frontiers | Research Topics

# Case reports in cardiovascular imaging 2022

**Edited by**
Antonios Karanasos, Riccardo Liga, Grigorios Korosoglou and Ali Yilmaz

**Published in**
Frontiers in Cardiovascular Medicine

ISSN 1664-8714
ISBN 978-2-8325-2949-2
DOI 10.3389/978-2-8325-2949-2

## About Frontiers

Frontiers is more than just an open access publisher of scholarly articles: it is a pioneering approach to the world of academia, radically improving the way scholarly research is managed. The grand vision of Frontiers is a world where all people have an equal opportunity to seek, share and generate knowledge. Frontiers provides immediate and permanent online open access to all its publications, but this alone is not enough to realize our grand goals.

## Frontiers journal series

The Frontiers journal series is a multi-tier and interdisciplinary set of open-access, online journals, promising a paradigm shift from the current review, selection and dissemination processes in academic publishing. All Frontiers journals are driven by researchers for researchers; therefore, they constitute a service to the scholarly community. At the same time, the *Frontiers journal series* operates on a revolutionary invention, the tiered publishing system, initially addressing specific communities of scholars, and gradually climbing up to broader public understanding, thus serving the interests of the lay society, too.

## Dedication to quality

Each Frontiers article is a landmark of the highest quality, thanks to genuinely collaborative interactions between authors and review editors, who include some of the world's best academicians. Research must be certified by peers before entering a stream of knowledge that may eventually reach the public - and shape society; therefore, Frontiers only applies the most rigorous and unbiased reviews. Frontiers revolutionizes research publishing by freely delivering the most outstanding research, evaluated with no bias from both the academic and social point of view. By applying the most advanced information technologies, Frontiers is catapulting scholarly publishing into a new generation.

## What are Frontiers Research Topics?

Frontiers Research Topics are very popular trademarks of the *Frontiers journals series*: they are collections of at least ten articles, all centered on a particular subject. With their unique mix of varied contributions from Original Research to Review Articles, Frontiers Research Topics unify the most influential researchers, the latest key findings and historical advances in a hot research area.

Find out more on how to host your own Frontiers Research Topic or contribute to one as an author by contacting the Frontiers editorial office: frontiersin.org/about/contact

# Case reports in cardiovascular imaging: 2022

**Topic editors**

Antonios Karanasos — Hippokration General Hospital, Greece
Riccardo Liga — Pisana University Hospital, Italy
Grigorios Korosoglou — GRN Klinik Weinheim, Germany
Ali Yilmaz — University Hospital Münster, Germany

**Citation**

Karanasos, A., Liga, R., Korosoglou, G., Yilmaz, A., eds. (2023). *Case reports in cardiovascular imaging: 2022*. Lausanne: Frontiers Media SA.
doi: 10.3389/978-2-8325-2949-2

# Table of contents

frontiers | Frontiers in Cardiovascular Medicine

TYPE Editorial
PUBLISHED 23 June 2023
DOI 10.3389/fcvm.2023.1222166



OPEN ACCESS

EDITED AND REVIEWED BY
Yohann Bohbot,
Centre Hospitalier Universitaire (CHU) d'Amiens, France

*CORRESPONDENCE
Grigorios Korosoglou
gkorosoglou@hotmail.com

RECEIVED 13 May 2023
ACCEPTED 16 June 2023
PUBLISHED 23 June 2023

CITATION
Karanasos A, Liga R and Korosoglou G (2023) Editorial: Case reports in cardiovascular imaging: 2022.
Front. Cardiovasc. Med. 10:1222166.
doi: 10.3389/fcvm.2023.1222166



# Editorial: Case reports in cardiovascular imaging: 2022

Antonios Karanasos[1], Riccardo Liga[2,3] and Grigorios Korosoglou[4,5]*

[1]1st Department of Cardiology, Athens Medical School, Hippokration Hospital, Athens, Greece, [2]Department of Surgical Pathology, University of Pisa, Pisa, Italy, [3]Cardiothoracic and Vascular Department, University Hospital of Pisa, Pisa, Italy, [4]Department of Cardiology, Vascular Medicine and Pneumology, GRN Hospital Weinheim, Weinheim, Germany, [5]Cardiac Imaging Center Weinheim, Hector Foundation, Weinheim, Germany

KEYWORDS

echocardiography, cardiac magnetic resonance (CMR), cardiac computed tomography (CCT), multimodal imaging, tissue characterization, cardiac masses, diagnostic classification, positron emission tomography (PET)

Editorial on the Research Topic
Case reports in cardiovascular imaging: 2022

Technical developments with several cardiovascular imaging techniques, including echocardiography, cardiac magnetic resonance (CMR), cardiac computed tomography angiography (CCTA) and positron emission tomography (PET) contributed to the profound understanding of cardiac physiology, as well as to precise diagnostic classification and risk stratification of patients with different cardiovascular disorders. Together with the wider availability of cardiovascular imaging and continuous training of cardiologists and radiologists in terms of image acquisition, analysis and interpretation within the clinical context, imaging techniques may not only provide the correct diagnosis, but also aid the monitoring of treatment strategies. In addition, artificial intelligence may standardize and harmonize the diagnostic processes, further enhancing the role of cardiovascular imaging in clinical practice. This taken together, along with continuous spread of knowledge among experts from different disciplines, like with the case series presented herein, will contribute to improved diagnostic work-up, patient management and outcomes.

The role of multimodality imaging is highlighted in the article by Yang D. et al. where using contrast echocardiography, CCTA and PET-CT a cardiac lymphoma was suspected. Using this multimodality imaging approach, the localization of the tumor in relation to neighboring structures of the heart could be verified, while extra cardiac spread helped classifying the structure as malignant, providing important information for the subsequent clinical treatment of the patient.

The role of cardiovascular imaging was again highlighted in another interesting case by Punzo et al. where CCTA and CMR aided determination of lesion morphology, anatomical localization, and tissue characterization in a patient with cardiac paraganglioma. Cardiac paragangliomas are rare extra-adrenal tumors, which arise from chromaffin cells of sympathetic ganglia and are frequently diagnosed incidentally in the absence of limiting clinical symptoms. The role of CMR, together with other imaging modalities, in the sense of a multimodal approach for the diagnosis of cardiac tumors has already been highlighted in a recent multi-center study (1) and has been discussed accordingly (2). The above-mentioned cases nicely confirm the importance of multimodality imaging and interdisciplinary discussion in this context.

In another interesting case report, Wa et al. demonstrated the importance of multimodality cardiovascular imaging for the establishment of the correct diagnosis in a relatively rare disease, cardiac sarcoidosis. Hereby, the presence of late gadolinium enhancement (LGE) in the right ventricle by CMR was indicative of sarcoidosis, whereas PET confirmed intense cardiac uptake in the septum and in the right ventricle. Imaging was used to guide endomyocardial biopsy, which indeed confirmed the presence of epithelioid nodules and lymphocytes indicative for cardiac sarcoidosis. Thereafter, the patient received immunosuppressive treatment with prednisolone, which led to resolution of the limiting symptoms and regression of the original lesion by PET.

In the same direction, Sharifkazemi et al. reported on 2 patients with large coronary artery fistulas, one from the left circumflex artery to the coronary sinus and one to the superior caval vein, which were both diagnosed using transesophageal echocardiography, CCTA and coronary angiography. This combined assessment by multimodality cardiovascular imaging helped to establish the diagnosis and estimate the exact course of the artery fistulas, which may help to predict the disease course and select the most suitable treatment option for the individual patient.

Another interesting case report by Nguyen et al. underlines the role of integration of clinical, multimodal imaging and histologic data for the diagnosis of concomitant intramyocardial and intrahepatic hydatic cysts in a young female patient with echinococcosis. The initial abdominal ultrasound revealed a large cyst in the liver, whereas echocardiography detected a cyst within lateral wall of the left ventricle. CCTA and CMR helped to localize and define typical features of the intramyocardial cyst, which was then treated by cardiac surgery and adjunctive pharmacotherapy.

Another promising development in the section of cardiovascular imaging is the increasing use of point-of-care ultrasound imaging for decision making in acute settings. Ngoc Le et al. were able to detect two large heterogeneous masses in the left ventricular wall and in the apical myocardium of a patients presenting with suspected acute ST-elevation myocardial infarction. This completely changed the initial diagnosis, modifying the treatment strategy in a patient with metastatic oesophageal carcinoma, where subsequent CCTA confirmed the presence of multiple cardiac and lung metastases.

In addition, imaging can shed light to characteristic of cardiac or vascular diseases, which are not completely understood in terms of pathology and pathophysiology. Thus, based on the report by Hong et al. a case of focal renal artery fibromuscular dysplasia was detected, which gradually progressed to a branch of the main renal artery 8 years after the initial treatment with a bare metal stent. Intravascular imaging has been used to evaluate vascular pathology in the renal arteries (3), and in this case excluded neointimal hyperplasia within the old stent and confirmed the presence of *de novo* eccentric intimal thickening, causing eccentric stenosis in the branch renal artery.

Given the wide epidemiology of inflammatory heart diseases and the relevant central role of cardiovascular imaging, six articles of the collection involved such cases, five of which involved valvular endocarditis. Interestingly, two papers reported cases of Libman-Sacks (LS) endocarditis (Liang et al.; Bui et al.), a form of non-bacterial thrombotic endocarditis (NBTE) that may develop in the presence of a hypercoagulable state, such as antiphospholipid antibody syndrome (APS) (4). Another case by Miao et al. highlighted the relevance of advanced non-invasive cardiac imaging techniques for the characterization of complex patients with blood culture-negative endocarditis, in whom novel innovations in three-dimensional echocardiography provided photorealistic images of cardiac structures, enabling finer anatomical characterization of the disease burden. Two last reports described the fate of patients with bacterial endocarditis caused by "conventional" germs from the streptococcus and staphylococcus family in patients with predisposing condition, such as a congenital heart disease (Yang G. et al.) and an implanted valvular prosthesis (Wu et al.). Both cases demonstrated how a detailed imaging assessment may allow a proper characterization of the endocarditis and of its complications, guiding the subsequent patient management.

Moving from valvular bacterial to autoimmune eosinophilic endocarditis, a paper by Li Y. et al. reported the characteristics and clinical course of the relatively rare Loeffler disease in a patient with multisystemic involvement of eosinophilic granulomatosis with polyangiitis (EGPA), where state-of-the-art cardiac magnetic resonance imaging allowed an in-depth depiction of disease progression.

Seven articles, on the other hand, dealt with cases of congenital heart diseases (CHD), each outlining the importance of a multiparametric imaging assessment to guide both diagnosis and patient management. Two papers described rare congenital anomalies involving the atrial chambers. In one case by Fukudome et al. the management of a patients with a very rare bronchogenic cyst in the right atrium was reported, describing the typical imaging features of the tumor and its preferential management strategy. In a second article, Li R. et al. reported on the clinical presentation, multimodality imaging assessment and final management strategy of a patient with a giant left atrial appendage aneurysm (LAAA). Another rare CHD with multi-chamber cardiac involvement was reported by Ge et al. In their article, a fatal case of double-chambered right ventricle associated with hypertrophic cardiomyopathy and incessant atrial flutter was described, and the specific role of the different cardiac imaging modalities was further discussed in this context. The possible risks of non-cardiac surgery in patients with unknown complex vascular malformations are outlined in the article by Zhang et al. reporting the 8th known case of azygos continuation of the inferior vena cava in a patient undergoing esophagectomy, indicating the benefit of a thorough pre-procedural vascular evaluation to avoid possibly fatal post-procedural complications.

In three articles of the current collection, non-invasive imaging identified the presence of congenital heart conditions that had been asymptomatic until late in the adulthood. The case by Deng et al. describes the finding of double orifice mitral valve by echocardiography. Despite its impressive visual appearance, this anomaly does not require a specific treatment unless combined with significant stenosis or insufficiency. In the case of

Tang et al. a simple chest radiograph performed for non-specific symptoms led to the discovery of the rare finding of supracardiac total anomalous pulmonary venous return, which was combined with a large atrial septal defect (ASD). The latter was assessed by a combination of TTE, CCTA, and cardiac catheterization, confirming the functional significance of the disorder and guided successful surgical correction. Finally, the case of Ma et al. illustrated how CCTA and TTE provided incremental information to the invasive angiogram for the diagnosis of a rare case of STEMI with cardiogenic shock in an acute setting. This condition was attributed to the rupture of a giant right sinus of Valsalva aneurysm, causing right coronary artery compression. Despite emergent surgical treatment the outcome was unfavourable in this patient, indicating the severity and poor prognosis of such a condition.

The use of imaging for the identification and management of complications following cardiac interventions is demonstrated in two articles of the collection. The cases presented by Zhou et al. underscore the need for vigilance and echocardiographic follow-up post neochord implantation. Two patients experienced recurrent dyspnoea due to early-intermediate rupture of neochords and were managed by elective reoperation. In another series by Wang et al. the management of the dislodgement of left atrial appendage closure (LAAC) devices is described. The authors used a combination of echocardiography and CCTA to identify the migration of two different devices used for LAAC, and managed to successfully retrieve them percutaneously through the femoral artery in one case and the femoral vein in the other case. Both interventions for complication management were guided using transoesophageal echocardiography.

The novel concept of using three-dimensional printing for procedural planning is illustrated in the article of Carrabba et al. In this interesting case, the authors used CCTA to reconstruct and print a 3d model of the left ventricle (LV) in a patient with ischemic LV dysfunction and LV aneurysm, scheduled for CABG and aneurysmatectomy. The printed model enhanced the 3D conceptualization of the procedure, leading to an improved LV function on this patient, with good agreement of the predicted and surgically attained residual LV volumes. Of course, the clinical value of this promising strategy still merits further investigation in future clinical trials.

In two of the articles of the collection, specific potential issues of imaging are addressed. Liao et al. presented a rare case of contrast-induced encephalopathy (CIE) with extreme manifestations due to contrast administered during a percutaneous coronary intervention. Further neuroimaging studies by brain CT, brain MRI and MRA disclosed the presence of moyamoya disease that in combination with electrolyte and thyroid function abnormalities were speculated to play a role in the severity and duration of the encephalopathy that eventually recovered following a standard treatment regimen for CIE. In the cases by Du et al. the issue of the "watershed" phenomenon in patients with mechanical circulatory support devices is highlighted. The sites of flow mix by cardiac output and mechanical circulatory support devices may be identified by CCTA as an arc-shaped low-attenuation filling defect that needs to be differentially diagnosed by thrombus. In such cases, repeating the examination in a different body position may lead to disappearance of the filling artifact and identification of the "watershed" site.

Finally, two articles illustrate the value of CT angiography in diagnosing vascular pathologies. The article by Ye et al. demonstrates the incremental value of CT angiography for the diagnosis of thrombotic foci in a patient with myocardial infarction due to histologically documented essential thrombocytosis and for guiding the type and duration of additional antithrombotic treatment, while the case by Li X et al. demonstrates the utility of multimodality imaging by colour Doppler ultrasound, CT angiography and digital subtraction angiography in the diagnosis, procedural planning and follow-up of a rare case of abdominopelvic arteriovenous malformation.

In conclusion, recent advances with non-invasive and invasive imaging are immense and decisive in modern cardiovascular medicine. The correct choice and interpretation of cardiovascular images enable precise diagnostic work-up of patients with cardiac diseases, guiding timely and efficient treatment. In addition, intracardiac or transesophageal imaging can effectively guide cardiac interventions during complications, which may occur during coronary or structural heart interventions. Many of the cases reported in our collection are very nice examples, showing how multimodality imaging can be incorporated in the daily clinical practice to improve patient care and resultant outcomes.

## Author contributions

AK wrote the first draft of the manuscript. AK, RL, and GK wrote sections of the manuscript. All authors contributed to the article and approved the submitted version.

## Conflict of interest

The authors declare that the research was conducted in the absence of any commercial or financial relationships that could be construed as a potential conflict of interest.

## Publisher's note

# References

1. Shenoy C, Grizzard JD, Shah DJ, Kassi M, Reardon MJ, Zagurovskaya M, et al. Cardiovascular magnetic resonance imaging in suspected cardiac tumour: a multicentre outcomes study. *Eur Heart J.* (2021) 43:71–80. doi: 10.1093/eurheartj/ehab635

2. Giusca S, Kelle S, Korosoglou G. When tissue and outcomes are the issue. Cardiac magnetic resonance for patients with suspected cardiac tumours. *Eur Heart J.* (2021) 43:81–3. doi: 10.1093/eurheartj/ehab625

3. Karanasos A, Van Mieghem N, Bergmann MW, Hartman E, Ligthart J, van der Heide E, et al. Multimodality intra-arterial imaging assessment of the vascular trauma induced by balloon-based and nonballoon-based renal denervation systems. *Circ Cardiovasc Interv.* (2015) 8:e002474. doi: 10.1161/CIRCINTERVENTIONS.115.002474

4. Habib G, Lancellotti P, Antunes MJ, Bongiorni MG, Casalta JP, Del Zotti F, et al. 2015 ESC guidelines for the management of infective endocarditis: the task force for the management of infective endocarditis of the European society of cardiology (ESC). endorsed by: european association for cardio-thoracic surgery (EACTS), the European association of nuclear medicine (EANM). *Eur Heart J.* (2015) 36:3075–128. doi: 10.1093/eurheartj/ehv319

frontiers in Cardiovascular Medicine

CASE REPORT
published: 23 February 2022
doi: 10.3389/fcvm.2022.840906

# Case Report: A Rare Case of Acute Anterior Myocardial Infarction Simultaneously Associated With Aortic Mural Thrombosis Due to Essential Thrombocytosis

*Sheng Ye, Wu-jie Xia and Peng Chen**

*Department of Cardiology, The Second Affiliated Hospital and Yuying Children's Hospital of Wenzhou Medical University, Wenzhou, China*

**Background:** Essential thrombocytosis (ET) simultaneously complicated with acute myocardial infarction and aortic thrombosis is extremely rare and associated with poor outcomes.

**Case:** A 54-year-old female was admitted to our emergency department with abdominal pain for 3 h. ST-segment elevation in leads V1–V3 on electrocardiography led to the diagnosis of acute anterior myocardial infarction. Coronary angiography demonstrated total occlusion of the proximal left anterior descending artery, and the patient was treated with angioplasty and placement of a drug-eluting stent. CT angiography revealed a massive mural thrombus located in the descending aorta. Bone marrow biopsy confirmed the diagnosis of ET. The patient was successfully treated with antithrombotic therapy and hydroxyurea.

**Conclusion:** At present, the clinical diagnosis and treatment of ET complicated with acute myocardial infarction and aortic thrombosis are mostly based on literature reports. Early target vessel revascularization, antiplatelet and anticoagulant combined with cytoreductive therapy may improve the prognosis. Clinicians should consider the risk of bleeding and thrombosis and create individualized treatment strategies for these patients.

**Keywords: acute myocardial infarction, aortic mural thrombosis, essential thrombocytosis, percutaneous coronary intervention, anticoagulation**

OPEN ACCESS

***Edited by:***
*Alessandro Zorzi, University Hospital of Padua, Italy*

***Reviewed by:***
*Gentian Denas, Rehabilitation Hospital of Motta di Livenza, Italy*
*Nicola Gasparetto, Ospedale di Treviso, Italy*

****Correspondence:***
*Peng Chen*
*chenpeng@wmu.edu.cn*

***Specialty section:***
*This article was submitted to Cardiovascular Imaging, a section of the journal Frontiers in Cardiovascular Medicine*

***Received:*** *21 December 2021*
***Accepted:*** *24 January 2022*
***Published:*** *23 February 2022*

***Citation:***
*Ye S, Xia W-j and Chen P (2022) Case Report: A Rare Case of Acute Anterior Myocardial Infarction Simultaneously Associated With Aortic Mural Thrombosis Due to Essential Thrombocytosis. Front. Cardiovasc. Med. 9:840906. doi: 10.3389/fcvm.2022.840906*

## INTRODUCTION

Essential thrombocytosis is a myeloproliferative disease that often leads to arterial thrombosis (1, 2). Essential thrombocytosis (ET) complicated with acute myocardial infarction (AMI) and aortic thrombosis is extremely rare and is therefore usually undiagnosed. Nevertheless, it is a life-threatening condition that requires emergency treatment. There is no standardized treatment strategy for the condition, although it is often treated with antithrombotic agents and hydroxyurea.

In this study, we reported a case of acute anterior myocardial infarction associated with aortic mural thrombosis due to ET. We successfully treated the patient with percutaneous coronary intervention combined with pharmacologic management.


**FIGURE 1 |** Twelve-lead ECG findings on admission and discharge. **(A)** Admission. **(B)** Discharge.

## CASE

A 54-year-old female was admitted to our emergency department with abdominal pain for 3 h. Her physical examination was unremarkable, and her vital signs were stable. The patient weighed 51 kg. Laboratory tests revealed a platelet count of 494 x $10^9$/L (normal range 100–300 x $10^9$/L). The troponin-I level was 0.132 ng/ml (normal range 0–0.034 ng/ml), and the D-dimer was 8 μg/ml (normal range 0–0.5 μg/ml). A 12-lead ECG revealed V1–V3 ST-segment elevation (**Figure 1A**). Acute anterior

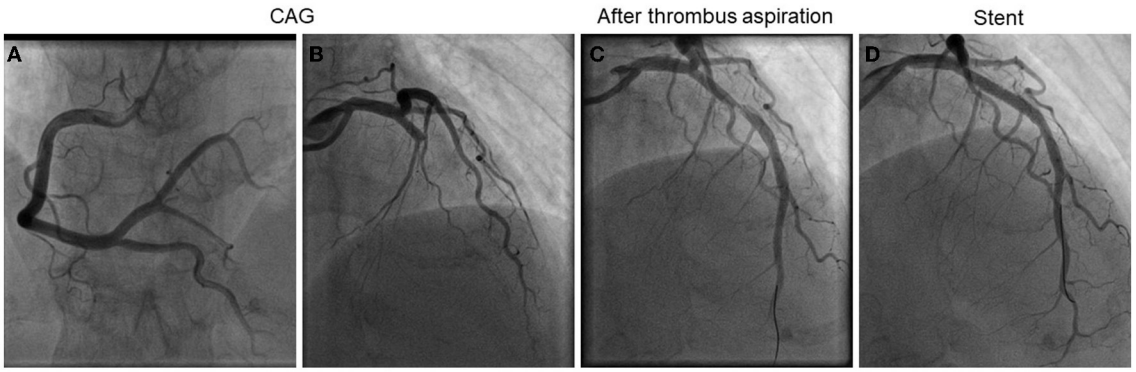


**FIGURE 2 |** Emergency coronary angiography and percutaneous coronary intervention. **(A)** Right coronary angiography. **(B)** Left coronary angiography. **(C)** After thrombus aspiration. **(D)** After stent.

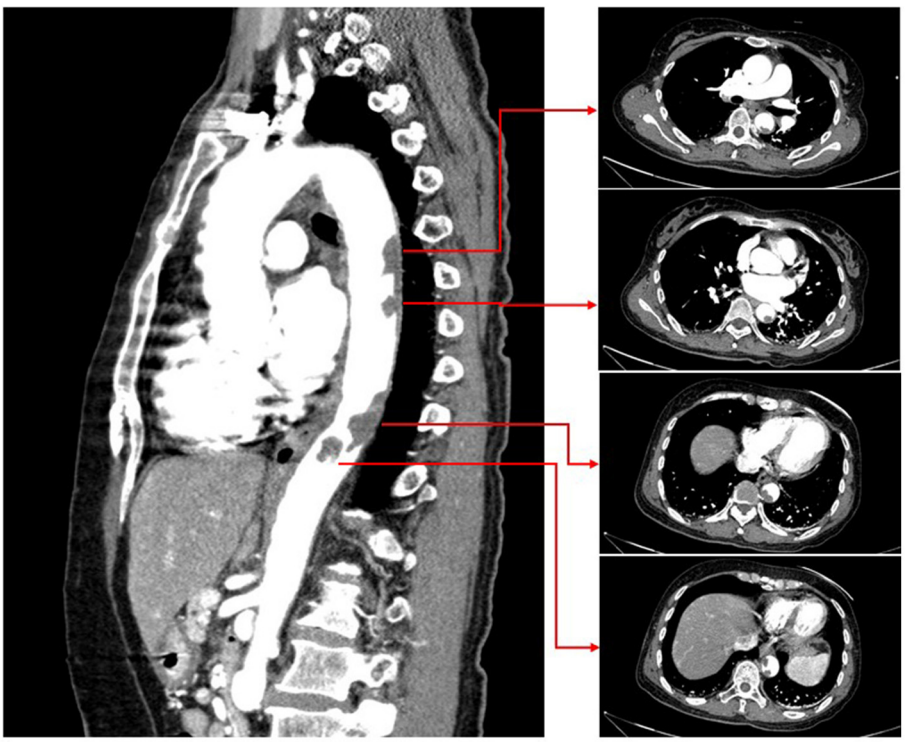

**FIGURE 3 |** CT angiography revealing massive mural thrombus in the descending aorta.

myocardial infarction was diagnosed, and the catheterization laboratory was engaged. Urgent coronary angiography revealed total occlusion of the proximal left anterior descending artery with thrombus (**Figure 2**). After thrombus aspiration, the patient was treated with angioplasty and placement of a drug-eluting stent (3 × 18 mm). The patient received unfractionated heparin (UFH) (6,000 IU) during percutaneous coronary intervention. Dual antiplatelet therapy was administrated, including aspirin (100 mg/day) and clopidogrel (75 mg/day). After the immediate percutaneous coronary intervention, the patient continued to complain of recurrent abdominal pain. Laboratory tests revealed a platelet count of 679 × $10^9$/L (normal range 100–300 × $10^9$/L), a troponin-I level of 42.1 ng/ml (normal range 0–0.034 ng/ml), and D-dimer 6.5 μg/ml (normal range 0–0.5 μg/ml). The CT angiography (CTA) revealed a massive mural thrombus in the descending aorta (**Figure 3**). The patient was started on enoxaparin (8,000 IU/day).

A bone marrow biopsy was performed based on the significantly elevated platelet count, and JAK2 V617F (the most prevalent mutation in ET) was detected. These results were

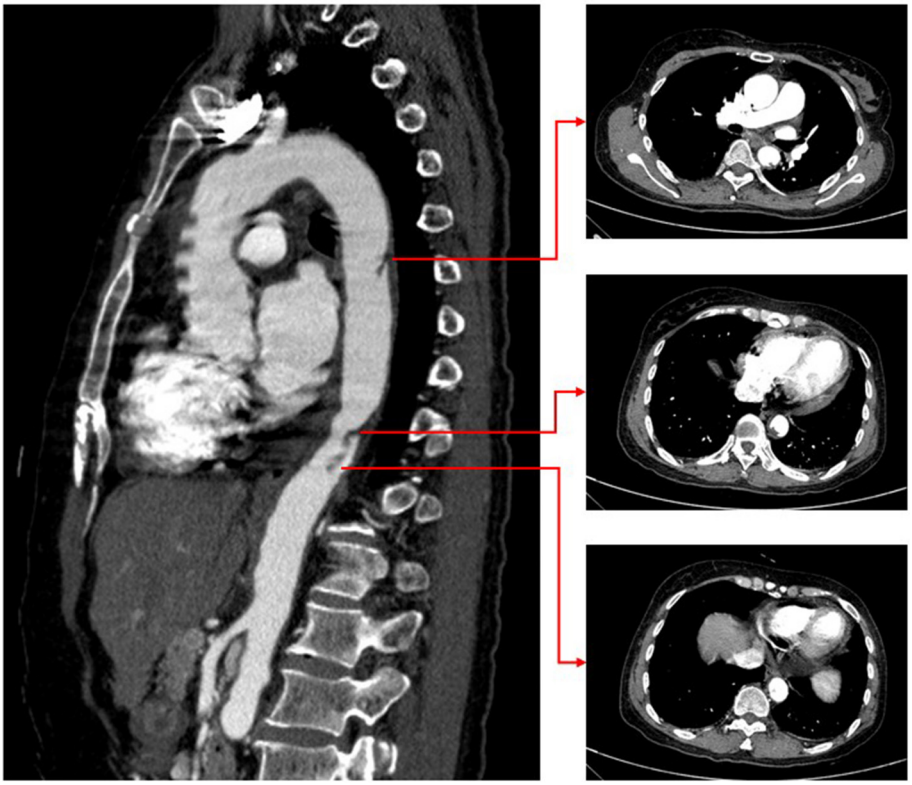

**FIGURE 4 |** Repeat CT angiography revealing significantly smaller aortic thrombus.

consistent with the diagnosis of ET. The patient denied a family history of myeloproliferative disease. The medications were modified to hydroxycarbamide (1,000 mg/day), enoxaparin (8,000 IU/day), aspirin (100 mg/day), and clopidogrel (75 mg/day). After 10 days of anticoagulation therapy, repeat CTA revealed that the size of the aortic mural thrombus had significantly decreased (**Figure 4**). The patient received another 10 days of anticoagulation therapy in the hospital. Laboratory tests revealed a platelet count of $299 \times 10^9$/L (normal range 100–300 $\times$ $10^9$/L), a troponin-I level of 0.032 ng/ml (normal range 0–0.034 ng/ml), and D-dimer 0.25 μg/ ml (normal range 0–0.5 μg/ml). Based on the D-dimer level, which is the most important laboratory indicator of thrombosis, having decreased to the normal range, we assumed that the thrombus had dissolved. However, she refused to undergo another CTA because of economic reasons. Considering the high risk of bleeding associated with triple antithrombotic therapy, anticoagulation was discontinued. The patient was ulti-mately discharged in stable clinical condition. The medications at discharge were modified to hydroxycarbamide (1,000 mg/day), aspirin (100 mg/day), and clopidogrel (75 mg/day). The ECG on discharge revealed Q wave in V1-V3 with T wave inversion (**Figure 1B**).

## DISCUSSION

Essential thrombocytosis (ET) is a myeloproliferative neoplasm, primarily the megakaryocytic system. It is characterized by a persistent increase in peripheral platelet levels. Hemorrhagic or thrombotic features are the primary clinical manifestations. The annual incidence of ET is about 0.3%. Thrombotic complications are the primary cause of death. However, when platelet levels are extremely elevated ($>$ 1,500 $\times$ $10^9$/L), the risk of bleeding increases.

Essential thrombocytosis (ET) that is complicated with AMI is rare (3, 4). Currently, the underlying pathogenesis is unclear, although it may be related to increased platelet count and aggregation. According to the literature, the left anterior descending artery is the most commonly obstructed site, although obstruction can also occur in the right coronary artery (5). At present, there is no standardized therapeutic strategy for acute myocardial infarction complicated with ET. Obstructions are mostly platelet thrombi in these patients, and there may be no atherosclerotic plaques in the coronary arteries. Thrombus aspiration can be used for treatment without coronary stent implantation. However, stents should be considered for patients with evident stenosis in the coronary artery after thrombus

aspiration. In our case, because of the severe thrombus burden and stenosis after repeated thrombus aspiration, the patient was treated with angioplasty and placement of a drug-eluting stent.

Aortic mural thrombosis due to ET is rarer (6). There are no appropriate guidelines for managing ET associated with aortic thrombosis. The choice is between pharmacologic and surgical therapy (7). Pharmacologic therapy for ET includes anticoagulation therapy and cytoreductive therapy with hydroxyurea (8). On the other hand, surgical therapy for aortic thrombosis is associated with high mortality and risk of complications and involves bleeding, cerebral and intestinal ischemia, and acute renal failure. Our patient suffered an AMI simultaneously associated with aortic thrombosis due to ET. Because we had previously implanted a drug-eluting stent in the left anterior descending artery, she required dual antiplatelet therapy. If we chose acute surgical treatment, the risk of bleeding would be extremely high. Therefore, we finally chose pharmacologic therapy. Fortunately, after treatment with aspirin, clopidogrel, enoxaparin, and hydroxyurea, the patient's condition stabilized, and repeat CTA revealed a significantly smaller aortic thrombus.

The primary therapeutic goals for ET include preventing thrombosis recurrence. Studies showed that oral anticoagulation (VKA or DOACs) combined with cytoreduction might provide a lower risk of recurrent thrombosis in patients with ET and VTE (9). However, the optimal antithrombotic strategy and duration for AMI and aortic mural thrombosis patients remain unclear. Based on the decreased size of aortic thrombus and D-dimer level in our case, triple antithrombotic therapy turned out to be effective. However, long-term triple antithrombotic therapy may increase bleeding risk. Because ET is a platelet disorder, antiplatelet therapy may be more critical for thromboembolic risk in ET with arterial thrombosis (10). At discharge, this patient's medications included dual antiplatelet therapy (aspirin and clopidogrel) for 12 months as well as cytoreductive therapy. Because the patient refused to undergo another CTA (for economic reasons), we asked her to present for follow-up platelet counts and D-dimer level to monitor thromboembolic risk.

In conclusion, we described a patient with ET who developed a rare combination of AMI and aortic mural thrombosis. This case teaches the importance of medical therapy when patients are not candidates for urgent surgery.

## DATA AVAILABILITY STATEMENT

The original contributions presented in the study are included in the article/supplementary material, further inquiries can be directed to the corresponding author.

## ETHICS STATEMENT

Written informed consent was obtained from the individual(s) for the publication of any potentially identifiable images or data included in this article.

## AUTHOR CONTRIBUTIONS

SY and PC drafted the manuscript and contributed to the case collection. W-jX provided figures and formalized the manuscript. PC reviewed the drafts and approved the final manuscript as submitted. All authors approved the submitted version.

## FUNDING

The research was funded by Grant 81901409 from the Youth Program of the National Natural Science Foundation of China and Grant Y2020015 from Wenzhou Municipal Science and Technology Bureau.

## REFERENCES

1. Angona A, Alvarez-Larrán A, Bellosillo B, Martínez-Avilés L, Garcia-Pallarols F, Longarón R, et al. Essential thrombocythemia: baseline characteristics and risk factors for survival and thrombosis in a series of 214 patients. *Med Clin.* (2015) 144:247–53. doi: 10.1016/j.medcle.2015.10.002
2. Mora B, Passamonti F. Developments in diagnosis and treatment of essential thrombocythemia. *Expert Rev Hematol.* (2019) 12:159–71. doi: 10.1080/17474086.2019.1585239
3. Daya SK, Gowda RM, Landis WA, Khan IA. Essential thrombocythemia-related acute ST-segment elevation myocardial infarction. A case report and literature review. *Angiology.* (2004) 55:319–23. doi: 10.1177/00033197040550312
4. Soucy-Giguère MC, Turgeon PY, Sénéchal M. What cardiologists should know about essential thrombocythemia and acute myocardial infarction: report of two cases and advanced heart failure therapies considerations. *Int Med Case Rep J.* (2019) 12:253–9. doi: 10.2147/IMCRJ.S217568
5. Gao W, Shen W, Luo X, Shi H, Jiang X, Pan J. ST-segment elevation myocardial infarction in patient with essential thrombocythemia without associated risk. *Int J Cardiol.* (2015) 180:223–5. doi: 10.1016/j.ijcard.2014.11.147
6. Geringer J, Fenderson J, Osswald M. Essential thrombocythemia complicated by occlusive thrombosis of the abdominal aorta. *Case Rep Hematol.* (2019) 2019:9454501. doi: 10.1155/2019/9454501
7. Suzuki K, Sezai A, Tanaka M. Unsuccessful surgical treatment of thoracic aortic thrombosis in a patient with essential thrombocythemia. *J Card Surg.* (2020) 35:236–8. doi: 10.1111/jocs.14286
8. Okada Y, Kimura F. Multiple aortic thrombi in essential thrombocythaemia. *Br J Haematol.* (2021) 193:862. doi: 10.1111/bjh.17353
9. Hamulyák EN, Daams JG, Leebeek FW, Biemond BJ, Te Boekhorst PA, Middeldorp S, et al. A systematic review of antithrombotic treatment of venous thromboembolism in patients with myeloproliferative neoplasms. *Blood Adv.* (2021) 5:113–21. doi: 10.1182/bloodadvances.2020003628
10. Bhat T, Ahmed M, Baydoun H, Ghandour Z, Bhat A, McCord D. Acute ST-segment elevation myocardial infarction in a young patient with essential thrombocythemia: a case with long-term follow-up report. *J Blood Med.* (2014) 5:123–7. doi: 10.2147/JBM.S53539

**Conflict of Interest:** The authors declare that the research was conducted in the absence of any commercial or financial relationships that could be construed as a potential conflict of interest.

**Publisher's Note:** All claims expressed in this article are solely those of the authors and do not necessarily represent those of their affiliated organizations, or those of the publisher, the editors and the reviewers. Any product that may be evaluated in this article, or claim that may be made by its manufacturer, is not guaranteed or endorsed by the publisher.

frontiers in Cardiovascular Medicine

CASE REPORT
published: 25 March 2022
doi: 10.3389/fcvm.2022.852682

# Case Report: Three-Dimensional Printing Model for Surgical Planning of Left Ventricular Aneurysm: Evolution Toward Tailoring Surgery

*Nazario Carrabba[1]*, Francesco Buonamici[2], Rocco Furferi[2], Monica Carfagni[2], Matteo Vannini[1], Renato Valenti[1], Alfredo Giuseppe Cerillo[1], Niccolò Marchionni[1] and Pierluigi Stefàno[1]*

[1] Cardiovascular and Thoracic Department of Careggi Hospital, Florence, Italy, [2] Department of Industrial Engineering of Florence, University of Florence, Florence, Italy

OPEN ACCESS

**Edited by:**
Grigorios Korosoglou,
GRN Klinik Weinheim, Germany

**Reviewed by:**
Joachim Lotz,
University of Göttingen, Germany
Sorin Giusca,
GRN Klinik Weinheim, Germany

***Correspondence:**
Nazario Carrabba
n.carrabba@virgilio.it;
carrabban@aou-careggi.toscana.it

**Specialty section:**
This article was submitted to Cardiovascular Imaging, a section of the journal Frontiers in Cardiovascular Medicine

**Received:** 11 January 2022
**Accepted:** 23 February 2022
**Published:** 25 March 2022

**Citation:**
Carrabba N, Buonamici F, Furferi R, Carfagni M, Vannini M, Valenti R, Cerillo AG, Marchionni N and Stefàno P (2022) Case Report: Three-Dimensional Printing Model for Surgical Planning of Left Ventricular Aneurysm: Evolution Toward Tailoring Surgery. Front. Cardiovasc. Med. 9:852682. doi: 10.3389/fcvm.2022.852682

A 59-year-old woman was admitted to the emergency department for heart failure (HF), New York Heart Association (NYHA) IV, showing an anterior, evolved myocardial infarction (MI) with a wide apical left ventricular aneurysm (LVA), ejection fraction (EF) 24%, and global longitudinal strain (GLS) −5. 5% by echo. Cardiac magnetic resonance imaging (MRI) confirmed an apical LVA without thrombus, EF 20%, and a transmural delayed enhancement in the myocardium wall. Coronarography showed a three-vessel disease with occluded proximal left anterior descending (LAD) and proximal right coronary artery (RCA). Based on the cardiac CT scan, we decided to generate a three-dimensional (3D) print model of the heart, for better prediction of residual LV volumes. After LVA surgery plus complete functional revascularization, an optimal agreement was found between predicted and surgical residual LV end-diastolic (24.7 vs. 31.8 ml/m$^2$) and end-systolic (54.1 vs. 69.4 ml/m$^2$) volumes, with an improvement of NYHA class, from IV to I. The patient was discharged uneventfully and at 6- and 12-month follow-up, the NYHA class, and LV volumes were found unchanged. This is a second report describing the use of the 3D print model for the preoperative planning of surgical management of LVA; the first report was described by Jacobs et al. among three patients, one with a malignant tumor and the remaining two patients with LVA. This article focused on the use of the 3D print model to optimize surgical planning and individualize treatment of LVA associated with complete functional revascularization, leading to complete recovery of LV function with a favorable outcome.

**Keywords: 3D printing model, left ventricular aneurysm, CAD, heart failure, surgical ventricular restoration**

## INTRODUCTION

After myocardial infarction (MI), patients with severe heart failure (HF) carry a poor prognosis, and despite major advances, long-term medical management alone might be insufficient (1). Cardiac transplantation and ventricular assist devices are definitive or temporary surgical therapies. Although it has been shown that mitral valve (MV) and surgical coronary revascularization (CR)

can lead to the improvement of symptoms in left ventricular aneurysm (LVA) patients, ventricular dilation and dysfunction might be so advanced that surgical reconstruction of the LV geometry must be attempted. We herein report a patient with LVA with severe systolic dysfunction, who underwent surgical LV reshaping using a 3D print model with the subsequent optimal recovery of systolic function (2).

## CASE PRESENTATION

Our patient was a 59-year-old woman admitted to the emergency department for HF, New York Heart Association (NYHA) IV, with dyspnea that started 10 days before. She was a former smoker, affected by hypercholesterolemia and hypertension, on angiotensin-converting enzyme (ACE) inhibitor treatment at the time of presentation. We started management of HF using high doses of loop diuretics i.v., beta blockers, ACE inhibitors, mineralocorticoids, statins, and aspirin. Routine blood investigations were notable for NT-proBNP 6,526 ng/dl and troponin-hs 196 ng/l. An anterior, evolved MI infarction was revealed by ECG, and a two-dimensional (2D)-echocardiogram showed a wide apical LVA (6 × 5.5 cm) without thrombus, EF 24% and global longitudinal strain (GLS) 5.5% (**Figures 1A–E** and **Supplementary Video 1**), and mild mitral regurgitation. The coronary angiogram showed a 60% stenosis of proximal left main and occlusion of proximal left anterior descending (LAD) as well as occlusion of proximal right coronary artery (RCA) (**Figures 1F–H**). To better evaluate LVA, further imaging was advised. Cardiac MRI confirmed an apical LVA without thrombus, EF 20%, and a transmural delayed enhancement in the myocardium wall, supplied by LAD, specifically, in the middle and apical segment of the septum, the distal segment of the anterior wall, and apical segments of LV, with microvascular obstruction observed in the septum (**Figures 1I–M**). Since the 3D volumetric sequences were not planned in an MRI protocol, to optimize surgical planning, based on the cardiac CT scan, we decided to generate a 3D print model of the LVA for a better prediction of the residual surgical LV volumes, LVA volume (47%), and the geometrical shape of MV, annulus, and papillary muscle attachment (**Table 1**). A dedicated contrast-enhanced CT scan (high pitch, dual source) was made according to the following protocol: retrospective ECG-gated spiral acquisition, with tube modulation. Thin reconstructions (0.4 mm) were exported into imaging processing software version 22.0 (Materialize Mimics Medical, Leuven, Belgium) to delineate and segment the left-sided structures, including the MV, annulus, and leaflets. All the phases were available, and diastolic and systolic phases were chosen for LV reconstruction. Patient-specific 3D models were then printed using tissue rigid material for left chambers. The models were printed using Fused Filament Fabrication technology; specifically, a Makerbot Replicator + machine was used to produce plastic models in the PLA material. A 0.1 mm layer height was selected during fabrication, to ensure valid resolution for the application. The cardiologist and cardiac surgeon used the 3D-printed models during their encounters with the patient, to illustrate the specific pattern of LVA and anticipated repair results. The patient expressed a markedly improved understanding of her LVA and planned operation.

After heart team discussion, the surgical ventricular restoration (SVR) of the LV chamber appeared as an attractive strategy, combined with complete CR. The risk in generating a small residual LV was discussed, as it is not trivial. To optimize surgical planning, we used a 3D print model of the LVA for a better prediction of the residual surgical LV volumes. The patient underwent SVR excluding dyskinetic portions of the anterior wall and septum, reshaping the LV with a stitch that encircled the transitional zone between contractile myocardium and aneurysmal tissue, and using a "Gore-Tex" patch to reestablish ventricular wall continuity. A complete functional CR was also attempted, using the left anterior internal mammary artery for the marginal branch and saphenous graft for RCA. The operation improved the size and geometry of the left ventricle, reduced wall tension and paradox movement, and enhanced overall systolic function, EF 54% (**Figures 2A,B**), and also GLS (average −14) and LV torsion (3.6, 1.3–2.1 deg/cm) (**Supplementary Videos 2–4**). In addition, the geometry of papillary muscle was preserved, without significant change in the interpapillary muscle distance and tenting height (**Figures 3A,B**), with a trivial residual mitral regurgitation (MR). Importantly, an optimal agreement was found between the predicted and surgical residual LV volumes (**Table 1**), with an improvement of NYHA class from IV to I. The patient remained uneventful and was discharged 7 days after surgery. At 6- and 12-month follow-up, the patient remained in NYHA class I, and LV volumes were found unchanged.

## DISCUSSION

Heart failure is a major health problem, with increasing prevalence due to the aging of the population and the increased survival after MI. Patients with severe HF have a poor prognosis, and despite major advances, long-term medical management alone may be insufficient. Cardiac transplantation and ventricular assist devices are permanent or temporary surgical therapies (3, 4). After an MI, the LVA is located at the apex or in the anterior wall in 90% of cases, and in the posterior–inferior wall in the remaining 10%. Although it has been shown that MV and surgical CR can lead to the improvement of symptoms in LVA patients, ventricular dilation and dysfunction might be so advanced that surgical reconstruction of the LV geometry must be attempted (5). Certainly, the concept of reducing LV volume to improve global contractile function is not new. Currently, the remodeling of the LVA is performed mostly with the surgical techniques developed by Dor and Jatene (6). The STICH trial did not show improved survival with surgical CR associated with SVR in comparison to CR alone (7). However, a *post hoc* analysis of that trial showed that a postoperative LVESVI of 70 ml/m$^2$ or lower resulted in

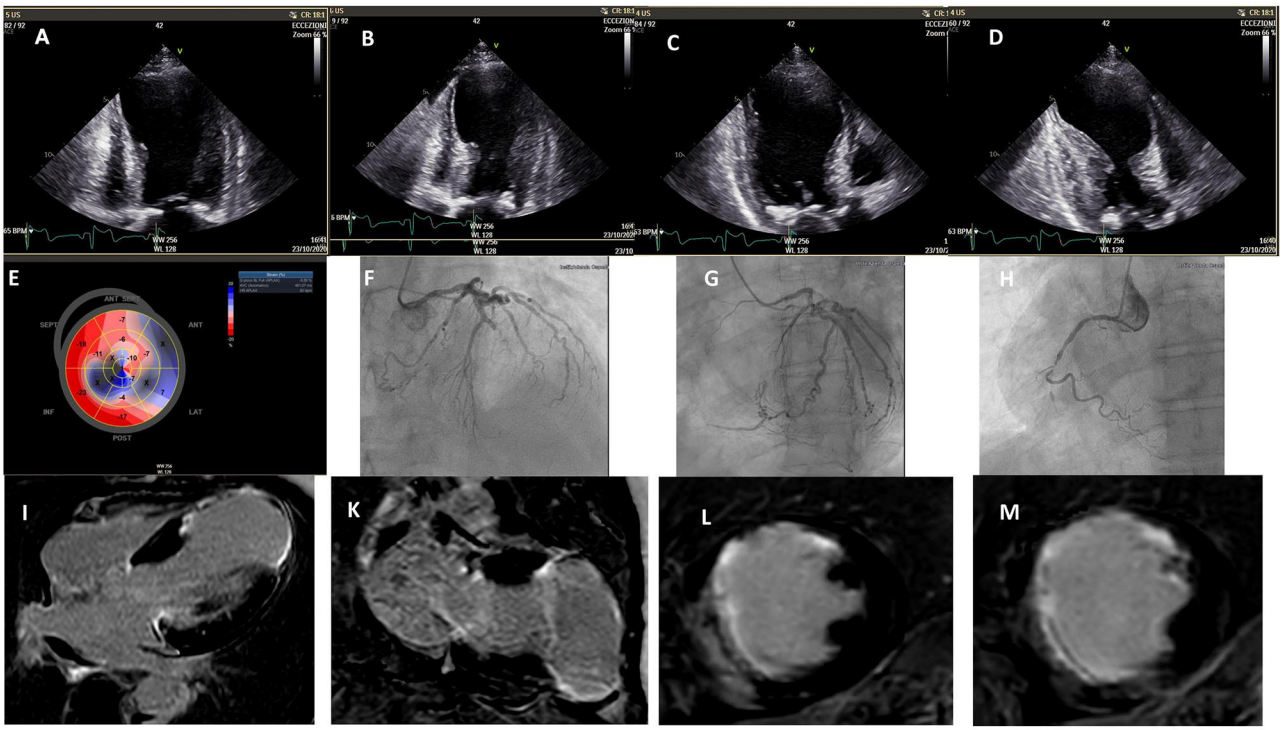


**FIGURE 1 |** 2D echo: **(A–D)** left ventricular aneurysm: systolic and diastolic phase; **(E)** baseline global longitudinal strain; coronary angiograms; **(F)** occlusion of the proximal left anterior descending coronary artery; **(G)** circumflex artery; **(H)** occlusion of proximal right coronary artery; cardiac MRI; **(I–M)** transmural delayed enhancement in the myocardium wall supplied by LAD.

**TABLE 1 |** Left ventricular volumes before, planned, and after surgery.

| | LV-EDV | LV-ESV | SV | EF (%) |
|---|---|---|---|---|
| **3D-printed model** | | | | |
| Before surgery (mL/m$^2$) | 101.8 | 77.1 | 24.7 | 24 |
| Planned (mL/m$^2$) | 54.1 | 24.7 | 29.4 | 54 |
| After surgery (mL/m$^{2)}$ | 69.4 | 31.8 | 37.3 | 54 |

*LV, left ventricular; EDV, end diastolic volume; ESV, end systolic volume; SV, stroke volume; EF, ejection fraction.*

improved survival, compared with CR alone (8). In agreement with these results, the most recent ESC/EACTS guidelines recommend SVR in combination with CR in selected HF patients with a scar in the LAD territory, especially, if a postoperative LVESVI below 70 ml/m$^2$ can be predictably achieved (class of recommendation IIb; level of evidence B) (9). In addition, when the removal of LVA, in comparison with the baseline LVESVi, is <30%, the beneficial effect of this surgical intervention could be lower than that expected, and in this case, the surgical intervention would be contraindicated (8). Beyond the surgeon's experience, optimal pre-procedural planning based on imaging is of pivotal importance to achieve a more detailed analysis of the heart structures and accurate measurements of LV volumes (10). Volumetric image acquisition plays a critical role in 3D printing. Not only does it determine the geometric accuracy of the 3D model, but also it characterizes tissue properties and directs the choice of the appropriate printing materials. A number of modern cardiovascular imaging techniques have been used to acquire 3D image data for 3D printing. Contrast-enhanced multidetector row CT with electrocardiographic gating/triggering has been the most commonly used imaging modality for 3D printing because of its fast acquisition, superb spatial resolution, and excellent ability of tissue characterization differentiating metal implants and calcific lesions from soft tissues. The temporal resolution of modern CT varies in the range of 75–200 ms, depending on its make and model. Compared with CT, 3D cardiac magnetic resonance has a relatively lower spatial resolution and longer acquisition time. However, because of the absence of ionizing radiation, the 3D cardiac MRI with free-breathing technique has been frequently used in modeling the structures of the cardiac chambers and great vessels in pediatric patients and young adults for 3D printing. On the other hand, because of the wide availability, high temporal resolution, and ease of performing echocardiography at the bedside, echocardiography has been used to acquire images for 3D printing, especially for imaging of valve disease. The main limitation of 3D echocardiography is the relatively low signal-to-noise ratio, which makes image post-processing and 3D modeling more challenging. Furthermore, because of the tradeoff between the size of the acoustic window and

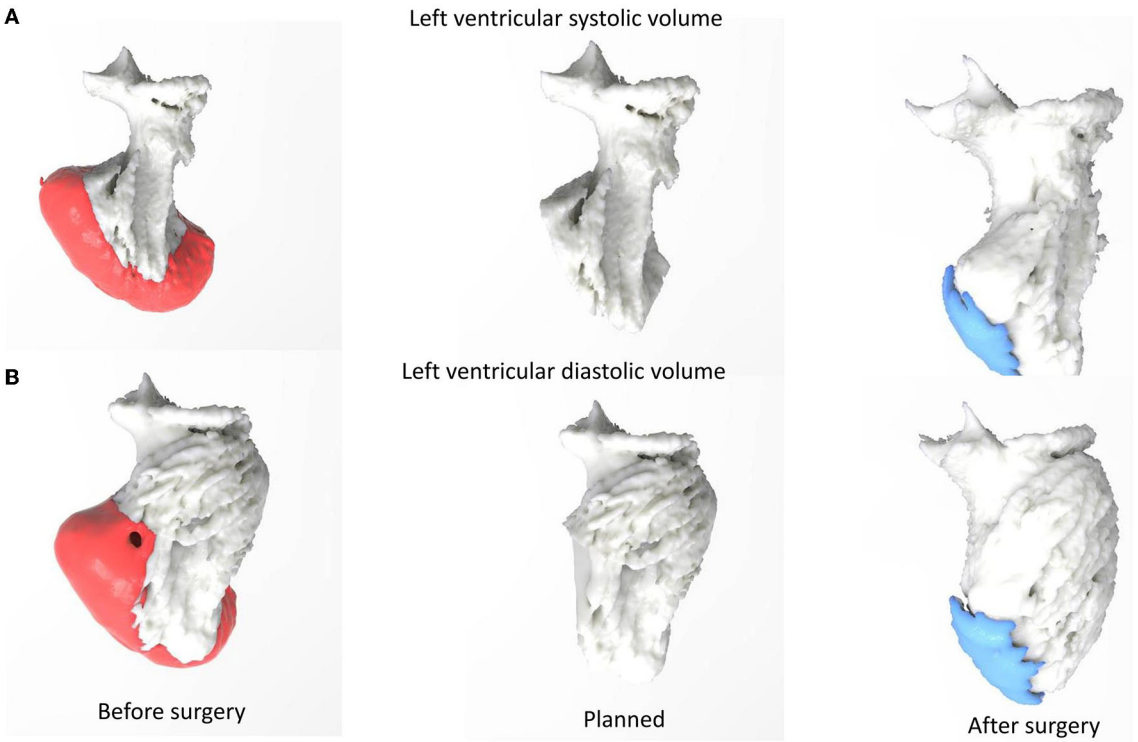


**FIGURE 2 |** 3D print model: **(A)** left ventricular systolic volume, **(B)** left ventricular diastolic volume before, planned, and after surgery.

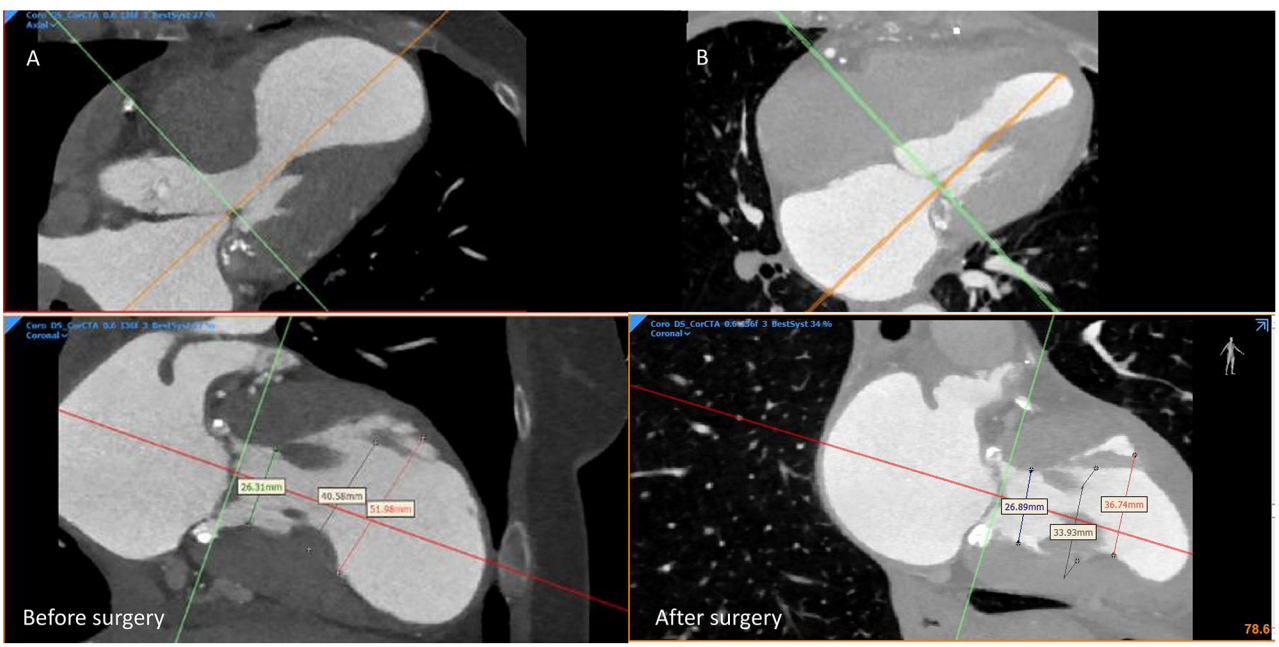


**FIGURE 3 |** CT scan: the geometrical shape of the mitral valve, annulus, and papillary muscle attachment **(A)** before surgery, **(B)** after surgery.

the spatiotemporal resolution, 3D modeling of the complete heart anatomy using echocardiography remains difficult. The usefulness of 3D models is particularly felt in cardiac surgery and interventional cardiology, where a detailed knowledge of patient-specific anatomy is fundamental to guide procedures (10). Indeed, the possibility of obtaining a 3D virtual model of the heart structure and physically printing the hollow heart anatomy introduces a radical revolution in interventional planning and in surgeons' training. In the treatment of LVA, for instance, the use of the 3D print model may help the surgeon accurately predicting LVESVI avoid the risk of a restrictive pattern or a distorted ventricular shape generating a severe MR. The 3D-printed model has been applied in the field of medical education and training, procedural planning and simulation, device innovation, and also communication to the patients (11). From a surgeon's and interventional cardiologist's perspective, printed models add 3D spatial and tactile dimensions to a patient's specific cardiovascular disease, thus, leading to improved 3D conceptualization and enhanced visuospatial skills (12). The ultimate goals are to optimize pre-procedural planning, to tailor the procedure to the patient's specific anatomy, to be prepared for possible complications, and to shorten operative and extracorporeal circulation times, reducing postoperative multiorgan dysfunction. From the patient's perspective, personalized 3D models have the potential to alleviate anxiety about the upcoming procedure by improving understanding of the disease and the anticipated operation, and by enhancing the patient–doctor relationship and communication.

## CONCLUSION

Nowadays, a personalized surgical approach is mandatory to satisfy the different needs of post-infarct LV remodeling. Patient-specific 3D-printed models can be used for a comprehensive assessment of the LVA, pre-procedural planning, and patient education, translating into excellent results. Optimal planning of SVR is of crucial relevance in preventing a restrictive pattern or a distorted ventricular shape, potentially translating into poor outcomes. Based on a 3D-printing model, it is conceivable that, in the near future, a tailored approach to different phenotypes of LVA will make the planning of the most appropriate residual LV volumes possible in the individual patient.

## DATA AVAILABILITY STATEMENT

The raw data supporting the conclusions of this article will be made available by the authors, without undue reservation.

## ETHICS STATEMENT

The studies involving human participants were reviewed and approved by Careggi Hospital EC. The patients/participants provided their written informed consent to participate in this study.

## AUTHOR CONTRIBUTIONS

NC: substantial contributions to the conception or design of the work, agree to be accountable for all aspects of the work in ensuring that questions related to the accuracy or integrity of any part of the work are appropriately investigated and resolved, and drafting the work or revising it critically for important intellectual content. FB: substantial contributions to the conception or design of the work and agree to be accountable for all aspects of the work in ensuring that questions related to the accuracy or integrity of any part of the work are appropriately investigated and resolved. RF and MC: substantial contributions to the conception or design of the work and provide approval for publication of the content. MV, RV, and AC: substantial contributions to the conception or design of the work, or the acquisition, analysis, or interpretation of data for the work. NM and PS: substantial contributions to the conception or design of the work and provide approval for publication of the content. All authors contributed to the article and approved the submitted version.

## SUPPLEMENTARY MATERIAL

The Supplementary Material for this article can be found online at: https://www.frontiersin.org/articles/10.3389/fcvm.2022.852682/full#supplementary-material

**Supplementary Video 1 |** 2D (2- 4-chamber and short axis view) and 3D echo of left ventricle aneurysm before surgery.

**Supplementary Video 2 |** Time-volume curve of left ventricular and ejection fraction after surgery.

**Supplementary Video 3 |** Left ventricular global longitudinal strain after surgery.

**Supplementary Video 4 |** Left ventricular torsion after surgery.

## REFERENCES


1. Bahit MC, Kochar A, Granger CB. Post-myocardial infarction heart failure. *JACC Heart Fail.* (2018) 3:179–86. doi: 10.1016/j.jchf.2017.09.015
2. Jacobs S, Grunert R, Mohr FW, Falk V. 3D imaging of cardiac structures using 3D heart models for planning in heart surgery: a preliminary study. Interact. *Cardiovasc Thorac Surg.* (2008) 7:6–9. doi: 10.1510/icvts.2007.156588
3. Rose EA, Gelijns AC, Moskowitz AJ, Heitjan DF, Stevenson LW, et al. The randomized evaluation of mechanical assistance for the treatment of congestive heart failure (REMATCH) study group. Long-term use of a left ventricular assist device for end- heart failure. *N Engl J Med.* (2001) 20:1435–43. doi: 10.1056/NEJMoa012175
4. Moss AJ, Zareba W, Hall WJ, Klein H, Wilber DJ, Cannom DS, et al. The multicenter automatic defibrillator implantation trial ii investigators. Prophylactic implantation of a defibrillator stage in patients with myocardial infarction and reduced ejection fraction. *N Engl J Med.* (2002) 12:877–83. doi: 10.1056/NEJMoa013474
5. Alderman EL, Fisher LD, Litwin P, Kaiser GC, Myers WO, Maynard C, et al. Results of coronary artery surgery in patients with poor left ventricular function (CASS). *Circulation.* (1983) 68:785–95. doi: 10.1161/01.CIR.68.4.785
6. Dor V, Saab M, Coste P, Kornaszewska M, Montiglio F. Left ventricular aneurysm: a new surgical approach. *Thorac Cardiovasc Surg.* (1989) 37:11–9. doi: 10.1055/s-2007-1013899

7. Jones RH, Velazquez EJ, Michler RE, et al. STICH Hypothesis 2 investigators. Coronary bypass surgery with or without surgical ventricular reconstruction. *N Engl J Med*. (2009) 360:1705–17. doi: 10.1056/NEJMoa0900559
8. Michler RE, Rouleau JL, Al-Khalidi HR, et al. STICH Trial Investigators. Insights from the STICH trial: change in left ventricular size after coronary artery bypass grafting with and without surgical ventricular reconstruction. *J Thorac Cardiovasc Surg*. (2013) 146:1139–45. doi: 10.1016/j.jtcvs.2012.09.007
9. Windecker S, Kolh P, Alfonso F, Collet JP, Cremer J, Falk V, et al. 2014 ESC/EACTS Guidelines on myocardial revascularization: the Task Force on Myocardial Revascularization of the European Society of Cardiology (ESC) and the European Association for CardioThoracic Surgery (EACTS) Developed with the special contribution of the European Association of Percutaneous Cardiovascular Interventions (EAPCI). *Eur Heart J*. (2014) 35:2541–619. doi: 10.1093/eurheartj/ehu278
10. Harb SC, Rodriguez LL, Vukicevic M, Kapadia SR, Little SH. Three-dimensional printing applications in percutaneous structural heart interventions. *Circ Cardiovasc Imaging*. (2019) 12:e009014. doi: 10.1161/CIRCIMAGING.119.009014
11. Bartel T, Rivard A, Jimenez A, Mestres CA, Müller S. Medical three-dimensional printing opens up new opportunities in cardiology and cardiac surgery. *Eur Heart J*. (2018) 39:1246–54. doi: 10.1093/eurheartj/ehx016
12. Wang DD, Qian Z, Vukicevic M, et al. 3D Printing, Computational Modeling, and Artificial Intelligence for Structural Heart Disease. *J Am Coll Cardiol Img*. (2021). 14:41–60. doi: 10.1016/j.jcmg.2019.12.022

**Conflict of Interest:** The authors declare that the research was conducted in the absence of any commercial or financial relationships that could be construed as a potential conflict of interest.

frontiers in Cardiovascular Medicine

CASE REPORT
published: 31 March 2022
doi: 10.3389/fcvm.2022.780646

# Case Report: Esophagectomy and Azygos Continuation of the Inferior Vena Cava: A Lethal Combination

*Yan Zhang[1], Zheng Ding[1], Teng Mu[1], Xue Pan[2]*, Guoqing Zhang[1]* and Xiangnan Li[1]**

[1] Department of Thoracic Surgery and Lung Transplantation, The First Affiliated Hospital of Zhengzhou University, Zhengzhou, China, [2] School of Nursing and Health, Zhengzhou University, Zhengzhou, China

Azygos continuation of the inferior vena cava (IVC) is rare in the general population and even rarer among patients with esophageal carcinoma. In 90% of cases, this congenital IVC variant is isolated and does not affect the patient's growth or development. However, thoracic surgery such as esophagectomy would be fatal if the flow through this connection was interrupted. We present a case of minimally invasive esophagectomy in a patient with azygos continuation of the IVC.

**Keywords: esophageal carcinoma, esophagectomy, azygos continuation, congenital inferior vena cava variant, artificial vascular bypass**

OPEN ACCESS

***Edited by:***
*Avi Leader,*
*Rabin Medical Center, Israel*

***Reviewed by:***
*Hugo Ten Cate,*
*Maastricht University Medical Centre, Netherlands*
*Amir Ben Yehuda,*
*Yitzhak Shamir Medical Center, Israel*

****Correspondence:***
*Xue Pan*
*xuepan321@163.com*
*Guoqing Zhang*
*drzhangguoqing@163.com*
*Xiangnan Li*
*lxn-2000@163.com*

***Specialty section:***
*This article was submitted to Cardiovascular Imaging, a section of the journal Frontiers in Cardiovascular Medicine*

***Received:*** *21 September 2021*
***Accepted:*** *09 March 2022*
***Published:*** *31 March 2022*

***Citation:***
*Zhang Y, Ding Z, Mu T, Pan X, Zhang G and Li X (2022) Case Report: Esophagectomy and Azygos Continuation of the Inferior Vena Cava: A Lethal Combination. Front. Cardiovasc. Med. 9:780646. doi: 10.3389/fcvm.2022.780646*

## INTRODUCTION

Azygos continuation of the IVC is rare in the general population. In a large series of 55,457 pregnant women who underwent prenatal examinations, an incidence of 0.02% (11/55457) was determined for azygos continuation of the IVC. Most of these cases (90%) were not associated with other anatomical variants (1). Azygos continuation of the IVC is considerably rarer in patients with esophageal carcinoma, and only six cases have been reported (2–4). Awareness of this type of combined condition is crucial in esophagectomy, and it would be fatal if the azygos vein was divided while following the usual procedure. Here, we report a case of minimally invasive esophagectomy in a patient with azygos continuation of the IVC. Written informed consent was obtained from the patients' legal guardian for the publication of any potentially identifiable images or data included in this article.

## CASE PRESENTATION

A 61-year-old female had dysphagia, and a lower thoracic squamous cell carcinoma (SCC) was detected *via* an upper gastrointestinal endoscopy (distance from incisor tooth, 30–35 cm) at a local hospital. Potential metastasis was ruled out by chest and abdomen CT scan, brain MRI and bone scintigraphy. The physical examination and laboratory tests were unremarkable. A cT3N0M0 primary SCC of the esophagus was diagnosed, and a minimally invasive McKeown esophagogastrectomy was performed on March 28, 2021, without a detailed preoperative evaluation for vascular malformation.

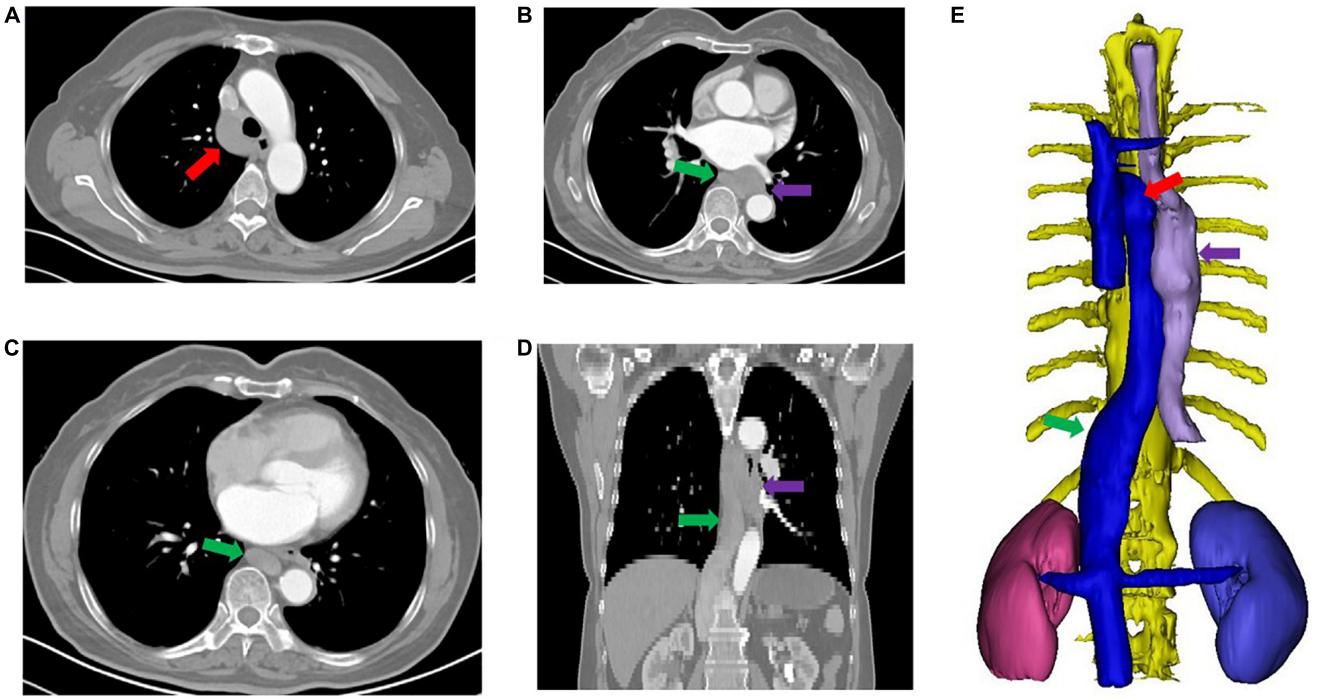


**FIGURE 1 |** CT reconstruction showing azygos continuation of the inferior vena cava (not preoperatively recognized). **(A–D)** Show the enlarged arch of the azygos vein and azygos vein. **(E)** Shows hepatic segment absence of the inferior vena cava with azygos continuation. The red arrow shows the enlarged arch of the azygos vein; the green arrow shows the azygos vein; the purple arrow shows the tumor.

During the surgery, the arch of the azygos vein was unusually enlarged and was unfortunately routinely divided without recognizing an azygos continuation of the IVC. The patient developed progressive hypotension and oliguria after 60 min, and repeated doses of dopamine and ephedrine did not improve this deterioration. The esophagogastrectomy was completed after the use of a large amount of vasopressors to maintain the patient's blood pressure. Unfortunately, the patient's condition progressively deteriorated.

The final diagnosis was obtained after reviewing the patient's preoperative CT scan. The absence of the hepatic segment of the IVC was detected, and the 3D CT reconstruction showed an azygos continuation of the IVC (**Figure 1**). Then, the patient was transferred to our tertiary hospital for further treatment.

An emergency digital subtraction angiography (DSA) of the inferior vena cava and double renal vein was performed 24 h post-operation. Angiography demonstrated a large thrombus at the azygos vein from the level of the diaphragm to the level where it was divided during surgery (**Figure 2A**). The patient underwent a thrombectomy and the placement of an inferior vena cava filter above the bilateral renal vein (**Figure 2B**). Artificial vascular bypass grafting was used to further reconstruct the venous drainage: the proximal part was anastomosed to the right atrium, and the distal end of the graft was anastomosed to the azygos vein at the level where it was divided during surgery. The artificial vessel was easily located on the postoperative routine CT evaluation (**Figure 2C**) (April 3, 2021). Unfortunately, the patient remained anuric after surgery, and continuous renal replacement therapy (CRRT) was used to provide renal support.

On April 6, 2021, the patient suffered from sudden cardiac arrest and died despite emergency rescue efforts. A pulmonary embolism was deemed the most likely cause of sudden death according to dilation of the pulmonary artery detected by bedside ultrasound (**Figure 3**). Unfortunately, effective management such as thrombolytic therapy and hemodynamic support was not initiated because of failure of rescue.

## DISCUSSION

Embryogenesis of the IVC (between the 6th and 8th weeks of embryonic life) is a complex process, and it involves the formation of several anastomoses between several embryonic veins. In general, the IVC is composed of four segments: a hepatic, a suprarenal, a renal, and an infrarenal segment. Failure to form the right subcardinal-hepatic anastomosis is thought to be the embryonic event of azygos continuation of the IVC. Consequently, blood is shunted from the suprasubcardinal anastomosis through the retrocrural azygos vein.

This malformation does not affect the patient's growth and development in most cases. However, it would be fatal if the patient suffered from diseases that needed to be treated with surgical intervention, such as a right transthoracic

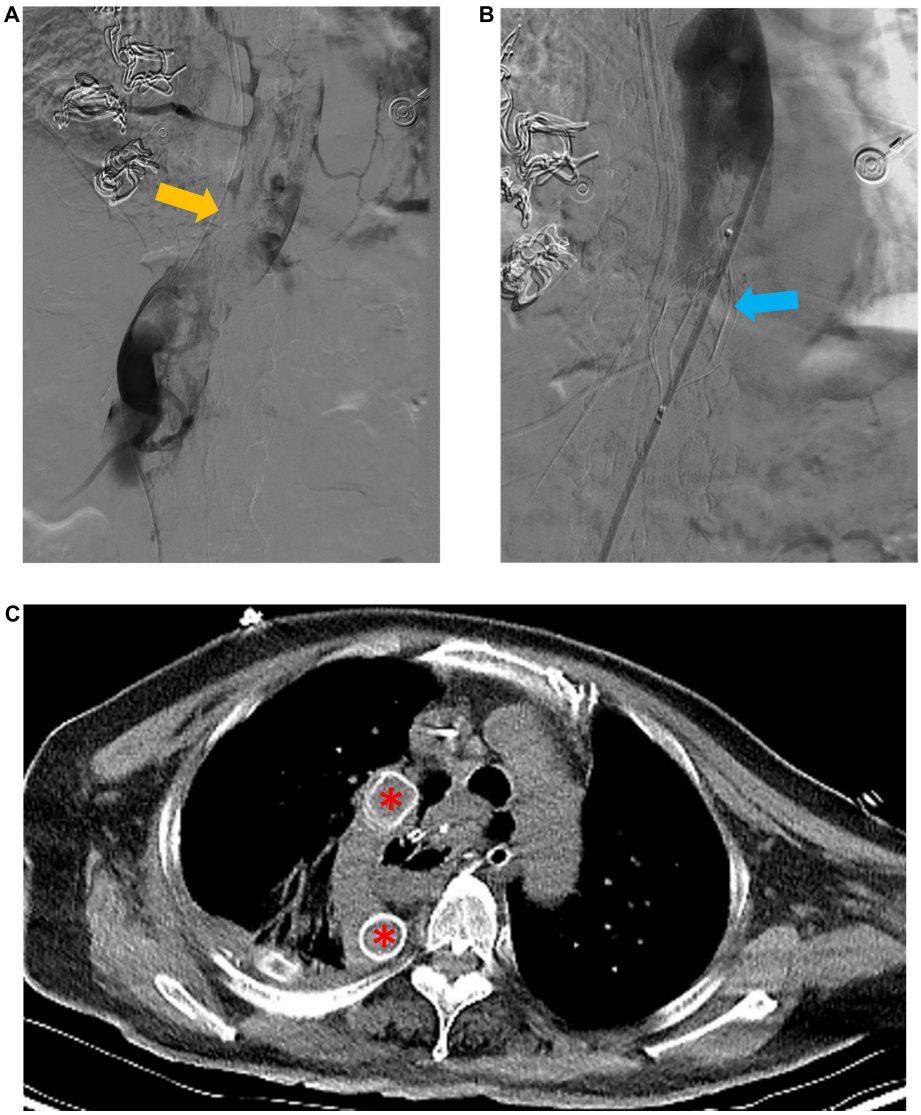


**FIGURE 2 |** Emergency digital subtraction angiography (DSA) of the inferior vena cava and artificial vascular bypass to reconstruct venous drainage. **(A)** Shows a large thrombus (yellow arrow) in the azygos vein. **(B)** Shows the inferior vena cava filter (blue arrow) superior to the bilateral renal vein. **(C)** Shows the well-located artificial vessel (red asterisk).

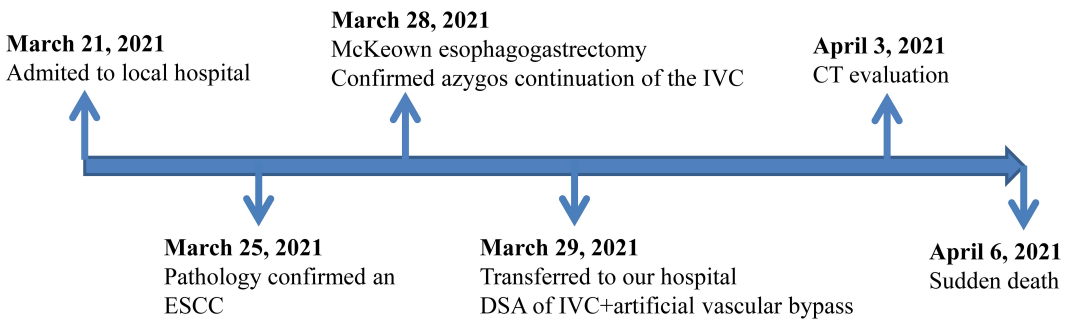


**FIGURE 3 |** Timeline of events of the patient from admission to discharge.

**TABLE 1 |** Reported cases of azygos continuation of the inferior vena cava in patients undergoing esophagectomy.

| Author | Country | Age, sex | Operation | Combined malformation | Arch of azygos vein | Discharge status |
|---|---|---|---|---|---|---|
| Bronshtein et al. (1) | Hungary | 52 y, male | Open | No | Protected | Alive |
| Veltman et al. (2) | Spain | 62 y, male | Open | No | Divided | Died within 1 day |
| Wang et al. (3) | China | 52 y, male | Open | No | Divided | Died within 15 h |
| Wang et al. (3) | China | 56 y, male | Open | Double IVC | Protected | Alive |
| Palotás et al. (4) | Netherlands | 62 y, female | Open | No | Divided | Alive |
| Martín-Malagón et al. (5) | Japan | 58 y, male | NR | Double IVC | Protected | Alive |
| Zhang et al. | China | 61 y, female | Minimally invasive | No | Divided | Died within 9 days |

*IVC, inferior vena cava; y, year.*

esophagectomy (3, 5). Considering the unremarkable physical examination and laboratory test results of patients with such an anomaly, recognition of the warning signs (enlarged azygos vein and arch of the azygos vein) of this anomaly as visualized on preoperative CT and during intraoperative exploration is vital. To date, there have been only six reported cases of azygos continuation of the IVC in patients undergoing esophagectomy (2–4, 6) (**Table 1**). Three patients were safely discharged with adequate arch of azygos vein protection (3, 4). Unfortunately, the arches of the azygos vein in the other three patients were routinely divided: one patient died within 15 h after esophagectomy (3), one patient died within 1 day after esophagectomy (5) and one survived after experiencing dangerous postoperative complications (acute renal insufficiency, hypotension, and huge azygos vein thrombus) (2). Similarly, there is also a report of an NSCLC patient who died after ligation of the azygos vein (7). However, we should note that it is likely that the true incidence is much higher, as death cases are less likely to be published.

Interestingly, the case of a patient reported by Veltman et al. survived even though the enlarged azygos was divided (2). Furthermore, eight patients with interruption or stenotic lesion of the IVC without a well-developed azygos/hemiazygos continuation have been reported (8). In such patients, venous return from the bilateral kidneys and lower extremities occurs exclusively through potential vessel variation or the collateral veins, such as (accessory) hemiazygos venous return, paravertebral collaterals (9) and portocaval communication. However, under circumstances of surgical ligation, compensatory collaterals do not have enough time to develop and are not sufficient for vein return. Similar to the case reported by Martín-Malagón et al. (5), artificial vascular graft was used to reconstruct the damaged arch of azygos vein in our study. Unfortunately, the two patients undergoing artificial vascular bypass died due to thromboembolic events, which may be additional evidence of a hypercoagulable state related to cancer or a cava filter. Scholars have pointed out that immediate reconstruction of the damaged arch of the azygos vein has important clinical importance in preventing graft thrombosis formation (5). Furthermore, active graft thrombosis prophylaxis after reconstruction of the arch of the azygos vein maybe of great clinical importance (10, 11).

We describe a patient who died after undergoing esophagectomy due to the presence of an azygos continuation of the IVC, and we systematically reviewed the limited literature related to this anomaly. The implications of this study for clinical practice are as follows. (1) Any patient who undergoes esophagectomy should have their CT reviewed for macrovascular malformations by the surgical team to prevent complications. Additionally, intraoperative exploration is the last opportunity to recognize an enlarged azygos vein and arch of the azygos vein to prevent fatal complications. (2) In some rare conditions (hemiazygos venous return, and abundant paravertebral collaterals), ligation of the enlarged azygos is not necessarily fatal, and a "wait and see" strategy may be reasonable. (3) In most cases, artificial vascular reconstruction is necessary and may be an appropriate intervention.

## DATA AVAILABILITY STATEMENT

The data that support the findings of this study are available from the corresponding author upon reasonable request.

## ETHICS STATEMENT

Written informed consent was obtained from the patients' legal guardian for the publication of any potentially identifiable images or data included in this article.

## AUTHOR CONTRIBUTIONS

YZ, ZD, and TM contributed to the conception and design of the study. YZ organized the data, performed the statistical analysis, and wrote the first draft of the manuscript. YZ, XP, GZ, and XL wrote the sections of the manuscript. All authors contributed to manuscript revision, read, and approved the submitted version.

## FUNDING

This study was supported by the National Natural Science Foundation of China (No. 32070623) and Provincial and Ministerial Co-construction Medical Science and Technology Project of Henan Province (SBGJ202002015).

## REFERENCES


1. Bronshtein M, Khatib N, Blumenfeld Z. Prenatal diagnosis and outcome of isolated interrupted inferior vena cava. *Am J Obstet Gynecol.* (2010) 202:398.e1–4. doi: 10.1016/j.ajog.2009.11.014
2. Veltman ES, Ruurda JP, van Berge Henegouwen MI. Inferior vena cava agenesis in a patient with esophagectomy for esophageal cancer. *Dis Esophagus.* (2013) 26:338–9. doi: 10.1111/j.1442-2050.2011.01264.x
3. Wang J, Yang L, Xin Y, Zhang H, Zuo Z, Li W, et al. Surgical treatment in patients with azygos continuation of the inferior vena cava. *J Regional Anat Operat Surg.* (2011) 20:469.
4. Palotás A, Paszt A, Szentpáli K, Lázár G. Esophageal cancer complicated with azygos continuation of the inferior vena cava. *Interact Cardiovasc Thorac Surg.* (2003) 2:361–3. doi: 10.1016/S1569-9293(03)00075-6
5. Martín-Malagón A, Bravo A, Arteaga I, Rodríguez L, Estévez F, Alarcó A. Ivor Lewis esophagectomy in a patient with enlarged azygos vein: a lesson to learn. *Ann Thorac Surg.* (2008) 85:326–8. doi: 10.1016/j.athoracsur.2007.06.039
6. Shintakuya R, Mukaida H, Mimura T, Ikeda T, Takiyama W, Yoshimitsu M, et al. A case of thoracic esophageal cancer with an unusual type of duplicated inferior vena cava. *Gen Thorac Cardiovasc Surg.* (2014) 62:327–30. doi: 10.1007/s11748-014-0372-3
7. Effler DB, Greer AE, Sifers EC. Anomaly of the vena cava inferior; report of fatality after ligation. *J Am Med Assoc.* (1951) 146:1321–2.
8. Koc Z, Oguzkurt L. Interruption or congenital stenosis of the inferior vena cava: prevalence, imaging, and clinical findings. *Eur J Radiol.* (2007) 62:257–66. doi: 10.1016/j.ejrad.2006.11.028
9. Bass JE, Redwine MD, Kramer LA, Huynh PT, Harris JH Jr. Spectrum of congenital anomalies of the inferior vena cava: cross-sectional imaging findings. *Radiographics.* (2000) 20:639–52. doi: 10.1148/radiographics.20.3.g00ma09639
10. Toth S, Flohr TR, Schubart J, Knehans A, Castello MC, Aziz F. A meta-analysis and systematic review of venous thromboembolism prophylaxis in patients undergoing vascular surgery procedures. *J Vasc Surg Venous Lymphat Disord.* (2020) 8:869–81.e2. doi: 10.1016/j.jvsv.2020.03.017
11. Comerota AJ, Thakur S. Management of anticoagulation and platelet inhibition in reconstructive vascular surgery. *Vascular.* (2008) 16:S48–54.


**Conflict of Interest:** The authors declare that the research was conducted in the absence of any commercial or financial relationships that could be construed as a potential conflict of interest.

frontiers | Frontiers in Cardiovascular Medicine

CASE REPORT
published: 08 April 2022
doi: 10.3389/fcvm.2022.771538

# Cardiac Lymphoma Diagnosed by Multi-Modality Imaging: A Case Report

*Dayan Yang*[1], *Tangna Wu*[1], *Lini Gao*[1], *Lili Liu*[1], *Fujin Liu*[2] *and Xiangxiang Jing*[1]*

[1] Department of Ultrasonography, Hainan General Hospital (Hainan Affiliated Hospital of Hainan Medical University), Haikou, China, [2] Department of Pathology, Hainan General Hospital (Hainan Affiliated Hospital of Hainan Medical University), Haikou, China

A 79-year-old female patient who presented with a cardiac mass detected by conventional echocardiography was ultimately diagnosed with a malignant tumor by myocardial contrast echocardiography. A positron emission tomography/computed tomography examination showed tumors in the right atrium consistent with the findings of the contrast-enhanced ultrasound. Finally, the patient was confirmed by pathology to have cardiac lymphoma. Because no lesions were found elsewhere in the body, primary cardiac lymphoma was diagnosed by combining multi-modal imaging examination and pathological examination. Although conventional echocardiography may identify a cardiac mass, it is difficult to identify whether they are malignant or not. Myocardial contrast echocardiography helps to identify the location, shape, and size of the mass, its relationship with the surrounding tissue, and evaluate its blood supply. Thus, this imaging modality is of great value for identifying the likely etiology of a cardiac mass. Multi-modal imaging is complementary to echocardiography for determining the location of cardiac masses, invasion of surround structures, extra cardiac spread, and determination of whether a mass is likely benign or malignant. Multi-modality imaging provides an important basis for clinical treatment and decision-making.

**Keywords: myocardial contrast echocardiography, cardiac lymphoma, diagnosed, ultrasound, cardiac tumor, multi-modality medical imaging**

OPEN ACCESS

***Edited by:***
*Sanjeev Bhattacharyya, Barts Heart Centre, United Kingdom*

***Reviewed by:***
*Christoph Sinning, University Medical Center Hamburg-Eppendorf, Germany*
*Natallia Maroz-Vadalazhskaya, Minsk, Belarus*
*Ying Wang, Xuzhou Medical University, China*
*Kunming Qi, Xuzhou Medical University, China*

***Correspondence:**
*Xiangxiang Jing*
*ljjxx2000@126.com*

***Specialty section:***
*This article was submitted to Cardiovascular Imaging, a section of the journal Frontiers in Cardiovascular Medicine*

***Received:*** *06 September 2021*
***Accepted:*** *14 March 2022*
***Published:*** *08 April 2022*

***Citation:***
*Yang DY, Wu TN, Gao LN, Liu LL, Liu FJ and Jing XX (2022) Cardiac Lymphoma Diagnosed by Multi-Modality Imaging: A Case Report. Front. Cardiovasc. Med. 9:771538. doi: 10.3389/fcvm.2022.771538*

## INTRODUCTION

Primary cardiac lymphoma is a very rare extranodal lymphoma. Non-Hodgkin's lymphoma is the diagnosis for 80–90% of all lymphoma patients, with one-third of tumors diagnosed in lymphoid tissue outside the lymph nodes or lymphoid tissue organs of agglomeration. Lymphoma can occur in any part of the body with different clinical manifestations, although its physical signs are mostly primary organ enlargement or local tumor formation. Primary cardiac lymphoma accounts for 1% of primary cardiac tumors and 0.5% of extranodal lymphomas (1). The final diagnosis of cardiac lymphoma is determined by pathology, which causes some trauma to the patient and has certain limitations. In addition, cardiac imaging can also provide some valuable information, such as the mass's location, shape, and size.

Here, we present the case of a 79-year-old female patient who had a cardiac mass detected by conventional echocardiography (ECG). She was diagnosed with a malignant tumor by myocardial contrast ECG, to which pathology confirmed the tumor was a cardiac lymphoma.

## CASE DESCRIPTION

A 79-year-old female patient had been complaining of chest pain for over 2 weeks. She described a tingling in the pre-cardiac area that was unrelated to breathing or activity, and could not be relieved by rest. She reported no radiating pain. Occasionally, the patient experienced night sweats, fatigue, acid reflux, and belching. Nausea, vomiting, and abdominal pain were also present. The vomiting of the gastric contents ultimately resolved itself. Before presentation, however, she had a continuous fever for 4–5 days with a peak body temperature of 38.5°C, which was occasionally accompanied by a dry cough. Self-reported use of oral antipyretics reduced her temperature to normal. The patient experiences lack of sleep, poor appetite, and a poor mental state. She had a history of cerebral infarction. No obvious change in body weight had recently occurred. The patient denied a family history of high blood pressure, diabetes, and coronary heart disease.

The patients physical examination upon admission revealed a temperature of 36.4°C, pulse rate of 103 bpm, breathing rate of 20 breaths/min, and blood pressure of 99/75 mmHg. Physical examination revealed that her superficial lymph nodes were not enlarged. There were no abnormal heaves. The apex beat was 0.5 cm inside the midline of the fifth intercostal space. No cardiac murmurs or rubs were heard and no other abnormalities were found during the rest of the examination. A blood routine examination revealed no obvious abnormality. Her white blood cell count was $5.01 \times 10^9$/L, lymphocyte percentage was 19.4%, red blood cell count was $3.77 \times 10^{12}$/L, hemoglobin concentration was 109 g/L, and platelet count was $71 \times 10^9$/L. Multi-tumor marker protein chromatin immunoprecipitation (ChIP) detection (female, 12 items) showed no special abnormalities. Her ferritin concentration was 529.08 ng/ml, and the values of five key cardiac enzymes were as follows: aspartate aminotransferase, 149.6 U/L; lactate dehydrogenase, 809.0 U/L; α-hydroxybutyrate dehydrogenase, 602.0 U/L; phosphocreatine kinase isozyme, 27.4 U/L; and C-reactive protein, 37.26 mg/L. Her 72-h blood bacterial culture was negative. Her erythrocyte sedimentation rate was measured, and three results of the tuberculosis antibody ChIP, four results of coagulation, four results of blood transfusion, and liver and kidney functions were all normal.

Conventional ECG revealed that the patient's right atrium was enlarged, and a hypoechoic mass (40 mm × 39 mm) was found to be connected to the bottom of the lateral wall. The mass appeared to oscillate with the cardiac cycle in the tricuspid valve orifice, causing right ventricular inflow tract stenosis in diastolic periods. The right and the left ventricles were both roughly normal in size. A large amount of pericardial effusion was detected (**Figures 1A–D**). Subsequently, an IE33 ultrasound machine (Philips, Amsterdam, Netherlands), of which the probe frequency was 2.5 MHz, was used to obtain myocardial contrast ECG images. An ultrasound contrast agent was purchased from SonoVue (Bracco, Italy) and was reconstituted by adding 5 ml of 0.9% sodium chloride solution, then injected intravenously.

After injection, the contrast agent rapidly filled the right atrium and the right ventricle, followed by the left atrium and the left ventricle. After several cardiac cycles, a large amount of scattered ultrasound contrast agent was observed in the right atrial mass (**Figures 2A,B**). Contrast-enhanced computed tomography (CT) revealed a mass near the aortic arch, which was mildly enhanced in the arterial phase (**Figure 3A**) and reduced in the venous phase (**Figure 3B**). When evaluating inflammation by positron emission tomography (PET)/CT (**Figure 4**), masses in the right atrium, the walls of the right atrium and the right ventricle were discovered to be non-homogeneously thickened. In addition, 18F-fluorodeoxyglucose uptake was increased. The ascending aorta–para-aortic soft tissue density mass and increased 18F-fluorodeoxyglucose metabolism indicated that both the right atrial and aorta-ascending–para-aorta tumors were malignant.

Finally, a pathological examination of the cell mass in the pericardial effusion (**Figure 5**) diagnosed it as diffuse large B-cell non-Hodgkin's lymphoma. The immunohistochemical results were as follows: BCL-2 (+, 90%), $CD19^+$, $CD20^+$, $CD5^+$, $CD79a^+$, c-Myc (+, 30%), Ki-67 (+, 80%), and MUM-$1^+$.

With the collection of multi-modality imaging data and histologic findings, the patient's heart mass was finally diagnosed as cardiac lymphoma which needed to be differentiated from other space-occupying cardiac lesions. Because it was a mass with a rich blood supply, while benign lesions or thrombi in the heart tend to have poor blood supply, it was considered to be a malignant mass on imaging and was confirmed as lymphoma by pathological examination.

The patient declined treatment and ultimately died 1 year later.

## DISCUSSION

Primary cardiac lymphoma is described as an extranodal lymphoma involving only the heart and/or pericardium, presenting with cardiac symptoms that are accompanied by the development of the main tumor mass in the heart or pericardium (2). The latter definition is more applicable in clinical practice. Cardiac lymphoma is a malignant tumor which usually occurs in the right cardiac system, especially the right atrium which may, possibly, abnormally collect lymphatic fluid from the whole body (3). Its clinical manifestations are atypical and includes arrhythmia, chest pain, and fever (4). In the present case, a primary cardiac lymphoma located in the right atrium was discovered.

Although cardiac imaging can also provide useful information, the diagnosis of cardiac lymphoma depends on the pathology results. Chemotherapy is the preferred treatment of heart lymphoma (5). According to the World Health Organization classification, lymphoma with positive expressions of both C-Myc and Bcl-2 or Bcl-6 detected by immunohistochemistry is known as a double-expression lymphoma, which has a poor prognosis (6). In the present study, the patient had positive expressions of both c-Myc and Bcl-2. In such cases, early detection and treatment are very important for the health of the patient.

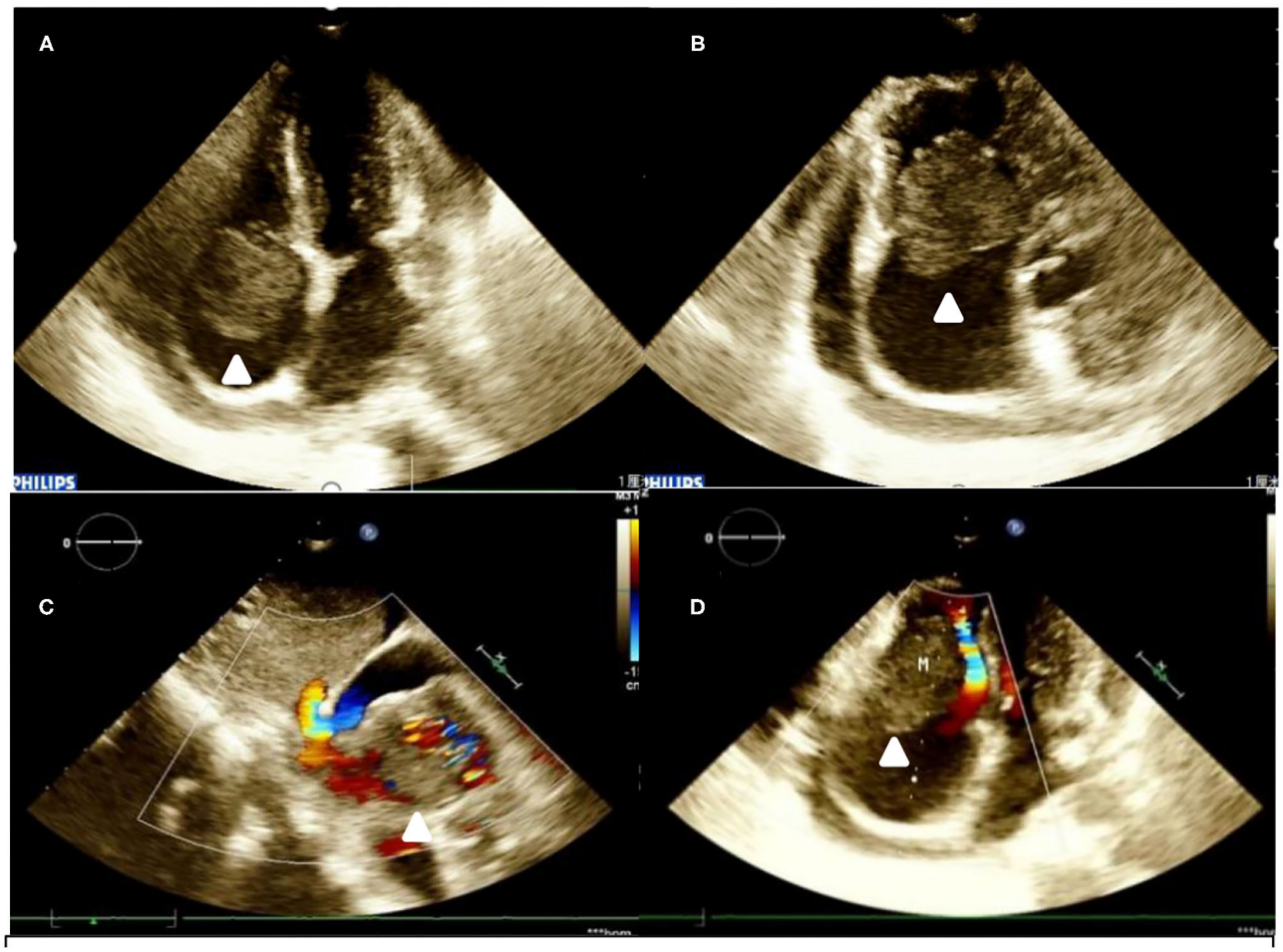


**FIGURE 1 |** Transthoracic echocardiogram. **(A,B)** A hypoechoic mass is seen at the base of the right atrium lateral wall. It is highly mobile and oscillates through the tricuspid valve in diastole. **(C)** Color Doppler flow imaging in subcostal two-chamber view. **(D)** Color Doppler flow imaging in four-chamber view).

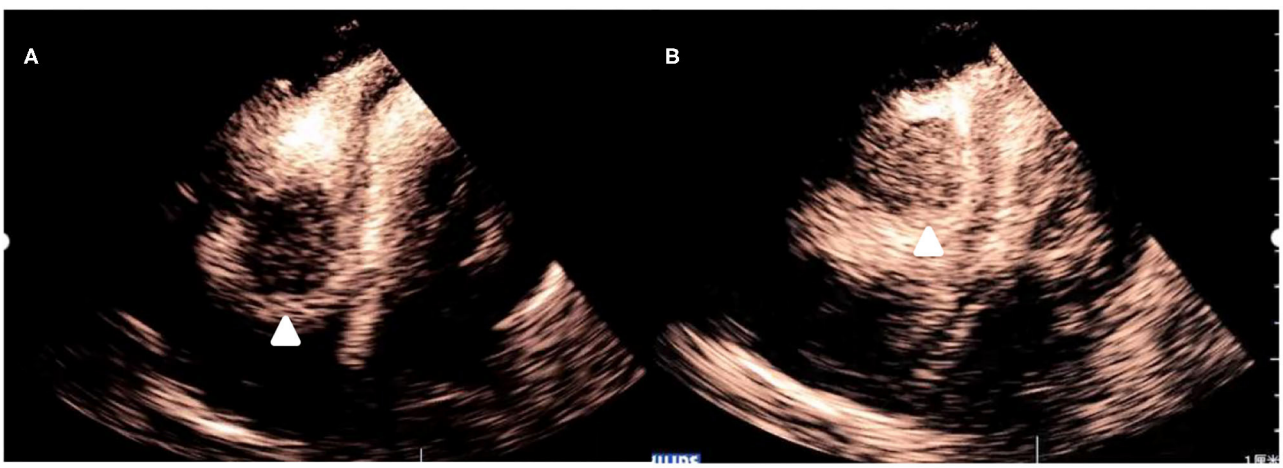


**FIGURE 2 |** Myocardial contrast echocardiography images of the mass. **(A)** After administration of the contrast agent, there is partial enhancement of the mass. **(B)** After several cardiac cycles, there is an increase in enhancement of the mass.

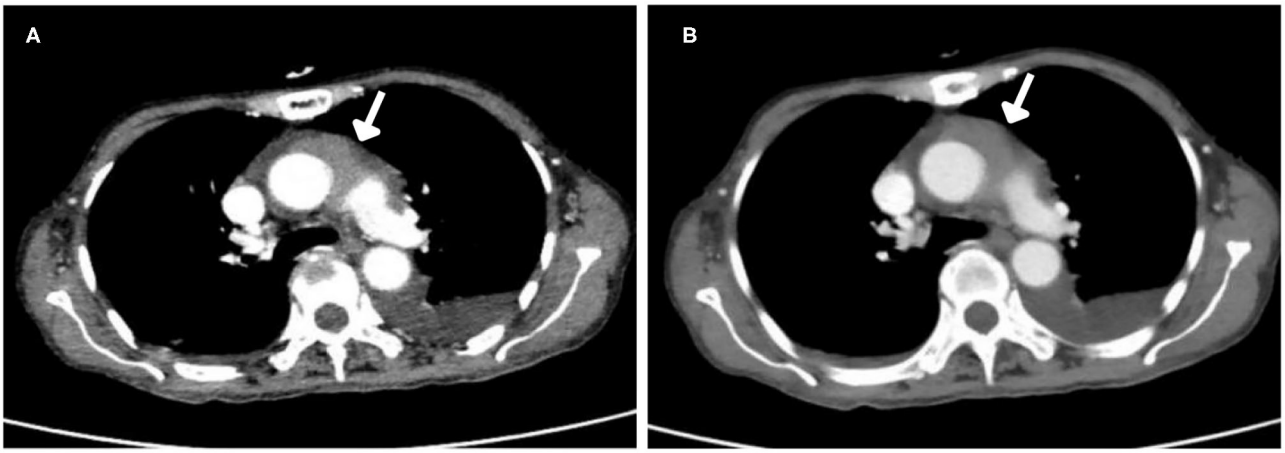


**FIGURE 3 |** Computed tomography (CT) images. **(A)** Arterial phase. The mass was mildly enhanced in the arterial phase. **(B)** Venous phase. The mass enhancement was reduced in the venous phase.

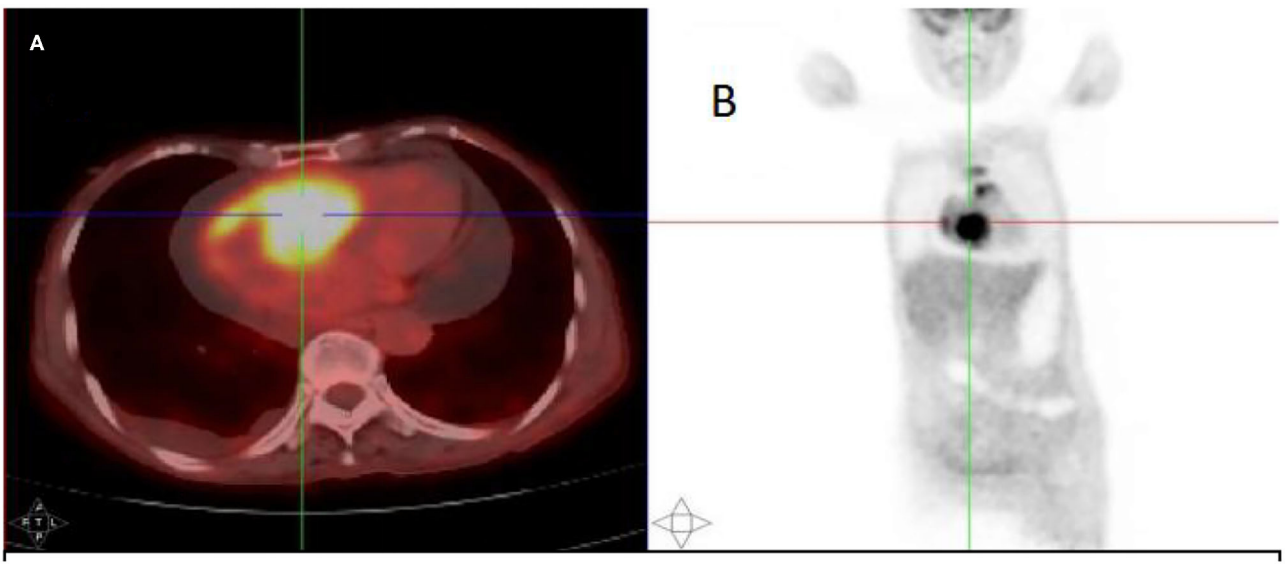


**FIGURE 4 |** The 18F-fluorodeoxyglucose positron emission tomography (PET)/CT scan. **(A)** A mass in the right atrium with high radiotracer uptake. **(B)** Whole-body maximum-intensity projection PET images showed high radiotracer uptake in both the right atrium and aorta-ascending para-aorta.

Coronary angiography is required to exclude coronary artery stenosis in patients being considered for cardiac surgery. Both CT and cardiac MRI are complementary imaging modalities to ECG. The CT scan is also important to show the extent of the lesion in the case of a potential differential diagnosis like renal cell carcinoma with spread *via* the inferior vena cava in the case of myxoma. Additionally, magnetic resonance imaging (MRI) has high spatial resolution and good tissue contrast. Hence, it can clarify the anatomical position relationship of each structure, divide the boundary between the tumor and normal tissue, and judge benign and malignant tumors by their behavioral characteristics, all of which are helpful in guiding the surgical treatment and prognosis evaluation. Although MRI is the gold standard for evaluating the heart's structure and function, ultrasonic cardiography is more convenient to perform and much more reasonably priced. In addition, conventional ECG can evaluate the effect of the mass on cardiac function and morphology. It is also able to identify space-occupying lesions, but it cannot effectively distinguish malignant lesions from benign ones. With the development of ultrasonic techniques, contrast-enhanced ultrasound (CEUS) is found to be capable of effectively and directly identifying the location, shape, and size of space-occupying lesions and discerning their relationship with surrounding tissues. Multi-modality imaging data are very helpful for the diagnosis of cardiac masses and for patient management.

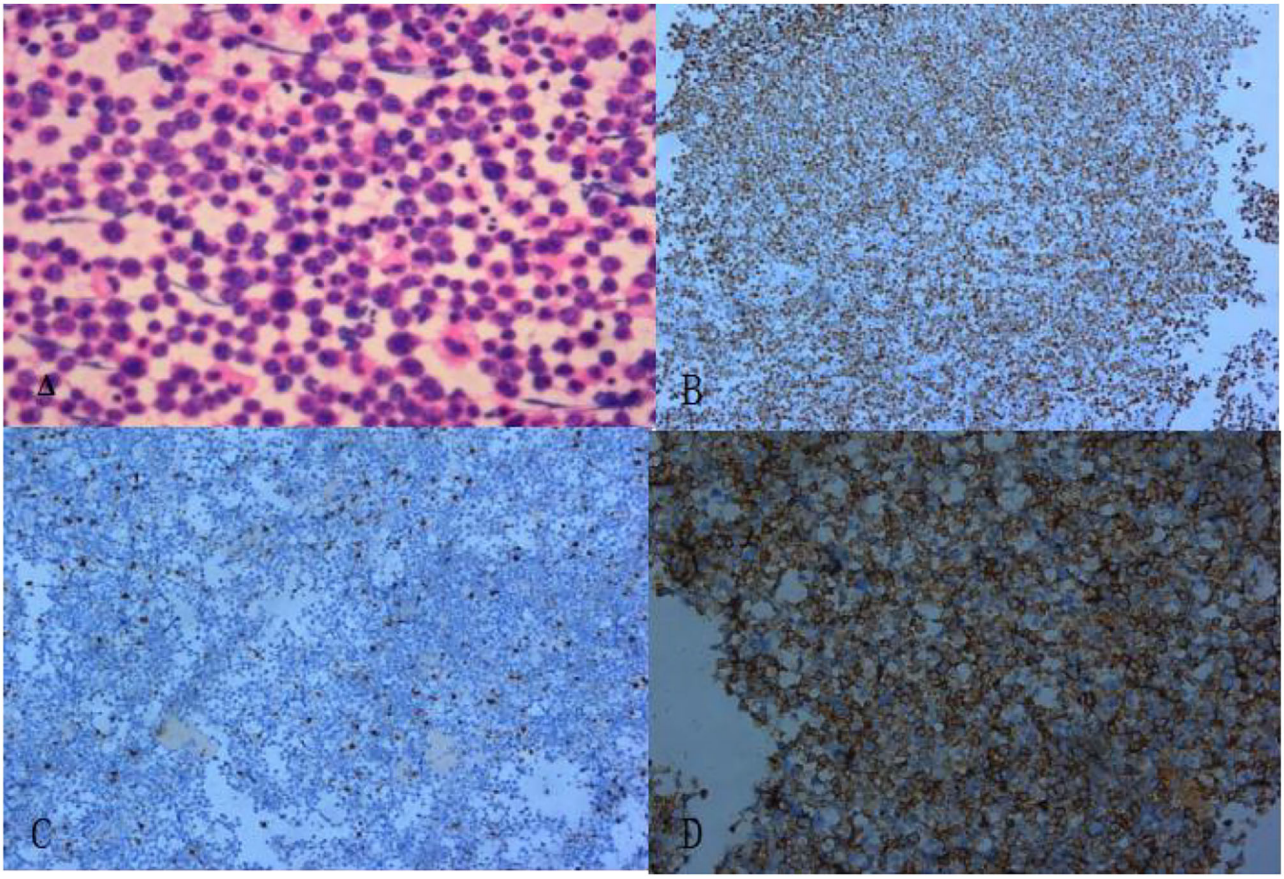


**FIGURE 5 |** The pathological section revealed diffuse enlargement of lymphocytes. **(A)** Hematoxylin and eosin staining (×200). **(B)** Ki-67 markers (+) (×100). **(C)** CD3 markers (–) (×100). **(D)** CD20 markers (+) (×100).

Contrast-enhanced ultrasound is also important for diagnosing cardiac space-occupying lesions. To date, there have been few reports of cardiac lymphoma diagnosed by myocardial contrast ECG. Non-neoplastic heart lesions show no enhancement due to the lack of blood flow. Benign tumors show some sparse enhancement due to poor blood supply. Malignant tumors are rich in newly formed blood vessels. Therefore, they show significant enhancement in medical imaging procedures. Shimizu et al. (7) applied myocardial contrast ECG with 1.5-harmonic imaging to an atrioventricular groove tumor of a patient with malignant lymphoma. Contrast ECG initially showed a single central lesion and some patchy echogenic foci within the tumor, all of which were indicative of arterial components. Subsequently, the tumor was homogenously enhanced, reflecting parenchymal hyperperfusion. Although the initial tumor-enhancement pattern was not observed in the present case, uniform enhancement and high perfusion were present. The mass was misdiagnosed as benign during a traditional ultrasound examination. However, CEUS indicated a malignancy. Thus, the ultrasound enhancement result was more accurate. CEUS can assist in clarifying benign or malignant lesion manifestation and is recommended for application in clinical practice. However, perfusion patterns specific to each tumor have yet to be elucidated (8) and require further exploration in the future.

Detailed collection of non-invasive data and histologic findings suggest an advantage of multi-modality imaging and may ensure more effective management of patients with cardiac tumors.

## DATA AVAILABILITY STATEMENT

The original contributions presented in the study are included in the article/supplementary material, further inquiries can be directed to the corresponding author/s.

## ETHICS STATEMENT

Written informed consent was obtained from the individual(s) for the publication of any

potentially identifiable images or data included in this article.

## AUTHOR CONTRIBUTIONS

XXJ contributed to the conception of the case report. DYY contributed to the manuscript writing. TNW, LLL, and LNG contributed to the clinical data collection. FJL contributed to the pathological diagnos. All authors contributed to the article and approved the submitted version.

## FUNDING

This study was funded by Hainan Provincial Science and Technology Special Fund (ZDYF2019136 and ZDYF2020140).

## REFERENCES

1. Burke A, Tavora F. The 2015 WHO classification of tumors of the heart and pericardium. *J Thorac Oncol.* (2016) 11:441–52. doi: 10.1016/j.jtho.2015.11.009
2. Petrich A, Cho SI, Billett H. Primary cardiac lymphoma: an analysis of presentation, treatment, and outcome patterns. *Cancer.* (2011) 117:581–9. doi: 10.1002/cncr.25444
3. Soon G, Ow GW, Chan HL, Ng SB, Wang S. Primary cardiac diffuse large B-cell lymphoma in immunocompetent patients: clinical, histologic, immunophenotypic, and genotypic features of 3 cases. *Ann Diagn Pathol.* (2016) 24:40–6. doi: 10.1016/j.anndiagpath.2016.05.005
4. Maschio M, Mengarelli A, Zarabla A, Giannarelli D, Maialetti A, Gumenyuk S, et al. Role of pregabalin in treatment of polyneuropathy in multiple myeloma patients: a retrospective study. *Clin Neuropharmacol.* (2019) 42:167–71. doi: 10.1097/WNF.0000000000000360
5. Gyoten T, Doi T, Nagura S, Yamashita A, Fukahara K, Kotoh K, et al. Primary cardiac malignant lymphoma: survival for 13 years after surgical resection and adjuvant chemotherapy. *Ann Thorac Surg.* (2015) 99:1060–2. doi: 10.1016/j.athoracsur.2014.05.074
6. Menguy S, Frison E, Prochazkova-Carlotti M, Dalle S, Dereure O, Boulinguez S, et al. Double-hit or dual expression of MYC and BCL2 in primary cutaneous large B-cell lymphomas. *Mod Pathol.* (2018) 31:1332–42. doi: 10.1038/s41379-018-0041-7
7. Shimizu M, Takahashi H, Tatsumi K. Myocardial contrast echocardiography with 1.5-harmonic imaging in the diagnosis of cardiac malignant lymphoma. *J Am Soc Echocardiogr.* (2005) 18:882. doi: 10.1016/j.echo.2004.09.006
8. Xiachuan Q, Xuebin L, Yongjie W. Case of cardiac hemangioma diagnosed by myocardial contrast echocardiography. *Circ Cardiovasc Imaging.* (2019) 12:e008811. doi: 10.1161/CIRCIMAGING.118.008811

**Conflict of Interest:** The authors declare that the research was conducted in the absence of any commercial or financial relationships that could be construed as a potential conflict of interest.

**Publisher's Note:** All claims expressed in this article are solely those of the authors and do not necessarily represent those of their affiliated organizations, or those of the publisher, the editors and the reviewers. Any product that may be evaluated in this article, or claim that may be made by its manufacturer, is not guaranteed or endorsed by the publisher.

frontiers | Frontiers in Cardiovascular Medicine

CASE REPORT
published: 10 May 2022
doi: 10.3389/fcvm.2022.888825

# Case Report: Giant Congenital Left Atrial Appendage Aneurysm Presenting With Acute Massive Cerebral Infarction and Refractory Atrial Fibrillation: A Case Report and Literature Review

*Rui Li[1], Fei Ma[1], Han Xiong Guan[2], Yue Ying Pan[2], Li Gang Liu[3], Dao Wen Wang[1] and Hong Wang[1]**

*[1] Division of Cardiology, Department of Internal Medicine, Hubei Key Laboratory of Genetics and Molecular Mechanism of Cardiologic Disorders, Tongji Hospital, Tongji Medical College, Huazhong University of Science and Technology, Wuhan, China, [2] Department of Radiology, Tongji Hospital, Tongji Medical College, Huazhong University of Science and Technology, Wuhan, China, [3] Division of Cardiothoracic and Vascular Surgery, Tongji Hospital, Tongji Medical College, Huazhong University of Science and Technology, Wuhan, China*

OPEN ACCESS

**Edited by:**
*Grigorios Korosoglou, GRN Klinik Weinheim, Germany*

**Reviewed by:**
*Sivasankaran Sivasubramonian, Sree Chitra Tirunal Institute for Medical Sciences and Technology (SCTIMST), India*
*Ioannis Drosos, University Hospital Frankfurt, Germany*

***Correspondence:**
*Hong Wang*
*hong_wang1988@126.com*

**Specialty section:**
*This article was submitted to Cardiovascular Imaging, a section of the journal Frontiers in Cardiovascular Medicine*

**Received:** *03 March 2022*
**Accepted:** *11 April 2022*
**Published:** *10 May 2022*

**Citation:**
*Li R, Ma F, Guan HX, Pan YY, Liu LG, Wang DW and Wang H (2022) Case Report: Giant Congenital Left Atrial Appendage Aneurysm Presenting With Acute Massive Cerebral Infarction and Refractory Atrial Fibrillation: A Case Report and Literature Review. Front. Cardiovasc. Med. 9:888825. doi: 10.3389/fcvm.2022.888825*

**Background:** Congenital left atrial appendage aneurysm (LAAA) is a rare cardiac anomaly with a variety of presentations, from being asymptomatic to potentially serious complications such as systemic thromboembolism and atrial tachyarrhythmia.

**Case Presentation:** We report a case of congenital giant LAAA in a 35-year-old man presenting with acute massive cerebral infarction and atrial fibrillation (AF) with rapid ventricular rate. The AF was refractory to conventional antiarrhythmic agents, such as amiodarone and electrical cardioversion, but restored and maintained sinus rhythm after surgical resection of LAAA. The patient remained free of events and was in sinus rhythm during half-year follow-up.

**Conclusion:** Giant LAAA has the potential causing serious complications and should be managed surgically in most cases.

**Keywords: left atrial appendage aneurysm, echocardiography, atrial fibrillation, acute cerebral infarction, case report**

## INTRODUCTION

Left atrial appendage aneurysm (LAAA) is a rare entity that can be congenital or acquired in etiology (1, 2). Congenital LAAAs are caused by dysplasia of pectinate muscles in the appendage (3). A lot of LAAAs were asymptomatic and were discovered incidentally during echocardiographic exams (4, 5). Others developed symptoms or signs after the second to third decade of life,

**Abbreviations:** LAA, left atrial appendage; LAAA, left atrial appendage aneurysm; TTE, transthoracic echocardiography; TEE, transesophageal echocardiography; CEUS, contrast-enhanced ultrasound; CT, computed tomography; MRI, magnetic resonance imaging; AF, atrial fibrillation; AO, aorta; LA, left atrium; LV, left ventricle; RA, right atrium; RV, right ventricle; SVT, supraventricular tachycardia; ECG, electrocardiogram.

such as palpitations, chest pain, dyspnea on exertion, and atrial tachyarrhythmia (6–9). A small percentage of patients were diagnosed after complications, mainly systemic thromboembolism (10–14). Surgical resection is the recommended standard therapy in the literature although some reports suggested the conservative management with clinical monitoring as an optional strategy in some asymptomatic patients (13, 15, 16). Herein, we present a case of a giant LAAA in a 35-year-old man who presented with acute massive cerebral infarction and refractory atrial fibrillation (AF) with rapid heart rate. Of interest, sinus rhythm was restored after LAAA resection.

## CASE PRESENTATION

A 35-year-old man who had no previous medical history and cardiac history suddenly lost consciousness and was referred to our hospital 10 h after the onset of the stroke. At the time of admission, his coma was rated 7 on the Glasgow Coma Scale (GCS), and he displayed left-sided hemiplegia. He had sinus rhythm with paroxysmal AF (**Figure 1A**) and normal blood pressure (111/68 mmHg). Computed tomography (CT) revealed massive cerebral infarction in the right-sided frontotemporal insula (**Figure 2A**) and the basal ganglia area with the right middle cerebral artery thrombus (**Figure 2B**). Due to the massive infarction, he was referred to a neurosurgeon who performed decompressive craniectomy (DC) plus temporalis muscle attachment treatment at 26 h after admission. The patient's mental status improved and became clear 10 days postoperatively, although he was still having left hemiplegia and aphasia. Thereafter, he was experiencing paroxysmal atrial tachycardia with mild ST-segment elevation in leads V2–V5 (**Figure 1B**). On day 16, the patient was then referred to the cardiology department for further cardiac evaluation.

The chest x-ray revealed a greatly enlarged left border of the heart (**Figure 2C**). Transthoracic echocardiography (TTE) (Vivid E9; GE Healthcare, Norway) revealed a giant echo-free cystic structure adjacent to the posterolateral wall of the left ventricle (LV) and compressed the anterolateral LV wall during the entire cardiac cycle (**Figure 2D**). The apical 4-chamber views with color Doppler demonstrated that this cavity was probably related to and communicated with the left atrium (LA) *via* a broad neck (**Figure 2E**). Contrast-enhanced echocardiography was performed then, which showed that the contrast agent filled the LA and the cystic structure was simultaneously with no filling defect (**Figure 2F**). Further transesophageal echocardiography (TEE) confirmed that the enlarged cavity measuring 9.3 cm × 5.7 cm was arising from the LA and communicating with the LA through a 2.6 cm-wide orifice, with a big chicken-wing morphology and with intense spontaneous echo contrast but no obvious thrombi (**Figures 2G,H**). To-and-fro blood flows through the orifice were detected by color Doppler image (**Figure 2I**). There were no other cardiac anomalies, and congenital LAAA was diagnosed. Computed tomography (CT) confirmed the echocardiographic findings and showed a giant LAAA measuring 9.3 cm × 6.4 cm × 3.8 cm that was compressing the LV wall (**Figures 2J,K**).

On day 17, the patient was frequently experiencing attacks of atrial tachycardia with a very rapid ventricular rate of 200–240 beats/min (**Figure 1C**) and reduced blood pressure to 80–90/50–60 mmHg. The AF was refractory to conventional antiarrhythmic agents such as amiodarone. Standard biphasic electrical cardioversion was performed several times, which could not convert AF but only maintain sinus rhythm for a short time. Intravenous injections of beta-blocker continuously and cedilanid intermittently were applied to slow the heart rate. Given the potential risk of thromboembolic events and the refractory AF with rapid heart rate causing hemodynamic instability, prompt surgical resection of LAAA was considered. Due to the high bleeding risk of the patient, anticoagulation therapy was not performed by oral anticoagulants but by using low molecular weight heparin, after the electrical cardioversion.

The patient was then referred to the cardiothoracic surgery department the next day. He underwent LAAA resection through median sternotomy aided by cardiopulmonary bypass on day 37. A huge LAAA measuring about 9.5 cm in long axis was visualized with intact pericardium during the operation (**Figures 3A,B**). There was no thrombus inside the cavity of the aneurysm (**Figure 3B**). Histopathology examination revealed focal chronic inflammation with myocardial atrophy and degeneration and increased interstitial fibrosis, which are typical histological features of LAAA (**Figures 3C,D**).

The patient had an uneventful postoperative course. Interestingly, the sinus rhythm was restored and maintained since LAAA resection. He was discharged home in sinus rhythm 6 days post LAAA resection. Antiarrhythmic agents were not used after resection, and the anticoagulation agents were discontinued 1 month later after discharge. At 6-month follow-up, he was still in sinus rhythm (**Figure 1D**) and free of adverse events. **Table 1** summarizes the clinical presentation and management of the patient.

## DISCUSSION

Left atrial appendage aneurysm is a rare abnormality characterized by either local or diffuse outpouching and enlargement of the left atrial appendage (17), which is generally considered to be either congenital or acquired as a result of mitral valve disease or syphilitic myocarditis (18). Herein, we report on a rare congenital giant LAAA, causing acute cerebral infection and refractory AF. Due to the unusual initial presentation of the patient, prompt diagnosis and proper management were challenging and required interdisciplinary considerations.

Congenital LAAA was firstly described in two children by Dr. Parmley in 1962 (19). Most studies about LAAA are individual case reports (4, 8, 13), and to date, about 150 cases of this defect have been reported in the literature (7, 10, 20). Although this disease is rare, its consequences are potentially hazardous and late diagnosis is common. In addition, no widely accepted consensus exists in regard to the management of this entity.

The presentation of LAAA was greatly variable. About one-third of LAAA was discovered incidentally during the echocardiographic exam and was asymptomatic at the time

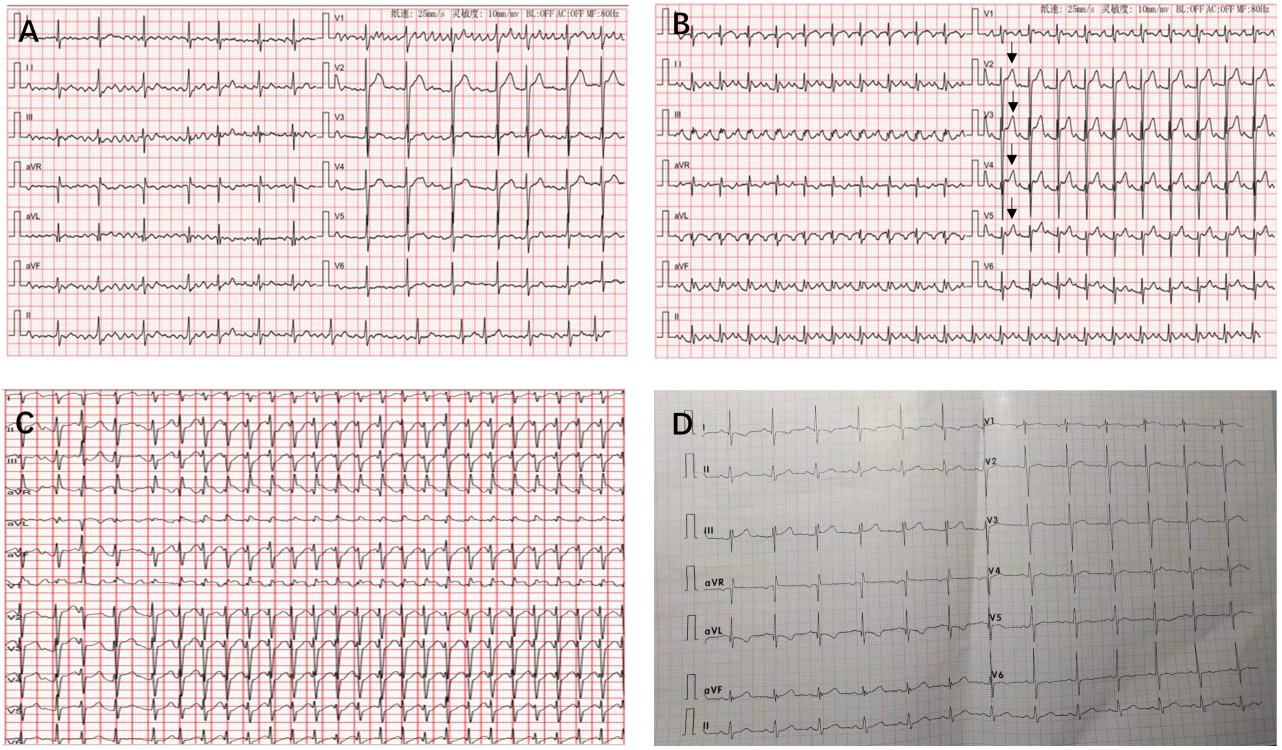


**FIGURE 1 |** Twelve-lead electrocardiograms revealing atrial fibrillation **(A)**, atrial flutter with mild ST-segment elevation in leads V2–V5 (arrows) **(B)**, atrial tachycardia with a rapid ventricular rate of 238 beats/min was recorded when he was experiencing attacks of atrial tachycardia **(C)**, and sinus rhythm at 6-month follow-up **(D)**.

of diagnosis (21). Others develop symptoms or signs of the disease in about the third decade of life (13). Some symptoms of this disease may not be related to the heart, so that the diagnosis is challenging in such cases. The most common manifestations are heart palpitations (43%), shortness of breath (22%), heart rhythm disturbances (15%), embolic disorders of cerebral circulation (11%), and chest pain, and discomfort (7%) (8, 22). Cough and hiccups have been described as very rare and atypical presentations (7, 8). Heart rhythm disturbances, mainly supraventricular tachycardia and AF, occur as a result of structural remodeling of the LAA (9, 22). Finally, thromboembolic events may occur as a serious complication of AF and LAA dilatation with subsequent blood stasis and thrombosis of the aneurysmal cavity (10, 23). In the literature, there are a small number of LAAA being diagnosed after thromboembolic events, such as stroke (24).

In our case, the patient presented with cerebral infarction, a thromboembolic complication of LAAA. His cerebral infarction was massive and required decompressive craniectomy, which has not been reported before. Due to the initial neurological presentation, the diagnosis of LAAA in the case was delayed until the patient suffered AF episodes. Moreover, the AF in the patient was with extremely quick heart rate that was refractory to antiarrhythmic agents and electrical cardioversion and causing dropping of blood pressure. Interestingly, during the AF episode, the ST-segment elevation in the precordial leads was recorded. As previously reported, it was likely caused by embolic occlusion of a coronary artery (11) or by external compression of the coronary arteries by LAAA (20, 25, 26). In our case, the compression of the left coronary artery or its divisions was more likely since no elevation of serial myocardial injury biomarkers was recorded.

The following diagnostic criteria for this congenital form have been proposed by Foale et al.: (1) origin from an otherwise normal atrial chamber; (2) well-defined communication with the atrial cavity; (3) location within the pericardium; and (4) distortion of the LV by an aneurysm (10, 27). There are two types of LAAA, extrapericardial and intrapericardial types (18). In extrapericardial type, the LA or LAA is prolated through the pericardial defect and compressed in it, which leads to the aneurysmal expansion of the extrapericardial part of LA. The case we presented and discussed here was intra pericardial type of LAAA.

According to the above criteria, imaging exams are essential tools for diagnosis and precise evaluation of LAAA, which are important for the subsequent treatment (28). Imaging modalities used to diagnose the LAAA include chest x-ray, echocardiography, CT, and magnetic resonance imaging (MRI) (10, 18). Convexity of the LA contour on a chest x-ray should raise the possibility of LAAA and require a differential diagnosis from a pericardial cyst and heart or mediastinal tumors (15, 18). TTE is considered the primary method of diagnosis but with low diagnostic accuracy and sensitivity. TTE usually shows a large saccular echo-free structure laterally to LV. It can, however, hardly in most cases show the connection and communication

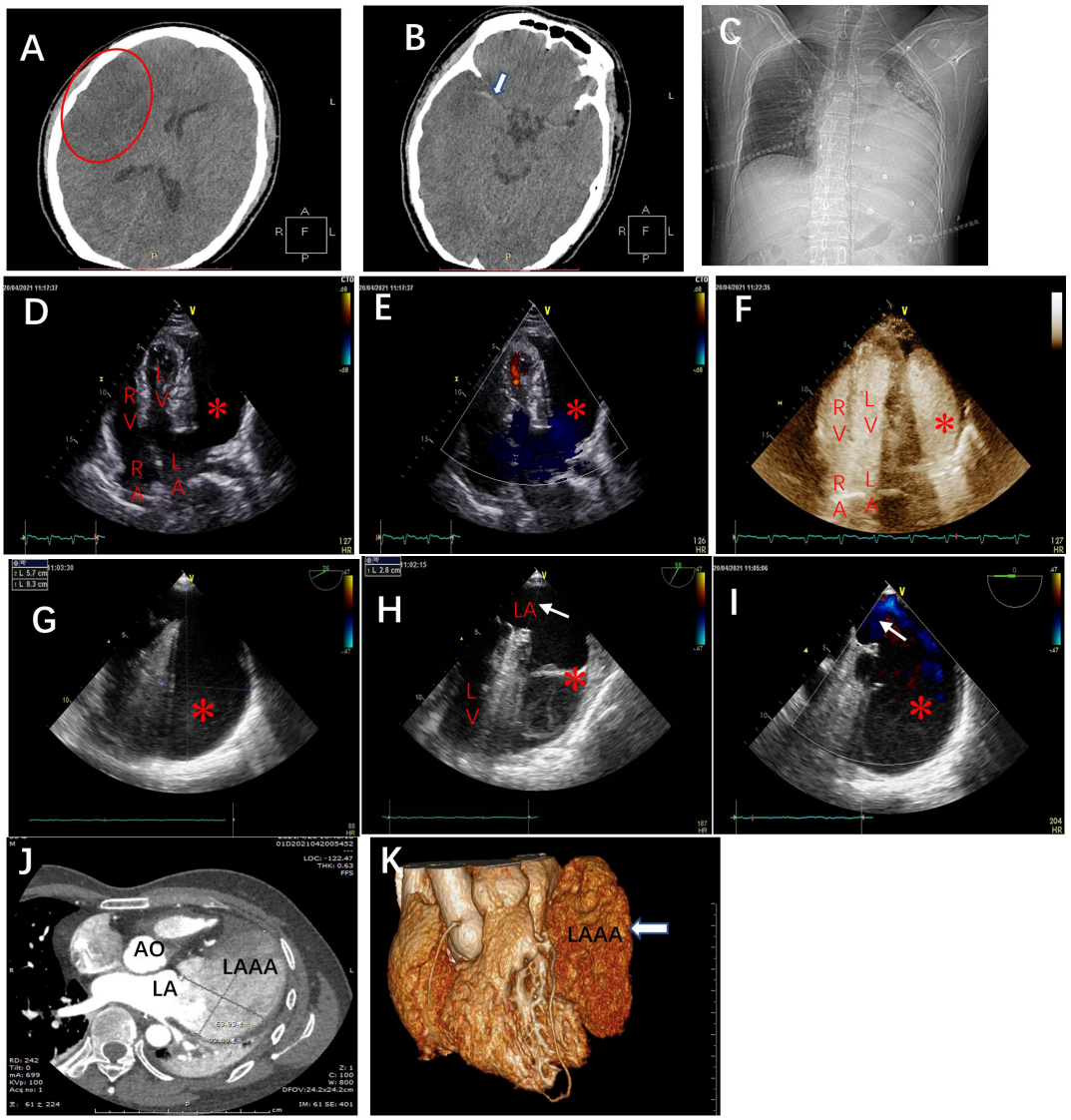


**FIGURE 2 |** The brain computed tomography scans at admission revealed **(A)** massive cerebral infarction in the right-sided frontotemporal insula (red circle) and **(B)** the basal ganglia area with right middle cerebral artery thrombus (white arrow). **(C)** The chest X-ray in the cardiology department demonstrating the abnormal left heart border. Transthoracic echocardiography (TTE), apical four-chamber view **(D)**, and the view with color doppler **(E)** revealing an echo-free cavity (red star) adjacent to and compressing the LV and the probable communication of the cavity with the LA; TTE with contrast showing the contrast filling in the LA and the cavity simultaneously without filling defect in the cavity **(F)**; TEE, the mid-esophageal 2-chamber and LAA view demonstrating a giant cavity (red star) measuring 9.3 cm × 5.7 cm **(G)** and its connection to LA *via* a 2.6 cm-wide orifice (white arrow) **(H)** and the to-and-fro blood flows between LA and the cavity (red star) through the orifice (white arrow) **(I)**. Axial computed tomography scan **(J)** and 3D reconstruction **(K)** demonstrate a 9.3 cm × 6.4 cm × 3.8 cm giant LAAA. AO: aorta; RA: right atrium; LA: left atrium; RV: right ventricle; LV: left ventricle.

between the LA and the echo-free cavity and, therefore, cannot make the definite diagnosis of LAAA in many cases and sometimes make the diagnosis mistakenly as a pericardial cyst or effusion (3, 17). Khaled A. Shams reported a case with aneurysmally dilated LA pushing the heart to the right side, and thus a dextro-posed heart was misdiagnosed as dextro-cardia with rheumatic heart disease and AF for a long time till the disease progressed to cardiogenic shock (29). Contrast-enhanced echocardiography can demonstrate the connection of LA and the cavity, which clearly shows the LAAA border, and more importantly the presence of a thrombus, which is a key element for therapeutic choice (21). TEE can provide clear visualization of the structure and composition of the LAAA and its connection with LA and should be mandatory if the diagnosis is ambiguous after TTE (30). Cardiac CT and MRI can clearly visualize LAAA with similar diagnostic accuracy as TEE. Moreover, they are more advantageous in assessing surrounding structures as probable compression of left coronary arteries and pulmonary veins. In most cases and in our case, LAAA was initially diagnosed by contrast-enhanced echocardiography

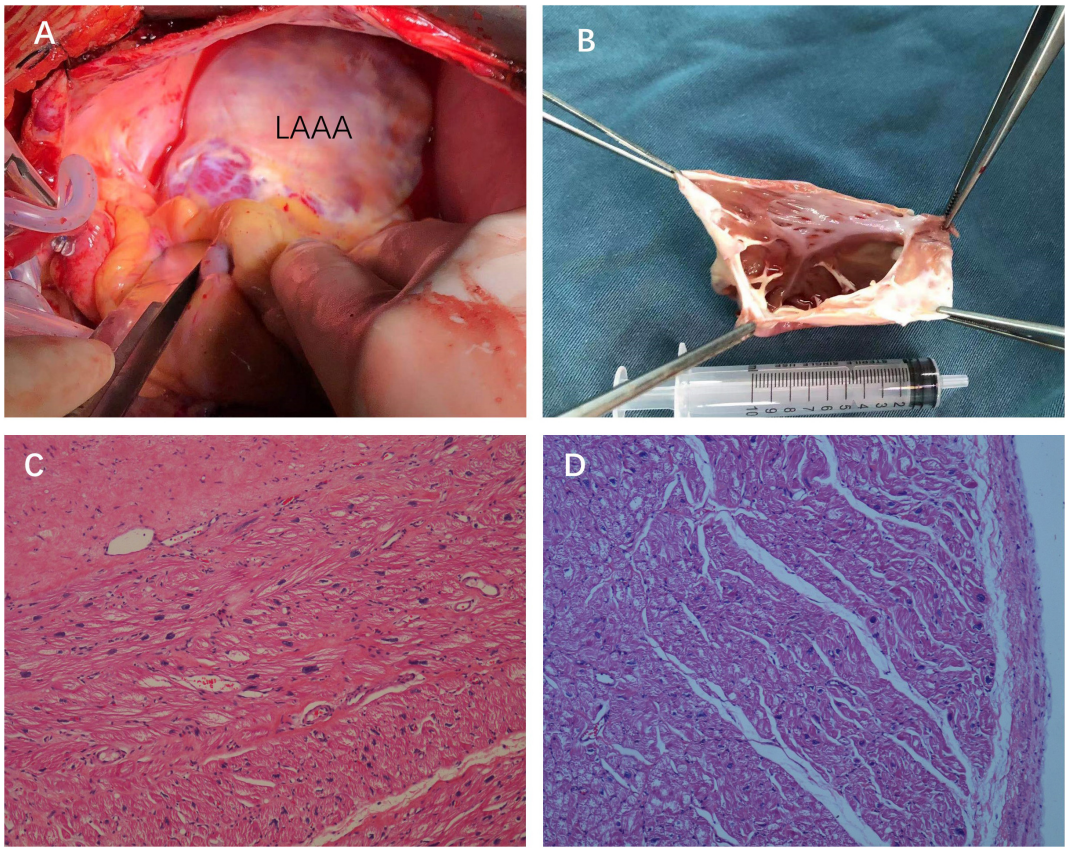


**FIGURE 3 |** Intraoperative views **(A)** and the surgical specimen of the LAAA with no thrombus inside the cavity of the aneurysm **(B)**. Hematoxylin and eosin staining of the resected left atrial appendage tissues showing the wall of the aneurysm composed of the myocardium and fibrotic tissue [**(C,D)**, 2007×].

and TEE and was further confirmed by cardiac CT or MRI (18, 21).

The early surgical intervention seems to be the standard of treatment once the diagnosis is established in the current literature, even in asymptomatic cases, aimed to prevent the occurrence of serious complications (10, 31). However, some reports suggested conservative management without or with delayed surgical treatment, which may be an option for patients with no or mild symptoms (13, 15). Because of the rarity of this entity, a direct comparison of medical treatments such as anticoagulation and antiarrhythmic therapies with surgical intervention is not available in the current literature. Thus, if conservative management was chosen, the patient should be closely monitored and anticoagulants may be considered (13, 15).

The recommendation of surgical occlusion in symptomatic patients is based on non-randomized or observational cohort studies (32) as it can prevent thromboembolic complications and atrial arrhythmias associated with the LA enlargement. Transcatheter device occlusion (33) has also been reported for the occlusion of narrow neck LAAs with a high rate of success (34). Available data in small studies suggest that LAA closure using LARIAT epicardial suture is a good alternative for stroke risk reduction (35). However, the incidence of major complications such as perforation of the left atrial appendage, pleural effusion, and thrombosis is also high, and more data regarding device safety and efficacy are needed (36). Moreover, due to the size limitations of currently available occluders, usually not larger than 33 mm, there is no report of device occlusion in really giant LAA by far (37).

**TABLE 1 |** Timeline of events.

| Days (d) | • Events |
|---|---|
| D1 | • Lost consciousness and referred to our hospital 10 h later, left-sided hemiplegia. |
| | • GLS 7, AF, normal blood pressure |
| | • Head CT revealed massive cerebral infarction and right middle cerebral artery thrombus referred to neurosurgery |
| D2 | • Decompressive craniectomy (DC) |
| D16 | • AF, transferred to cardiology |
| | • Chest x-ray, TTE, TEE, Contrast-enhanced echocardiography, Coronary CT angiography clarified the diagnosis of left atrial appendage aneurysm |
| D17 | • Frequently attacks of atrial tachycardia, refractory to conventional antiarrhythmic agents and electrical cardioversion |
| D18 | • Transferred to cardiothoracic surgical ward |
| D37 | • LAAA resection |
| D43 | • Discharged from hospital |

Various successful approaches to aneurysmectomy with or without cardiopulmonary bypass have been described, such as median sternotomy, left thoracotomy, mini-thoracotomy, and endoscopy (1, 38). Recently, catheter closure of a giant LAAA was reported, providing a novel non-invasive approach to treating LAAA (3). Removal of the aneurysm usually results in complete resolution of atrial arrhythmias as seen in previous reports (20, 39), although a concomitant full maze procedure was suggested in another study of LAAA with chronic AF. However, concomitant AF surgery may increase the risk of requiring a permanent pacemaker (40). In our case, considering the large size of LAAA, resection *via* median sternotomy and cardiopulmonary bypass was used. A full maze procedure was not adopted in the patient, but sinus rhythm was restored right after the operation and maintained as of the time of writing.

In our opinion, surgical intervention should be taken in symptomatic LAAA or in secondary prevention of thromboembolic events. In asymptomatic cases or in primary prevention, risk stratification for thromboembolic events is the key for the choice of management strategies. The early surgical intervention should be taken in cases with a high risk of thromboembolic events. However, in addition to spontaneous echo contrast and thrombi in the aneurysm, no other reliable indicators can predict embolic complications (21). A study suggested that the presence of AF/flutter was the only predictor of thrombus formation and embolic events (10). Whether the size, orifice, and morphology of LAAA can predict embolic events need to be studied in the future.

## LIMITATIONS

This is only a case report with a literature review, and such a study has inherent limitations and may not be able to provide the true perspective of the disease. Again, the LAAA is a very rare disease and a case series study is hard to perform in the real world. Also, this study does not allow us to establish a cause–effect relationship between LAAA and massive cerebral infarction.

## CONCLUSION

We described here a unique case with a giant LAAA that presented with acute massive cerebral infarction and refractory AF with very rapid heart rate, which has never been described before in the literature. LAAA was detected initially by TTE and thereafter confirmed by contrast-enhanced echocardiography and TEE. Surgical resection was performed promptly after frequently occurring AF with rapid heart rate, and the patient had favorable outcome. Giant LAAA has a high risk of causing significant morbidity as in our case and should be managed by surgical intervention in most cases.

## DATA AVAILABILITY STATEMENT

The original contributions presented in the study are included in the article/supplementary material, further inquiries can be directed to the corresponding author.

## ETHICS STATEMENT

Written informed consent was obtained from the individual(s) for the publication of any potentially identifiable images or data included in this article.

## AUTHOR CONTRIBUTIONS

RL wrote the report, performed the literature research, and took the pictures. RL and FM performed echocardiography, including TEE and contrast-enhanced echocardiography. LL performed surgery. HG and YP provided CT images. HW revised the report and performed the literature research. DW reviewed the manuscript. All authors read and approved the final manuscript.

## FUNDING

This work was supported by grants from the National Natural Science Foundation of China (81770793).

## ACKNOWLEDGMENTS

We thank the patients, the nurses, and clinical staff who are providing care for the patient.

## REFERENCES

1. Victor S, Nayak VM. Aneurysm of the left atrial appendage. *Tex Heart Inst J.* (2001) 28:111–8.
2. Pomerantzeff PM, Freyre HM, de Almeida Brandao CM, Pereira Barreto AC, Almeida de Oliveira S. Aneurysm of the left atrial appendage. *Ann Thorac Surg.* (2002) 73:1981–3. doi: 10.1016/s0003-4975(02)03408-2
3. Kothandam S, Ramasamy R. Planning and execution of catheter closure of a giant left atrial appendage aneurysm causing recurrent cardioembolism. *Ann Pediatr Cardiol.* (2020) 13:353–6. doi: 10.4103/apc.APC_76_20
4. Yakut K, Varan B, Erdogan I. Asymptomatic giant congenital left atrial aneurysm. *Turk J Pediatr.* (2019) 61:117–9. doi: 10.24953/turkjped.2019.01.019
5. Veiga VC, Rojas SS, Silva Junior A, Patricio ML, Marum EC, Abensur H. Left atrial appendage aneurysm: echocardiographic diagnostic. *Arq Bras Cardiol.* (2008) 90:e36–8. doi: 10.1590/s0066-782x2008000500014
6. Gan GC, Bhat A, Desai H, Eshoo S. Cardiac vignette: giant left atrial appendage aneurysm. *Heart Lung Circ.* (2015) 24:e81–5. doi: 10.1016/j.hlc.2015.02.005
7. Asfalou I, Boumaaz M, Raissouni M, Sabry M, Benyass A, Zbir EM. Huge left atrial appendage aneurysm revealed by chronic hiccups. *J Saudi Heart Assoc.* (2017) 29:293–6. doi: 10.1016/j.jsha.2017.03.009
8. Bamous M, Aithoussa M, Abetti A, Boulahya A. Congenital left atrial appendage aneurysm: atypical presentation. *Ann Pediatr Cardiol.* (2017) 10:293–4. doi: 10.4103/apc.APC_4_17
9. Morin J, Cantin L, Pasian S, Philippon F, Beaudoin J. Giant left atrial appendage aneurysm mimicking mediastinal mass and associated with

incessant atrial arrhythmias. *J Atr Fibrillation.* (2017) 9:1539. doi: 10.4022/jafib.1539
10. Aryal MR, Hakim FA, Ghimire S, Giri S, Pandit A, Bhandari Y, et al. Left atrial appendage aneurysm: a systematic review of 82 cases. *Echocardiography.* (2014) 31:1312–8. doi: 10.1111/echo.12667
11. Chowdhury UK, Seth S, Govindappa R, Jagia P, Malhotra P. Congenital left atrial appendage aneurysm: a case report and brief review of literature. *Heart Lung Circ.* (2009) 18:412–6. doi: 10.1016/j.hlc.2008.10.015
12. Nakai Y, Asano M, Nomura N, Mishima A. Surgical management of an aneurysm of the left atrial appendage to prevent potential sequelae. *Interact Cardiovasc Thorac Surg.* (2013) 17:586–7. doi: 10.1093/icvts/ivt252
13. Chen Y, Mou Y, Jiang LJ, Hu SJ. Congenital giant left atrial appendage aneurysm: a case report. *J Cardiothorac Surg.* (2017) 12:15. doi: 10.1186/s13019-017-0576-6
14. Tidake A, Gangurde P, Mahajan A. Congenital left atrial appendage aneurysm associated with a systemic embolism. *Cardiol Young.* (2015) 25:597–9. doi: 10.1017/S1047951114000857
15. Valentino MA, Al Danaf J, Morris R, Tecce MA. Giant left atrial appendage aneurysm: a case of mistaken identity. *J Cardiol Cases.* (2017) 15:129–31. doi: 10.1016/j.jccase.2016.12.010
16. Plonska-Gosciniak E, Larysz B, Jurczyk K, Kasprzak JD. Five-chambered heart: a 20-year story of left atrial appendage aneurysm. *Eur Heart J.* (2009) 30:1014. doi: 10.1093/eurheartj/ehn613
17. Wang HQ, Zhang Z, Yang H, Wu S, Fu YH, Song ZM, et al. A huge congenital left atrial appendage aneurysm. *Chin Med J (Engl).* (2017) 130:3011–2. doi: 10.4103/0366-6999.220301
18. Wang B, Li H, Zhang L, He L, Zhang J, Liu C, et al. Congenital left atrial appendage aneurysm: a rare case report and literature review. *Medicine (Baltimore).* (2018) 97:e9344. doi: 10.1097/MD.0000000000009344
19. Parmley LF Jr. Congenital atriomegaly. *Circulation.* (1962) 25:553–8. doi: 10.1161/01.cir.25.3.553
20. Belov DV, Moskalev VI, Garbuzenko DV, Arefyev NO. Left atrial appendage aneurysm: a case report. *World J Clin Cases.* (2020) 8:4443–9. doi: 10.12998/wjcc.v8.i19.4443
21. Yanli Z, Xiaocong W, Liping P, Yan M, Wei Y, Shu J. Diagnosis of a giant left atrial appendage aneurysm by contrast-enhanced echocardiography: case report and literature review. *J Clin Ultrasound.* (2021) 49:293–7. doi: 10.1002/jcu.22962
22. Harland DR, Suma V, Muthukumar L, Port SC, Werner PH, Tajik AJ. Giant congenital left atrial appendage aneurysm presenting with recurrent supraventricular tachycardia and chest pain. *CASE (Phila).* (2019) 3:129–32. doi: 10.1016/j.case.2019.01.003
23. Jiang B, Wang X, Liu F, Song L. Left atrial appendage aneurysm. *Interact Cardiovasc Thorac Surg.* (2020) 30:495–6. doi: 10.1093/icvts/ivz283
24. Itaya H, Aoki C, Hatanaka R, Fukuda I. Resection of left atrial appendage aneurysm and full maze procedure as curative management for stroke recurrence. *Gen Thorac Cardiovasc Surg.* (2020) 68:295–7. doi: 10.1007/s11748-018-1048-1
25. Tandon R, Arisha MJ, Nanda NC, Kumar S, Wander GS, Srialluri S, et al. Incremental benefit of three-dimensional transthoracic echocardiography in the assessment of left atrial appendage aneurysm leading to severe extrinsic compression of a coronary artery. *Echocardiography.* (2018) 35:685–91. doi: 10.1111/echo.13901
26. Wagdy K, Samaan A, Romeih S, Simry W, Afifi A, Hassan M. Giant left atrial appendage aneurysm compressing the left anterior descending coronary artery. *Echocardiography.* (2016) 33:1790–2. doi: 10.1111/echo.13296
27. Foale RA, Gibson TC, Guyer DE, Gillam L, King ME, Weyman AE. Congenital aneurysms of the left atrium: recognition by cross-sectional echocardiography. *Circulation.* (1982) 66:1065–9. doi: 10.1161/01.cir.66.5.1065
28. Brenneman DJ, Pitkin AD, Gupta D, Bleiweis MS, Reyes KM, Chandran A. Left atrial appendage aneurysm characterized by multimodal imaging. *World J Pediatr Congenit Heart Surg.* (2020) 11:N161–3. doi: 10.1177/2150135118769327
29. Shams KA. When the left atrium becomes a monster: a case report. *Eur Heart J Case Rep.* (2020) 4:1–4. doi: 10.1093/ehjcr/ytaa128
30. Agmon Y, Khandheria BK, Gentile F, Seward JB. Echocardiographic assessment of the left atrial appendage. *J Am Coll Cardiol.* (1999) 34:1867–77. doi: 10.1016/s0735-1097(99)00472-6
31. Hui C, Luo S, An Q. Giant congenital left atrial appendage aneurysm. *Cardiol Young.* (2017) 27:577–9. doi: 10.1017/S1047951116002791
32. Kanderian AS, Gillinov AM, Pettersson GB, Blackstone E, Klein AL. Success of surgical left atrial appendage closure: assessment by transesophageal echocardiography. *J Am Coll Cardiol.* (2008) 52:924–9. doi: 10.1016/j.jacc.2008.03.067
33. Sick PB, Schuler G, Hauptmann KE, Grube E, Yakubov S, Turi ZG, et al. Initial worldwide experience with the WATCHMAN left atrial appendage system for stroke prevention in atrial fibrillation. *J Am Coll Cardiol.* (2007) 49:1490–5. doi: 10.1016/j.jacc.2007.02.035
34. Reddy VY, Doshi SK, Kar S, Gibson DN, Price MJ, Huber K, et al. 5-year outcomes after left atrial appendage closure: from the PREVAIL and PROTECT AF trials. *J Am Coll Cardiol.* (2017) 70:2964–75. doi: 10.1016/j.jacc.2017.10.021
35. Musat D, Mittal S. LARIAT trial updates. *J Atr Fibrillation.* (2018) 11:1806. doi: 10.4022/jafib.1806
36. Chatterjee S, Herrmann HC, Wilensky RL, Hirshfeld J, McCormick D, Frankel DS, et al. Safety and procedural success of left atrial appendage exclusion with the lariat device: a systematic review of published reports and analytic review of the FDA MAUDE database. *JAMA Intern Med.* (2015) 175:1104–9. doi: 10.1001/jamainternmed.2015.1513
37. Evangeliou AP, Sotiroglou E, Charitakis N, Loufopoulos G, Varassas C, Papadopoulos S, et al. An asymptomatic patient with an additional cardiac chamber giant left atrial appendage. *Case Rep Cardiol.* (2020) 2020:6519089. doi: 10.1155/2020/6519089
38. Ruttkay T, Scheid M, Gotte J, Doll N. Endoscopic resection of a giant left atrial appendage. *Innovations (Phila).* (2015) 10:282–4. doi: 10.1097/IMI.0000000000000172
39. Burke RP, Mark JB, Collins JJ Jr, Cohn LH. Improved surgical approach to left atrial appendage aneurysm. *J Card Surg.* (1992) 7:104–7. doi: 10.1111/j.1540-8191.1992.tb00786.x
40. Huffman MD, Karmali KN, Berendsen MA, Andrei AC, Kruse J, McCarthy PM, et al. Concomitant atrial fibrillation surgery for people undergoing cardiac surgery. *Cochrane Database Syst Rev.* (2016) 2016:CD011814. doi: 10.1002/14651858.CD011814.pub2

**Conflict of Interest:** The authors declare that the research was conducted in the absence of any commercial or financial relationships that could be construed as a potential conflict of interest.

frontiers | Frontiers in Cardiovascular Medicine

CASE REPORT
published: 13 May 2022
doi: 10.3389/fcvm.2022.893355

# Case Report: Two Cases of Watershed Phenomenon in Mechanical Circulatory Support Devices: Computed Tomography Angiography Imaging and Literature Review

*Guiying Du, Jiwang Zhang, Junbo Liu and Lijuan Fan**

*Department of Radiology, TEDA International Cardiovascular Hospital, Tianjin, China*

Mechanical circulatory support (MCS) has become a processing technique used in end-stage heart failure (ESHF) because it can significantly improve survival and quality of life in patients with ESHF as either a transitional support therapy or a permanent replacement therapy before heart transplant. However, various potential complications associated with MCS need to be considered, especially aortic root thrombus formation. It's critical to have an appropriate diagnosis of aortic root thrombus and "watershed" because the prognosis and treatment are different. Both "watershed" and aortic root thrombus formation can be characterized by computed tomography angiography. The CT manifestations of two patients who had MCS device implantation in our hospital (one with intra-aortic balloon pumps + extracorporeal membrane oxygenators, the other with left ventricular assist devices) were reported, and a literature review that recognized of "watershed" phenomenon in the aortic root was conducted.

**Keywords: left ventricular assist devices, extracorporeal membrane oxygenators, case report, computed tomography angiography, watershed phenomeno, aortic root thrombus formation**

OPEN ACCESS

***Edited by:***
*Ana Teresa Timoteo,*
*Hospital de Santa Marta, Portugal*

***Reviewed by:***
*Hiroyuki Kamiya,*
*Asahikawa Medical University, Japan*
*Valeria Pergola,*
*University Hospital of Padua, Italy*

****Correspondence:***
*Lijuan Fan*
*lijuanfan111@sina.com*

***Specialty section:***
*This article was submitted to Cardiovascular Imaging, a section of the journal Frontiers in Cardiovascular Medicine*

***Received:*** *10 March 2022*
***Accepted:*** *26 April 2022*
***Published:*** *13 May 2022*

***Citation:***
*Du G, Zhang J, Liu J and Fan L (2022) Case Report: Two Cases of Watershed Phenomenon in Mechanical Circulatory Support Devices: Computed Tomography Angiography Imaging and Literature Review. Front. Cardiovasc. Med. 9:893355. doi: 10.3389/fcvm.2022.893355*

## INTRODUCTION

There are an increasing number of therapies available for people with end-stage heart failure, particularly in the form of Mechanical circulatory support (MCS). It is intended to be used as a bridge to cardiac transplantation for patients with severe, refractory heart failure who have failed medical treatment (1). MCS devices such as intra-aortic balloon pumps (IABP), extracorporeal membrane oxygenators (ECMO), and left ventricular assist devices (LVAD) are commonly employed (1, 2).

For all this, various potential complications associated with MCS need to be taken into consideration, especially aortic root thrombus formation. Aortic root thrombosis is a rare complication that was recently recognized in continuous-flow left ventricular assist device therapy and is associated with significant mortality in MCS patients (3, 4). It can lead to serious consequences such as stroke, acute myocardial infarction, and even death (4). The "watershed," also known as the "mixing zone" or "mixing cloud," has been reported in ECMO implantation and

is the specific location where the left ventricle cardiac output and ECMO flow mix. It is typically located along the ascending aorta (AAO), depending on the balance between the left ventricle cardiac output and the ECMO flow (5, 6). In clinical practice, an accurate diagnosis of aortic root thrombosis and "watershed" is essential because the prognosis and therapy are diverse. Both the "watershed" and the aortic root thrombus formation can be characterized by computed tomography angiography (CTA; 7–9). The CTA of two patients who had mechanical circulatory assist device implantation in our institution (one with IABP + ECMO, the other with LVAD) was evaluated. The two cases where the arc-shaped low-attenuation filling defect disappeared with the change of position represent a "watershed" phenomenon that can be seen in AAO.

## CASE PRESENTATION

### Case 1

#### Left Ventricular Assist Devices Implantation

A 56-year-old man with ischemic heart disease and a severely reduced ejection fraction underwent implantation of a "HeartCon" (TICH, Tianjin, China) continuous-flow left ventricular assist device. His medical history also included myocardial infarction, heart failure (NYHA IV), first-degree atrioventricular block, pulmonary arterial hypertension, and coronary artery bypass surgery. The LVAD has augmented the innate cardiac pumping function by creating an artificial blood flow conduit from the left ventricle to the descending aorta (DAO), thereby supplying the systemic circulation and maintaining proper tissue perfusion. The pump speed was 2,400 rpm. The blood pressure was 90/67 mmHg. The CTA was used for follow-up after 6 months of LVAD implantation.

### Case 2

#### Intra-Aortic Balloon Pumps and Extracorporeal Membrane Oxygenators Implantation

A 37-year-old man suffered from acute myocarditis, cardiogenic shock, arrhythmia-bradycardia, third-degree atrioventricular block, and paroxysmal tachycardia. His medical history also included acute liver injury, acute kidney injury, acute respiratory failure, and mixed acid-base balance disorder. The patient's circulatory failure could not be repaired by IABP alone, and the veno-arterial ECMO (VA-ECMO) was implanted to stabilize circulatory collapse according to the indications for the use of cardiopulmonary support. The patient was admitted to the hospital for emergency coronary angiography, but the right coronary artery was not visualized. This examination was to assess the state of the right coronary artery.

## COMPUTED TOMOGRAPHY ANGIOGRAPHY SCANNING

The CTA of the two cases was performed using a prospective ECG-gated sequence in the arterial phase and iterative reconstruction with a 256-slice CT scanner (GE Revolution). Attenuation-based kV assist and automatic mA, as well as the bolus tracking technique, is used in CTA. A region of interest (1 $cm^2$) is commonly positioned in the AAO for tracking the contrast bolus, and the acquisition is started with a 2-s delay after reaching a threshold of 300 HU. A non-ionic iodine contrast agent (Ioversol, Hengrui Jiangsu, China, iodine 350 mg/ml) was injected into an antecubital vein at 5.0 ml/s, followed by a 30 ml saline flush at the same rate. The patient was in the supine position at the first scan and changed to the right lateral decubitus position at the second scan (**Figures 1a,b**).

## COMPUTED TOMOGRAPHY ANGIOGRAPHY IMAGING

### Case 1

In this case, an ECG-gated multidetector CTA showed a filling defect in the root of the aorta and no visualization of the bypass of the right coronary artery when the patient was in the supine position, while the DAO was filling well (**Figure 2A**). After turning the position to the right lateral decubitus position, the arc-shaped low-attenuation filling defect disappeared, and the bypass of the right coronary artery was filled with the contrast agent (**Figure 2B**). Transthoracic conventional echocardiography and two-dimensional spectral Doppler show that the blood flow velocity of the aortic valve was extremely low and there was no thrombus formation in the aortic root (**Figure 2C**).

### Case 2

In this case, the ECG-gated multidetector CT angiography showed a filling defect in the root of the aorta with no visualization of the right coronary artery when the patient was in the supine position, while the DAO was filling well (**Figure 3a**). After turning the patient to the right lateral decubitus position, the arc-shaped low-attenuation filling defect disappeared. In addition, changing the patient's scanning position resulted in the good filling of the right coronary artery that was not filled on scanning in the supine position (**Figure 3b**). Transthoracic conventional echocardiography and two-dimensional spectral Doppler show that the blood flow velocity of the aortic valve was extremely low and there was no thrombus formation in the aortic root (**Figure 3c**).

## FOLLOW-UP AND OUTCOMES

While awaiting a heart transplant, the vital signs of Case 1 have stabilized and his circulatory function has improved.

The patient from Case 2 has healed. The left ventricular ejection fraction has gone back to normal, and the blood circulation has stabilized.

## DISCUSSION

In two of our patients with MCS implantation, there was a low-attenuation filling defect in the aortic root on CTA, which

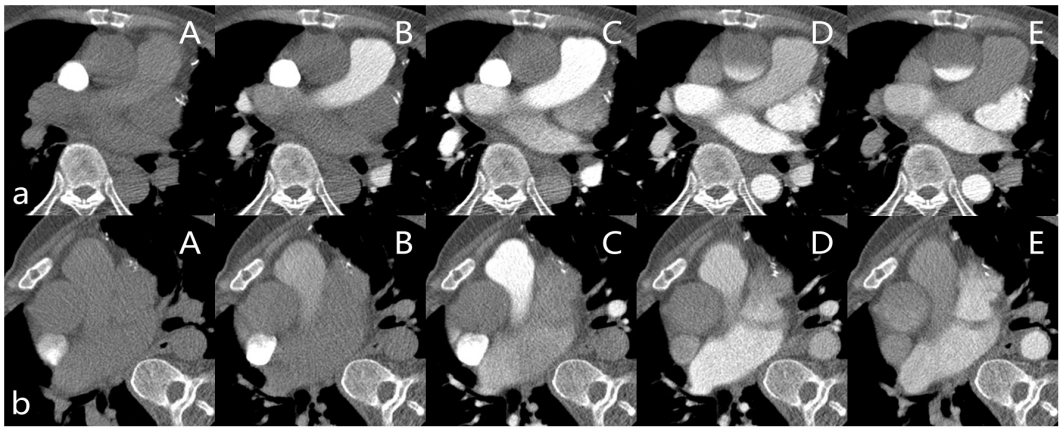


**FIGURE 1 | (a)** Patient in the supine position. (A–E) are the slices of the AAO after the contrast agent injects 9s, 13s, 18s, 23s, and 28s in the Smart Prep Series. **(b)** Patient in the right lateral decubitus position. (A–E) are the slices of the AAO after the contrast agent injects 9s, 13s, 18s, 23s, and 27s in the Smart Prep Series.

disappeared after altering the patient's position, thus confirming that it was not a true thrombosis but a "watershed" in the aortic root. This "watershed" of the aortic root is caused by the opposite bleeding between MCS flows and the left ventricle. Meanwhile, several other complications of MCS, such as thrombus formation, also deserve our attention. Because the prognosis and therapy for aortic root thrombosis and "watershed" vary, it's vital to get an accurate diagnosis.

## "WATERSHED" PHENOMENON OF MCS ON COMPUTED TOMOGRAPHY ANGIOGRAPHY

Extracorporeal membrane oxygenators is commonly utilized as a bridge to recovery and the installation of ventricular assist devices in refractory cardiogenic shock, and the veno-arterial configuration is used for cardiovascular support (10–12). In most ECMO patients, the left ventricle maintains some residual output and so provides an antegrade blood flow to the systemic circulation *via* the aortic valve (6). But the flow rate at the aortic root is extremely low (13). In addition, ECMO flow is in contrast to antegrade native cardiac output. Blood stasis can develop as a result of retrograde blood flow in the AAO during VA-ECMO, which can lead to intracardiac or extracardiac thrombosis (14). The LVAD is able to unload the left ventricle effectively and provide the heart with real rest, and the aortic valve is almost in a closed state (15). Due to the location of the LVAD outflow cannula, the local blood flow pattern might be influenced, resulting in a stagnant flow zone in the backflow portion. Such stagnation zones may cause the formation of thrombosis (16).

Computed tomography angiography is a widely available and capable technique that can be employed to evaluate thrombosis in the aorta in patients with MCS (7, 17, 18). In our center, two patients who got IABP + ECMO and LVAD surgery also underwent CTA. The aortic root contrast medium fills slowly on CTA in which the blood displays a filling defect in the root of the aorta with no visualization of the right coronary artery or coronary artery bypass while the patients were supine. The arc-shaped low-attenuation filling defect disappeared when the position was changed to the right lateral decubitus position and the right coronary artery or the bypass of the coronary artery was filled with the contrast agent, both of which displayed the "watershed" phenomenon on CTA in the root of the aorta. The changes strongly demonstrate that the arc-shaped low-attenuation filling defect in the root of the aorta is not a thrombus formation. Meanwhile, echocardiography reveals that no thrombus formation occurs even if the pressures and flows of aortic roots are extremely low.

The pressures and flows of the left ventricle outflow trace are low, and the oxygen content of the blood coming from the left ventricle is unknown. The "watershed" phenomenon may put the coronary artery and supra-aortic branches at risk of poor perfusion and hypoxemia (5, 8). Thus, cardiac ischemia may occur in patients receiving MCS support. In our cases, there was no contrast agent filling in the right coronary (the bypass of the right coronary artery) on CTA, which demonstrated that perfusion and flow of the right coronary (the bypass of the right coronary artery) were inadequate. With insufficient blood supply, the myocardium could be injured. Right heart failure is a complication of MCS, particularly in LVAD patients, and the insufficient blood supply to the coronary could be one of the causes.

Furthermore, if MCS flow perfusion levels do not reach the origins of supra-aortic arteries, brain circulation may be limited. The first case shows that a portion of the supra-aortic branches was receiving blood from the LVAD circuit, implying that brain circulation may be restricted. The supra-aortic branches are not reached by the scanning scope in case two.

## AORTIC ROOT THROMBUS FORMATION

The MCS implantation such as ECMO and LVAD has various severe complications, including thrombosis. The majority of

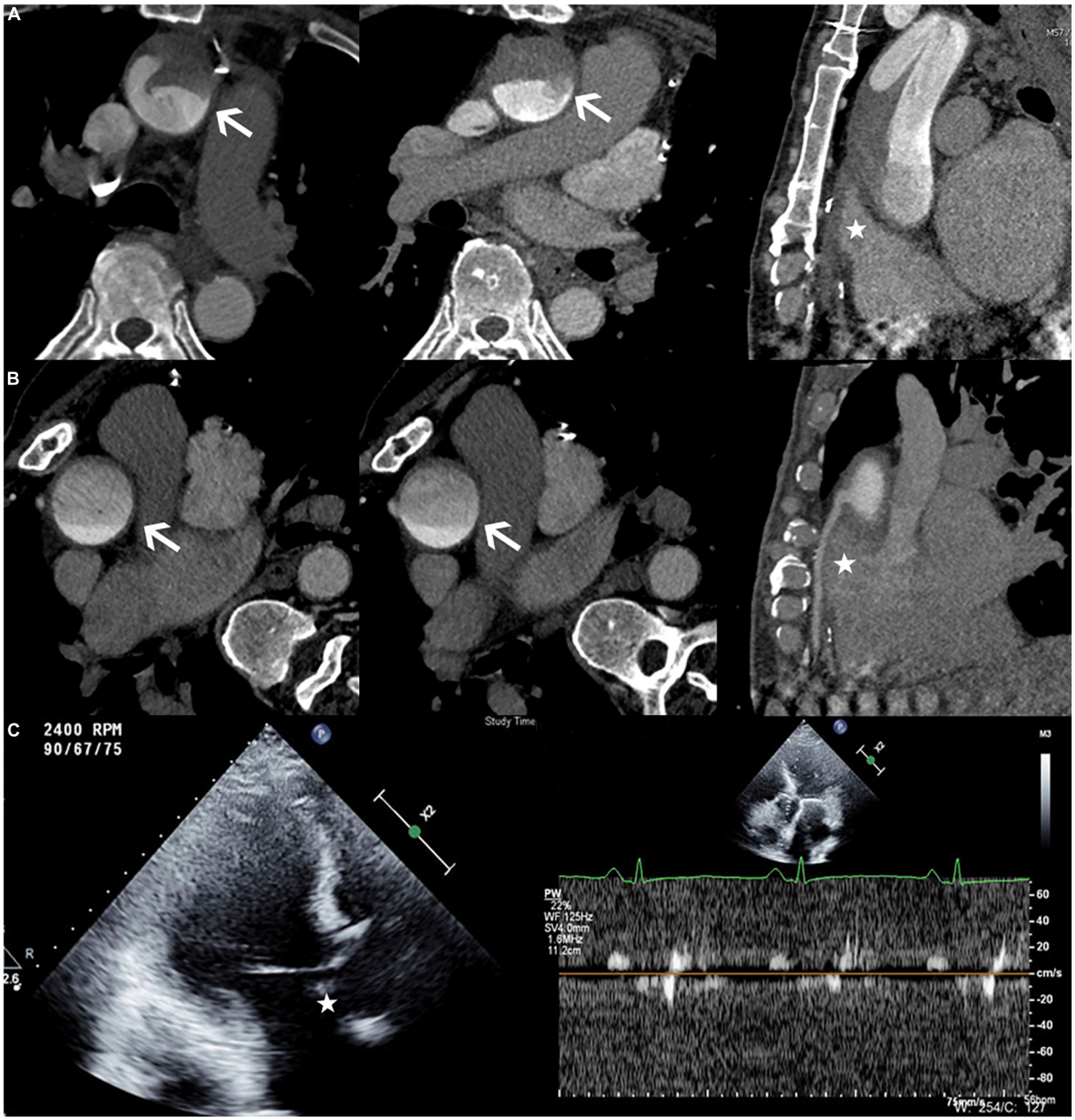


**FIGURE 2 | (A)** Patient in the supine position. The axial view demonstrating an arc-shaped low-attenuation filling defect (white arrow) was seen in the root of the aorta, while the DAO was filling well. The multiplanar reformatted image from the CTA showed no contrast agent filling in the bypass of the right coronary artery (white star). **(B)** Patient in the right lateral decubitus position. The arc-shaped low-attenuation filling defect disappeared (white arrow), and the bypass of the right coronary artery filled well (white star). **(C)** The echocardiography (Philips EPIQ 7C; 45° reclining position; Three-chamber view) demonstrated the extremely low velocity of the aortic valve and no thrombus formation in the aortic root (white star).

thrombosis instances documented are ventricular, while intra-aortic thrombosis is extremely rare, with only a few examples reported in the literature, and the mortality of patients is extremely high (14, 15, 19). Devastating complications such as strokes, acute myocardial infarction, or even death can be caused by thrombus deposition in the aortic root (4). Not only is there decreased blood flow velocity in the aortic root, but the increased levels of clotting factors also lead to an increased risk of thrombosis in MCS patients (12, 20–22). The thrombus in the aortic root shows a permanent filling defect that does not alter with the filling and clearance of the contrast agent (15). The "watershed" phenomenon has no additional effect on the coagulation status or the stability of blood circulation.

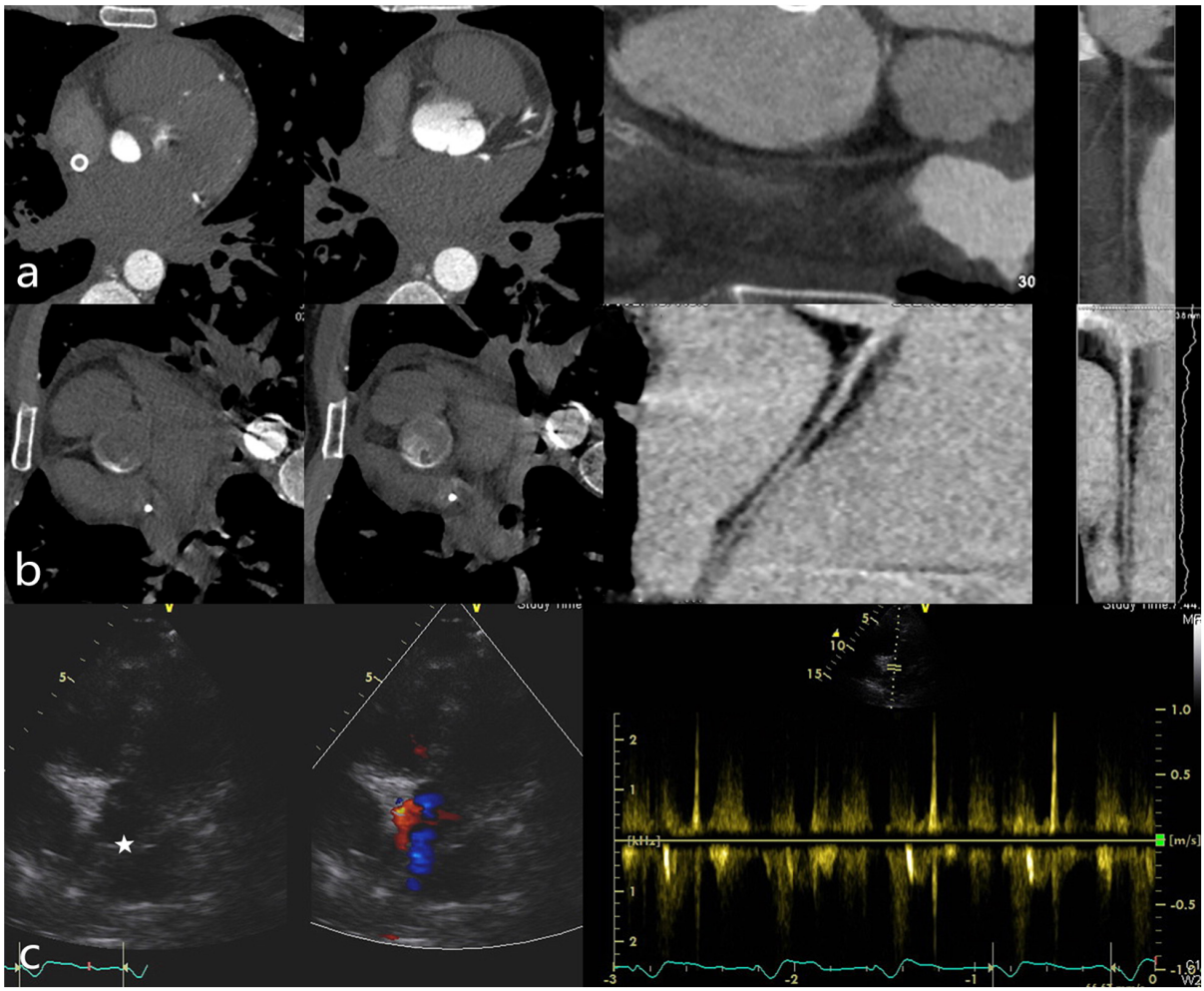


**FIGURE 3 | (a)** Patient in the supine position. The axial view demonstrated an arc-shaped low-attenuation filling defect ("watershed" phenomenon) in the root of the aorta while the DAO was filling well. The multiplanar reformatted image from the CTA showed no contrast agent filling in the right coronary. **(b)** Patient in the right lateral decubitus position. The arc-shaped low-attenuation filling defect disappeared and the right coronary filled well. (Left dominant coronary artery; **(c)** The echocardiography (GE Vivid E95; 45° reclining position; Five-chamber view) demonstrated the extremely low velocity of the aortic valve and there was no thrombus formation in the aortic root (white star).

To our knowledge, the "watershed" phenomenon has never been mentioned on LVAD. What's more, this is the first report of the discriminate "watershed" phenomenon and thrombus formation with MCS implantation verified by CTA. The diagnosis of the aortic root "watershed" phenomenon described here may lead to a false diagnosis. When a patient undergoes a CTA scanning, altering the right lateral position for supplementary scanning is critical for detecting this sign and distinguishing it from thrombosis.

## CONCLUSION

The signs of the "watershed" phenomenon are not common in patients with MCS, and it is necessary for radiologic technologists and radiologists to accumulate experience in scanning and diagnosis, as well as pay attention to distinguishing it from thrombosis. Accurate identification of aortic root thrombosis is critical for both clinical and postoperative management. With proper evaluation and diagnosis, patients can have favorable prognoses.

## DATA AVAILABILITY STATEMENT

The original contributions presented in the study are included in the article/supplementary material; further inquiries can be directed to the corresponding author/s.

## ETHICS STATEMENT

All subjects gave written informed consent in accordance with the Declaration of Helsinki. The protocol was approved by

the institutional review board (IRB) of TEDA International Cardiovascular Hospital. The present study involved no potential risk to patients.

## AUTHOR CONTRIBUTIONS

GD and LF: responsibility for the integrity of the work as a whole, from inception to finished article. GD and JL: acquisition of imaging. GD and JZ: analysis and interpretation of imaging. All authors were involved in drafting the article or revising it critically for important intellectual content, and all authors approved the final version to be published.

## FUNDING

National Key Research and Development Plan of China: Implantable Artificial Heart and Ventricular Auxiliary Device Project (2017YFC0111005).

## ACKNOWLEDGMENTS

We would like to extend our sincerest thanks to the entire Department of Radiology (TEDA International Cardiovascular Hospital, Tianjin, China) for their assistance.

## REFERENCES

1. Simon MA, Bachman TN, Watson J, Baldwin JT, Wagner WR, Borovetz HS. Current and future considerations in the use of mechanical circulatory support devices: an update, 2008-2018. *Annu Rev Biomed Eng.* (2019) 21:33–60. doi: 10.1146/annurev-bioeng-062117-121120
2. Sodhi N, Lasala JM. Mechanical circulatory support in acute decompensated heart failure and shock. *Interv Cardiol Clin.* (2017) 6:389. doi: 10.1016/j.iccl.2017.03.008
3. Fried J, Garan AR, Shames S, Masoumi A, Yuzefpolskaya M, Takeda K, et al. Aortic root thrombosis in patients supported with continuous-flow left ventricular assist devices. *J Heart Lung Transplant.* (2018) 37:1425–32. doi: 10.1016/j.healun.2018.07.012
4. Delmaczynska E, Newham R. To explore the prevalence and outcomes of advance care planning for patients with left ventricular assist devices: a review. *J Clin Nurs.* (2019) 28:1365–79. doi: 10.1111/jocn.14748
5. Rozencwajg S, Wu EL, Heinsar S, Stevens M, Chinchilla J, Fraser JF, et al. A mock circulation loop to evaluate differential hypoxemia during peripheral venoarterial extracorporeal membrane oxygenation. *Perfusion.* (2022) 2022:2676591211056567. doi: 10.1177/02676591211056567
6. Gehron J, Schuster M, Rindler F, Bongert M, Böning A, Krombach G, et al. Watershed phenomena during extracorporeal life support and their clinical impact: a systematic in vitro investigation. *ESC Heart Fail.* (2020) 7:1850–61. doi: 10.1002/ehf2.12751
7. Li X, Kondray V, Tavri S, Ruhparwar A, Azeze S, Dey A, et al. Role of imaging in diagnosis and management of left ventricular assist device complications. *Int J Cardiovasc Imaging.* (2019) 35:1365–77. doi: 10.1007/s10554-019-01562-4
8. Hoeper MM, Tudorache I, Kühn C, Marsch G, Hartung D, Wiesner O, et al. Extracorporeal membrane oxygenation watershed. *Circulation.* (2014) 130:864–5.
9. Angleitner P, Röggla M, Laufer G, Wiedemann D. Watershed of veno-arterial extracorporeal life support. *Eur J Cardiothorac Surg.* (2016) 50:785. doi: 10.1093/ejcts/ezw185
10. Tickoo M, Bardia A. Anesthesia at the edge of life: mechanical circulatory support. *Anesthesiol Clin.* (2020) 38:19–33. doi: 10.1016/j.anclin.2019.11.002
11. Bardia A, Schonberger RB. Postcardiotomy venoarterial extracorporeal membrane oxygenation (VA ECMO) in adult patients - many questions, few answers, and hard choices. *J Cardiothorac Vasc Anesth.* (2018) 32:1183–4. doi: 10.1053/j.jvca.2017.10.037
12. Thomas J, Kostousov V, Teruya J. Bleeding and thrombotic complications in the use of extracorporeal membrane oxygenation. *Semin Thromb Hemostas.* (2017) 2017:20–9. doi: 10.1055/s-0037-1606179
13. Thompson AF, Luan J, Al Aklabi MM, Cave DA, Ryerson LM, Noga ML. Pediatric extracorporeal membrane oxygenation (ECMO): a guide for radiologists. *Pediatr Radiol.* (2018) 48:1488–502. doi: 10.1007/s00247-018-4211-z
14. Nishihara T, Kudamatsu N, Hamada T, Nakata Y, Yamamoto W, Nandate H, et al. A case report of thrombotic complete obstruction of the ascending aorta as a complication of Venoarterial extracorporeal membrane oxygenation support: steps to prevent thrombosis. *J Cardiothorac Surg.* (2020) 15:185. doi: 10.1186/s13019-020-01239-3
15. Leontiadis E, Koertke H, Bairaktaris A, Koerfer R. Thrombosis of the ascending aorta during mechanical circulatory support in a patient with cardiogenic shock. *Interact Cardiovasc Thorac Surg.* (2010) 11:510–1. doi: 10.1510/icvts.2010.240689
16. Tran BC, Nijjar PS. Role of contrast CT for the diagnosis and the prognosis of suspected LVAD thrombosis[J]. *J Cardiac Surg.* (2017) 32:162–5. doi: 10.1111/jocs.13094
17. Kar B, Delgado RM, Frazier OH, Gregoric ID, Harting MT, Wadia Y, et al. The effect of LVAD aortic outflow-graft place-ment on hemodynamics and flow: implantation technique and computer flow modeling. *Tex Heart Inst J.* (2005) 32:294–8.
18. Carr CM, Jacob J, Park SJ, Karon BL, Williamson EE, Araoz PA. CT of left ventricular assist devices. *Radiographics.* (2010) 30:429–44. doi: 10.1148/rg.302095734
19. Madershahian N, Weber C, Scherner M, Langebartels G, Slottosch I, Wahlers T. Thrombosis of the aortic root and ascending aorta during extracorporeal membrane oxygenation. *Intens Care Med.* (2014) 40:432–3. doi: 10.1007/s00134-013-3173-8
20. Weber C, Deppe AC, Sabashnikov A, Slottosch I, Kuhn E, Eghbalzadeh K, et al. Left ventricular thrombus formation in patients undergoing femoral veno-arterial extracorporeal membrane oxygenation. *Perfusion.* (2017) 33:283–8. doi: 10.1177/0267659117745369
21. Veenis JF, Brugts JJ, Yalcin YC, Roest S, Bekkers JA, Manintveld OC, et al. Aortic root thrombus after left ventricular assist device implantation and aortic valve replacement. *ESC Heart Failure.* (2020) 7:3208–12. doi: 10.1002/ehf2.12921
22. Tanna MS, Reyentovich A, Balsam LB, Dodson JA, Vainrib AF, Benenstein RJ, et al. Aortic root thrombus complicated by left main coronary artery occlusion visualized by 3D echocardiography in a patient with continuous-flow left ventricular assist device. *Echocardiography.* (2017) 34:306–10. doi: 10.1111/echo.13425

**Conflict of Interest:** The authors declare that the research was conducted in the absence of any commercial or financial relationships that could be construed as a potential conflict of interest.

**Publisher's Note:** All claims expressed in this article are solely those of the authors and do not necessarily represent those of their affiliated organizations, or those of the publisher, the editors and the reviewers. Any product that may be evaluated in this article, or claim that may be made by its manufacturer, is not guaranteed or endorsed by the publisher.

frontiers | Frontiers in Cardiovascular Medicine

CASE REPORT
published: 27 May 2022
doi: 10.3389/fcvm.2022.915876

# Case Report: Bronchogenic Cyst in the Right Atrium of a Young Woman

*Yuya Fukudome[1], Michinari Hieda[2]*, Shiho Masui[2], Taku Yokoyama[2], Shutaro Futami[2], Shohei Moriyama[2], Kei Irie[2], Mitsuhiro Fukata[2], Tomoki Ushijima[3], Akira Shiose[3] and Koichi Akashi[2]*

[1] Heart Center, Kyushu University Hospital, Fukuoka, Japan, [2] Department of Medicine and Bio-systemic Science, Hematology, Oncology, and Cardiovascular Medicine, School of Medicine, Kyushu University Hospital, Fukuoka, Japan, [3] Department of Cardiovascular Surgery, Kyushu University Hospital, Fukuoka, Japan

A 31-year-old woman was referred to our hospital for evaluation of a cardiac mass in the right atrium. Cardiac magnetic resonance imaging indicated a cystic mass filled with fluid accumulation in the right atrium. The mass was identified as a cardiac cyst and was surgically removed. Pathological examination revealed an extremely rare bronchogenic cyst. Bronchogenic cysts are benign congenital abnormalities of primitive foregut origins that form in the mediastinum during embryonic development. There is unusual clinical dilemmas surrounding the treatment plan for cardiac surgery or biopsy of cardiac masses, especially in patients with rare cardiac cysts. The anatomical location of the cyst can be related to various clinical symptoms and complications. In cases of indeterminate cardiac cysts, direct cyst removal without prior biopsy is of utmost importance.

**Keywords: bronchogenic cyst, cardiac mass, cardiac biopsy, cardiac MRI, imaging**

OPEN ACCESS

***Edited by:***
*Grigorios Korosoglou, GRN Klinik Weinheim, Germany*

***Reviewed by:***
*Alexandros Kallifatidis, St. Luke's Hospital, Greece*
*Janek Salatzki, Heidelberg University, Germany*

***Correspondence:**
*Michinari Hieda*
*hieda.michinari.265@m.kyushu-u.ac.jp*

***Specialty section:***
*This article was submitted to Cardiovascular Imaging, a section of the journal Frontiers in Cardiovascular Medicine*

***Received:*** *08 April 2022*
***Accepted:*** *02 May 2022*
***Published:*** *27 May 2022*

***Citation:***
*Fukudome Y, Hieda M, Masui S, Yokoyama T, Futami S, Moriyama S, Irie K, Fukata M, Ushijima T, Shiose A and Akashi K (2022) Case Report: Bronchogenic Cyst in the Right Atrium of a Young Woman. Front. Cardiovasc. Med. 9:915876. doi: 10.3389/fcvm.2022.915876*

## INTRODUCTION

The incidence of primary cardiac tumors is approximately 0.02%, with three-quarters of cardiac tumors are benign. Among these benign cardiac tumors, cardiac myxoma is the most frequent. Other major types of benign cardiac tumors include fibromas, rhabdomyomas, papillomas, lipomas, papillary fibroelastomas, hemangiomas, and bronchogenic cysts (1).

Bronchogenic cysts in the atrial septum are extremely rare. Regarding the intracardiac bronchogenic cysts, they have been reported in only 22 cases, to date (2). They are benign congenital cysts of primitive foregut origin that form in the mediastinum during embryonic development (3–5). These bronchogenic cysts represent 6% to 15% of primary mediastinal masses (6), and may develop in the neck, spinal dura mater, sub-diaphragm, diaphragm (7), or retroperitoneal regions (8). The heart is derived from the mesoderm, and its development differs from that of the ectoderm-derived respiratory system. The embryonic cardiac primordium is close to the primordial bronchial tree and foregut. Therefore, it has been indicated that migration of the embryonic cardiac primordium to the cardiac muscle site during abnormal budding may be involved in cardiac cyst development (9). In addition, ectopic bronchogenic cysts are often misdiagnosed preoperatively, because they have no imaging features and have different clinical manifestations (10). Therefore, multimodality imaging is the most important approach to establish an accurate diagnosis.

## CASE PRESENTATION

A 31-year-old woman presented to a local physician 2 months before her referral with palpitations and shortness of breath. At the time, a paroxysmal atrial fibrillation was detected by a

Holter-electrocardiogram examination. Thereafter, successful catheter ablation of paroxysmal atrial fibrillation was performed. Presence of a cardiac tumor in the right atrium was suspected during catheter ablation. Therefore, the patient was referred to our hospital for further evaluation.

On presentation to our hospital, the patient had no symptoms. The patient's medical history included asthma, emergency cesarean section for pregnancy-induced hypertension, paroxysmal atrial fibrillation, gestational diabetes, and type 2 diabetes mellitus. The patient was managed with edoxaban (60 mg daily) for paroxysmal atrial fibrillation and dapagliflozin (5 mg), sitagliptin (50 mg), and metformin (500 mg) for type 2 diabetes mellitus. The patient had no other pertinent family medical history.

Her height, weight, body mass index, and body surface area were 157.8 cm, 64.6 kg, 25.94 kg/$m^2$, and 1.66 $m^2$, respectively. The patient had body temperature, 37.2°C; blood pressure, 130/88 mmHg; pulse rate, 108 bpm; and $O_2$ saturation measured by pulse oximetry, 98% on room air. Normal heart and lung sounds were ausculated without any murmur. The abdomen was soft and tender. There was no edema in the lower legs. Her blood test results are shown in **Table 1**. A 12-lead electrocardiogram showed normal sinus rhythm. Chest radiography revealed a cardiothoracic ratio of 43.9% without pleural effusion or pulmonary congestion. Transthoracic echocardiography revealed normal left ventricular ejection fraction (71%) and diastolic function (E/e': 9.0) without valvular diseases. Although we attempted to visualize the tumor in the right atrium using a subcostal approach, it was unclear due to obesity.

Transesophageal echocardiography revealed a 16 × 10 mm isoechoic mass lesion on the right interatrial septum. The mass had a clear border, smooth surface, and broad base without mobility and apparent feeding vessels (**Figure 1**; **Supplementary Videos 1, 2**). A plain thoracic computed tomography (CT) revealed a high-intensity nodule on the right interatrial septum at the border of the inferior vena cava (**Figure 2A**). The absorption value was 110 HU and size was 13 × 9 mm. Moreover, there was no change in absorption value before and after contrast enhancement. Cardiac MRI showed a 14-mm nodule attached to the inter atrial septum. The nodule showed little higher signal than its surrounding muscle on a T1-weighted image. In addition, the tumor had high signal intensity on a T2-weighted image. No significant abnormal enhancement in LV wall and nodule on a late gadolinium enhancement image. Based on these findings, the nodule was suggested to be a cystic mass including liquid component (**Figures 2B,C**). In addition, whole-body positron emission tomography-CT showed no fluorodeoxyglucose accumulation in the lesion.

The right atrial cyst was resected using minimally invasive cardiac surgery *via* right mini-thoracotomy. After aortic clamping, induction of cardiac arrest, and incision of the right atrium, a white mass with a smooth surface appeared on the posterior wall of the right atrium-inferior vena cava junction. A yellowish-white viscous mucous material was found in the mass with no thrombus (**Figure 3**). The mass was completely resected, and the right atrial posterior wall defect in the inferior vena cava was reconstructed using a bovine pericardial patch. Pathohistological evaluation revealed multilineage ciliated columnar epithelium and mucous glands present, resembling the respiratory epithelium in the intima of some cyst walls (**Figure 4**). No findings, such as nuclear irregularities or atypical cells, suggested malignancy. Therefore, the patient was diagnosed with a bronchogenic cyst (11).

The patient's postoperative course was favorable and uneventful. She was discharged 21 days later without any

**TABLE 1 |** Blood data on presentation in our hospital.

| Measure | Data | Reference range |
|---|---|---|
| White blood cell count ($10^3/\mu L$) | 12.42 | 3.3–8.6 |
| Red blood cell count ($10^6/\mu L$) | 5.69 | 3.86–4.92 |
| Hemoglobin (g/dL) | 11.4 | 11.6–14.8 |
| Hematocrit (%) | 38.8 | 35.1–44.4 |
| Platelet count ($10^3/\mu L$) | 521 | 158–348 |
| Fibrinogen (mg/dL) | 250 | 200–400 |
| Fibrinogen degradation product (μg/mL) | 2.5 | ≦ 5.0 |
| D-dimer (μg/mL) | 0.5 | ≦ 1.0 |
| PT-INR (INR) | 1.17 | 0.90–1.10 |
| Total protein (g/dL) | 8.2 | 6.6–8.1 |
| Albumin (g/dL) | 4.9 | 4.1–5.1 |
| Blood urea nitrogen (mg/dL) | 13 | 8–20 |
| Creatinine (mg/dL) | 0.44 | 0.46–0.79 |
| Urea acid (mg/dL) | 2.8 | 2.6–5.5 |
| Total-bilirubin (mg/dL) | 0.5 | 0.4–1.5 |
| Direct-bilirubin (mg/dL) | 0.1 | 0.0–0.3 |
| Aspartate aminotransferase (U/L) | 24 | 13–30 |
| Alanine aminotransaminase (U/L) | 65 | 7–23 |
| Lactic dehydrogenase (U/L) | 167 | 124–222 |
| Alkaline phosphatase (U/L) | 58 | 38–113 |
| Gamma-glutamyl transpeptidase (U/L) | 55 | 9–32 |
| Creatine kinase (U/L) | 49 | 41–153 |
| Glucose (mg/dL) | 100 | 73–109 |
| Total-cholesterol (mg/dL) | 201 | 142–248 |
| HDL-cholesterol (mg/dL) | 43 | 48–103 |
| LDL-cholesterol (mg/dL) | 116 | 65–163 |
| Triglyceride (mg/dL) | 424 | 30–117 |
| C-reactive protein (mg/dL) | 0.08 | ≦ 0.14 |
| Na (mmol/L) | 138 | 138–145 |
| K (mmol/L) | 4.8 | 3.6–4.8 |
| Cl (mmol/L) | 101 | 101–108 |
| IgG (mg/dL) | 1124 | 861–1747 |
| IgA (mg/dL) | 602 | 93–393 |
| IgM (mg/dL) | 128 | 50–269 |
| CH-50 (U/mL) | 60.0 | 31.6–57.6 |
| Hb A1c (%) | 6.7 | 4.9–6.0 |
| Troponin T (ng/mL) | 0.004 | ≦ 0.014 |
| Soluble interleukin-2 receptor (U/mL) | 256 | 156.6–474.5 |
| Brain natriuretic peptide (pg/mL) | 4.5 | 0.0–18.4 |
| Carcinoembryonic antigen (ng/mL) | 0.7 | ≦ 3.2 |
| Carbohydrate antigen 19–9 (U/mL) | 9.1 | ≦ 37.0 |
| Neuron-specific enolase (ng/mL) | 14.3 | ≦ 15.1 |
| Cytokeratin 19 Fragment (ng/mL) | 1.4 | ≦ 3.5 |
| Squamous cell carcinoma antigen (ng/mL) | 1.2 | 0.6–2.3 |

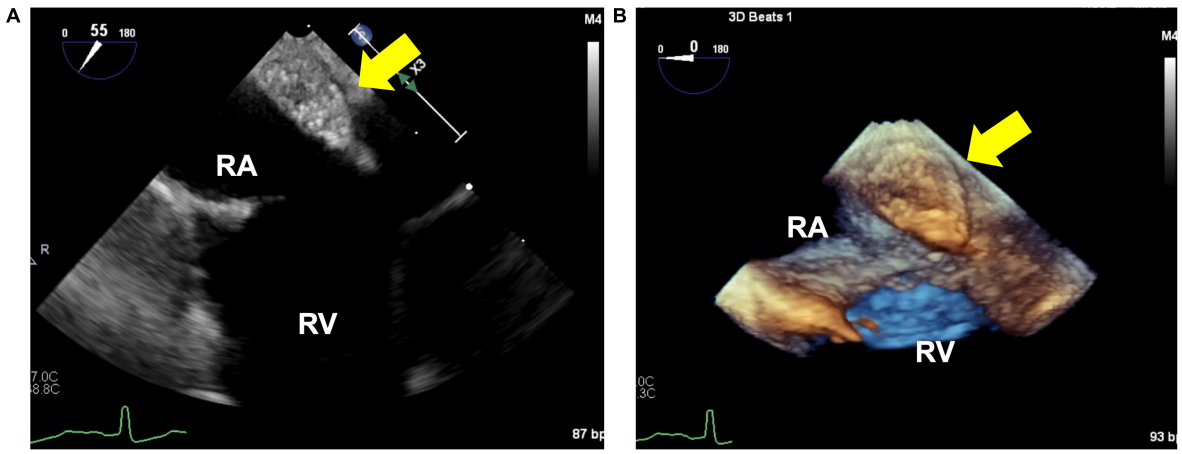


**FIGURE 1 |** 2-dimensional **(A)** and 3-dimensional **(B)** image of the isoechoic mass using transesophageal echocardiography. **(A)** 16×10×10 mm isoechoic mass. This image shows an isoechoic mass on the right interatrial septum near the inferior vena cava. **(B)** Mass is well-defined, has a smooth surface, and broadly adherent to the atrial.

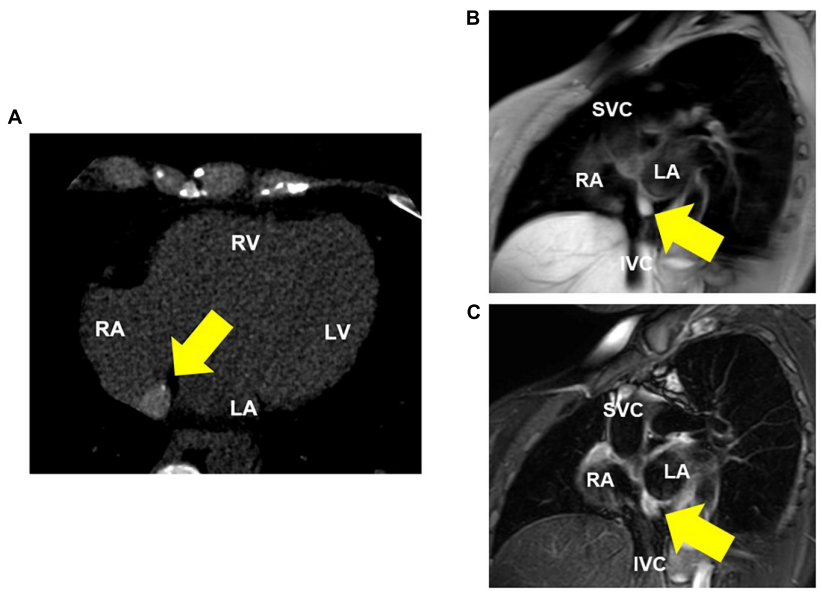


**FIGURE 2 |** Thoracic computed tomography (CT) and MRI (T1 and T2-weighted) images. **(A)** CT shows a high-intensity nodule on the interatrial septum. **(B)** Cardiac MRI (T1-weighted image) reveals a nodule that is little higher signal than its surrounding muscle. **(C)** Cardiac MRI (T2-weighted image) reveals a high-intensity nodule on the interatrial septum, suggesting a cystic lesion with fluid components. RA, right atrium; RV, right ventricle; LA, left atrium; LV, left ventricle; SVC, superior vena cava; IVC, inferior vena cava.

complications. Currently, the patient visits the hospital as an outpatient without recurrence.

## DISCUSSION

This was an extremely rare case of bronchogenic cyst occurring in a right atrium, in which establishing an accurate preoperative diagnosis was difficult. The differential diagnoses of intra-cardiac tumors include myxomas, lipomas, papillary fibroelastomas, metastatic tumors, cardiac cysts, or thrombi. Myxomas are the most frequent benign cardiac tumors occurring in adulthood: asymptomatic in 0–20% of cases (12). Lipomas are adipocyte-derived masses occurring in the epicardial myocardium, with approximately 25% of these lesions occur in the intracardiac lumen (13). These tumors are generally observed as isoechoic masses when the capillary blood flow in the stalk becomes obstructed, the mass becomes necrotic, and its echo-image is hypoechogenic (14). Papillary fibroelastomas generally occur on the valvular surface and are most commonly found in the aortic valve (15). In this present case, tumor markers were not elevated, leading to ruling out a metastatic cardiac tumor.

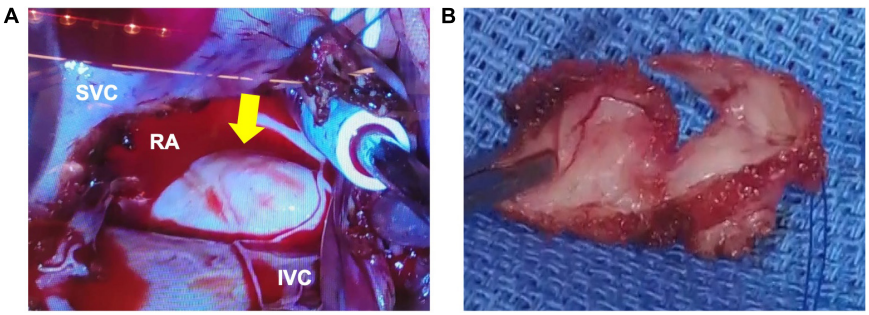


**FIGURE 3 |** Macroscopic findings during surgery. **(A)** The outer surface of the mass is white, smooth, and soft. **(B)** A yellowish-white viscous mucous material is found in the mass. There are no thrombi inside or outside the cyst. RA, right atrium; RV, right ventricle; LA, left atrium; LV, left ventricle; SVC, superior vena cava; IVC, inferior vena cava.

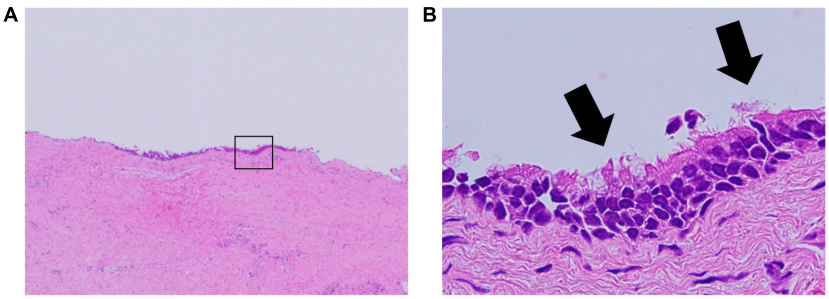


**FIGURE 4 |** Pathology of the bronchogenic cyst. **(A)** Hematoxylin and eosin stain; original magnification, 20×. **(B)** The ciliated columnar epithelium suggests a bronchogenic cyst; original magnification, 400×.

**TABLE 2 |** Literature review of recent intra-cardiac bronchogenic cysts.

| No | References | Age | Sex | Location | Symptoms | Arrythmia | Treatment |
|---|---|---|---|---|---|---|---|
| 1 | Foley (28) | 28 | F | IAS | Incidentally | No | Conservative |
| 2 | Shiferaw (29) | 42 | M | Myocardium | Chest pain, fatigue | No | Unrelated sudden death |
| 3 | Hui (9) | 36 | F | IAS | Palpitation | No | Resection |
| 4 | | 29 | F | IAS | Dyspnea | No | Resection |
| 5 | Olsen (30) | 50 | F | IAS | Cough, dyspnea | No | Resection |
| 6 | Forcillo (31) | 41 | F | IVS | No, heart murmur | No | Resection |
| 7 | Grozavu (32) | 42 | F | Pericardium | Dull chest pain | No | Resection |
| 8 | Wang (33) | 41 | M | LV wall | precordial pain | No | Resection |
| 9 | Smer (34) | 50 | M | IAS | Tachycardia | Af | Resection |
| 10 | Shiohira (35) | 77 | F | AVS | Syncope | Wenckebach AVB, Vf | Resection |
| 11 | Nishida (36) | 78 | M | IVS | Unknown | Af, PVC | Unrelated death |
| 12 | Eriko (20) | 36 | M | IAS | Chest discomfort | Third-degree AVB | Resection and PM |
| 13 | Blesneac (37) | 10 | F | IVS | Incidentally | PVC, PAC | Resection |
| 14 | Van Praet (38) | 58 | M | IAS | Stroke | No | Resection |
| 15 | Gimpel (39) | 71 | F | Pericardium | Dysphagia, SOB | No | Resection |
| 16 | Li (40) | 17 | M | LA, RSPV | Chest pain, dyspnea | No | Resection |
| 17 | Fukada (41) | 42 | F | IAS | Dyspnea on exertion | No | Resection |
| 18 | Essam (42) | 31 | F | IAS | Retrosternal pain | Tachycardia, atrial flutter | Resection |
| 19 | Luo (10) | 47 | M | IAS | SOB | No | Resection |

*M, male; F, female; LV, left ventricle; LA, left atrium; IAS, Inter atrial septum; IVS, Inter ventricular septum; AVS, atrio-ventricular septum; RSPV, right superior pulmonary vein; AVB, atrioventricular block; Af, atrial fibrillation; Vf, ventricular fibrillation; PVC, Premature Ventricular Contraction; PAC, premature atrial contraction; AF, atrial flutter; SOB, shortness of breath; PM, pacemaker.*

The D-dimer level also indicated a low likelihood of thrombosis. Pericardial cysts are rare benign disease that often identified incidentally on chest X-ray or trans-thoracic echocardiography, the majority of cases of this disease are asymptomatic. Since complex type pericardial cysts are defined as the presence of solid compornents, it was difficult to distinguish between pericardial

cysts and this case. However, these diseases are more likely to be located at the right cardiophrenic angle followed by the left cardiophrenic angle in mediastinal sites (16). Thus, we ruled out pericardial cysts. Although, differential diagnosis as an extra-cardiac tumors include substernal thyroid, thymic tumor, intra-thoracic cystic hygroma, serous cyst, and aortic aneurysm, all they were excluded by multimodality imaging studies. In this case, multimodality imaging suggested that the cystic lesion contained both fluid and blood. Thus, the preoperative clinical diagnosis was suspected to be a right atrial cyst.

Cardiovascular magnetic resonance (CMR) imaging is an important diagnostic tool for evaluating patients with suspected cardiac tumors. A previous study demonstrated that CMR diagnoses were 25% no mass, 16% pseudo mass, 16% thrombus, 17% benign tumor, and 23% malignant tumor (17). Compared to the final diagnosis, the CMR diagnosis was accurate in 98.4% of patients; patients with CMR diagnoses of pseudo mass and the benign tumor had mortality rates similar to those without masses, but patients with malignancy [hazard ratio (HR) 3.31 (2.40–4.57)] and thrombus [HR 1.46 (1.00–2.11) (17). The CMR diagnosis had more prognostic value than clinical factors such as left ventricular ejection fraction, coronary artery disease, or history of extracardiac malignancy ($P < 0.001$) (17). Therefore, we should perform CMR for evaluating patients with suspected cardiac tumors since CMR diagnosis is a powerful independent predictor of mortality over clinical risk factors (18).

We reviewed all case reports of recent intra-cardiac bronchogenic cyst published and summarized them in **Table 2**. Common symptoms of bronchogenic cysts include cough, fever, and dyspnea (19). Miwa et al. reported a case of a bronchogenic cyst in the lower interatrial septum that demonstrated complete atrioventricular block (20). In this case, the patient had paroxysmal atrial fibrillation and a cyst in the right interatrial septum near the inferior vena cava. Although the causal relationship between tumors and arrhythmias is not clear, arrhythmia of unknown origin in younger patients may lead clinicians to suspect a cardiac tumor. Furthermore, in some cases, obstruction of the superior vena cava (SVC) and dysphagia have been reported (21, 22). In addition, bronchogenic cysts can cause compression into the left atrium, pulmonary veins, or coronary arteries (23, 24). Regarding these reasons, it might be essential to focus on the anatomical location of the cyst accurately.

Whether to perform a surgery or biopsy first is a dilemma in diagnosing rare cardiac tumors or cysts. Puncture aspiration biopsy was an option for preoperative diagnosis. However, biopsy of a cystic lesion could rupture the trachea, thoracic cavity, or pericardial cavity. In addition, there has been a reported case of cystic infection after endobronchial ultrasonography-guided fine needle aspiration. Therefore, cystic lesions in the intra-cardiac cavity should not be considered for a needle aspiration (25). Given these complications, direct surgical resection is recommended without prior tumor biopsy (26). In addition, bronchogenic cyst is a risk of malignant transformation in adulthood, and risk of complications increase over time. Therefore, bronchogenic cysts are recommended for preferably early surgery (27). Since it could not be judged whether the tumor was benign or malignant, we decided to resect it directly. It must be emphasized that preoperative diagnosis can also be complicated by the extreme rarity of such cases. This case describes the usefulness of multimodality imaging in diagnosing bronchogenic cysts preoperatively with minimal complications.

## CONCLUSION

There is a clinical dilemma surrounding the treatment plan for cardiac surgery or biopsy of cardiac masses, especially in patients with rare cardiac cysts. The anatomical location of the cyst is related to various clinical symptoms and complications. Therefore, multimodality imaging might be practical for assessing the exact anatomical location of cysts and avoiding various complications. This case describes a rare bronchogenic cyst in the right atrium and highlights the importance of multimodality imaging for appropriate diagnosis and management. In cases of indeterminate cardiac cysts, direct removal of the cyst without previous biopsy is of utmost importance.

## DATA AVAILABILITY STATEMENT

The raw data supporting the conclusions of this article will be made available by the authors, without undue reservation.

## ETHICS STATEMENT

Ethical review and approval was not required for this study on human participants in accordance with the local legislation and institutional requirements. The patients/participants provided their written informed consent to participate in this study.

## AUTHOR CONTRIBUTIONS

YF and MH contributed significantly to the writing and editing to the manuscript. MH, SMa, TY, SF, KI, SMo, and MF managed the patient. TU and AS performed the surgeries. All authors critically revised the report, commented on the drafts of the manuscript, and approved the final version for publication.

## ACKNOWLEDGMENTS

We thank to acknowledge all staffs who contributed to this case diagnosis, therapy, and decision-making.

## SUPPLEMENTARY MATERIAL

The Supplementary Material for this article can be found online at: https://www.frontiersin.org/articles/10.3389/fcvm.2022.915876/full#supplementary-material

## REFERENCES


1. Kamiya H, Yasuda T, Nagamine H, Sakakibara N, Nishida S, Kawasuji M, et al. Surgical treatment of primary cardiac tumors: 28 Years' experience in kanazawa university hospital. *Jpn Circ J.* (2001) 65:315–9. doi: 10.1253/jcj.65.315
2. Kawase Y, Takahashi M, Takemura H, Tomita S, Watanabe G. Surgical treatment of a bronchogenic cyst in the interatrial septum. *Ann Thorac Surg.* (2002) 74:1695–7. doi: 10.1016/s0003-4975(02)03863-8
3. Maier HC. Bronchiogenic cysts of the mediastinum. *Ann Surg.* (1948) 127:476–502. doi: 10.1097/00000658-194803000-00010
4. Suen HC, Mathisen DJ, Grillo HC, LeBlanc J, McLoud TC, Moncure AC, et al. Surgical management and radiological characteristics of bronchogenic cysts. *Ann Thorac Surg.* (1993) 55:476–81. doi: 10.1016/0003-4975(93)91022-f
5. Kobza R, Oechslin E, Jenni R. An intrapericardial bronchogenic cyst. *Interact Cardiovasc Thorac Surg.* (2003) 2:279–80. doi: 10.1016/s1569-9293(03)00044-6
6. Gutiérrez GS, Gutiérrez FG, Bastianelli GA, Vaccarino GN. Bronchogenic cyst in an unusual location. *Asian Cardiovasc Thorac Ann.* (2021) 29:44–6. doi: 10.1177/0218492320960271
7. Simonetti S, Canalís E, Macías L, Carrasco MA. Clinico-pathological features of the intradiaphragmatic bronchogenic cysts: report of a case and review of the literature. *Pathologica.* (2018) 110:116–20.
8. Itoh H, Shitamura T, Kataoka H, Ide H, Akiyama Y, Hamasuna R, et al. Retroperitoneal bronchogenic cyst: report of a case and literature review. *Pathol Int.* (1999) 49:152–5. doi: 10.1046/j.1440-1827.1999.00837.x
9. Jiang H, Wang H, Wu H, Li X. Bronchogenic cyst of the interatrial septum. *J Cardiothorac Surg.* (2013) 8:171. doi: 10.1186/1749-8090-8-171
10. Luo Y, Chen D, Yang X. Bronchogenic cyst in the right atrium: a case report. *Asian J Surg.* (2022) 45:1162–64. doi: 10.1016/j.asjsur.2021.12.072
11. St-Georges R, Deslauriers J, Duranceau A, Vaillancourt R, Deschamps C, Beauchamp G, et al. Clinical spectrum of bronchogenic cysts of the mediastinum and lung in the adult. *Ann Thorac Surg.* (1991) 52:6–13. doi: 10.1016/0003-4975(91)91409-o
12. Yuda S, Nakatani S, Yutani C, Yamagishi M, Kitamura S, Miyatake K. Trends in the clinical and morphological characteristics of cardiac myxoma: 20-year experience of a single tertiary referral Center in Japan. *Circ J.* (2002) 66:1008–13. doi: 10.1253/circj.66.1008
13. da Silveira WL, Nery MW, Soares EC, Leite AF, Nazzetta H, Batista MA, et al. Lipoma of the right atrium. *Arq Bras Cardiol.* (2001) 77:361–8. doi: 10.1590/s0066-782x2001001000006
14. Fyke FE III, Seqard JB, Edwards WD, Miller FA Jr., Reeder GS, Schattenberg TT, et al. Primary cardiac tumors: experience with 30 consecutive patients since the introduction of two-dimensional echocardiography. *J Am Coll Cardiol.* (1985) 5:1465–73. doi: 10.1016/s0735-1097(85)80364-8
15. Gowda RM, Khan IA, Nair CK, Mehta NJ, Vasavada BC, Sacchi TJ. Cardiac papillary fibroelastoma: a comprehensive analysis of 725 cases. *Am Heart J.* (2003) 146:404–10. doi: 10.1016/s0002-8703(03)00249-7
16. Khayata M, Alkharabsheh S, Shah NP, Klein AL. Pericardial cysts: a contemporary comprehensive review. *Curr Cardiol Rep.* (2019) 21:64. doi: 10.1007/s11886-019-1153-5
17. Shenoy C, Grizzard JD, Shah DJ, Kassi M, Reardon MJ, Zagurovskaya M, et al. Cardiovascular magnetic resonance imaging in suspected cardiac tumour: a multicentre outcomes study. *Eur Heart J.* (2021) 43:71–80. doi: 10.1093/eurheartj/ehab635
18. Giusca S, Kelle S, Korosoglou G. When tissue and outcomes are the issue. cardiac magnetic resonance for patients with suspected cardiac tumours. *Eur Heart J.* (2021) 43:81–3. doi: 10.1093/eurheartj/ehab625
19. Lateef N, Kuniyoshi J, Latif A, Ahsan MJ, Shaikh K, DeVrieze B, et al. Cardiac Tamponade as a complication of bronchogenic cyst. *Proc (Bayl Univ Med Cent).* (2020) 34:172–4. doi: 10.1080/08998280.2020.1795594
20. Miwa E, Tani T, Okada Y, Furukawa YA. Rare cardiac tumor: bronchogenic cyst of interatrial septum. *Echocardiography.* (2017) 34:474–5. doi: 10.1111/echo.13445
21. Sarper A, Ayten A, Golbasi I, Demircan A, Isin E. Bronchogenic cyst. *Tex Heart Inst J.* (2003) 30:105–8.
22. Liu HS, Li SQ, Cao ZL, Zhang ZY, Ren H. Clinical features and treatment of bronchogenic cyst in adults. *Chin Med Sci J.* (2009) 24:60–3. doi: 10.1016/s1001-9294(09)60061-4
23. Han SJ, Cho HJ, Kang MW, Yu JH, Na MH, Kang SK. A life-threatening bronchogenic cyst. *Korean J Thorac Cardiovasc Surg.* (2018) 51:69–71. doi: 10.5090/kjtcs.2018.51.1.69
24. Azeem F, Finlay M, Rathwell C, Awad WI. A near fatal presentation of a bronchogenic cyst compressing the left main coronary artery. *J Thorac Cardiovasc Surg.* (2008) 135:1395–6. doi: 10.1016/j.jtcvs.2007.09.082
25. Gamrekeli A, Kalweit G, Schäfer H, Huwer H. Infection of a bronchogenic cyst after ultrasonography-guided fine needle aspiration. *Ann Thorac Surg.* (2013) 95:2154–5. doi: 10.1016/j.athoracsur.2012.10.071
26. Kirmani B, Kirmani B, Sogliani F. Should asymptomatic bronchogenic cysts in adults be treated conservatively or with surgery? *Interact Cardiovasc Thorac Surg.* (2010) 11:649–59. doi: 10.1510/icvts.2010.233114
27. Fievet L, D'Journo XB, Guys JM, Thomas PA, De Lagausie P. Bronchogenic cyst: best time for surgery? *Ann Thorac Surg.* (2012) 94:1695–9. doi: 10.1016/j.athoracsur.2012.06.042
28. Foley JR, Irwin RB, Abidin N. Multimodality characterization of interatrial cyst. *J Am Coll Cardiol.* (2012) 59:2217. doi: 10.1016/j.jacc.2011.11.071
29. Shiferaw K, Lobrinus AJ, Grabherr S, Michaud K, Mangin P, Schrag B. One case, 3 rare simultaneous findings: intramyocardial bronchogenic cyst, P.H558r variant of Scn5a gene, and granular cell tumor of the esophagus. *Am J Forensic Med Pathol.* (2012) 33:335–8. doi: 10.1097/PAF.0b013e318264e9ef
30. Olsen M, Mitchell TA, Percival TJ, Helsel BS. Interatrial bronchogenic cyst resection. *Ann Thorac Surg.* (2015) 100:709–11. doi: 10.1016/j.athoracsur.2014.10.025
31. Forcillo J, Dion D, Sauvageot C, Jeanmart H. Intraventricular bronchogenic cyst: a rare congenital anomaly. *Ann Thorac Surg.* (2015) 100:1101–3. doi: 10.1016/j.athoracsur.2014.11.059
32. Grozavu C, Fera A, Iliaş M, Pantile D. Intrapericardial development of a bronchogenic cyst - case report. *Chirurgia (Bucur).* (2016) 111:345–9.
33. Wang J, Zhu Q, Liang B, Shi H, Han P, Kong X. Left ventricular bronchogenic cyst. *Ann Thorac Surg.* (2016) 101:744–6. doi: 10.1016/j.athoracsur.2015.03.083
34. Smer A, Alla VM, Abuissa H. A 50-year-old man with incidental cardiac mass. *Heart.* (2017) 103:189. doi: 10.1136/heartjnl-2016-310337
35. Shiohira S, Sasaki T, Maeda S, Kawabata M, Goya M, Hirao K. Bronchogenic cyst of the atrioventricular septum presenting with ventricular fibrillation. *HeartRhythm Case Rep.* (2017) 3:389–91. doi: 10.1016/j.hrcr.2017.05.005
36. Nishida N, Hata Y, Nomoto K. Intramyocardial bronchogenic cyst: histological appearance and a review of the literature. *Cardiovasc Pathol.* (2017) 28:64–7. doi: 10.1016/j.carpath.2017.03.005
37. Blesneac C, Horvath E, Muntean I, Benedek T, Toganel R. Intracardiac bronchogenic cyst associated with ventricular septal defect: an extremely rare feature in children. *Eur Heart J Cardiovasc Imaging.* (2018) 19:1074. doi: 10.1093/ehjci/jey078
38. Van Praet KM, Stamm C, Sündermann SH, Meyer A, Unbehaun A, Montagner M, et al. Minimally invasive cardiac surgery: removal of an interatrial intraseptal bronchogenic cyst through a periareolar approach. *Innovations (Phila).* (2018) 13:230–2. doi: 10.1097/imi.0000000000000502
39. Gimpel D, Conway J, Meikle F, Lin Z, McCormack DJ, El-Gamel A. Acute shortness of breath due to reoccurrence of an intrapericardial bronchogenic cyst. *Respirol Case Rep.* (2019) 7:e00431. doi: 10.1002/rcr2.431
40. Li Z, Xiang D, Gao L, Tan J, Zeng X. Resection of a giant bronchogenic cyst in the left atrium. *Can J Cardiol.* (2020) 36:967.e13–15. doi: 10.1016/j.cjca.2020.02.078
41. Fukada Y, Endo Y, Nakanowatari H, Kitagawa A, Tsuboi E, Irie Y. Bronchogenic cyst of the interatrial septum. *Fukushima J Med Sci.* (2020) 66:41–3. doi: 10.5387/fms.2019-29

42. Saad E, Singh P, Iskandar M. Atypical chest pain in a young woman with an interatrial bronchogenic cyst. *BMJ Case Rep.* (2021) 14:241736. doi: 10.1136/bcr-2021-241736

**Conflict of Interest:** The authors declare that the research was conducted in the absence of any commercial or financial relationships that could be construed as a potential conflict of interest.

**Publisher's Note:** All claims expressed in this article are solely those of the authors and do not necessarily represent those of their affiliated organizations, or those of the publisher, the editors and the reviewers. Any product that may be evaluated in this article, or claim that may be made by its manufacturer, is not guaranteed or endorsed by the publisher.

frontiers | Frontiers in Cardiovascular Medicine

CASE REPORT
published: 23 June 2022
doi: 10.3389/fcvm.2022.916096

# Case Report: A Rare Abdominopelvic Arteriovenous Malformation: Originating From Splenic Artery and Draining Into Portal Vein

*Xin Li[1†], Jiehua Li[1†], Mo Wang[1], Junwei Wang[1], Lunchang Wang[1], Hao He[1], Ming Li[1], Quanming Li[1] and Chang Shu[1,2*]*

[1] Department of Vascular Surgery, The Second Xiangya Hospital, Central South University, Changsha, China, [2] Center of Vascular Surgery, Chinese Academy of Medical Sciences and Peking Union Medical College, Fuwai Hospital, Beijing, China

**Background:** Abdominopelvic arteriovenous malformation is an uncommon congenital vascular lesion, for which the diagnosis and treatment are usually difficult. Though embolization and sclerotherapy are the primary treatment strategies, traditional surgical resection remains a valuable option.

**Case Presentation:** Herein, we present a 32-year-old female diagnosed with a massive abdominopelvic arteriovenous malformation that originates from the splenic artery and drains into the portal vein. The vascular lesion was evaluated with multiple imaging modalities and then surgically resected successfully. The patient was discharged post-operatively on day 6 and free of symptoms during the 12-month follow-up.

**Conclusion:** To our knowledge, the presented abdominopelvic arteriovenous malformation is the first to be reported in the literature, with such a rare condition originating from the splenic artery and draining into the portal vein.

**Keywords: abdominopelvic arteriovenous malformation, vascular malformation, splenic artery, portal vein, surgical resection**

OPEN ACCESS

***Edited by:***
*Yueqi Zhu,*
*Shanghai Jiao Tong University, China*

***Reviewed by:***
*Su Li Xin,*
*Shanghai Jiao Tong University, China*
*Hai Feng,*
*Capital Medical University, China*

****Correspondence:***
*Chang Shu*
*shuchang@csu.edu.cn*

*[†]These authors have contributed equally to this work and share first authorship*

***Specialty section:***
*This article was submitted to Cardiovascular Imaging, a section of the journal Frontiers in Cardiovascular Medicine*

***Received:*** *08 April 2022*
***Accepted:*** *25 May 2022*
***Published:*** *23 June 2022*

***Citation:***
*Li X, Li J, Wang M, Wang J, Wang L, He H, Li M, Li Q and Shu C (2022) Case Report: A Rare Abdominopelvic Arteriovenous Malformation: Originating From Splenic Artery and Draining Into Portal Vein. Front. Cardiovasc. Med. 9:916096. doi: 10.3389/fcvm.2022.916096*

## BACKGROUND

Abdominopelvic arteriovenous malformation (AVM) is an uncommon vascular lesion, for which the etiology is usually congenital, and the diagnosis and treatment are difficult. The AVM is characterized by abnormal connections between supplying arteries and draining veins (1). It may begin with an asymptomatic lesion, but often progresses over time and expands secondary to trauma or hormonal change, such as that during puberty or pregnancy (2). The symptoms range from mild discomfort to high-output cardiac failure or life-threatening hemorrhage (3). Though embolization and sclerotherapy are the primary treatment strategies, traditional surgical resection remains a valuable option (4–6).

Most pelvic AVMs are supplied by internal iliac arteries, inferior mesenteric artery, or the median sacral artery (7–9), and are often drained into iliac, pudendal, or obturator veins (10–12). However, for the current case we present here, the AVM rarely had a single feeding artery from the splenic artery and two draining veins into the portal vein, which, to our knowledge, has not been reported before. The patient was asymptomatic and physical examination revealed aberrant abdominal vascular bruits. The massive abdominopelvic AVM was evaluated with multiple imaging modalities and successfully treated with surgical resection.

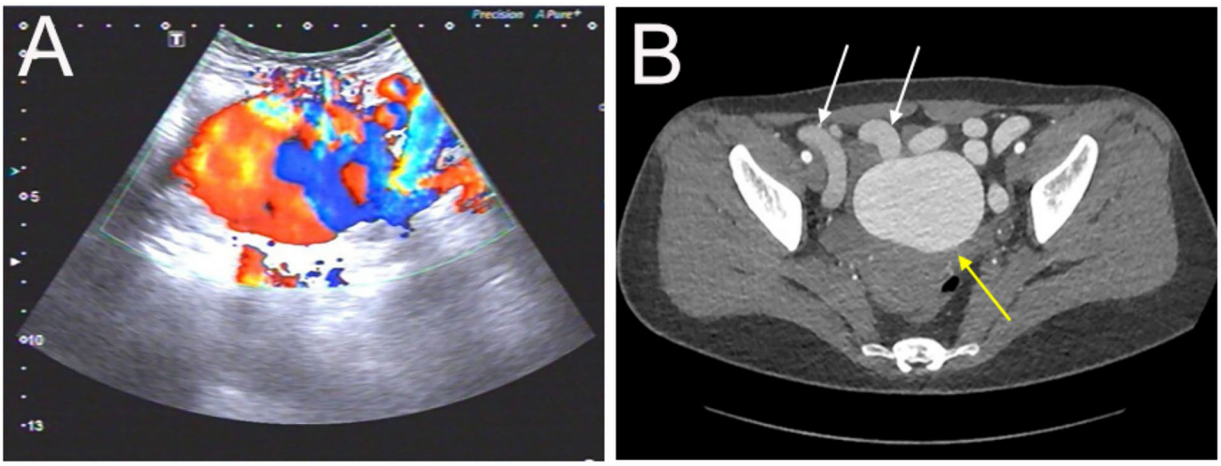


**FIGURE 1 |** Evaluation of the abdominopelvic arteriovenous malformation (AVM) with color Doppler ultrasound and CT angiography. **(A)** The ultrasound revealed a pelvic mass with an abundant blood flow signal. **(B)** The axial view of CT angiography showed the nidus of AVM (yellow arrow) and dilated outflow veins (white arrows) (the aneurysm was measured as 72 × 56 mm).

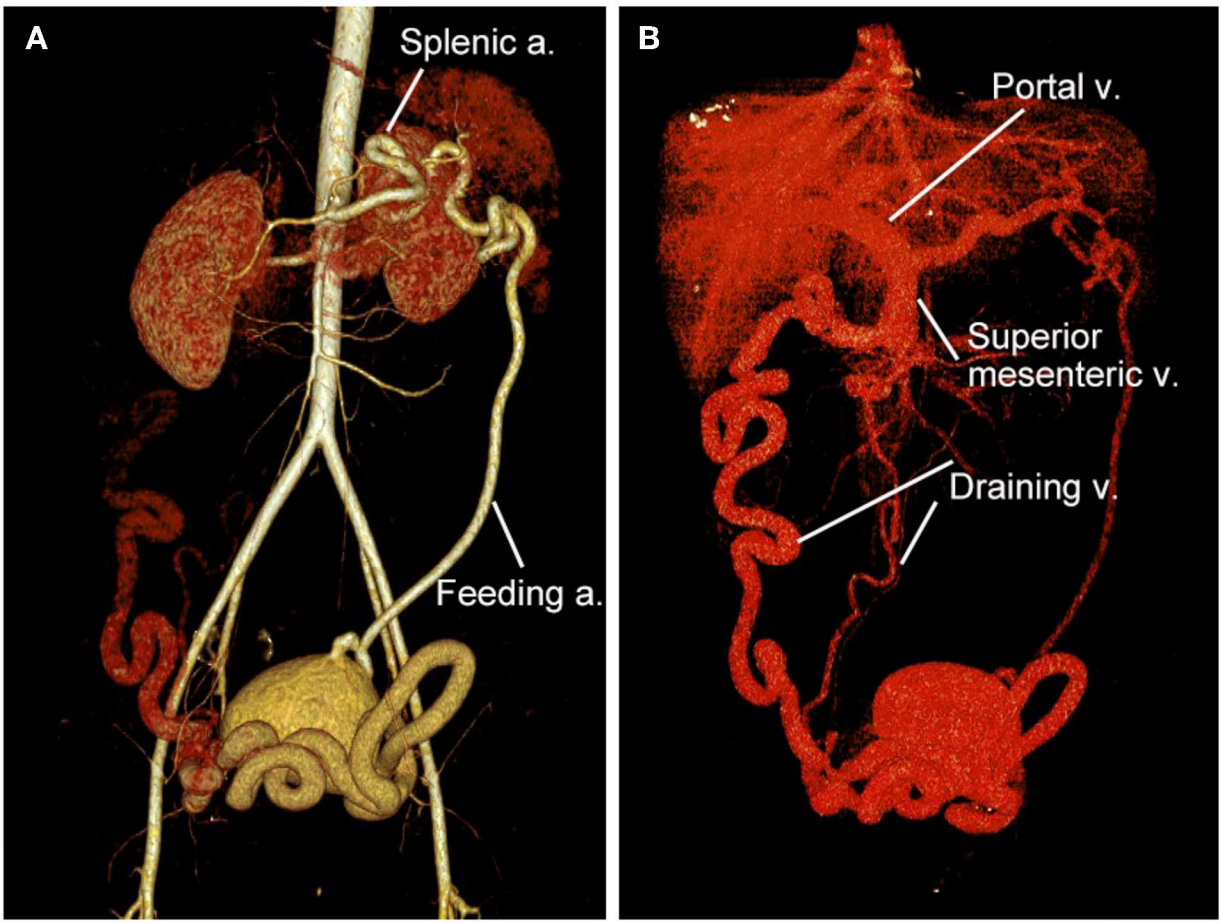


**FIGURE 2 |** 3D reconstruction of CT angiography of the abdominopelvic arteriovenous malformation (AVM). **(A)** Arterial phase of CT angiography showed the AVM had a single feeding artery originating from the splenic artery. **(B)** Venous phase of CT angiography showed the AVM had two draining veins into the superior mesenteric vein and then the portal vein.

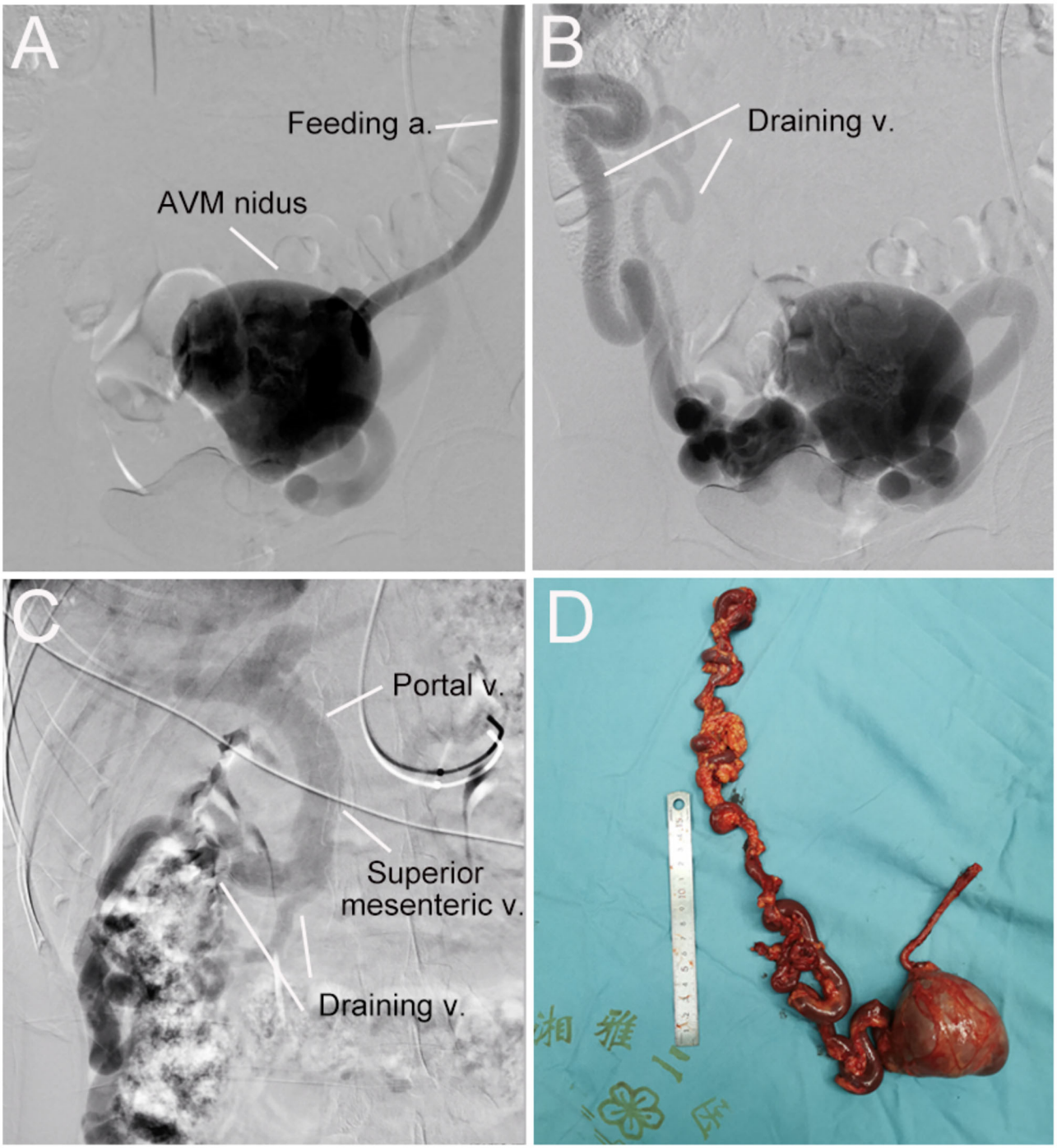


**FIGURE 3 |** Digital subtraction angiography (DSA) and resected vascular lesion of the abdominopelvic arteriovenous malformation (AVM). **(A)** DSA showed the feeding artery and AVM nidus. **(B)** DSA showed the AVM nidus and two draining veins. **(C)** DSA showed draining veins flowed into the superior mesenteric vein and then the portal vein. **(D)** the AVM lesion was surgically removed successfully.

## CASE PRESENTATION

A 32-year-old woman was admitted to our center due to the finding of a pelvic mass with hypervascularity 2 years ago. She was generally asymptomatic and had no related family history. On physical examination, her mass was not palpable, but vascular bruits could be easily auscultated on the abdomen, especially in the peri-umbilicus area. The ultrasound revealed a pelvic mass with an abundant blood flow signal (**Figure 1A**). CT angiography (CTA) showed the nidus of pelvic arteriovenous malformation

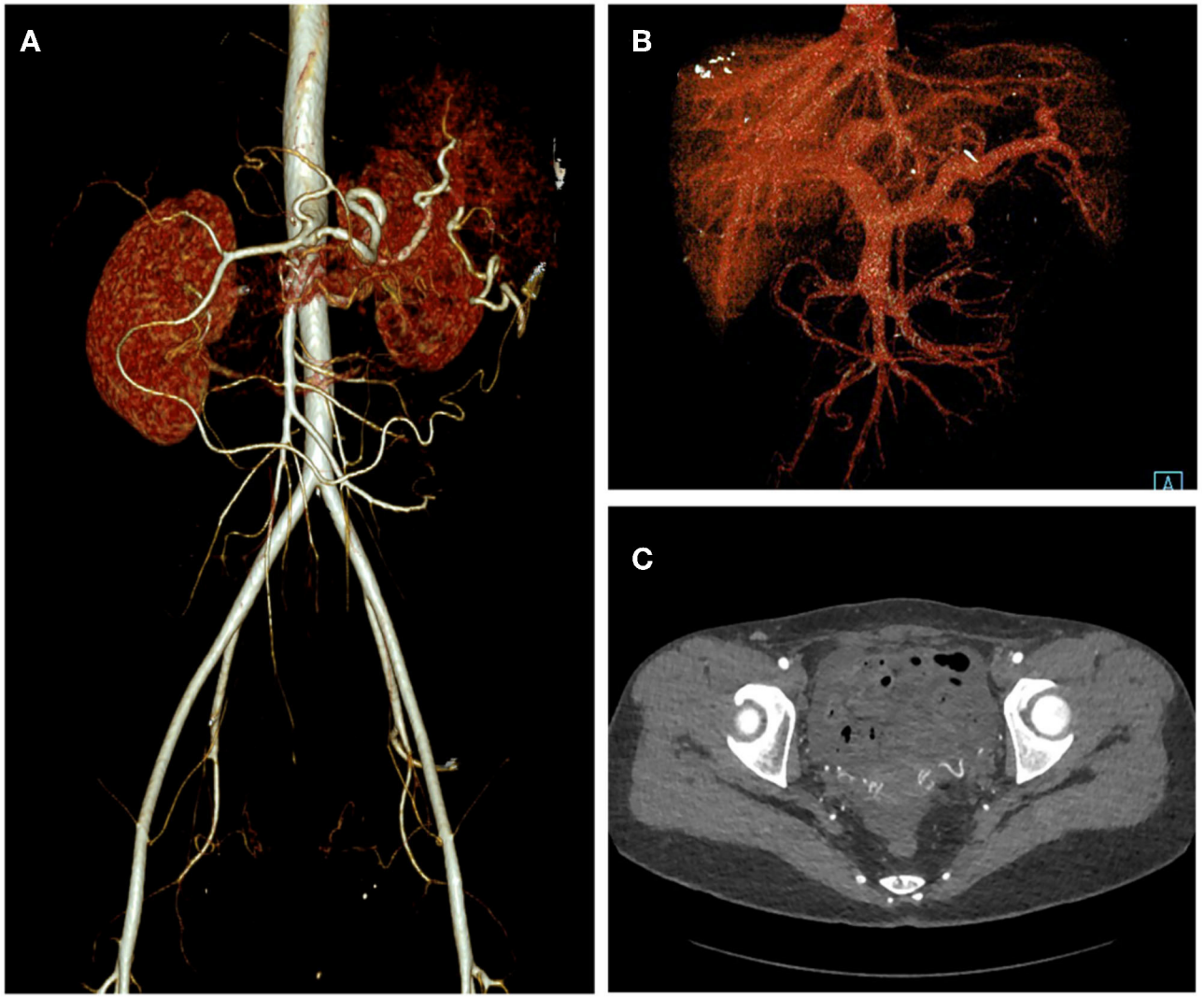


**FIGURE 4 |** One-month post-operative CT angiography of the patient. Arterial phase **(A)**, Venous phase **(B)**, and axial view **(C)** of the CT angiography showed elimination of the abdominopelvic AVM.

(AVM) and aneurysmal-dilated vessel (measured 72 × 56 mm) (**Figure 1B**). The 3D reconstruction of CTA demonstrated that the AVM had a single feeding artery originating from the splenic artery and two draining veins into the superior mesenteric vein, and then, a portal vein (**Figure 2**). Digital subtraction angiography (DSA) was used to further evaluate the AVM (**Figures 3A–C**). It was confirmed that the AVM finally drained into the portal vein and there were no other feeding arteries from bilateral internal iliac arteries (**Supplemenatry Video 1**). Considering the risk of aneurysm rupture and hemorrhage, the patient was treated with surgical resection of the AVM and ligation of the feeding artery and draining veins (**Figure 3D**). She recovered well after the operation and was discharged post-operatively on day 6. The 1-month follow-up CTA showed elimination of the abdominopelvic AVM (**Figure 4**) and the patient was doing well during the following 12 months.

## DISCUSSION AND CONCLUSION

Arteriovenous malformation (AVM) belongs to the entity of vascular malformations, which are generally classified into slow-flow (venous, capillary, and lymphatic malformation) and fast-flow malformations (arteriovenous fistula and arteriovenous malformation) (13). AVM is an uncommon medical condition and accounts for 8% of vascular malformations (14). It could appear on almost any part of the body, including the abdominal and pelvic cavity (15). The composition of a typical AVM includes feeding arteries, draining veins, and the vascular shunting bypassing the capillary bed (also called "the nidus") (3). Specifically for our case, the AVM had a feeding artery from the splenic artery, two draining veins into the portal vein, and significant dilated vascular "nidus" formed in the pelvic cavity.

Pelvic AVM may be asymptomatic in some patients, and present as a pulsatile or vascularized mass on pelvic imaging. However, AVMs often progress throughout life, and a variety of symptoms could occur, such as urinary frequency or dysuria, pelvic pain, life-threatening hemorrhage, and high-output cardiac failure. It is well-known that the growth of AVM could be stimulated by various factors, such as puberty, pregnancy, and trauma. According to the Schobinger classification system, there are typically four stages for AVM lesions: stage I (quiescent), stage II (expansive), stage III (destructive), and stage IV (cardiac decompensation) (16). The current case had a stage II pelvic AVM that was asymptomatic, but with a significantly dilated vascular lesion. She presented no signs of heart failure or portal hypertension.

The pelvic AVMs are usually first detected and evaluated by color Doppler ultrasound, which could offer an impressive overview of the lesion with hypervascularity signals (17). MR angiography and CT angiography are important diagnostic tools to visualize the feeding arteries, draining veins, and location of shunting, as well as flow dynamics (16). However, digital subtraction angiography (DSA) remains a pre-requisite for the treatment of AVMs. DSA *via* transarterial, transvenous, and sometimes direct percutaneous access could profoundly evaluate the AVM. The successful treatment of AVM depends largely on the diagnostic imaging, which needs to provide information on the location, extension, composition, vessel diameters, and hemodynamics of AVM.

Treatment of AVM is notoriously challenging, as inappropriate treatment could stimulate the AVM lesion into an aggressive growth state (18). Although an asymptomatic lesion can be observed, it is preferable to treat the AVM before it progresses. Surgical resection of AVM lesions is an effective strategy and has been regarded as the gold standard for a long period, but it carries the risk of massive bleeding, incomplete resection of the lesion, and injury to adjacent organs. In recent decades, endovascular therapy using various embolic and sclerosing materials, either alone or in a combination with surgical resection, has become a widely accepted treatment option for patients with AVMs (19, 20). However, the endovascular strategy could still lead to significant recurrence and complication rate (21). Thus, the optimal treatment of AVM should be individualized and be based on the certain condition of AVM and the experience of surgeons.

Here we presented a condition of AVM that might not have been described in the literature before, which had a massive vascular nidus in the pelvic cavity with feeding artery from splenic artery and draining veins into portal vein. The AVM was profoundly evaluated with color Doppler ultrasound, CT angiography, and catheter angiography, and it was demonstrated as a well-localized lesion that did not involve other organs or the pelvic wall. For this case, surgical resection was considered to be a superior strategy to endovascular therapy. As the AVM had relatively simple angioarchitectures without involving vital adjacent vital organs, surgical resection could provide a definite and effective treatment, while interventional therapy had the risk of incomplete or ectopic embolization.

The patient was treated successfully with surgical resection of the AVM and ligation of the feeding artery and draining veins. A major concern of the surgery was that removal of the AVM might significantly decrease the blood flow into the liver and cause ischemic liver injury. Fortunately, the patient recovered well and showed no signs of liver injury after the operation. The post-operative CTA showed no evidence of residual arteriovenous connections, and she lived uneventfully during the 12-month follow-up.

## DATA AVAILABILITY STATEMENT

The original contributions presented in the study are included in the article/**Supplementary Material**, further inquiries can be directed to the corresponding author/s.

## ETHICS STATEMENT

The studies involving human participants were reviewed and approved by the institutional Ethics boards of the Second Xiangya Hospital. The patients/participants provided their written informed consent to participate in this study.

## AUTHOR CONTRIBUTIONS

XL and JL drafted the manuscript. CS and QL designed the study. HH and ML revised the manuscript. MW, JW, and LW were responsible for the collection of data or analysis. All authors read and approved the final manuscript.

## FUNDING

This work was supported by the National Natural Science Foundation of China (grant numbers: 81870345 and 82120108005) and the Natural Science Foundation of Hunan Province, China (grant number: 2020JJ2054).

## SUPPLEMENTARY MATERIAL

The Supplementary Material for this article can be found online at: https://www.frontiersin.org/articles/10.3389/fcvm.2022.916096/full#supplementary-material

**Supplementary Video |** Digital subtraction angiography of the massive abdominopelvic arteriovenous malformation.

## REFERENCES

1. Schimmel K, Ali MK, Tan SY, Teng J, Do HM, Steinberg GK, et al. Arteriovenous malformations-current understanding of the pathogenesis with implications for treatment. *Int J Mol Sci.* (2021) 22. doi: 10.3390/ijms22169037
2. Whitehead KJ, Smith MC, Li DY. Arteriovenous malformations and other vascular malformation syndromes. *Cold Spring Harb*

*Perspect Med.* (2013) 3:a006635. doi: 10.1101/cshperspect.a006635
3. Burrows PE. Vascular malformations involving the female pelvis. *Semin Intervent Radiol.* (2008) 25:347–60. doi: 10.1055/s-0028-1102993
4. Do YS, Kim YW, Park KB, Kim DI, Park HS, Cho SK, et al. Endovascular treatment combined with embolosclerotherapy for pelvic arteriovenous malformations. *J Vasc Surg.* (2012) 55:465–71. doi: 10.1016/j.jvs.2011.08.051
5. Visser A, FitzJohn T, Tan ST. Surgical management of arteriovenous malformation. *J Plast Reconstr Aesthet Surg.* (2011) 64:283–91. doi: 10.1016/j.bjps.2010.05.033
6. Lee BB, Do YS, Yakes W, Kim DI, Mattassi R, Hyon WS. Management of arteriovenous malformations: a multidisciplinary approach. *J Vasc Surg.* (2004) 39:590–600. doi: 10.1016/j.jvs.2003.10.048
7. Jacobowitz GR, Rosen RJ, Rockman CB, Nalbandian M, Hofstee DJ, Fioole B, et al. Transcatheter embolization of complex pelvic vascular malformations: results and long-term follow-up. *J Vasc Surg.* (2001) 33:51–5. doi: 10.1067/mva.2001.111738
8. Mallios A, Laurian C, Houbballah R, Gigou F, Marteau V. Curative treatment of pelvic arteriovenous malformation-an alternative strategy: transvenous intra-operative embolisation. *Eur J Vasc Endovasc Surg.* (2011) 41:548–53. doi: 10.1016/j.ejvs.2010.11.018
9. Yamada M, Iwamoto H, Konno O, Kihara Y, Akashi I, Okihara M. Pelvic arteriovenous malformation in a kidney transplant recipient. *Kidney Int.* (2021) 100:246. doi: 10.1016/j.kint.2020.12.003
10. Cho SK, Do YS, Shin SW, Kim DI, Kim YW, Park KB, et al. Arteriovenous malformations of the body and extremities: analysis of therapeutic outcomes and approaches according to a modified angiographic classification. *J Endovasc Ther.* (2006) 13:527–38. doi: 10.1583/05-1769.1
11. Choi SY, Do YS, Lee DY, Lee KH, Won JY. Treatment of a pelvic arteriovenous malformation by stent graft placement combined with sclerotherapy. *J Vasc Surg.* (2010) 51:1006–9. doi: 10.1016/j.jvs.2009.11.036
12. Murakami K, Yamada T, Kumano R, Nakajima Y. Pelvic arteriovenous malformation treated by transarterial glue embolisation combining proximal balloon occlusion and devascularisation of multiple feeding arteries. *BMJ Case Rep.* (2014) 2014. doi: 10.1136/bcr-2013-203492
13. Wassef M, Blei F, Adams D, Alomari A, Baselga E, Berenstein A, et al. Vascular anomalies classification: recommendations from the international society for the study of vascular anomalies. *Pediatrics.* (2015) 136:e203–14. doi: 10.1542/peds.2014-3673
14. Adams DM, Brandao LR, Peterman CM, Gupta A, Patel M, Fishman S, et al. Vascular anomaly cases for the pediatric hematologist oncologists-an interdisciplinary review. *Pediatr Blood Cancer.* (2018) 65. doi: 10.1002/pbc.26716
15. Christenson BM, Gipson MG, Smith MT. Pelvic vascular malformations. *Semin Intervent Radiol.* (2013) 30:364–71. doi: 10.1055/s-0033-1359730
16. Sadick M, Muller-Wille R, Wildgruber M, Wohlgemuth WA. Vascular anomalies (part I): classification and diagnostics of vascular anomalies. *Rofo.* (2018) 190:825–35. doi: 10.1055/a-0620-8925
17. Jain KA, Gerscovich EO. Sonographic spectrum of pelvic vascular malformations in women. *J Clin Ultrasound.* (1999) 27:523–30. doi: 10.1002/(sici)1097-0096(199911/12)27:9<523::aid-jcu6>3.0.co;2-6
18. Lee BB, Lardeo J, Neville R. Arterio-venous malformation: how much do we know? *Phlebology.* (2009) 24:193–200. doi: 10.1258/phleb.2009.009032
19. Lee BB, Baumgartner I, Berlien HP, Bianchini G, Burrows P, Do YS, et al. Consensus document of the international union of angiology (IUA)-2013. Current concept on the management of arterio-venous management. *Int Angiol.* (2013) 32:9–36.
20. Muller-Wille R, Wildgruber M, Sadick M, Wohlgemuth WA. Vascular anomalies (part II): interventional therapy of peripheral vascular malformations. *Rofo.* (2018). doi: 10.1055/s-0044-101266
21. Kim R, Do YS, Park KB. How to treat peripheral arteriovenous malformations. *Korean J Radiol.* (2021) 22:568–76.doi: 10.3348/kjr.2020.0981

**Conflict of Interest:** The authors declare that the research was conducted in the absence of any commercial or financial relationships that could be construed as a potential conflict of interest.

frontiers | Frontiers in Cardiovascular Medicine

CASE REPORT
published: 28 June 2022
doi: 10.3389/fcvm.2022.928192

# Case Report: An Unusual Presentation of Cardiovascular Involvement in Eosinophilic Granulomatosis With Polyangiitis

*Yajuan Li*[1,2], *Hui Zhou*[1,2*], *Yaou Zhou*[3] *and Haixiong Tang*[1,4]

[1] *Department of Radiology, Xiangya Hospital Central South University, Changsha, China,* [2] *National Clinical Research Center for Geriatric Disorders, Xiangya Hospital Central South University, Changsha, China,* [3] *Department of Rheumatology and Immunology, Xiangya Hospital Central South University, Changsha, China,* [4] *Department of Radiology, The Fourth People's Hospital of Chenzhou, Chenzhou, China*

**Background:** Because eosinophilic granulomatosis with polyangiitis (EGPA) is so rare and the symptoms so varied, it can be a challenge to get a correct diagnosis in clinical practice. Cardiovascular involvement is the main cause of death of EGPA. We are the first to report of cardiac magnetic resonance (CMR) findings about right-sided heart involvement in EGPA.

**Patient Findings:** The initial abnormalities detected by CMR were Löffler endocarditis with extensive thrombosis and left ventricular (LV) dysfunction. After active treatment, LV systolic function recovered and endocarditis with thrombosis significantly improved, but there was rapidly progressive pulmonary hypertension, enlargement of right atrium and right ventricle and persistent right-sided heart failure. The patient eventually died of sudden cardiac death 6 months after hospital discharge.

**Conclusions:** Löffler endocarditis and right-sided heart involvement are both rare presentations in patients with EGPA. CMR is a reliable non-invasive tool to precisely and comprehensively assess cardiovascular involvement in EGPA.

**Keywords: eosinophilic granulomatosis with polyangiitis, Löffler endocarditis, thrombosis, pulmonary hypertension, right-sided heart failure, cardiac magnetic resonance imaging**

OPEN ACCESS

***Edited by:***
*Ali Yilmaz,*
*University Hospital Münster, Germany*

***Reviewed by:***
*Luca Arcari,*
*M.G. Ospedale Vannini, Italy*
*Liqing Peng,*
*West China Fourth Hospital of Sichuan University, China*

***Correspondence:**
*Hui Zhou*
*huistanzhou@csu.edu.cn*

***Specialty section:***
*This article was submitted to Cardiovascular Imaging, a section of the journal Frontiers in Cardiovascular Medicine*

***Received:*** *25 April 2022*
***Accepted:*** *07 June 2022*
***Published:*** *28 June 2022*

***Citation:***
*Li Y, Zhou H, Zhou Y and Tang H (2022) Case Report: An Unusual Presentation of Cardiovascular Involvement in Eosinophilic Granulomatosis With Polyangiitis. Front. Cardiovasc. Med. 9:928192. doi: 10.3389/fcvm.2022.928192*

## INTRODUCTION

Eosinophilic granulomatosis with polyangiitis (EGPA) is a systemic necrotizing vasculitis of small- and medium-size vessels, characterized by extravascular granulomas, eosinophilia, and tissue infiltration by eosinophils of multiple organs, including heart, lungs, skin, gastrointestinal tract, kidneys, and peripheral nerves (1). Cardiac involvement in EGPA is associated with a poor prognosis and high mortality. Therefore, early diagnosis and treatment are essential to prevent the acceleration of cardiac involvement in patients with EGPA (1, 2). We describe a rare case of EGPA characterized by involvement of heart and pulmonary artery.

## CASE PRESENTATION

A 44-year-old female patient presented to our hospital with a 1-month history of dizziness, fatigue, chest tightness, and shortness of breath. She also had ecchymosis of the lower legs. The patient presented with a 10-year history of asthma, sinusitis, and nasal polyps (**Figure 1D**). Electrocardiograph (ECG) demonstrated QS waves in leads V2-V3, ST segment depression in leads V5-V6, and T-wave inversion. Blood pressure was 90/62 mmHg, pulse was 112 beats/minute. Laboratory findings (**Table 1**) showed increase in the percentage of eosinophils (47.8%), erythrocyte sedimentation rate (ESR) (32 mm/H), C-Reactive protein (CRP) (24.70 mg/L), N-terminal pro-B-type natriuretic peptide (NT-proBNP) (12,045 pg/mL), and troponin I (1.760 ng/mL). Diagnostic work up revealed negative anti-nuclear antibodies (ANA), ANCA, anti-MPO antibodies, and rheumatoid factor. The patient's renal function was normal and there was no evidence of blood infection. Diffusion-weighted imaging of the brain magnetic resonance imaging (MRI) revealed multiple acute cerebral infarctions (**Figure 1C**) with no obvious cerebrovascular stenosis on magnetic resonance angiography (MRA) (**Figure 1H**). Chest CT and Cardiac magnetic resonance (CMR) localizing images showed multiple patchy consolidations of both lungs and bilateral pleural effusion (**Figures 1A,B**). After completing a series of examinations and multi-disciplinary discussions, the patient met the inclusion criteria of the American College of Rheumatology 1990 criteria for the classification of EGPA (3). Transthoracic echocardiography showed numerous deposits in the mural left ventricular (LV) endocardium, obliteration of the apical portion of the left ventricle, enlarged left atrium, moderate pulmonary hypertension [the estimated systolic pulmonary artery pressure (eSPAP) was 46 mmHg] and a small pericardial effusion. $^{18}$F-FDG PET-CT showed accumulation of FDG in the lungs and myocardium. CMR was used to assess the cardiovascular involvement which was performed on a 3.0 T MRI at 8 days after admission, confirming Löffler endocarditis (endocardial thickening, edema and enhancement) with LV thrombus on cine, perfusion, and LGE images (**Figures 2A–F**, **Supplementary Videos 1–6**), LV volume enlargement and mildly reduced LV systolic function, normal right ventricular volume, and function (**Table 2**, **Supplementary Videos 1–4**).

Eosinophils reduced to normal (**Table 1**) and her symptoms gradually improved after treatment according to the 2015 EGPA Consensus Task Force recommendations (4). Chest CT showed that the diffuse lesions of both lungs were absorbed, and the pleural effusion was reduced after the treatment. Unfortunately, the patient was readmitted for dyspnea, bilateral lower limb edema and systemic ecchymosis after 10 months. Transthoracic echocardiography showed deposits in the mural LV endocardium were significantly reduced, the LV diameter returned to normal but greater diameter of right atrium (RA) and right ventricle (RV) with moderate-to-severe regurgitation of tricuspid valve and pulmonary valve, severe pulmonary hypertension (eSPAP was 71 mmHg). CMR imaging was performed again, showing enlargement of RA and RV (**Table 2**, **Figure 2J**, **Supplementary Videos 9–12**), significantly improved endocardial enhancement and overlying thrombus on cine, perfusion and LGE images (**Figures 2G–L**, **Supplementary Videos 7–12**), remarkably reduced RV systolic function but improvement of LV systolic function (**Table 2**, **Supplementary Videos 7–10**), new strip-like LGE in the lateral wall (**Figure 2L**), representing replacement fibrosis and increased diameters of pulmonary trunk from 28 mm to

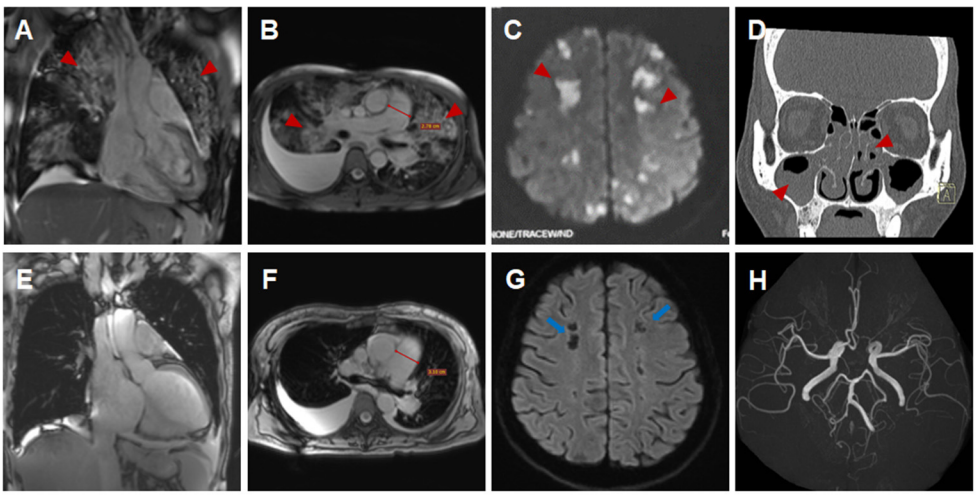


**FIGURE 1 |** Imaging findings of eosinophilic granulomatosis with polyangiitis **(A–D,H)** Imaging findings during the initial hospitalization (**A,D**, coronal view; **B,C,H**, transverse view). Multiple patchy consolidations of both lungs (**A,B**, triangular arrows) on CMR images, multiple acute cerebral infarctions (**C**, triangular arrows) with no obvious cerebrovascular stenosis (**H**, triangular arrows) on brain MR images and sinusitis and nasal polyps (**D**, triangular arrows) on reconstructed CT images. **(E–G)** Imaging findings during the subsequent hospitalization (**E**, coronal view; **F,G**, transverse view). Significantly absorbed multiple lesions of both lungs (**E,F**), the pulmonary hypertension with increased diameters of pulmonary trunk from 28 mm **(B)** to 32 mm **(F)** and multiple encephalomalacia (**G**, long arrows).

**TABLE 1 |** Laboratory findings during two separate hospitalizations.

| | The percentage of eosinophils | ESR | CRP | NT-proBNP | Troponin I |
|---|---|---|---|---|---|
| The initial admission | 47.8% | 32 mm/H | 24.70 mg/L | 12,045.00 pg/mL | 1.760 ng/mL |
| The initial discharge | 1.0% | 111 mm/H | 64.30 mg/L | 4,072.07 pg/mL | 0.020 ng/mL |
| The subsequent admission | 1.1% | 5 mm/H | 1.72 mg/L | 4,472.00 pg/mL | 0.020 ng/mL |
| The subsequent discharge | 0.7% | 7 mm/H | 5.11 mg/L | 5,451.00 pg/mL | 0.030 ng/mL |
| Reference range | 0.4–8.0% | 0–26 mm/H | 0–8.00 mg/L | <125 pg/mL | <0.040 ng/mL |

*ESR, erythrocyte sedimentation rate; CRP, C-Reactive protein; NT-proBNP, N-terminal pro-B-type natriuretic peptide.*

**TABLE 2 |** Comparison of CMR results during two separate hospitalizations.

| | The initial CMR | The subsequent CMR | Reference range |
|---|---|---|---|
| LVEF (%) | 46 | 60 | 57–81 |
| LVEDVI (mL/m2) | 70 | 75 | 51–95 |
| LVESVI (mL/m2) | 38 | 27 | 11–35 |
| RVEF (%) | 53 | 24 | 50–78 |
| RVEDVI (mL/m2) | 62 | 137 | 42–118 |
| RVESVI (mL/m2) | 29 | 105 | 6–54 |
| LA (cm2) | 21 | 22 | <24 |
| RA (cm2) | 15 | 32 | <23 |

*LVEF, left ventricular ejection fraction; LVEDVI, left ventricular end-diastolic volume indexed; LVESVI, left ventricular end-systolic volume indexed; RVEF, right ventricular ejection fraction; RVEDVI, right ventricular end-diastolic volume indexed; RVESVI, right ventricular end-systolic volume indexed; LA, left atrium; RA, right atrium.*

32 mm (**Figures 1B,F**). Multiple lesions of both lungs were significantly absorbed (**Figures 1E,F**) and encephalomalacia were formed (**Figure 1G**). Despite the patient received intensive immunosuppressive treatment combing glucocorticoid and immunosuppressant (cyclophosphamide) and aggressive anti-heart failure therapy, the symptoms of right-sided heart failure were not completely relieved and sudden cardiac death occurred 6 months after hospital discharge.

## DISCUSSION

Although EGPA belongs to the spectrum of ANCA-associated vasculitis, <50% of patients with EGPA are ANCA positive (1). Cardiac involvement occurs in approximately 15–60% of EGPA patients and can present as pericarditis, myocarditis, acute heart failure, acute myocardial infarction, valvular heart disease, and especially those who are ANCA negative (1, 2, 5). Löffler endocarditis is present in 50–60% hypereosinophilic syndrome (HES), but rarely reported in patient with EGPA (6). Through the literature search, there is no report of EGPA patient involving the right-sided heart so far.

For the evaluation of cardiac involvements, the unique advantage of CMR lies in the comprehensive evaluation of cardiac volume, function, and myocardial tissue characterization.

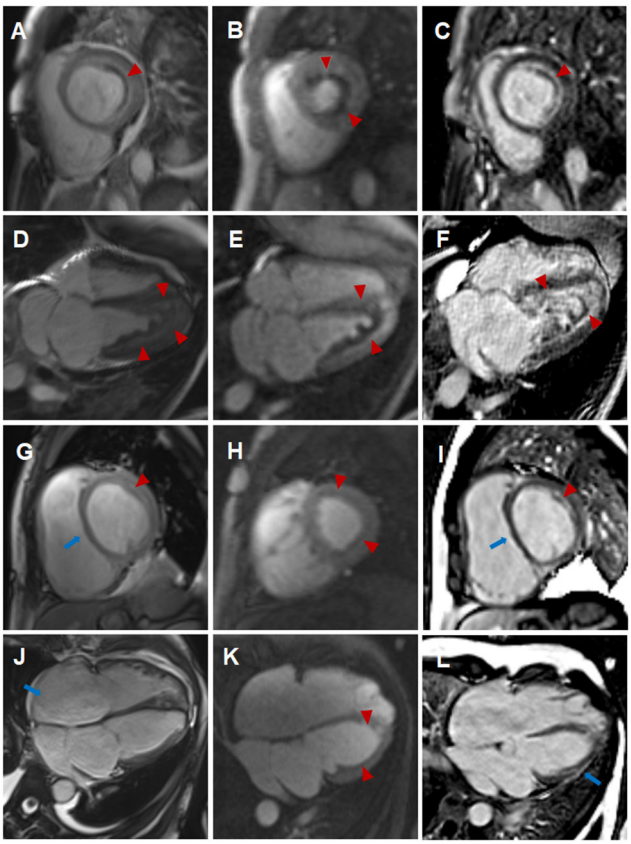


**FIGURE 2 |** Comparison of cardiovascular involvement detected by CMR during two separate hospitalizations **(A–F)** CMR findings during the initial hospitalization (**A–C**, short-axis view; **D–F**, four-chamber view). Distinct high-signal-intensity plane separating the thrombus from underlying myocardium on end-diastolic cine images (**A,D**, triangular arrows), endocardial surface hypoperfusion zone on perfusion images (**B,E**, triangular arrows) and endocardial enhancement and overlying non-enhancing thrombus on LGE images (**C,F**, triangular arrows). **(G–L)** CMR findings during the subsequent hospitalization (**G–I**, short-axis view; **J–L**, four-chamber view). Enlargement of right atrium and right ventricle, flat ventricular septum (**G,J**, long arrows) and significantly reduced high-signal-intensity plane and thrombus (**G,J**, triangular arrows) on cine images, significantly reduced endocardial surface hypoperfusion zone on perfusion images (**H,K**, triangular arrows) and significantly thinning endocardial enhancement and overlying thrombus (**I,L**, triangular arrows), new strip-like LGE in the lateral wall (**L**, long arrows) on LGE images, representing replacement fibrosis.

The initial abnormalities of this case detected by CMR were Löffler endocarditis with extensive thrombosis in LV and LV dysfunction. After treatment, pulmonary lesions and endocarditis with thrombosis were significantly improved, with LV systolic function recovered, but pulmonary hypertension rapidly progressed and right-sided heart enlargement and right-sided heart failure emerged. Pilania et al. (7) also reported that pulmonary arterial hypertension is a rare occurrence in ANCA-associated vasculitis. Löffler endocarditis of HES or EGPA progresses through three stages, namely acute necrotic stage (infiltration of eosinophils in the myocardium), thrombotic stage (mural thrombi formation along the damaged endocardium), and fibrotic stage (the granulation tissue changing into hyaline fibrosis), which may overlap (2, 8). Myocardial fibrosis may develop rapidly and immediate aggressive treatment may help to slow the progression of chronic heart failure (8–10). Right-sided heart failure can be a consequence of left ventricular dysfunction; however, Fitchett et al. (11) believed that right ventricular failure might in certain circumstances develop either before or after left ventricular failure when there is a diffuse myocardial disease. Therefore, we hypothesize that emerging right-sided heart failure of this patient could be induced by the combined effect of progressive and refractory pulmonary hypertension caused by pulmonary vasculitis and the diffuse myocardial damage. T1 and T2 mappings are new parametric quantitative sequences, which provide tissue-specific T1 and T2 values. Puntmann et al. (12) believed that T1 and T2 mappings may support non-invasive recognition of cardiac involvement and activity of myocardial inflammation. Cereda et al. (13) reported that CMR parameters of interstitial fibrosis including native T1 and extracellular volume fraction (ECV) were significantly more elevated in patients with EGPA in clinical remission compared to healthy subjects. Lagan et al. (14) also found that stable EGPA was associated with focal replacement (non-ischemic LGE) and diffuse interstitial myocardial fibrosis (elevated native T1 and ECV), but myocardial T2 and capillary permeability were no different in EGPA compared to control. Since the initial scanning machine was not equipped with mapping sequences, T1 and T2 mappings were underwent during the subsequent hospitalization and elevated native T1, ECV and normal T2 were found, which was consistent with the results of previous studies (13, 14).

Because EGPA is so rare and the symptoms so varied, it can be a challenge to get a correct diagnosis in clinical practice. EGPA with <50% ANCA positive can also easily be misdiagnosed as HES due to incomplete history collection. However, chief manifestations of cardiovascular involvement and therapeutic schedule of HES and EGPA are quite different (15). EGPA patients often present with pericarditis, myocarditis, valvular heart disease, restrictive cardiomyopathy and acute myocardial infarction from vasculitic pathology of coronary artery, while Löffler endocarditis is the common cardiac performance of HES. Corticosteroid therapy remains first drug of choice in both HES and EGPA, immunosuppressant (e.g., cyclophosphamide) should be added in EGPA patients with cardiac involvement.

There are still some limitations of this study. The histological examination of tissue biopsies of the lungs and the heart cannot be performed due to the high risk of thrombus shedding and more cases are needed to further validate our findings.

## CONCLUSION

Right-sided heart involvement is extremely rare in EGPA, but may be associated with a poor prognosis. CMR is a reliable non-invasive way to precisely and comprehensively assess cardiac volume, function, and myocardial tissue characterization. In this regard, we highly recommend CMR as initial and follow-up diagnostic tool to evaluate cardiovascular involvements for all the patients with EGPA.

## DATA AVAILABILITY STATEMENT

The original contributions presented in the study are included in the article/**Supplementary Material**, further inquiries can be directed to the corresponding author.

## ETHICS STATEMENT

The studies involving human participants were reviewed and approved by the Ethics Committee of the Xiangya Hospital of Central South University. The patients/participants provided their written informed consent to participate in this study. Written informed consent was obtained from the individual(s) for the publication of any potentially identifiable images or data included in this article.

## AUTHOR CONTRIBUTIONS

All authors listed have made a substantial, direct, and intellectual contribution to the work and approved it for publication.

## FUNDING

The Natural Science Foundation of Hunan Province (2021JJ31131), China.

## ACKNOWLEDGMENTS

The authors would like to acknowledge all who contributed to this case diagnosis, therapy and decision-making.

## SUPPLEMENTARY MATERIAL

The Supplementary Material for this article can be found online at: https://www.frontiersin.org/articles/10.3389/fcvm.2022.928192/full#supplementary-material

## REFERENCES


1. Liu S, Guo L, Zhang Z, Li M, Zeng X, Wang L, et al. Cardiac manifestations of eosinophilic granulomatosis with polyangiitis from a single-center cohort in China: clinical features and associated factors. *Ther Adv Chronic Dis.* (2021) 12:2040622320987051. doi: 10.1177/20406223209 87051
2. Wu EY, Hernandez ML, Jennette JC, Falk RJ. Eosinophilic Granulomatosis with Polyangiitis: Clinical Pathology Conference and Review. *J Allergy Clin Immunol Pract.* (2018) 6:1496–504. doi: 10.1016/j.jaip.2018.07.001
3. Masi AT, Hunder GG, Lie JT, Michel BA, Bloch DA, Arend WP, et al. The American college of rheumatology 1990 criteria for the classification of Churg-Strauss syndrome (allergic granulomatosis and angiitis). *Arthritis Rheum.* (1990) 33:1094–100. doi: 10.1002/art.1780330806
4. Groh M, Pagnoux C, Baldini C, Bel E, Bottero P, Cottin V, et al. Eosinophilic granulomatosis with polyangiitis (Churg-Strauss) (EGPA) Consensus Task Force recommendations for evaluation and management. *Eur J Intern Med.* (2015) 26:545–53. doi: 10.1016/j.ejim.2015.04.022
5. Watanabe K, Yamochi W, Oshitani T, Taniguchi H. Low-dose corticosteroid therapy improves refractory coronary vasospasm accompanied by eosinophilic granulomatosis with polyangiitis. *J Cardiol Cases.* (2021) 23:69–72. doi: 10.1016/j.jccase.2020.09.008
6. Ogbogu PU, Rosing DR, Horne MK 3rd. Cardiovascular manifestations of hypereosinophilic syndromes. *Immunol Allergy Clin North Am.* (2007) 27:457–75. doi: 10.1016/j.iac.2007.07.001
7. Pilania RK, Dhawan SR, Mathew JL, Singh S, Sodhi KS, Singh M. ANCA-associated vasculitis presenting as severe pulmonary hypertension and right heart failure. *Indian J Pediatr.* (2017) 84:799–801. doi: 10.1007/s12098-017-2379-0
8. Karthikeyan K, Balla S, Alpert MA. Non-infectious aortic and mitral valve vegetations in a patient with eosinophilic granulomatosis with polyangiitis. *BMJ Case Rep.* (2019) 12:e225947. doi: 10.1136/bcr-2018-225947
9. Ito T, Fujita SI, Kanzaki Y, Sohmiya K, Hoshiga M. Eosinophilic Granulomatosis with Polyangiitis (EGPA) with an unusual manifestation of mid-ventricular obstruction caused by endocardial thrombus. *Am J Case Rep.* (2018) 19:1197–203. doi: 10.12659/AJCR. 910861
10. Ferreira RM, Madureira P, Pinho T, Martins E, Pimenta S, Costa L. Silent acute myocarditis in eosinophilic granulomatosis with polyangiitis. *Acta Reumatol Port.* (2018) 43:309–13.
11. Fitchett DH, Sugrue DD, MacArthur CG, Oakley CM. Right ventricular dilated cardiomyopathy. *Br Heart J.* (1984) 51:25–8. doi: 10.1136/hrt.51.1.25
12. Puntmann VO, Isted A, Hinojar R, Foote L, Carr-White G, Nagel E. T1 and T2 mapping in recognition of early cardiac involvement in systemic sarcoidosis. *Radiology.* (2017) 285:63–72. doi: 10.1148/radiol.2017162732
13. Cereda AF, Pedrotti P, De Capitani L, Giannattasio C, Roghi A. Comprehensive evaluation of cardiac involvement in eosinophilic granulomatosis with polyangiitis (EGPA) with cardiac magnetic resonance. *Eur J Intern Med.* (2017) 39:51–6. doi: 10.1016/j.ejim.2016.09.014
14. Lagan J, Naish JH, Fortune C, Bradley J, Clark D, Niven R. et al. Myocardial involvement in eosinophilic granulomatosis with polyangiitis evaluated with cardiopulmonary magnetic resonance. *Int J Cardiovasc Imaging.* (2021) 37:1371–81. doi: 10.1007/s10554-020-02091-1
15. Jin X, Ma C, Liu S, Guan Z, Wang Y, Yang J. Cardiac involvements in hypereosinophilia-associated syndrome: case reports and a little review of the literature. *Echocardiography.* (2017) 34:1242–6. doi: 10.1111/echo.13573


**Conflict of Interest:** The authors declare that the research was conducted in the absence of any commercial or financial relationships that could be construed as a potential conflict of interest.

frontiers | Frontiers in Cardiovascular Medicine

CASE REPORT
published: 06 July 2022
doi: 10.3389/fcvm.2022.905344

# Percutaneous Retrieval of Left Atrial Appendage Closure Devices in Patients With Atrial Fibrillation: A Case Report

*Saihua Wang[1†], Juhua Zhang[2†], Shuwen Hao[1†], Luoning Zhu[1], Zhongping Ning[1*] and Zhihong Zhao[1*]*

[1] Department of Cardiology, Shanghai University of Medicine and Health Sciences Affiliated Zhoupu Hospital, Shanghai, China, [2] Department of Social Medicine and Health Career Management, School of Public Administration, Fudan University, Shanghai, China

OPEN ACCESS

**Edited by:**
*Ali Yilmaz,*
*University Hospital Münster, Germany*

**Reviewed by:**
*Christian Hendrik Heeger,*
*University Heart Center Luebeck, Germany*
*Muharrem Akin,*
*Hannover Medical School, Germany*
*Binhao Wang,*
*Ningbo First Hospital, China*

***Correspondence:**
*Zhongping Ning*
*ningzhongping88@163.com*
*Zhihong Zhao*
*zhihong_zhao@pku.org.cn*

*† These authors have contributed equally to this work*

**Specialty section:**
*This article was submitted to Cardiovascular Imaging, a section of the journal Frontiers in Cardiovascular Medicine*

**Received:** *27 March 2022*
**Accepted:** *30 May 2022*
**Published:** *06 July 2022*

**Citation:**
*Wang S, Zhang J, Hao S, Zhu L, Ning Z and Zhao Z (2022) Percutaneous Retrieval of Left Atrial Appendage Closure Devices in Patients With Atrial Fibrillation: A Case Report. Front. Cardiovasc. Med. 9:905344. doi: 10.3389/fcvm.2022.905344*

Left atrial appendage closure (LAAC) devices can be inadvertently released into unfavorable locations, which may allow them to migrate to a different position within the left atrial appendage or embolize from the heart into the aorta. In such instances, it can be challenging to remove the LAAC device. Here, we present two cases in which patients with atrial fibrillation experienced LAAC device exposure at an inappropriate site because of interventional operator error and device mismatch: (a) the LAAC device was dislodged into the aortic arch and retrieved percutaneously from the femoral artery route, and (b) in the left atrium, which was dislodged into the left atrium and retrieved *via* atrial transseptal puncture of the femoral vein.

**Keywords: atrial fibrillation, dislodgment, left atrial appendage closure, complications, retrieval**

## INTRODUCTION

Atrial fibrillation (AF) is one of the most common cardiac arrhythmias. Patients with AF are at high risk of ischemic stroke and require long-term or even life-long anticoagulation therapy. The left atrial appendage (LAA) is the site most prone to thrombosis in patients with AF. LAA occluders are not only an alternative method of anticoagulation therapy, but also a contraindication for oral anticoagulation, and several occluders, including those made in China, have been used in clinical practice (1). The device detachment after left atrial appendage closure (LAAC) has a low incidence rate but carries a fatal risk. Herein, we report two cases of LAAC device detachment in which the LAAC devices were removed *via* the percutaneous femoral artery or femoral vein retrieval. We also analyzed the possible treatment strategies following a review of the available literature.

## CASE DESCRIPTION

**Case 1** involved a 69-year-old male patient with a history of persistent AF, hypertension, diabetes, cerebral embolism, and transient ischemic attack for > 10 years. The patient had a history of taking warfarin but had self-discontinued the medication. Transthoracic echocardiography revealed the following findings: left atrium (LA), 44 mm; left ventricle (LV) end-systole, 46 mm; LV end-diastolic, 55 mm; LV ejection fraction, 58%; mitral calcification with minimal regurgitation; and minimal aortic regurgitation. Both the $CHA_2DS_2$-VASc and HAS-BLED scores

were 6 points. LA computed tomography angiography (CTA) excluded LA thrombus. The patient underwent a combination of catheter ablation and LAAC in a single procedure. Transesophageal echocardiography (TEE) measured an LAA ostial of 25–30 mm and an effective depth of 28 mm (**Figure 1A**). Digital subtraction angiography (DSA) measured the LAA opening as 28 mm and the depth as 31 mm (**Figure 1B**). The Watchman 33-mm device (Boston Scientific, Marlborough, MA, United States) was released, with a compression ratio of 15–24% and no residual peri-device leak (**Figure 1C**), then proceeded to complete AF pulmonary vein isolation ablation. After returning to the ward, the patient developed a cough and shortness of breath. Bedside echocardiography did not show the LAA occluder, and a chest CT scan revealed that the occluder was in the aortic arch (**Figure 1D**). A 5-French (Fr) Tig angiography catheter (Terumo Corporation, Tokyo, Japan) was sent through the radial artery to the aortic arch for relative fixation of the occluder. Next, the 5-Fr pigtail angiography catheter was sent through the 6-Fr sheath of the left femoral artery to the right femoral artery puncture site to delineate to ensure that the puncture site was located in the middle of the femoral artery. After a successful puncture of the right femoral artery, two ProGlide vascular staplers (Abbott, Chicago, IL, United States) were pre-set at the puncture site. A Watchman guide system 16-Fr sheath (Boston Scientific) was sent under the occluder through the femoral artery, and a 7-Fr guide catheter was sent through the sheath to the occluding umbrella. Next, the Amplatzer gooseneck snare, a 20 or 40-mm mesh basket guidewire (Medtronic, Minneapolis, MN, United States), was caught and covered. The occluder was pulled down to the descending aorta. Then, the 2.4-mm × 20-cm Raptor grasping device (Raptor US Endoscopy, Mentor, OH, United States) was advanced through the 16-Fr sheath into the LA to clamp the trabeculae of the umbrella. After intrathecal injection of ice-cold 0.9% saline, the vascular sheath was pushed, the occluding umbrella was recovered into the sheath (**Figures 1E,F**), and the Watchman occluder was removed (**Figure 1G**). When the vascular sheath was withdrawn, the femoral artery was sutured with ProGlide at the puncture site of the femoral artery. Then, the patient was returned to the ward safely, and LAAC was performed again 5 months later. In this later surgery, the 33-mm Watchman was placed, and DSA and TEE confirmed that the Watchman device was properly positioned (**Figures 1H–J**). The compression ratio was 15–20%, and there was no residual leakage. The postoperative follow-up re-examination of TEE was normal. Six months later, a chest CT showed that the LAA occluder was in a good position (**Figure 1K**).

**Case 2** involved an 86-year-old male patient with a history of persistent AF for 3 years and an implanted pacemaker because of bradyarrhythmia for 6 years. His $CHA_2DS_2$-VASc score was 5 points, and his HAS-BLED score was 2 points. After cryoablation, LAAC was performed, in which the diameter of the LAA opening as measured by TEE was 18.3–22 mm and the anchoring zone was 16.5–24.4 mm (**Figure 2A**). The LAA showed a chicken wing shape. The diameter of the opening of the LAA as measured by DSA was 28.6 mm, and the anchoring area was 31.5 mm (**Figure 2C**). A Lacbes 2834 device was delivered (**Figure 2D**). TEE showed that the shoulder of the fixed column was mildly exposed, and the residual shunt at the upper edge was 4.3 mm, which was within the allowable range. The occluder was slowly released after pulling it steadily (**Figure 2B**). After returning to the ward, the patient had no chest tightness or shortness of breath, but he did complain of drowsiness, and his blood pressure dropped to 58/41 mmHg, with a heart rate of 60 beats/min. Subsequently, dopamine 20 mg was administered intravenously while increasing the rate of fluid replacement to maintain blood pressure. Bedside echocardiography showed that the occluder had drifted in the LA, and the possibility of the occluder detaching was considered. Emergency LAA occlusion umbrella capture was performed under general anesthesia with endotracheal intubation and ventilator-assisted breathing. Under DSA, the occluder was seen floating in the LA (**Figure 2E**). The atrial septal puncture was performed twice through the right femoral vein route. Two 14-Fr cryoablation steerable sheaths were sent to the LA. A pigtail catheter (Terumo) was delivered across the mitral valve to prevent the occluder from crossing the mitral valve and traveling into the LV. The Raptor grasping device and pigtail catheters were sent through another sheath, and the latter was used to attempt to fix the occluder in an appropriate position, i.e., coaxial alignment of the jaws of the Raptor grasping device to the center of the Lacbes disc. Once the disc was grasped, sustained traction initially dislodged the proximal disc from the LA, and the occluder was pulled back to the sheath (**Figures 2F–H**); then, the Lacbes 2636 device was placed in the LAA (**Figures 2I,J**). After discharge, warfarin was used to control the international normalized ratio (INR) to 2–3. Results of the 3-month postoperative follow-up re-examination of TEE were normal. Long-term oral administration of clopidogrel antiplatelet drugs was enacted. During the follow-up period, the patient's quality of life was good, and persistent follow-up will be conducted.

## DISCUSSION

The LAA is the most common site of atrial thrombus in AF (2). LAAC is a viable strategy for stroke risk reduction in patients with non-valvular AF who can tolerate systemic oral anticoagulation therapy but are unsuitable candidates for long-term anticoagulation (3). Occluder detachment is one of the most serious complications of LAAC. Complications have been reported in the ASAP study, which included thoracotomy and percutaneous interventional methods (4, 5). Most occluder detachments occur during the perioperative period but can also happen any time from hospital discharge to 1 year later (6, 7). LAA detachment is usually asymptomatic unless the patient is hemodynamically affected; for example, in our case 2, the occluder fell into the LA and hung on the mitral valve, resulting in a drop in blood pressure. If the occluder lodges in the mitral valve or aortic valve, it may lead to sudden death.

We described two cases of percutaneous retrieval of dislodged LAAC devices from the LA and aorta through the femoral artery and femoral vein routes, respectively. In case 1, after LAAC, the ablation catheter was touched and the occluder fell out of the LAA

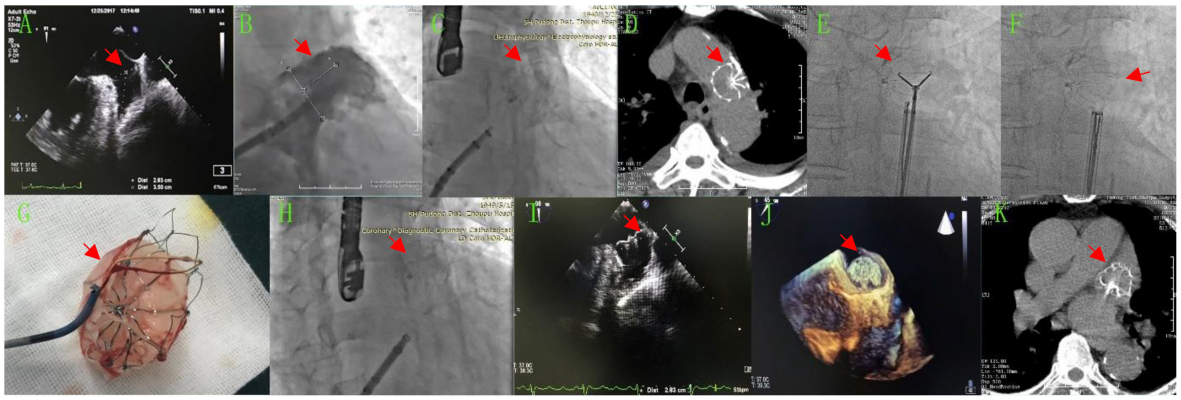

**FIGURE 1 |** After LAAC, the occluder fell off into the aortic arch and was feathered out, before the 33-mm Watchman device was occluded again. **(A,I,J)** LA TEE images. **(A)** Preoperative LAA: ostial of 25–30 mm and an effective depth of 28 mm. **(I,J)** Two-dimensional and 3-dimensional images after the second closure with the Watchman device. **(B,C,E,F,H)** DSA images. **(B)** Preoperative LAA with an opening of 28 mm and a depth of 31 mm. **(C)** After occlusion with the 33-mm Watchman device. **(E,F)** Endoscopic Raptor forceps were used to clamp the umbrella trabeculae and drag it into the sheath. **(H)** Second closure with the Watchman device. **(D,K)** Chest CT image. **(D)** Occluder in the aortic arch. **(K)** LAAC with the Watchman device. **(G)** Modified occluder.

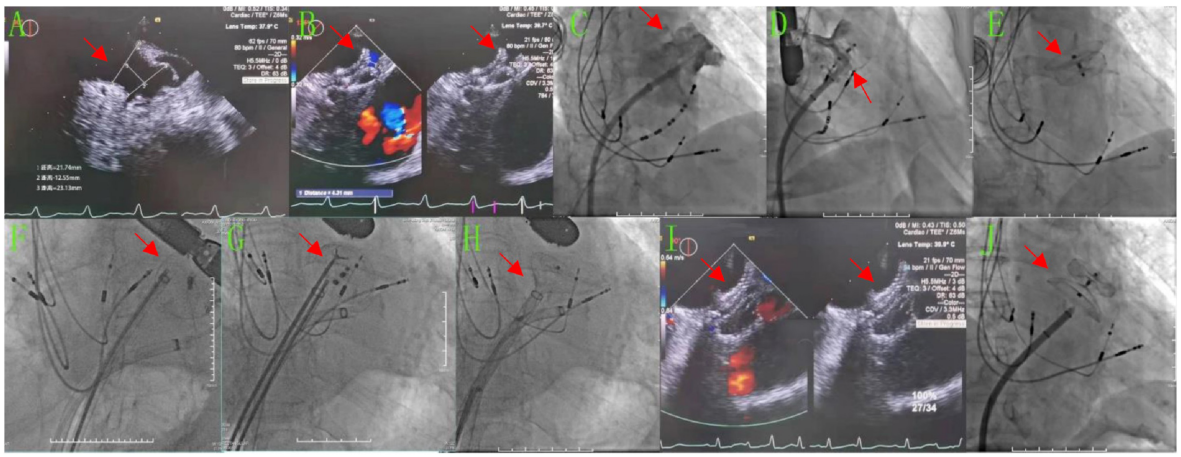

**FIGURE 2 |** After LAAC, the occluder detached into the LA and was retrieved, before the Lacbes 2834 device was occluded again. **(A,B,I)** TEE images. **(A)** Preoperatively, the diameter of the LAA opening was 18.3–22 mm and the diameter of the anchoring area was 16.5–24.4 mm. **(B)** The Lacbes 2834 was placed in LAA, the fixed column was exposed, and the residual shunt at the upper edge was 4.3 mm. **(I)** After the second LAAC procedure with Lacbes 2636, the covering disc adhered well and had no residual shunt. **(C–H,J)** DSA images. **(C)** Preoperatively, the diameter of the LAA change opening was 28.56 mm and the diameter of the anchoring area was approximately 31.47 mm. **(D)** After closure with the Lacbes 2834 device. **(E)** The Lacbes fell into the LA. **(F–H)** Endoscopic Raptor forceps were used to clamp the umbrella trabeculae and drag them into the sheath. **(J)** After the second LAAC procedure with the Lacbes 2636 device.

during pulmonary vein isolation. In case 2, after cryoablation, LAAC was performed, and because the selected occluder size is small for the LAA, it fell out of the LAA. The Raptor grasping device was designed by gastroenterologists for retrieving foreign bodies, which has a hybrid jaw configuration that combines alligator and rat tooth capabilities into a single device, increasing its gripping ability. Its design played a key role in tightly grabbing and withdrawing the devices in our cases. However, caution is recommended while engaging the LAAC device due to the risk of vascular wall damage from inadvertently grasping the vascular wall; in this series, 14-Fr and 16-Fr sheaths provided a large enough lumen and support to accommodate full device retrieval.

The findings of the concrete analysis of 18 cases of LAA occluder detachment published from 2013 to 2021 (4, 6–17) are as follows: the duration of occluder detachment occurs from the day the patient is discharged to 1 year later; among these patients, 70% are asymptomatic, while 30% have hemodynamic instability, arrhythmia, and cerebral infarction. Reasons for occluder detachment include the variable shape of the LAA, the fixed type of occluder, the unsuitability of the occluder for the LAA, and no clear reason. The positions where the occluder falls off include the aorta (32%), the LV (29%), and the LA (25%), and looseness in the LAA also contributes to occluder detachment (14%), which can cause mitral valve damage, hemodynamic instability, or ventricular arrhythmia. The following procedures can be performed simultaneously: thoracotomy to remove the LAA occluder, aortic valve replacement, mitral valve replacement or repair, atrial fibrillation (AF) Maze surgery or ablation, and

LAA resection or suture or clipping. The occluder can be percutaneously retrieved from the LA cavity, LAA, or the LV cavity, and even from the aorta. When percutaneous retrieval is expected to be difficult, surgical retrieval should be actively considered (3).

The materials used for percutaneous retrieval of occluders include a 14-Fr cryoablation Agilis sheath, 16-Fr LAA occluder introducer sheath, and 4-Fr Agilis sheath for mitral valve clipping (MitraClip; Abbott), or 27-Fr sheath used for wireless pacemaker (Micra; Medtronic). The capture devices include the gooseneck snare, Ensnare (Merit Medical Inc., South Jordan, UT, United States), a self-made capture device, or Raptor grasping device. It should be noted that the iatrogenic patent foramen ovale was caused by percutaneous retrieval of the occluder through the fossa ovalis.

In conclusion, we herein reported two case studies of LAA occluder detachment where the occluder dislodged and drifted in the aortic arch in one case and the LA in the other. Both occluders were successfully retrieved *via* a femoral artery or femoral vein route, respectively. The causes, characteristics, and removal methods of the LAA occluder were summarized by combining our cases with those reported previously.

## DATA AVAILABILITY STATEMENT

The original contributions presented in this study are included in the article/**Supplementary Material**, further inquiries can be directed to the corresponding author/s.

## ETHICS STATEMENT

The studies involving human participants were reviewed and approved by the China Medical University. The patients/participants provided their written informed consent to participate in this study. Written informed consent was obtained from the individual(s) for the publication of any potentially identifiable images or data included in this article.

## AUTHOR CONTRIBUTIONS

ZZ participated in research design and data acquisition and analysis. SH, SW, JZ, and ZZ participated in the writing of the manuscript. JZ, LZ, and ZN participated in the performance of the research. All authors have read and approved the manuscript.

## FUNDING

This work was supported by the Shanghai Pudong Top-level Clinical Discipline Fund Project (PWYgf2021-04), the Shanghai Key Medical Specialty Program Construction Fund (ZK2019B25), Shanghai Pudong Science and Technology Development Fund (Pkj2021-y33), and the Shanghai Pudong Health Committee Key Sub-Specialized Construction Fund (PWZY2020-08).

## ACKNOWLEDGMENTS

We thank LetPub (www.letpub.com) for its linguistic assistance during the preparation of this manuscript.

## SUPPLEMENTARY MATERIAL

The Supplementary Material for this article can be found online at: https://www.frontiersin.org/articles/10.3389/fcvm.2022.905344/full#supplementary-material

## REFERENCES

1. He B, Jiang LS. [A brief discussion: the impact of "2019 Chinese society of cardiology (CSC) expert consensus statement on left atrial appendage closure in the prevention of stroke in patients with atrial fibrillation" on the evolution of technical development of LAAC in China]. *Zhonghua Xin Xue Guan Bing Za Zhi.* (2021) 49:212–6. doi: 10.3760/cma.j.cn112148-20210131-00113
2. Schotten U, Verheule S, Kirchhof P, Goette A. Pathophysiological mechanisms of atrial fibrillation: a translational appraisal. *Physiol Rev.* (2011) 91:265–325. doi: 10.1152/physrev.00031.2009
3. Chinese Society of Cardiology of Chinese Medical Association, Editorial Board of Chinese Journal of Cardiology. [2019 Chinese society of cardiology (CSC) expert consensus statement on left atrial appendage closure in the prevention of stroke in patients with atrial fibrillation]. *Zhonghua Xin Xue Guan Bing Za Zhi.* (2019) 47:937–55. doi: 10.3760/cma.j.issn.0253-3758.2019.12.002
4. Gupta P, Szczeklik M, Selvaraj A, Lall KS. Emergency surgical retrieval of a migrated left atrial appendage occlusion device. *J Card Surg.* (2013) 28:26–8. doi: 10.1111/jocs.12038
5. Reddy VY, Mobius-Winkler S, Miller MA, Neuzil P, Schuler G, Wiebe J, et al. Left atrial appendage closure with the Watchman device in patients with a contraindication for oral anticoagulation: the ASAP study (ASA plavix feasibility study with Watchman left atrial appendage closure technology). *J Am Coll Cardiol.* (2013) 61:2551–6. doi: 10.1016/j.jacc.2013.03.035
6. Turagam MK, Neuzil P, Dukkipati SR, Petru J, Skalsky I, Weiner MM, et al. Percutaneous retrieval of left atrial appendage closure devices with an endoscopic grasping tool. *JACC Clin Electrophysiol.* (2020) 6:404–13. doi: 10.1016/j.jacep.2019.11.015
7. Martinez-Lopez D, de Villarreal Soto JE, Mosquera VMO, Gil AF. Emergency surgical retrieval of a migrated LAmbre device through the mitral valve. *Eur J Cardiothorac Surg.* (2021) 60:1475–6. doi: 10.1093/ejcts/ezab342
8. Nunes A, Pissarra D, Tavares Silva M, Almeida PB, Silva JC, Maciel MJ. Embolization of a left atrial appendage closure device. *Rev Port Cardiol (Engl Ed).* (2021) 40:247–8. doi: 10.1016/j.repc.2019.12.010
9. Maan A, Turagam MK, Dukkipati SR, Reddy VY. Percutaneous extraction of a migrated WATCHMAN device after seven months. *J Innov Card Rhythm Manag.* (2021) 12:4572–4. doi: 10.19102/icrm.2021.120701
10. Lubis AC, Iqbal M, Munawar DA, Hartono B, Munawar MA. Simple percutaneous retrieval technique for an embolized Watchman left atrial appendage closure device in the thoracic aorta using a homemade snare. *Int Heart J.* (2021) 62:1153–5. doi: 10.1536/ihj.20-790
11. Tschishow WN, Israel CW. [Dislodgement of a left atrial appendage occluder : step-by-step management by retrograde extraction with a "home-made snare" and two sheaths]. *Herzschrittmacherther Elektrophysiol.* (2020) 31:430–3. doi: 10.1007/s00399-020-00726-3
12. Sun X, Hong D, Liu H, Li H. Acute mitral valve injury following percutaneous left atrial appendage occlusion: a case report and literature review. *Heart Surg Forum.* (2020) 23:E743–5. doi: 10.1532/hsf.3157

13. Takayuki G, Grimmig O, Soren J, Dirk F. Asymptomatic dislocation of a Watchman left atrial appendage occluder. *Asian Cardiovasc Thorac Ann.* (2019) 27:394–5. doi: 10.1177/0218492318805620
14. El-Gabry M, Shehada SE, Wendt D, Mourad F. Emergent surgical removal of a migrated left atrial appendage occluder. *Eur J Cardiothorac Surg.* (2018) 54:191–2. doi: 10.1093/ejcts/ezy005
15. Sanhoury M, Fassini G, Dello Russo A, Lumia G, Bartorelli A. Early dislodgment and migration of a left atrial appendage closure device. *Am J Cardiol.* (2017) 120:1905–7. doi: 10.1016/j.amjcard.2017.07.077
16. Lee OH, Lee H, Kim JS. Successful retrieval of a dislodged left atrial appendage closure device. *JACC Cardiovasc Interv.* (2017) 10:98–100. doi: 10.1016/j.jcin.2016.10.044
17. Pisani P, Sandrelli L, Fabbrocini M, Tesler UF, Medici D. Left-atrial-appendage occluder migrates in an asymptomatic patient. *Tex Heart Inst J.* (2014) 41:443–4. doi: 10.14503/THIJ-13-3173

**Conflict of Interest:** The authors declare that the research was conducted in the absence of any commercial or financial relationships that could be construed as a potential conflict of interest.

frontiers | Frontiers in Cardiovascular Medicine

CASE REPORT
published: 13 July 2022
doi: 10.3389/fcvm.2022.942808

# Case Report: A Huge Calabash Heart: A Rare Case of Supracardiac Total Anomalous Pulmonary Venous Return

*Jianjun Tang*[1†], *Zhihong Wu*[1†], *Jia He*[1], *Qingdan Hu*[1], *Jun Yao*[2], *Lin Hu*[1], *Shenghua Zhou*[1] *and Mingxian Chen*[1*]

[1] *The Second Xiangya Hospital of Central South University, Changsha, China,* [2] *Hongjiang First Hospital of Traditional Chinese Medicine, Huaihua, China*

A 46-year-old woman was admitted to the cardiovascular department because of a 3-month history of palpitations and exertional dyspnea. She had a history of a successful pregnancy at a very young age. The chest radiograph presented a "calabash" configuration. Echocardiogram discovered a large atrial septal defect with a suspected pulmonary vein abnormality. Cardiac CT revealed supracardiac total anomalous pulmonary venous return, whereby, all the pulmonary veins drain into a vertical vein and, finally, to the superior vena cava. Cardiac catheterization was consistent with anomalous pulmonary venous drainage without pulmonary hypertension. Finally, she underwent a successful surgical repair and appeared asymptomatic before her discharge.

**Keywords: heart, congenital heart disease, supracardiac total anomalous pulmonary venous return, structural heart disease, enlargement**

OPEN ACCESS

***Edited by:***
*Ali Yilmaz,*
*University Hospital Münster, Germany*

***Reviewed by:***
*Florian Bönner,*
*Heinrich Heine University of Düsseldorf, Germany*
*Patrick Doeblin,*
*German Heart Center Berlin, Germany*

***Correspondence:**
*Mingxian Chen*
*xymignxianchen@csu.edu.cn*

*[†] These authors have contributed equally to this work*

***Specialty section:***
*This article was submitted to Cardiovascular Imaging, a section of the journal Frontiers in Cardiovascular Medicine*

***Received:*** *13 May 2022*
***Accepted:*** *13 June 2022*
***Published:*** *13 July 2022*

***Citation:***
*Tang J, Wu Z, He J, Hu Q, Yao J, Hu L, Zhou S and Chen M (2022) Case Report: A Huge Calabash Heart: A Rare Case of Supracardiac Total Anomalous Pulmonary Venous Return. Front. Cardiovasc. Med. 9:942808. doi: 10.3389/fcvm.2022.942808*

## INTRODUCTION

Total anomalous pulmonary venous return (TAPVR) is a rare congenital heart defect. Anatomically, TAPVR is caused by the failure of connection between the left atrium and the common pulmonary vein, while resulting in persisting communication between the pulmonary and systemic veins (1). The incidence of TAPVR is 0.05 to 0.09 per 1,000 live births accounting for only 1.5% of children with congenital heart disease. Patients with TAPVR are usually symptomatic at a very young age, and a few 7% of them without surgical correction can survive into adulthood (2). Herein, we reported an adult patient with TAPVR who underwent a successful surgical repair.

## CASE PRESENTATION

A 46-year-old woman was presented to our hospital with a history of palpitations and exertional dyspnea for 3 months. She was incidentally found to have a heart murmur during cough treatment at a local hospital in December 2019. However, she did not look for further inspection. Palpitations were correlated with an atrial flutter on Holter monitoring. She was referred to our hospital for further cardiac assessment and management.

Physical examination showed a blood pressure of 105/68 mmHg in the left arm, a heart rate of 106 bpm, and oxygen saturation of 96–98% under room air between the upper and lower limbs. Her jugular venous pulsations were normal. Auscultation revealed that her lungs were clean. A cardiac examination found a right ventricular heave, but no thrills. Cardiac auscultation revealed normal heart sounds, with no added sounds. There was no hepatomegaly, peripheral clubbing, or edema.

## INVESTIGATIONS

Chest radiograph showed an increased cardiothoracic ratio at.95 with no evidence of heart failure. It found that both lung fields and costophrenic angles are clear. The cardiac enlargement resembles a "calabash" configuration (**Figure 1**). The mediastinum is widened in relation to the heart border.

A cardiac CT scan was performed to further present the anomalous PV and to check any remaining pulmonary venous drainage into the left atrium. Three-dimensional images further delineated the supracardiac TAPVR in coronal view (**Figure 2A**) and sagittal view (**Figure 2B**). It shows that there were several pulmonary veins draining separately into the collecting vein. The collecting vein, located above the left atrium, ascended, and formed a dilated vertical vein. The vertical vein drained into the SVC by a dilated left innominate vein was observed. Other CT findings include no pulmonary venous obstruction, a large ASD, and cardiomegaly with the dilated right ventricular forming the right lateral heart border.

Cardiac catheterization was subsequently performed, which revealed common drainage of pulmonary veins into a collecting vein. This vein ascended and formed a left innominate vein and finally drained into the SVC (**Figure 3**). Hemodynamic data were obtained as follows: femoral artery pressure was 74/48 mm Hg, main pulmonary artery pressure was 28/9 (11) mm Hg, right ventricular (RV) pressure was 31/2 (11) mm Hg, and left atrium pressure was 11/4 (7) mm Hg. Oxygen saturation from arterial blood gas was 96% under room air. The calculated pulmonary vascular resistance (PVR) was.87 wood unit. The pulmonary blood flow was 20.76 L/min, while the systemic blood flow was 2.93 L/min.

Her ECG showed atrial flutter at a rate of 141 bpm. Her QRS axis was 120°, and there was a right bundle branch with a QRS duration of 100 ms.

Transthoracic echocardiography presented a left innominate vein connected to the superior vena cava and formed an abnormal connection-supracardiac TAPVR. It was found in large

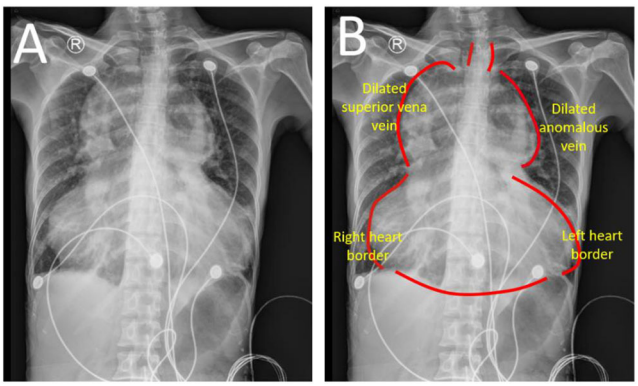


**FIGURE 1 |** Chest radiograph **(A,B)**. A huge "calabash" heart presented as appearance according to chest radiograph. The mediastinum is obviously in relation to heart border. TAPVR, total anomalous pulmonary venous return.

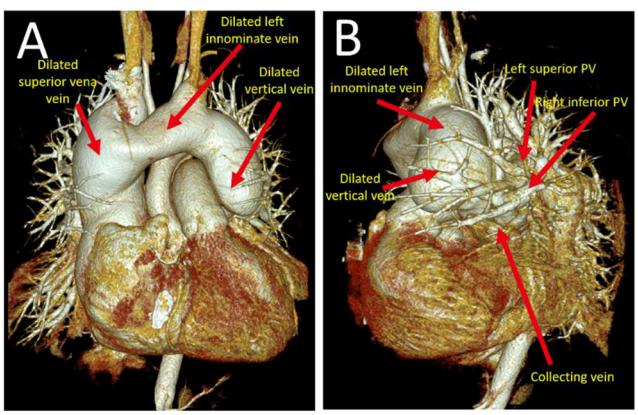


**FIGURE 2 |** A three-dimensional cardiac CT scan further delineated the supracardiac TAPVR in coronal view **(A)** and sagittal view **(B)**. Pulmonary veins drained into a collecting vein. Later followed by left upper pulmonary vein to form an anomalous dilated vertical vein which eventually drains into left innominate vein and superior vena cava. TAPVR, total anomalous pulmonary venous return.

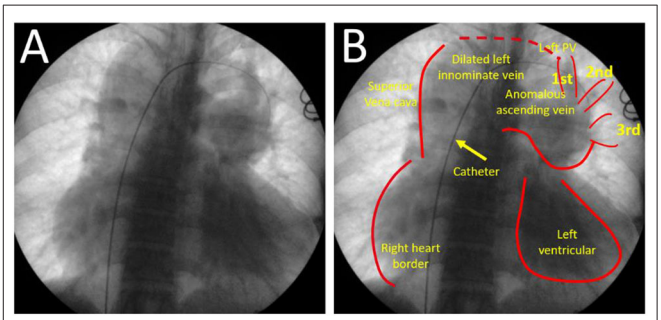


**FIGURE 3 |** Cardiac catheter angiogram **(A,B)** from femoral vein approach. It presented pulmonary veins drained into the collecting vein, and then join to form an anomalous vertical vein into left innominate vein and superior vena cava.

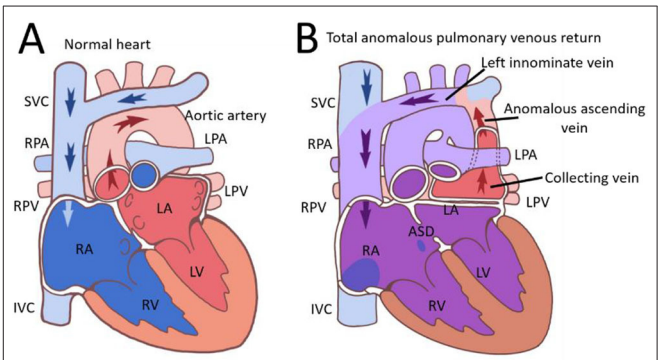


**FIGURE 4 |** Images of normal heart **(A)** and supracardiac TAPVR **(B)** were presented. ASD, atrial septal defect; IVC, superior vena cava; LA, left atrium; LPA, left pulmonary artery; LPV, left pulmonary vein; LV, left ventricular; RPA, right pulmonary artery; RPV, right pulmonary vein; SVC, superior vena cava; TAPVR, total anomalous pulmonary venous return.

right chambers, a small left side of the heart, and the common pulmonary vein behind the left atrium at the two-dimensional view of the parasternal long axis. Color Doppler found a flow from the common pulmonary vein to the superior vena cava through a vertical vein and left the innominate vein at the two-dimensional view of the suprasternal axis.

The patient was referred to our hospital for surgical repair. She underwent a successful surgical correction of TAPVC and atrial septal defect (ASD) closure. At the procedure, she was diagnosed with supracardiac TAPVC and found excessively dilated SVC, innominate vein, and right heart chamber. The pulmonary artery was larger than the aorta (ratio = 2.5:1). The large ASD was measured at 31 × 22 mm diameter and the vertical vein was at 22 × 26 mm diameter. The LA was connected to the PV confluence through the anastomosis. A patching material has been used to close the large ASD. The patient immediately presented pulmonary edema after surgery but was relieved a few days later after medical treatment. The patient was discharged well on the sixth postoperative day. No palpitations and exertional dyspnea during the half-year follow-up.

## DISCUSSION

Total anomalous pulmonary venous return (TAPVC) is a rare congenital heart defect. The TAPVC incidence rate was 5–9 per 100,000 live births. TAPVC is caused by the failure of connection between pulmonary veins and the morphologic left atrium. Then the pulmonary vein drains abnormally *via* a venous channel into the morphologic right atrium in TAPVC. TAPVC is usually divided into types according to the location of pulmonary venous outflow into the systemic circulation: supracardiac (**Figure 4**), cardiac, infracardiac, and mixed. The most common type of TAPVC is supracardiac TAPVC, accounting for approximately half of all the patients with TAPVC.

Patients with TAPVC are usually symptomatic at a very young age, and a few of them without surgical correction can survive into adulthood. The clinical presentation of TAPVC is mainly determined by the degree of pulmonary venous drainage obstruction and the magnitude of the left-to-right shunt. In TAPVC with obstructed pulmonary venous return, patients were usually severely ill with severe cyanosis and respiratory distress. All blood enters the left atrium through an atrial septal defect. Patients with unobstructed TAPVC usually appeared with a cardiac murmur, heart failure, and cyanosis, but were less ill. TAPVC is rarely discovered in adults because rare cases can survive until 50 years of age. It was reported that the oldest patient was 57 years old and underwent successful TAPVR repair (3). Also, the oldest patient was 63 years old and survived without TAPVR repair (4). Our patient lived with no symptoms found until her 46th year because of palpitations and exertional dyspnea caused by atrial flutter.

In this case, this patient was particularly unusual that she has been living without symptoms until her nearly fifth decade of life without the need for medication. Two factors, the absence of the pulmonary venous obstruction and a large ASD, contribute to the long-time survival of this patient in supracardiac TAPVR. A large ASD provided a satisfactory cardiac output and the amount of mixing of the oxygenated blood. It can explain the lack of cyanosis and normal blood pressure in this patient. Cardiac CT provides accurate anatomical delineation of pulmonary venous pathways and their connections (5). According to the CT scan of this patient, no unobstructed pulmonary venous circulation was observed. Cardiac catheterization showed no pulmonary over-circulation and normal cardiac output. A cardiac CT scan and catheterization showed that this patient had no pulmonary venous obstruction and a large ASD.

The "calabash" configuration on the chest radiograph is uncommonly observed in supracardiac TAPVR. The SVC and right heart dilation formed a right-sided configuration and the dilated innominate vein mainly consists of this left-sided configuration. There is also a non-specific appearance of the chest radiograph in some patients, and then used as such CT scan and echocardiography for accurate diagnosis of TAPVR. This patient was firstly reported as "calabash" appearance on the chest radiograph and was diagnosed by CT scan and echocardiography. A cardiac CT scan presented venous system enlargement, but also aortic system disuse atrophy. Disuse atrophy probably resulted from a reduction of aortic effective blood circulation, while right heart dilation is caused by excessive pulmonary blood circulation. Cardiac hemodynamic assessment in the patient showed no pulmonary hypertension and for further surgical repair.

Surgical repair is an immediate need in most cases once the diagnosis of TAPVC is made. However, the timing of the surgery depends on the type of TAPVC, as well as the condition of the patients. The surgical mortality is <5% when a repair is performed in patients without obstructed pulmonary veins. This patient successfully underwent TAPVC surgical correction and closed ASD. Although circulation (the pulmonary veins returning to the left atrium) was normalized by the surgery, the patient presented pulmonary edema because of aortic disuse atrophy post-operation. Risk factors associated with poor outcomes are pulmonary venous obstruction before repair, younger age at repair, pulmonary vein size, and univentricular heart (6). However, the long-term outcome after surgical repair of TAPVC is also excellent. Because successful repair results in normal circulation, the patients usually grow and develop normally with few symptoms.

## DATA AVAILABILITY STATEMENT

The original contributions presented in the study are included in the article/supplementary material, further inquiries can be directed to the corresponding author.

## ETHICS STATEMENT

The studies involving human participants were reviewed and approved by the Second Xiangya Hospital of Central South University. The patients/participants provided their written informed consent to participate in this study. Written informed

consent was obtained from the individual(s) for the publication of any potentially identifiable images or data included in this article.

## AUTHOR CONTRIBUTIONS

MC, JT, and QH participated in the study design and drafted the manuscript. LH and SZ contributes to data collection. MC and JT were responsible for writing the manuscript. ZW and JH contributes to the manuscript revision. All authors contributed to the article and approved the submitted version.

## FUNDING

Financial support was obtained from the National Natural Science Foundation of China Grant No. 81800302 and the Provincial Natural Science Foundation of Hunan Grant No. 2019JJ50871.

## ACKNOWLEDGMENTS

The authors would like to thank Shuang Zhang and Zhuo Wang for their modifications.

## REFERENCES

1. Verma M, Pandey NN, Kumar S, Saxena A. Beating the odds: a rare case of supracardiac total anomalous pulmonary venous return (TAPVR) in an adult patient. BMJ Case Rep. (2018) 2018:bcr2017221074. doi: 10.1136/bcr-2017-221074
2. Burroughs JT, Edwards JE. Total anomalous pulmonary venous connection. *Am Heart J.* (1960) 59:913–31. doi: 10.1016/0002-8703(60)90414-2
3. Mitsubishi T. Successful repair of total anomalous pulmonary venous drainage (supracardiac type): the adult case in Japan (57-year-old female). *Jpn J Thorac Surg.* (1986) 39:837.
4. Wetzel U, Scholtz W, Bogunovic N, Körfer J, Haas NA, Blanz U, et al. Successful correction of a total anomalous venous connection in a 63-year-old male–case report and review of the literature. *Congenit Heart Dis.* (2010) 5:470–5. doi: 10.1111/j.1747-0803.2009.00372.x
5. Vyas HV, Greenberg SB, Krishnamurthy R, MR. imaging and CT evaluation of congenital pulmonary vein abnormalities in neonates and infants. *Radiographics.* (2012) 32:87–98. doi: 10.1148/rg.321105764
6. Karamlou T, Gurofsky R, Al Sukhni E, Coles JG, Williams WG, Caldarone CA, et al. Factors associated with mortality and reoperation in 377 children with the total anomalous pulmonary venous connection. *Circulation.* (2007) 115:1591–8. doi: 10.1161/CIRCULATIONAHA.106.635441

**Conflict of Interest:** The authors declare that the research was conducted in the absence of any commercial or financial relationships that could be construed as a potential conflict of interest.

**Publisher's Note:** All claims expressed in this article are solely those of the authors and do not necessarily represent those of their affiliated organizations, or those of the publisher, the editors and the reviewers. Any product that may be evaluated in this article, or claim that may be made by its manufacturer, is not guaranteed or endorsed by the publisher.

frontiers | Frontiers in Cardiovascular Medicine

TYPE Case Report
PUBLISHED 22 July 2022
DOI 10.3389/fcvm.2022.937758



OPEN ACCESS

EDITED BY
Grigorios Korosoglou,
GRN Klinik Weinheim, Germany

REVIEWED BY
Anastasios Nikolaos Panagopoulos,
University of Nebraska Medical Center,
United States
Sorin Giusca,
GRN Klinik Weinheim, Germany

*CORRESPONDENCE
Tongshuai Chen
chentongshuai@163.com
Jingquan Zhong
18560086597@163.com

†These authors have contributed equally to this work and share first authorship

SPECIALTY SECTION
This article was submitted to Cardiovascular Imaging, a section of the journal Frontiers in Cardiovascular Medicine

RECEIVED 06 May 2022
ACCEPTED 27 June 2022
PUBLISHED 22 July 2022

CITATION
Ge J, Hu T, Liu Y, Wang Q, Fan G, Liu C, Zhang J, Chen S, Maduray K, Zhang Y, Chen T and Zhong J (2022) Case report: Double-chambered right ventricle diagnosed in a middle-aged female with hypertrophic cardiomyopathy and atrial flutter: A rare case.
*Front. Cardiovasc. Med.* 9:937758.
doi: 10.3389/fcvm.2022.937758



# Case report: Double-chambered right ventricle diagnosed in a middle-aged female with hypertrophic cardiomyopathy and atrial flutter: A rare case

Junye Ge[1†], Tong Hu[1†], Yan Liu[1], Qian Wang[2], Guanqi Fan[1], Chuanzhen Liu[3], Jun Zhang[3], Shiming Chen[4], Kellina Maduray[1], Yun Zhang[1], Tongshuai Chen[1*] and Jingquan Zhong[1,5*]

[1]The Key Laboratory of Cardiovascular Remodeling and Function Research, Chinese Ministry of Education, Chinese National Health Commission and Chinese Academy of Medical Sciences, The State and Shandong Province Joint Key Laboratory of Translational Cardiovascular Medicine, Department of Cardiology, Qilu Hospital, Cheeloo College of Medicine, Shandong University, Jinan, China, [2]Department of Radiology, Qilu Hospital, Shandong University, Jinan, China, [3]Department of Cardiovascular Surgery, Qilu Hospital, Shandong University, Jinan, China, [4]Department of Pathology, Qilu Hospital, Shandong University, Jinan, China, [5]Department of Cardiology, Qilu Hospital (Qingdao), Cheeloo College of Medicine, Shandong University, Qingdao, China

Double-chambered right ventricle (DCRV) is a rare congenital heart defect in adults, manifesting with progressive right ventricular outflow tract obstruction. We describe the first case of DCRV coexisting with hypertrophic cardiomyopathy, which is complicated by atrial flutter. A middle-aged woman with recurrent symptomatic atrial flutter who had previously been diagnosed with biventricular hypertrophic cardiomyopathy was admitted to our department. Echocardiography and cardiac magnetic resonance revealed asymmetrical interventricular septal hypertrophy, and abnormal muscle bundles within the right ventricle, generating an obstructive gradient. Genetic testing detected a hypertrophic cardiomyopathy-associated mutation: *MYH7*, c.4135G > A, p. Ala1379Thr. A diagnosis of DCRV complicated by hypertrophic cardiomyopathy and atrial flutter was made. Surgical intervention was performed, which included radiofrequency ablation, removal of abnormal muscle bundles, and ventricular septal defect repair. Intraoperative transesophageal echocardiography demonstrated the well-corrected right ventricular outflow tract. Free of early postoperative complications, the patient was discharged in sinus rhythm on the 11th day after the surgery. Unfortunately, the patient died from a sudden death 38 days following the surgery. In conclusion, the coexistence of DCRV with hypertrophic cardiomyopathy in patients is an uncommon condition. The present case highlights the importance of diagnostic imaging in the management of this disorder.

KEYWORDS

**double-chambered right ventricle, hypertrophic cardiomyopathy, atrial flutter, echocardiography, cardiac magnetic resonance**

## Introduction

Double-chambered right ventricle (DCRV) is a rare congenital heart disease (CHD) characterized by abnormal muscle bundles, resulting in intra-cavity obstruction in which the right ventricle (RV) is divided into a high-pressure chamber near the tricuspid valve and a low-pressure chamber near the pulmonary valve (PV) (1). DCRV accounts for only 0.5–2% of all CHD cases (2). Hypertrophic cardiomyopathy (HCM) is the most common genetic cardiac disease. About 2/3 of patients experience left ventricular outflow tract obstruction, known as hypertrophic obstructive cardiomyopathy (HOCM) (3). Yamamoto et al. first described HOCM in a DCRV patient with Noonan syndrome (2). Imaging examinations play an important role in the diagnosis of DCRV with HCM. Here, we present a case of DCRV complicated by HCM and atrial flutter (AFL). To our knowledge, such a combination has never been reported before.

## Case presentation

A 45-year-old woman presenting with a 10-year history of palpitations and recent aggravation accompanied with dyspnea was referred to our center. She was originally diagnosed with biventricular HCM yet did not receive relevant treatment. Assessment of family medical history revealed that her mother died of a sudden cardiac death (SCD). Upon physical examination, the patient's vital signs were stable, with the exception of tachycardia (112 beats/min) and a loud grade 4/6 systolic ejection murmur in the 4th intercostal space along the left sternal border. Routine 12-lead electrocardiography displayed recurrent AFL at a ventricular rate of 112 beats/min (**Figure 1A**). Transthoracic echocardiography (TTE) revealed mildly reduced left ventricular ejection fraction (EF: 45%), mild pericardial effusion, biatrial enlargement (left atrium: 54 mm × 68 mm × 58 mm; right atrium: 59 mm × 43 mm) (**Figure 2A**), biventricular hypertrophy and asymmetrical interventricular septal hypertrophy (20 mm) (**Figure 2B**). The anomalous muscle bundles inferior to the infundibulum divided the RV into two cavities, inducing right ventricular outflow tract (RVOT) obstruction (**Figures 2C,D** and **Supplementary Videos 1, 2**). The peak pressure gradient of RVOT was approximately 44 mmHg, and the forward flow velocity was measured at 333 cm/s (**Figure 2E**). The obstructive gradient, however, may have been underestimated due to the inability of color Doppler to align turbulent flow. Furthermore, a small left to right membranous ventricular septal defect (VSD) (0.3 cm) shunt was discovered in the high-pressure chamber (**Figure 2F** and **Supplementary Video 3**). Cardiac magnetic resonance (CMR) further confirmed the presence of sub-infundibular obstruction, biventricular hypertrophy, and interventricular septal hypertrophy (basal segment: 22.5 mm, middle segment: 25.5 mm, distal segment: 21 mm). A dumbbell-shaped RV and flow acceleration at the RVOT were observed during systole (**Figures 3A,B** and **Supplementary Video 4**). CMR assessed RV function with a right ventricular ejection fraction of 63%, right ventricular end-diastolic volume of 61 ml, and right ventricular end-systolic volume of 23 ml. No signs of stenosis were identified in the infundibulum, PV, and pulmonary artery (PA) (**Figure 3C**). Scattered patchy late gadolinium enhancement (LGE) was seen within the left ventricular myocardium, particularly in the left ventricular anterior wall and interventricular septum (**Figure 3D**). The native T1 mapping revealed a markedly increased T1 value at basal IVS from 1,123 to 1,260 ms (**Figures 3E,F**). The reference native T1 value of our 1.5T scanner was 1,035 ms. Genetic testing detected one HCM-associated mutation: *MYH7*, c.4135G > A, p. Ala1379Thr. *MYH7* is the most frequent pathogenic gene of HCM, accounting for 40–44% of HCM cases (3).

The final diagnosis was DCRV complicated by HCM and AFL. Despite the administration of an adequate amount of amiodarone, successful conversion of AFL was not achieved. Since the patient suffered from renal dysfunction (serum creatinine: 175 μmol/L; GFR by Cockcroft-Gault: 39.49 ml/min), oral rivaroxaban (15 mg) was administered daily following admission. The HCM Risk-SCD formula was applied for risk stratification, resulting in a 4.26% 5-year risk of SCD. The decision not to implant an ICD was made after carefully analyzing the clinical benefits and the patient's preferences. Surgery was performed via the median sternotomy approach. AFL was terminated by ablation of the cavotricuspid isthmus. Intraoperatively, a 1.5-cm subvalvular VSD was identified, larger than that shown on TTE. The muscular stenosis tunnel was resected, and a pericardial patch was used for VSD repair. Intraoperative transesophageal echocardiography (TEE) demonstrated well-corrected RVOT (**Figures 2G,H** and **Supplementary Videos 5–6**). The pathology report revealed myocardial fiber hypertrophy, degeneration and necrosis of some myocardial fibers, fibrous scar formation, local subendocardium fibrous tissue hyperplasia, hyaline degeneration, and hyperplasia of elastic fibers in the focal subendocardium, all of which were consistent with HCM (**Figure 4**). On the first postoperative day, the electrocardiography showed coronary sinus rhythm (**Figure 1B**). Sinus rhythm recovered on the 8th day after the operation (**Figure 1C**). The patient was discharged on the 11th

**Abbreviations:** DCRV, double-chambered right ventricle; RVOT, right ventricular outflow tract; CHD, congenital heart disease; RV, right ventricle; HCM, hypertrophic cardiomyopathy; HOCM, hypertrophic obstructive cardiomyopathy; AFL, atrial flutter; SCD, sudden cardiac death; TTE, transthoracic echocardiography; EF, ejection fraction; VSD, ventricular septal defect; CMR, cardiac magnetic resonance; LGE, late gadolinium enhancement; PV, pulmonary valve; PA, pulmonary artery; TEE, transesophageal echocardiography.


FIGURE 1
Electrocardiography. **(A)** Electrocardiography upon admission showed Type I atrial flutter. **(B)** Post-operative electrocardiography (1st day) showed coronary sinus rhythm. **(C)** Post-operative electrocardiography (8th day) showed recovered sinus rhythm.

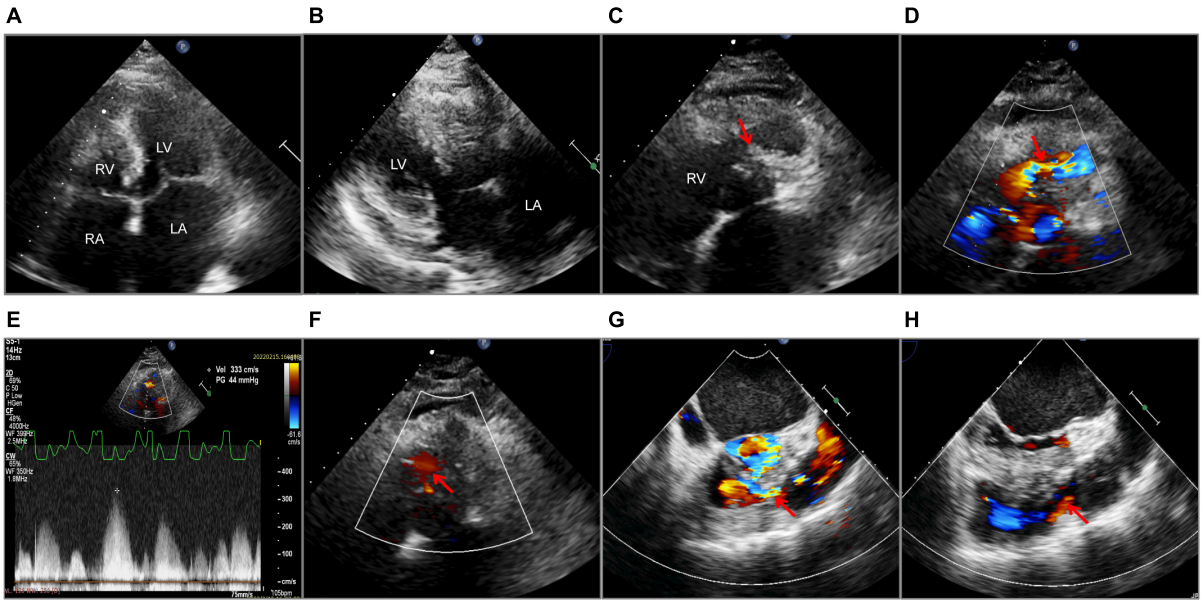


FIGURE 2
Echocardiography. Transthoracic echocardiography **(A–F)**. **(A)** A 2-D apical four-chamber view with enlarged atria. **(B)** Left ventricular hypertrophy and interventricular septal hypertrophy. **(C)** Muscular septation within the right ventricle (the red arrow). **(D)** Flow acceleration showed by Color Doppler at the right ventricular outflow tract (the red arrow). **(E)** The systolic pressure gradient of the right ventricular outflow tract. **(F)** Ventricular septal defect (the red arrow) detected by Color Doppler. Transesophageal echocardiography **(G,H)**. Color Doppler flow of the right ventricular outflow tract before **(G)** and after operation **(H)**, as shown by the red arrows. LA, left atrium; RA, right atrium; LV, left ventricle; RV, right ventricle; Vel, velocity; PG, pressure gradient.

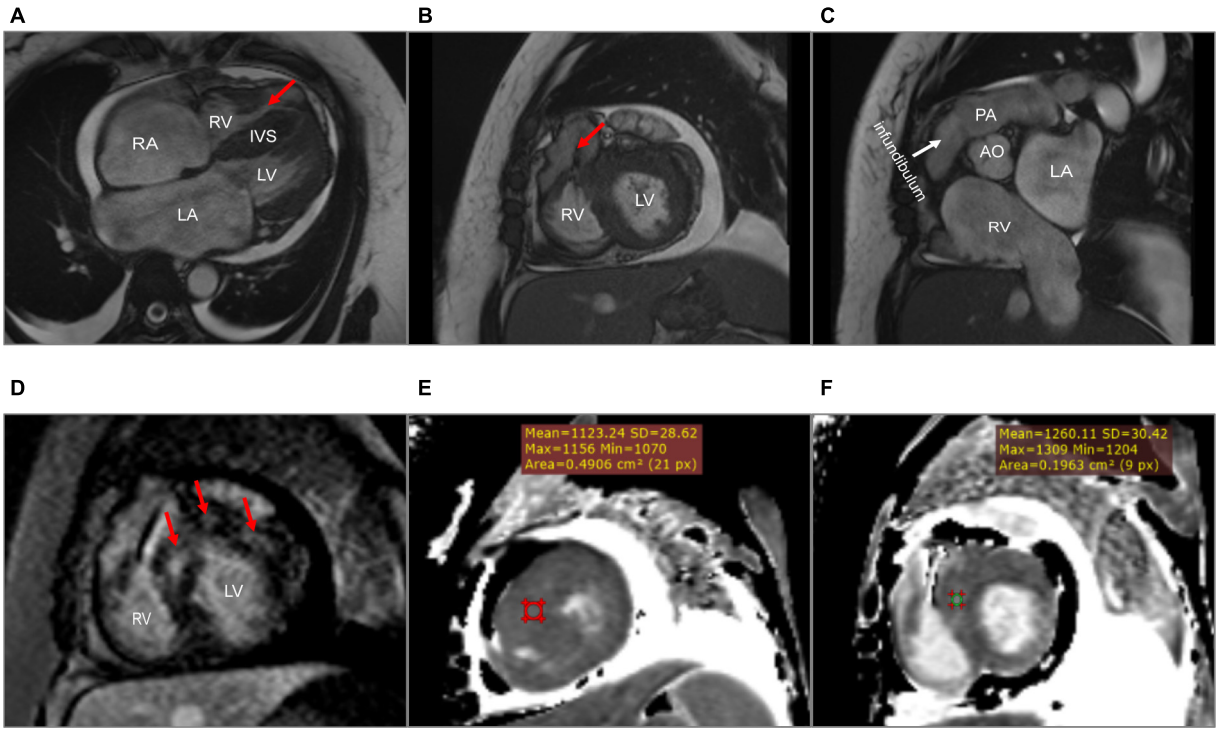


FIGURE 3
Cardiac magnetic resonance. **(A)** A dumbbell-shaped right ventricle indicated right ventricular outflow tract obstruction (the red arrow). **(B)** A flow void sign at the right ventricular outflow tract (the red arrow). **(C)** No stenosis of infundibulum, pulmonary valve, and pulmonary artery. **(D)** Scattered patchy late gadolinium enhancement within the left ventricular myocardium (red arrows), particularly in the left ventricular anterior wall and the interventricular septum. **(E,F)** The native T1 mapping revealed the markedly increased T1 value at the basal interventricular septum from 1,123 to 1,260 ms. LA, left atrium; RA, right atrium; LV, left ventricle; RV, right ventricle; IVS, interventricular septum; PA, pulmonary artery; AO, aorta.

day after the surgery with no early postoperative complications. Unfortunately, the patient died from a sudden death 38 days after the surgery. Since no autopsy was performed, the cause of death could not be confirmed. The mechanism of death was presumed to be arrhythmic.

## Discussion

Double-chambered right ventricle is a rare disease in which the pressure gradient across the obstruction frequently surpasses 20 mmHg, accompanied by a high pulmonary blood flow volume (4). Approximately, 80–90% of patients additionally present with other cardiac anomalies, including VSD (seen in up to 90% of patients with DCRV), atrial septal defect, subaortic stenosis, aortic valve regurgitation, PV stenosis, and so on (4). However, DCRV complicated by HCM is an extremely rare coexistence. Several cases reported this unique condition complicated with HCM (2, 5, 6). With respect to the combination of arrhythmias, Alvarez et al. reported that, in two adult patients diagnosed with DCRV, complicated by sustained monomorphic ventricular tachycardia, tachycardia did not reoccur after surgical excision of the abnormal muscle bundles (7). This report is the first to describe DCRV complicated by HCM and AFL; therefore, it offers guidance for clinical practice.

The symptoms of DCRV are often atypical, similar to those that present in other types of cardiovascular diseases. The most prevalent symptoms are shortness of breath and reduced exercise endurance (8). As the severity of RV blockage increases in adults, even light physical exertion might cause considerable dyspnea. DCRV is most commonly diagnosed in infants and children. However, it can occasionally be detected in adults due to misdiagnosis or the absence of symptoms at a young age (8, 9). There is, currently, a knowledge gap regarding DCRV diagnosis, which is further exacerbated by HCM. In our case, the patient has been previously diagnosed with HCM and AFL, while DCRV was overlooked. According to Said et al., preoperative TTE had a 74% success rate in detecting DCRV; however, as knowledge of DCRV grew, the accuracy of diagnosis improved (6). Thus, considerable experience and advanced diagnostic techniques are of vital importance. Echocardiography is an effective diagnostic tool for DCRV. TTE is initially used to assess cardiac structure; however, limitations arise when diagnosing DCRV in adults due to the unique shape of the RV and its retrosternal position

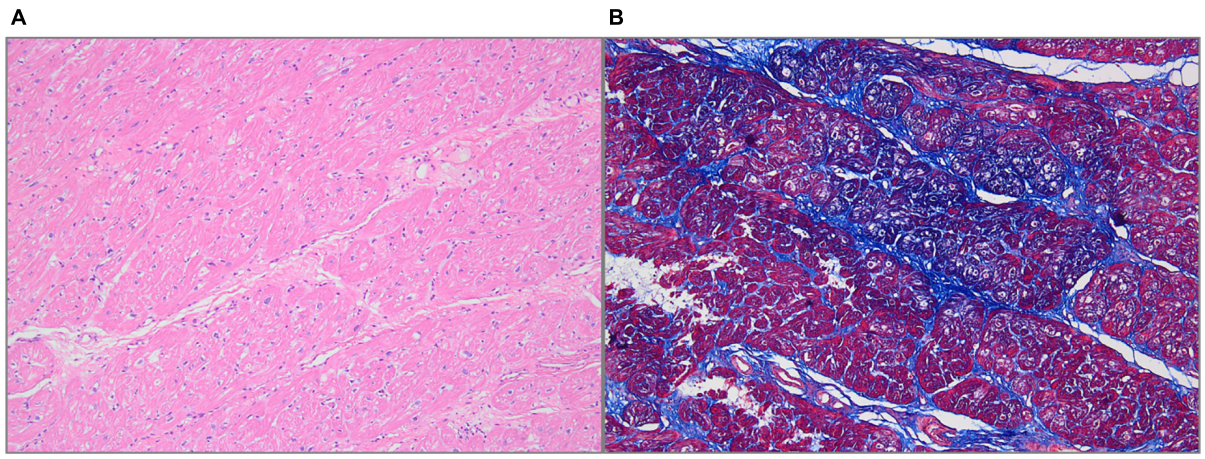


FIGURE 4
Histologic features. **(A)** Hematoxylin-Eosin staining showed myocardial fiber hypertrophy, degeneration and necrosis of some myocardial fibers, and hyaline degeneration (100× magnification). **(B)** Masson staining showed fibrous tissue hyperplasia (100× magnification).

(10). Obesity and emphysema are additional factors that limit the use of TTE in adults (11). The subcostal view tends to provide better visualization of the RVOT, while it is much clearer in infants or children than in adults (10). TTE successfully confirmed the presence of DCRV complicated by HCM and VSD in our case. Due to improved visualization of the RVOT and the ability to precisely observe aberrant muscle bundles and estimate the gradient pressure, TEE is a more effective method for diagnosing DCRV (10). Hoffman et al. compared the success rates of the two echocardiography methods in the diagnosis of DCRV; the study found that TEE was more effective, and the combined application of both methods further improved the accuracy (4). At present, CMR is the best non-invasive examination method for the diagnosis of DCRV, while TEE is deemed unnecessary (12). By carefully modifying the direction and angle of CMR scans, the features of the RVOT and the anatomy of the heart can be clearly shown. Comparatively, TEE is confined to the interface between the esophagus and the heart. In addition, LGE by CMR is able to detect the presence of multiple myocardial fibrosis. If VSD is opened in the proximal high-pressure cavity, the shunt velocity from left to right is low, limiting the shunt volume. Therefore, VSD was undetectable by CMR in our case. Cardiac catheterization and angiography are invasive means often used to confirm the diagnosis and obtain precise blood flow information (12). However, with the continuous improvement of non-invasive techniques, such as echocardiography and CMR, angiography may gradually lose position when diagnosing DCRV (8).

As the only RVOT lesion inferior to the infundibulum (1), DCRV needs to be distinguished from other types of lesions that produce RVOT obstruction, such as anomalies at the infundibular region, PV, the superior valvular region, left or right PA, and peripheral PA (12, 13). The position of the auscultation murmur indicated a lower level of obstruction in this patient. We confirmed the diagnosis of DCRV by echocardiography and CMR without abnormalities in the infundibular region, PV, and PA. It is important to note that the diagnosis of DCRV coexisting with VSD is, to some extent, similar to tetralogy of Fallot (TOF). DCRV has a pressure difference in the RV between the proximal high-pressure cavity and the distal low-pressure cavity, whereas the infundibular region is generally normal. However, for TOF, a pressure difference exists between the PA and RV or within the transition zone in the infundibular region due to PV or infundibulum stenosis.

Although DCRV anatomy is congenital and the RVOT may be non-obstructive at birth, the progressive hypertrophy of aberrant muscle bundles causes RVOT obstruction to develop or worsen (8, 14). RVOT obstruction progresses rapidly in young adults with DCRV, who usually present with severe obstruction around the age of 30 or 40 (15). Nonetheless, it was discovered that, in some patients who did not receive surgical treatment, the severity of RVOT blockage did not worsen over time (16). Surgical treatment is considered to be an effective way to remove RVOT obstruction. The severity of the blockage and lesion usually determines whether or not surgery is necessary (4). Since some patients with DCRV do not experience progressive RVOT blockage during the normal course of the disease, basic follow-up is sufficient for patients with no significant lesions and little or no pressure gradient in the RV (4, 16, 17). Negative inotropic drugs, such as beta-blockers and calcium channel antagonists, may be effective in improving symptoms (2, 12). If the obstruction worsens during follow-up, surgical repair may

be considered. McElhinney et al. recommend surgical repair in adults who present with symptoms or severe obstruction (pressure gradient more than 40 mmhg) despite not having any symptoms (17). Some authors advocated for early surgical therapy even in the absence of symptoms, given the progressive development of blockage and symptoms (8). The European Society of Cardiology guideline recommends surgical treatment of DCRV, even if the obstruction pressure gradient is low (IIa) (13). Further evidence is expected to be gathered to determine the optimum surgical option. With a low recurrence and mortality rate, the long-term prognosis of surgical treatment is excellent, resulting in most patients remaining symptom free after surgery (8). In our case, the morphology of ECG changed significantly on the 1st day after operation: P wave was deeply inverted (negative) in leads II, III, and aVF, and positive in lead V1. According to its characteristics, the P wave was indicative of coronary sinus rhythm. Coronary sinus rhythm might be related to the delayed recovery of sinus node function after the conversion of AFL. The ECG showed sinus P wave morphology on the 8th day after the operation. The P wave was wide with a notch on the peak caused by bi-atrial enlargement. A complete right bundle branch block produced pathological ST segments in leads V1-V3, which could be related to surgical excision.

The combination of HCM is one of the unique features of this case. A study showed that the annual incidence of cardiovascular mortality is 1–2% in adult patients with HCM (18). SCD is one of the leading causes of death in patients with HCM, which is often correlated with lethal arrhythmias, including ventricular tachycardia, ventricular fibrillation, and a complete atrioventricular conduction block. Regarding HCM management in clinical practice, the risk stratification of SCD is of the utmost importance. ICD implantation is the only reliable way to prevent SCD in patients with HCM. Predictive factors of SCD in adult patients with HCM include early age of the onset, non-sustained ventricular tachycardia, maximum LV wall thickness of $\geq$ 30 mm, family history of early SCD, unexplained syncope, enlarged left atrial size, severe left ventricular outflow tract obstruction, LGE, multiple genetic mutations, and so on (19). In this case, the HCM Risk-SCD model was used to stratify risk. It divides adult patients with HCM into three risk levels: low risk (5-year risk $<$ 4%), intermediate risk (5-year risk with $\geq$ 4%– $<$ 6%), high risk (5-year risk $\geq$ 6%) (19). ICD implantation is suggested in high-risk patients and generally not recommended in low-risk patients. In intermediate-risk patients, ICD may be taken into consideration. In our case, after discussion and shared decision-making, ICD implantation was not performed.

There were some limitations in this case. Sudden death occurred 38 days after the surgery. Thromboembolic events are one of the most common complications of AFL or atrial fibrillation with biatrial enlargement. In this patient, adequate rivaroxaban was given after admission and discharge. Moreover, preoperative TEE showed no thrombus in the left atrium. Therefore, it may be possible to rule out the occurrence of thromboembolic events. CMR showed scattered patchy LGE in the left ventricular myocardium. In a large cohort study, myocardial fibrosis revealed by CMR was linked to an increased risk of ventricular tachyarrhythmias in patients with HCM (20). Since no autopsy was performed, it was impossible to ascertain the exact cause of death. We postulated that ventricular arrhythmia, which may be related to multiple myocardial fibrosis, was a significant contributing factor.

In conclusion, DCRV is typically accompanied with other lesions and rarely manifests as a standalone abnormality. Echocardiography and CMR are essential in the diagnosis of DCRV. Due to the low risk of complications and a favorable long-term prognosis, surgery has been proved to be fundamental in removing the obstruction. In patients with HCM, with a moderate 5-year SCD risk determined by the HCM Risk-SCD model, LGE may be indicative of a poor prognosis. Clinicians should recognize early the risk factors of SCD and stratify risk to make the best decision in patients with DCRV complicated by HCM.

## Data availability statement

The raw data supporting the conclusions of this article will be made available by the authors, without undue reservation.

## Ethics statement

Written informed consent was obtained from the participant/s for the publication of this case report. Written informed consent was obtained from the individual(s) for the publication of any potentially identifiable images or data included in this article.

## Author contributions

JG, TH, YL, and TC contributed to conception and design of the case. JG and TH wrote the first draft of the manuscript. QW, GF, CL, JZ, SC, KM, and YZ wrote sections of the manuscript. YL, QW, CL, JZ, SC, and YZ contributed to the clinical treatment of this case. TC and JQZ contributed to the review of the manuscript. All authors contributed to manuscript revision, read, and approved the submitted version.

## Funding

This study was supported by the Qingdao Key Health Discipline Development Fund and National Natural Science Foundation of China (81970282).

## Conflict of interest

The authors declare that the research was conducted in the absence of any commercial or financial relationships that could be construed as a potential conflict of interest.

## Publisher's note

All claims expressed in this article are solely those of the authors and do not necessarily represent those of their affiliated organizations, or those of the publisher, the editors and the reviewers. Any product that may be evaluated in this article, or claim that may be made by its manufacturer, is not guaranteed or endorsed by the publisher.

## Supplementary material

The Supplementary Material for this article can be found online at: https://www.frontiersin.org/articles/10.3389/fcvm.2022.937758/full#supplementary-material

SUPPLEMENTARY VIDEO 1
Transthoracic echocardiography showed anomalous muscle bundles at the right ventricular outflow tract.

SUPPLEMENTARY VIDEO 2
Transthoracic echocardiography showed flow acceleration at the right ventricular outflow tract.

SUPPLEMENTARY VIDEO 3
Transthoracic echocardiography showed ventricular septal defect.

SUPPLEMENTARY VIDEO 4
Cardiac magnetic resonance clearly showed the double-chambered right ventricle and accelerated blood flow during systole.

SUPPLEMENTARY VIDEO 5
Transesophageal echocardiography showed flow acceleration at the right ventricular outflow tract.

SUPPLEMENTARY VIDEO 6
Transesophageal echocardiography showed a well-corrected right ventricular outflow tract.

## References

1. Loukas M, Housman B, Blaak C, Kralovic S, Tubbs RS, Anderson RH. Double-chambered right ventricle: a review. *Cardiovasc Pathol.* (2013) 22:417–23.

2. Yamamoto M, Takashio S, Nakashima N, Hanatani S, Arima Y, Sakamoto K, et al. Double-chambered right ventricle complicated by hypertrophic obstructive cardiomyopathy diagnosed as Noonan syndrome. *ESC Heart Fail.* (2020) 7:721–6. doi: 10.1002/ehf2.12650

3. Cheng Z, Fang T, Huang J, Guo Y, Alam M, Qian H. Hypertrophic cardiomyopathy: from phenotype and pathogenesis to treatment. *Front Cardiovasc Med.* (2021) 8:722340. doi: 10.3389/fcvm.2021.722340

4. Hoffman P, Wójcik AW, Rózański J, Siudalska H, Jakubowska E, Włodarska EK, et al. The role of echocardiography in diagnosing double chambered right ventricle in adults. *Heart.* (2004) 90:789–93.

5. Tyczyński P, Śpiewak M, Chmielewski P, Kotliński K, Deptuch T, Witkowski A, et al. Double chambered right ventricle in a patient with hypertrophic cardiomyopathy. A unique coexistence. *Kardiol Pol.* (2021) 79:891–2. doi: 10.33963/KP.a2021.0023

6. Said SM, Burkhart HM, Dearani JA, O'Leary PW, Ammash NM, Schaff HV. Outcomes of surgical repair of double-chambered right ventricle. *Ann Thorac Surg.* (2012) 93:197–200.

7. Alvarez M, Tercedor L, Lozano JM, Azpitarte J. Sustained monomorphic ventricular tachycardia associated with unrepaired double-chambered right ventricle. *Europace.* (2006) 8:901–3. doi: 10.1093/europace/eul084

8. Kahr PC, Alonso-Gonzalez R, Kempny A, Orwat S, Uebing A, Dimopoulos K, et al. Long-term natural history and postoperative outcome of double-chambered right ventricle–experience from two tertiary adult congenital heart centres and review of the literature. *Int J Cardiol.* (2014) 174:662–8. doi: 10.1016/j.ijcard.2014.04.177

9. Darwazah AK, Eida M, Bader V, Khalil M. Surgical management of double-chambered right ventricle in adults. *Tex Heart Inst J.* (2011) 38:301–4.

10. Lascano ME, Schaad MS, Moodie DS, Murphy D Jr. Difficulty in diagnosing double-chambered right ventricle in adults. *Am J Cardiol.* (2001) 88:816–9.

11. Romano MM, Furtado RG, Dias CG, Jurca M, Almeida-Filho OC, Maciel BC. Double-chambered right ventricle in an adult patient diagnosed by transthoracic echocardiography. *Cardiovasc Ultrasound.* (2007) 5:2. doi: 10.1186/1476-7120-5-2

12. Bashore TM. Adult congenital heart disease: right ventricular outflow tract lesions. *Circulation.* (2007) 115:1933–47.

13. Baumgartner H, Bonhoeffer P, De Groot NM, de Haan F, Deanfield JE, Galie N, et al. ESC guidelines for the management of grown-up congenital heart disease (new version 2010). *Eur Heart J.* (2010) 31:2915–57.

14. Hartmann AF Jr, Goldring D, Carlsson E. Development of right ventricular obstruction by aberrant muscular bands. *Circulation.* (1964) 30:679–85. doi: 10.1161/01.cir.30.5.679

15. Oliver JM, Garrido A, González A, Benito F, Mateos M, Aroca A, et al. Rapid progression of midventricular obstruction in adults with double-chambered right ventricle. *J Thorac Cardiovasc Surg.* (2003) 126:711–7. doi: 10.1016/s0022-5223(03)00044-8

16. Simpson WF Jr, Sade RM, Crawford FA, Taylor AB, Fyfe DA. Double-chambered right ventricle. *Ann Thorac Surg.* (1987) 44:7–10.

17. McElhinney DB, Chatterjee KM, Reddy VM. Double-chambered right ventricle presenting in adulthood. *Ann Thorac Surg.* (2000) 70:124–7.

18. Elliott PM, Gimeno JR, Thaman R, Shah J, Ward D, Dickie S, et al. Historical trends in reported survival rates in patients with hypertrophic cardiomyopathy. *Heart.* (2006) 92:785–91. doi: 10.1136/hrt.2005.068577

19. Elliott PM, Anastasakis A, Borger MA, Borggrefe M, Cecchi F, Charron P, et al. 2014 ESC Guidelines on diagnosis and management of hypertrophic cardiomyopathy: the task force for the diagnosis and management of hypertrophic cardiomyopathy of the European society of cardiology (ESC). *Eur Heart J.* (2014) 35:2733–79. doi: 10.1093/eurheartj/ehu284

20. Adabag AS, Maron BJ, Appelbaum E, Harrigan CJ, Buros JL, Gibson CM, et al. Occurrence and frequency of arrhythmias in hypertrophic cardiomyopathy in relation to delayed enhancement on cardiovascular magnetic resonance. *J Am Coll Cardiol.* (2008) 51:1369–74.

frontiers | Frontiers in Cardiovascular Medicine

TYPE Case Report
PUBLISHED 18 August 2022
DOI 10.3389/fcvm.2022.985111



OPEN ACCESS

EDITED BY
Sanjeev Bhattacharyya,
Barts Heart Centre, United Kingdom

REVIEWED BY
Apostolos Vrettos,
Barts Health NHS Trust,
United Kingdom
Aliki Tsagkridi,
Barts Heart Centre, United Kingdom

*CORRESPONDENCE
Xin Chen
chen_heart@hotmail.com

SPECIALTY SECTION
This article was submitted to Cardiovascular Imaging, a section of the journal Frontiers in Cardiovascular Medicine

RECEIVED 03 July 2022
ACCEPTED 01 August 2022
PUBLISHED 18 August 2022

CITATION
Liang H, Ma C and Chen X (2022) Case report: Mitral valve replacement for Libman-Sacks endocarditis and cerebral embolism of primary antiphospholipid syndrome. *Front. Cardiovasc. Med.* 9:985111. doi: 10.3389/fcvm.2022.985111



# Case report: Mitral valve replacement for Libman-Sacks endocarditis and cerebral embolism of primary antiphospholipid syndrome

Huili Liang, Chunyan Ma and Xin Chen*

Department of Cardiovascular Ultrasound, Clinical Medical Research Center of Imaging in Liaoning Province, The First Affiliated Hospital of China Medical University, Shenyang, China

Antiphospholipid syndrome (APS) is a systemic autoimmune disease characterized by recurrent arteriovenous thrombosis and/or morbid pregnancy. Valve involvement is the most common cardiac manifestation of APS, with lesions characterized by valve thickening and vegetations known as Libman-Sacks endocarditis (LSE). This report discussed a rare case of a 26-year-old young woman diagnosed with primary APS with multiple cerebral infarctions and right middle cerebral artery occlusion that occured 3 years ago. During the investigation, transthoracic echocardiography (TTE) revealed vegetations on both leaflets of the mitral valve with mild to moderate mitral regurgitation. One year following corticosteroid and anticoagulant treatment, mitral valve fibrosis and moderate to severe regurgitation were noted, after which mitral mechanical valve replacement was finally performed. Accordingly, this report suggests that LSE occurrence should be alerted during the examination of APS patients especially in those with cerebrovascular disease. Furthermore, establishing an early diagnosis and conducting close follow-ups are necessary for its timely intervention and treatment.

KEYWORDS

**antiphospholipid syndrome, Libman-Sacks endocarditis, cerebral embolism, mitral valve, mitral regurgitation**

## Introduction

Libman-Sacks endocarditis (LSE) is a common manifestation in patients with antiphospholipid syndrome (APS) who have cardiac valve involvement; however, it is often ignored due to its asymptomatic nature during the early stages. As the disease progresses, serious complications such as valve dysfunction and cerebrovascular

embolism, may occur (1). Therefore, achieving an early and accurate LSE diagnosis as well as performing timely treatment in patients with APS are crucial in preventing disease progression and improving prognosis (2). This report discusses a rare case of LSE complicated by cerebral embolism in a patient with primary APS who underwent mechanical mitral valve replacement.

## Case presentation

A 26-year-old young woman was hospitalized in the Rheumatology and Immunology department of a local hospital due to elevated blood pressure, elevated creatinine and head and neck erythema 5 years ago (**Table 1**). Laboratory tests revealed that the rheumatism antibody test was negative, and anti-β2 glycoprotein-1 antibody (anti-β2GP1) was >90 Umol/L. Because the patient had no history of abortion or oral estrogen-containing hormonal contraception and lacked diagnostic criteria, such as recurrent arteriovenous thrombosis, probable APS was diagnosed. The patient was then treated with 10 mg/days oral methylprednisolone. Two years later, the patient suffered from sudden slurred speech, numbness, and motor dysfunction in her right hand and numbness in her left lower extremities 2 months ago. Then, she was subsequently admitted to our hospital. An emergency brain computed tomography (CT) demonstrated multiple lacunar cerebral infarctions. Moreover, her physical examination demonstrated red spots on the head and neck with associated pruritus. Electrocardiography (ECG) showed sinus rhythm with 87 bpm. Her laboratory investigations revealed the following biochemical indicators: anti-β2 glycoprotein-1 antibody (anti-β2GP1)-IgG 210.5 CU (0.0–20.0 CU); anticardiolipin antibody (aCL)-IgG, aCL-IgA were increased with aCL-IgG 468.9 CU (0.0–20.0 CU), aCL-IgM 4.3 CU (0.0–20.0 CU), aCL-IgA 24.4 CU (0.0–20.0 CU) and positive lupus anticoagulant (LA). Prothrombin time was 37.4 s (11.0–14.3 s), and activated partial thromboplastin time was increased with 54.3 s (32.0–43.0 s). Creatinine was 133 μmol/L (41–73 μmol/L). However, testing for antinuclear antibody, anti-double-stranded DNA antibody, anti-U1RNP antibody, anti-SSA antibody, and anti-SSB antibody yielded negative results. The levels of hemoglobin, platelets, white cell count, C-reactive protein (CRP), erythrocyte sedimentation rate (ESR), C3 and C4, protein C and S, and urea and liver function indicators were within normal limits.

Magnetic resonance imaging (MRI) of the brain was then performed, showing multiple infarctions and softening lesions in the right thalamus, paraventricular area, and cerebellar hemisphere (**Figure 1**). Magnetic resonance arteriography (MRA) showed right middle cerebral artery occlusion. A carotid ultrasound scan was normal. Transthoracic echocardiogram (TTE) demonstrated that the cusps of the anterior and posterior mitral valve leaflets were thickened. Additionally, verrucous and nodular vegetations with heterogeneous echo-density could be seen at the commissural border of both mitral valve leaflets (**Figures 2A,C**). The vegetations were firmly attached to the surface of the valve without obvious independent motion. Mild to moderate mitral regurgitation was detected at the central commissure when the valve closed (**Figures 2B,D**) with an effective regurgitant orifice area (EROA) of 0.25 $cm^2$ and the regurgitant volume of 36 mL. The other valves were morphologically normal. The left ventricular function was normal, with a left ventricular ejection fraction (LVEF) of 60%. Repeated blood cultures were negative, and the patient had no recent history of fever. Considering these findings, the patient was diagnosed with primary APS, LSE, and cerebral infarction. Symptomatic treatment was provided to her during hospital admission with sufficient low molecular weight heparin and warfarin anticoagulation. Oral prednisolone acetate (15 mg/day) and warfarin were administered after her discharge.

One year later, the patient again sought medical care due to chest tightness and shortness of breath for 2 months. Chest X-ray and chest CT were normal. Additionally, cardiac auscultation revealed a grade 3/6 apical systolic murmur. Follow-up TTE showed thickening and fibrosis of the anterior and posterior mitral valve cusps, mild stenosis (transmitral mean gradient of 3 mmHg and mitral valve area of 2.6 $cm^2$) and moderate to severe regurgitation of the mitral valve (**Figure 3**) with EROA of 0.40 $cm^2$ and the regurgitant volume of 58 mL. The other valves were normal. The left ventricular function was normal, with a left ventricular ejection fraction (LVEF) of 64%. Repeated blood cultures were again negative. Mitral valve mechanical valve replacement was then performed, which intraoperatively revealed thickening and multiple small nodular vegetations on the mitral valve. No perforation or destruction of the mitral valve was identified. Histopathology demonstrated fibrous tissue hyperplasia with hyaline degeneration and no inflammatory cell infiltration (**Figure 4**). Postoperatively, oral prednisolone acetate and warfarin were administered with an international normalized ratio (INR) target of 3.0–4.0. During her 17-month follow-up, the patient was clinically stable, the symptoms of cerebral infarction were relieved, and no new infarct was found on the follow-up brain CT. TTE revealed no mitral regurgitation with normal ventricular function.

## Discussion

Antiphospholipid syndrome is a non-inflammatory systemic autoimmune disease with an incidence of five new cases/100,000 persons per year and a prevalence of 40–50 cases/100,000 persons (3) and is more common in young women (4). "Definite" APS must have recurrent arteriovenous thrombosis and/or morbid pregnancy (habitual abortion, or stillbirth in the middle and late stages) as its main clinical

TABLE 1 Timeline of the patient's clinical course.

| | |
|---|---|
| 2017 | Diagnosed with probable APS at a local hospital. Oral methylprednisolone was administered |
| December 2019 | Sudden slurred speech, numbness and motor dysfunction in the right hand and numbness in the left lower extremities 2 months ago |
| 3 December 2019 | Emergency brain CT scan showed multiple lacunar cerebral infarctions. The patient was then hospitalized |
| 5 December 2019 | MRI showed multiple infarctions and softening lesions in the right thalamus, paraventricular area, and cerebellar hemisphere. MRA showed right middle cerebral artery occlusion. Autoimmune indicators were suggestive for primary APS |
| 10 December 2019 | TTE showed mitral valve vegetations and mild to moderate mitral regurgitation |
| 18 December 2019 | The patient was discharged home, receiving prednisolone acetate and oral warfarin |
| July 2020 | Chest tightness and shortness of breath were reported for 2 months. The patient was then rehospitalized |
| 22 July 2020 | Follow-up TTE showed moderate to severe mitral regurgitation |
| 30 July 2020 | Mitral valve mechanical valve replacement was performed |
| December 2021 | Postoperative TTE revealed no mitral regurgitation with normal ventricular function |

APS, antiphospholipid syndrome; CT, computed tomography; MRA, magnetic resonance arteriography; MRI, magnetic resonance imaging; TTE, transthoracic echocardiography.

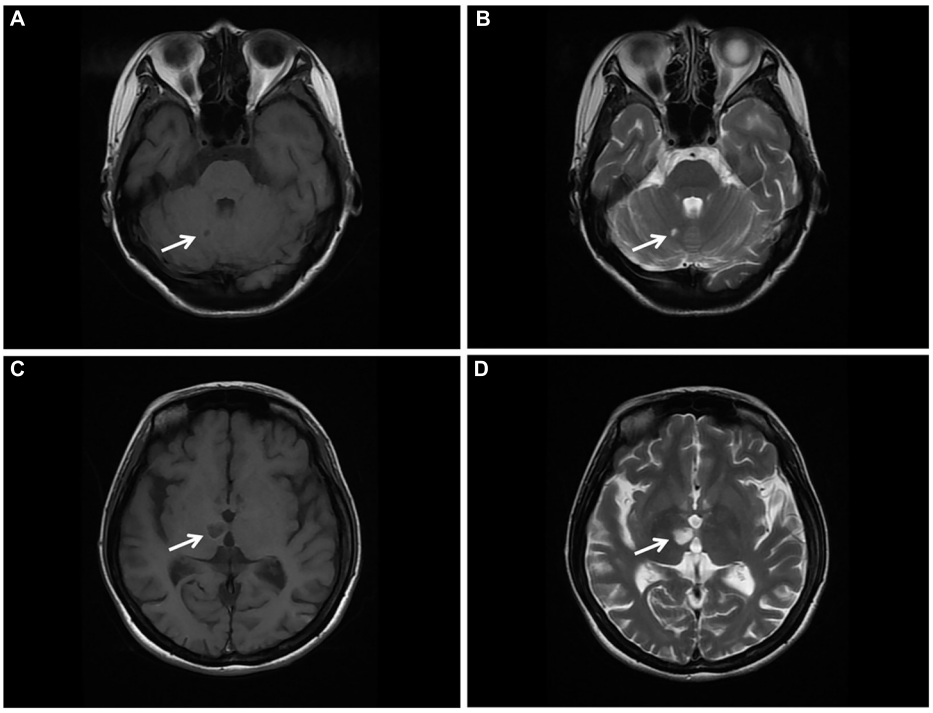


FIGURE 1
Brain MRI. **(A,B)** T1 and T2 sequences showing cerebral infarction with a clear border in the right cerebellar hemisphere (arrow). **(C,D)** T1 and T2 sequences showing cerebral infarction with a clear border in the right thalamus. MRI, magnetic resonance imaging (arrow).

manifestations (5). Additionally, laboratory tests should demonstrate persistently high titers of antiphospholipid antibodies, including aCL, LA, and anti-β2GP1 (5). APS can be divided into primary and secondary APS. Primary APS has been generally defined to cover diseases meeting the diagnostic criteria of APS without those that induce the production of antiphospholipid antibodies, such as autoimmune diseases and malignancies (5). APS occurring secondary to other diseases, such as systemic lupus erythematosus (SLE) and Sjogren syndrome, is traditionally termed secondary APS (5). Additionally, APS can also be divided into the following subtypes, including probable APS or pre-APS, seronegative APS, and catastrophic APS (6). The patient discussed in this case report was diagnosed with probable APS in a local hospital 5 years ago and was positive for antiphospholipid antibodies; however, there was a lack of certain components in the diagnostic criteria, such as thrombosis or recurrent abortion (6). While she was hospitalized 3 years ago, in conjunction with the results of her MRI, MRA and biochemical tests, she was diagnosed with primary APS. The clinical manifestations of APS are complex and diverse, and various body systems may be involved during the disease.

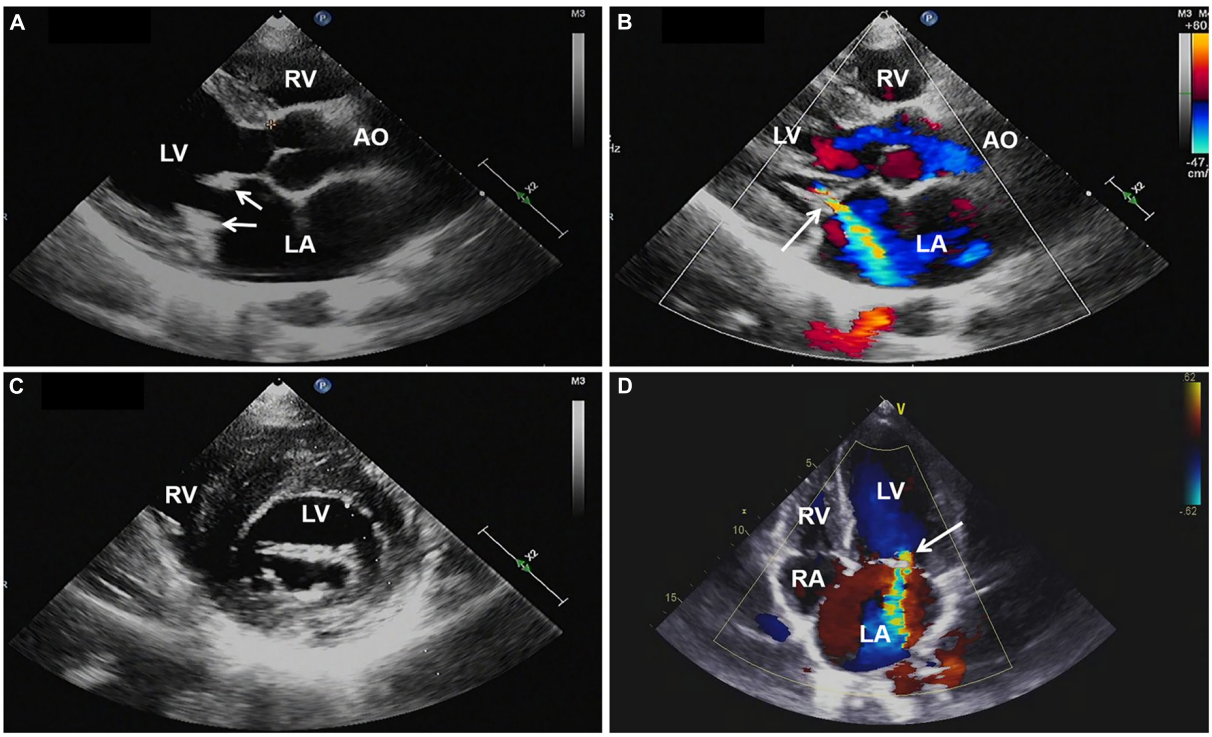


FIGURE 2
**(A,C)** Transthoracic echocardiography showing thickened mitral valve leaflets with verrucous, nodular, heterogeneous echoic vegetations located on the commissural border of both leaflet tips (arrows). **(B,D)** Color Doppler imaging revealing mild to moderate mitral regurgitation (arrow). AO, aorta; LA, left atrium; LV, left ventricle; RA, right atrium; RV, right ventricle; TTE, transthoracic echocardiography.

Involvement of the heart valve is the most common cardiac manifestation of APS, with 32% of APS cases demonstrating invasion of the heart valve and valvular damage (7). The lesions characterized by valve thickening and vegetations are defined as LSE. LSE is non-bacterial thrombotic endocarditis, which is most commonly seen in SLE, and a few cases have been reported in APS in recent years (2). Its pathogenesis involves the deposition of autoimmune complexes and complement, leading to valve thickening and the formation of fibrin-platelet thrombus on the valve. Antiphospholipid antibodies could activate endothelial cells, resulting in aggregation of monocytes and platelets, promoting the thrombosis of valves damaged by immune complex deposition, and aggravating valve damage and inflammatory changes (8). Echocardiography is the preferred investigation for LSE. Typical manifestations are verrucous and nodular vegetations of various sizes and shapes, which are usually small in size (<1 cm in diameter), and have irregular borders, heterogeneous echogenicity, and wide bases while being firmly attached to the valve surface (9). These are often located at the upstream, the commissural border of the valve leaflets, and can also involve the chordae tendineae and atrioventricular endocardial surface, without obvious voluntary motion (9). The mitral valve is most commonly involved, accounting for about 63% of cases, followed by the aortic valve, the tricuspid valve, and the pulmonary valve, which are rarely involved (10). Most patients have no obvious valve dysfunction with only mild regurgitation or less, and only 4–6% of patients have severe valve regurgitation (11). Zuily et al. have discovered that the incidence of LSE in the antiphospholipid antibody-positive group was three times that of the negative group, where moderate to severe mitral regurgitation was more likely to occur (12). Charles et al. have shown that the prevalence of LSE in double-positive or triple-positive patients is significantly higher than that in single-positive patients with antiphospholipid antibodies (13). All three antiphospholipid antibodies were positive in our patient, which might relate to the severity of valve regurgitation.

Studies have also found that LSE might be a common and under-recognized pathological process of embolic cerebrovascular disease, a potential embolic source of cerebrovascular embolism in patients with SLE and APS, and an independent risk factor of cerebrovascular events (8, 14, 15). Cerebrovascular events in patients with APS may be caused by the fragmentation of LSE or may be related to the hypercoagulable state caused by antiphospholipid antibodies (8). Erdozain et al. have shown that cerebrovascular events are more prevalent in patients with significant valvular lesions (15).

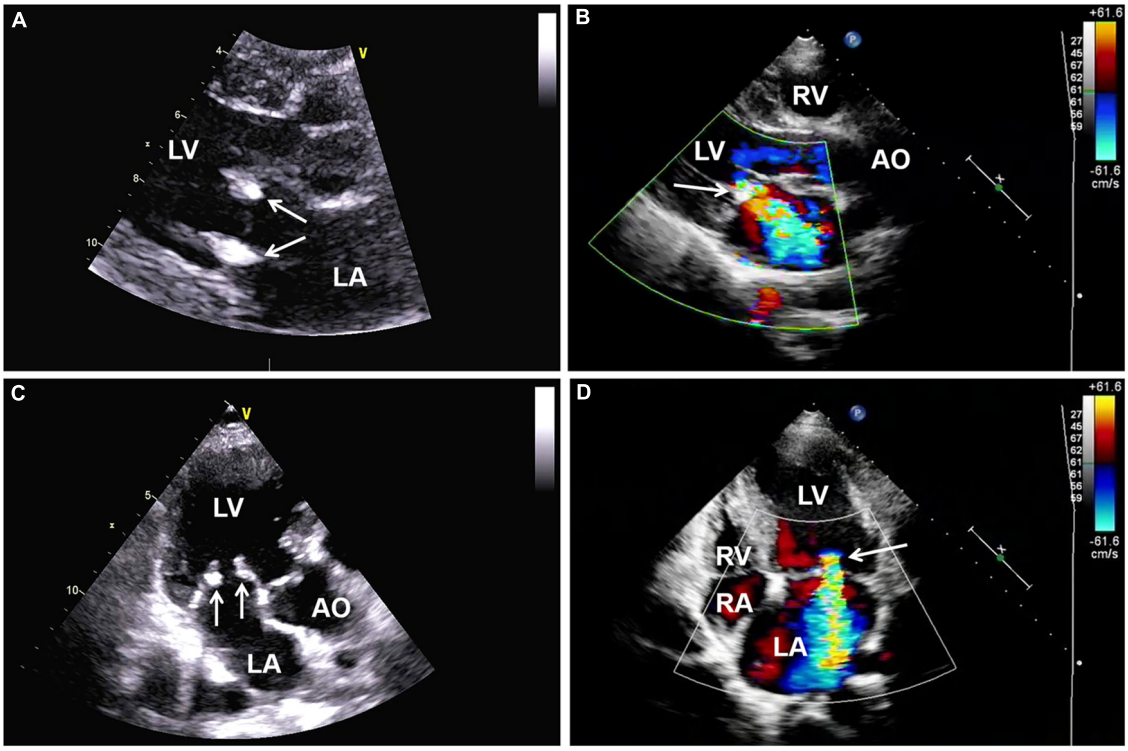


FIGURE 3
**(A,C)** Follow-up transthoracic echocardiography (TTE) demonstrating thickening and hyperechoic lesions of mitral valve leaflets (arrows), suggesting valvular fibrosis. **(B,D)** Color Doppler imaging showing moderate to severe regurgitation of the mitral valve. AO, aorta; LA, left atrium; LV, left ventricle; RA, right atrium; RV, right ventricle; TTE, transthoracic echocardiography.

In the present case report, the MRI scan exhibited small, multiple and scattered cerebral infarctions, while the MRA showed occlusion of the right middle cerebral artery. The cerebral vascular event of this patient was considered to be attributed to the combination of arterial embolism due to hypercoagulability and cardiogenic embolism as a result of LSE.

In patients with APS complicated by cerebrovascular embolism, early diagnosis and timely treatment of LSE are crucial. Controversy regarding LSE treatment in APS patients continues to exist. LSE treatment is usually performed using hormones, such as corticosteroids; however, studies have shown that corticosteroids can accelerate valve vegetation healing, which might lead to valve scarring and fibrosis, thus worsening valve dysfunction (4, 16). Therefore, scholars have suggested that corticosteroid therapy should not be recommended for APS valve lesions (4). Thus, for patients suffering from LSE with severe valvular regurgitation and cerebrovascular embolism, surgical treatment is still required to prevent further deterioration of the cardiac structure and function and recurrent embolism occurrence. Mechanical valve replacement continues to remain the preferred surgical treatment for young patients with LSE, and studies have shown that better outcomes are evident when performing mitral valve replacement compared to mitral valve repair (16). Native valve repair does not seem to alter the progression of valve thickening and calcification; hence, replacement is ultimately necessary. Regarding the patient in

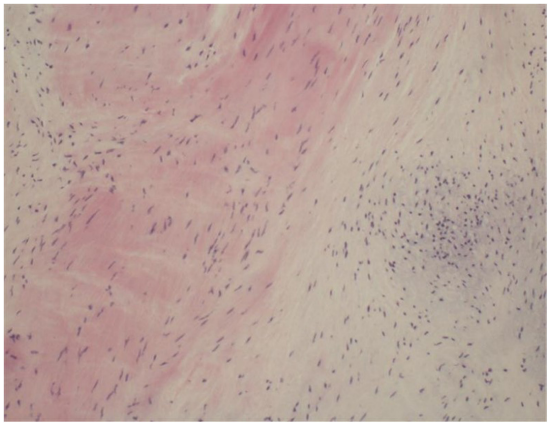

FIGURE 4
Histopathology of excised valve demonstrating fibrous tissue hyperplasia with hyaline degeneration and no inflammatory cell infiltration.

this case report, due to her poor response to medical treatment, the degree of mitral regurgitation was aggravated, which was further complicated by cerebral vascular embolism. Mitral valve mechanical valve replacement was performed to prevent the deterioration of the condition and recurrence of embolism. Due to the hypercoagulable state of APS, anticoagulants should be prescribed for long-term use following surgery to prevent thrombosis, with regular dosage readjustment.

## Conclusion

The findings of this case report suggest that clinicians should be more aware of LSE when performing echocardiography in patients with APS. Once the diagnosis is confirmed, close follow-up and timely treatment are necessary. Additionally, there were concerns that the use of corticosteroid agents may cause shrinking and scarring of heart valves; therefore, despite the indications for surgery for patients with LSE have not been sufficiently studied, severe valvular dysfunction, large vegetations and recurrent embolization despite therapeutic anticoagulation are generally accepted indications for surgical intervention.

## Data availability statement

The original contributions presented in this study are included in the article/supplementary material, further inquiries can be directed to the corresponding author.

## Ethics statement

Written informed consent was obtained from the individual(s) for the publication of any potentially identifiable images or data included in this article.

## Author contributions

HL: conceptualization, data interpretation, and drafting manuscript. XC: conceptualization, project administration, and supervision. CM: supervision. All authors have read and approved the submitted version.

## Conflict of interest

The authors declare that the research was conducted in the absence of any commercial or financial relationships that could be construed as a potential conflict of interest.

## Publisher's note

All claims expressed in this article are solely those of the authors and do not necessarily represent those of their affiliated organizations, or those of the publisher, the editors and the reviewers. Any product that may be evaluated in this article, or claim that may be made by its manufacturer, is not guaranteed or endorsed by the publisher.

## References

1. Eunjung C, Lena MM, Julie P, Mary CC, Katherine CW, Erin DM, et al. Multimodality evaluation of aortic insufficiency and aortitis in rheumatologic diseases. *Front Cardiovasc Med.* (2022) 12:874242. doi: 10.3389/fcvm.2022.874242

2. Jelena ZA, Hiroshi Y, Howard SR. Multiple embolic strokes as a result of Libman–Sacks endocarditis associated with lupus and secondary antiphospholipid antibody syndrome: A case report. *Eur Heart J Case Rep.* (2018) 17:yty094. doi: 10.1093/ehjcr/yty094

3. Polytarchou K, Varvarousis D, Manolis AS. Cardiovascular disease in antiphospholipid syndrome. *Curr Vasc Pharmacol.* (2020) 18:538–48. doi: 10.2174/1570161117666190830101341

4. Ishizu K, Isotani A, Yamaji K, Ando K. Immunosuppressive therapy to reduce mitral regurgitation in Libman-Sacks endocarditis: A case report. *Eur Heart J Case Rep.* (2019) 1:ytz133. doi: 10.1093/ehjcr/ytz133

5. Miyakis S, Lockshin MD, Atsumi T, Branch DW, Brey RL, Cervera R. International consensus statement on an update of the classification criteria for definite antiphospholipid syndrome (APS). *J Thromb Haemost.* (2006) 4:295–6. doi: 10.1111/j.1538-7836.2006.01753.x

6. Baker WF, Bick RL. The clinical spectrum of antiphospholipid syndrome. *Hematol Oncol Clin North Am.* (2008) 22:33–52. doi: 10.1016/j.hoc.2007.10.007

7. Rayan JR, Ghassan ED, Jawad F, Rachoin R. Complete resolution of a large bicuspid aortic valve thrombus with anticoagulation in primary antiphospholipid syndrome. *Front Cardiovasc Med.* (2017) 20:59. doi: 10.3389/fcvm.2017.00059

8. Andrea C, Carlos AM, Gerard E, Miguel AP, Jose LP, Josep F, et al. Heart valve surgery in patients with the antiphospholipid syndrome: Analysis of a series of nine cases. *Eur J Cardiothorac Surg.* (2010) 37:154–8. doi: 10.1016/j.ejcts.2009.06.046

9. Garcia D, Erkan D. Diagnosis and management of the antiphospholipid syndrome. *N Engl J Med.* (2018) 24:2010–21. doi: 10.1056/NEJMra1705454

10. Wong N, Ignasius AJ, Ewe SH, Yeo KK. Severe mitral regurgitation from Libman-Sacks endocarditis treated with MitraClip: A case report. *Eur Heart J Case Rep.* (2021) 11:ytab361. doi: 10.1093/ehjcr/ytab361

11. Hersh S, Ricardo B, Robin F, Sydney M, Muhamed S. Mitral valve Libman-Sacks endocarditis visualized by real time three-dimensional transesophageal echocardiography. *Echocardiography.* (2012) 29:E100–1. doi: 10.1111/j.1540-8175.2011.01602.x

12. Zuily S, Regnault V, Selton-Suty C, Eschwège V, Bruntz JF, Bode-Dotto E, et al. Increased risk for heart valve disease associated with antiphospholipid antibodies in patients with systemic lupus erythematosus: Meta-analysis of echocardiographic studies. *Circulation.* (2011) 12:215–24. doi: 10.1161/CIRCULATIONAHA.111.028522

13. Charles JL, Rekha M, Kyle K, Reto K, Robert DM. Antiphospholipid syndrome and the relationship between laboratory assay positivity and prevalence of non-bacterial thrombotic endocarditis: A retrospective cohort study. *J Thromb Haemost.* (2020) 18:1408–14. doi: 10.1111/jth.14798

14. Roldan CA, Sibbitt WL, Qualls CR, Jung RE, Greene ER, Gasparovic CM, et al. Libman-Sacks endocarditis and embolic cerebrovascular disease. *JACC Cardiovasc Imaging.* (2013) 6:973–83. doi: 10.1016/j.jcmg.2013.04.012

15. Erdozain JG, Ruiz-Irastorza G, Segura MI, Amigo MC, Espinosa G, Pomar JL, et al. Cardiac valve replacement in patients with antiphospholipid syndrome. *Arthritis Care Res (Hoboken).* (2012) 64:1256–60. doi: 10.1002/acr.21670

16. Kenta H, Kazuaki W, Tomomitsu T, Atsuhiro Y, Shugo S, Hisao S, et al. Double-valve replacement for mitral and aortic regurgitation in a Patient with Libman-Sacks endocarditis. *Intern Med.* (2014) 53:1769–73. doi: 10.2169/internalmedicine.53.2232

frontiers | Frontiers in Cardiovascular Medicine

TYPE Case Report
PUBLISHED 14 October 2022
DOI 10.3389/fcvm.2022.993024



OPEN ACCESS

EDITED BY
Riccardo Liga,
Pisana University Hospital, Italy

REVIEWED BY
Alexander Van Rosendael,
Leiden University Medical Center (LUMC), Netherlands
Andrea Barison,
Gabriele Monasterio Tuscany Foundation (CNR), Italy
Natallia Maroz-Vadalazhskaya,
Belarusian State Medical University, Belarus

*CORRESPONDENCE
Ming Bai
baiming@vip.163.com

SPECIALTY SECTION
This article was submitted to Cardiovascular Imaging, a section of the journal Frontiers in Cardiovascular Medicine

RECEIVED 13 July 2022
ACCEPTED 26 September 2022
PUBLISHED 14 October 2022

CITATION
Wa Y, Niu X, Xu J, Jiang G, Hu S and Bai M (2022) Case report: A case of isolated cardiac sarcoidosis diagnosed by multimodal imaging and endomyocardial biopsy. *Front. Cardiovasc. Med.* 9:993024. doi: 10.3389/fcvm.2022.993024



# Case report: A case of isolated cardiac sarcoidosis diagnosed by multimodal imaging and endomyocardial biopsy

Yongling Wa, Xiaowei Niu, Jizhe Xu, Gaxue Jiang, Sixiong Hu and Ming Bai*

Department of Cardiology, First Hospital of Lanzhou University, Lanzhou, China

Due to its low incidence, isolated cardiac sarcoidosis (ICS) is often missed or misdiagnosed. Herein, we describe a case of ICS in a 52-year-old male patient. Advanced imaging, including cardiac magnetic resonance (CMR) and fluorine-18 fluorodeoxyglucose positron emission tomography (FDG-PET), could not only screen high-risk patients for establishing diagnosis, but also guide endomyocardial biopsy (EMB) for improving cardiac disease detection rate. This case highlights the importance of multimodal imaging for screening and necessity of EMB for diagnosis.

KEYWORDS

**cardiovascular imaging (CARD), isolated cardiac sarcoidosis, myocardial endocardial biopsy, multimodal imaging, CMR (cardiovascular magnetic resonance), FDG (18F-fluorodeoxyglucose)-PET/CT**

## Introduction

Sarcoidosis is a systemic disease that can occur in various organs. Although the most common clinical manifestation in > 90% of patients with sarcoidosis is enlargement of the hilar and mediastinal lymph nodes, circular erythema of the skin is the main symptom in some patients. However, some patients (approximately 5%) also have heart involvement called cardiac sarcoidosis (CS) that can develop in any part of the heart. The three most common clinical manifestations of CS are atrioventricular block, ventricular arrhythmia, and heart failure. Some studies reported that a small number of primary lesions in patients with sarcoidosis originate from the heart: isolated cardiac sarcoidosis (ICS). The definition of ICS was first established in the CS guidelines proposed by the Japanese Circulation Society (1–3). This case is unique in that it provides a preliminary diagnosis of ICS through multimodal imaging combined with identifying clinical manifestations. An accurate endomyocardial biopsy (EMB) was performed under the guidance of imaging to successfully make diagnosis (**Table 1**).

## Case description

A 52-year-old man presented to our hospital with palpitations and dizziness. Physical examination on admission did not show any skin or mucosal damage or superficial lymph node enlargement. Laboratory test results showed only a slight increase in troponin levels (0.032 ng/ml). In addition, electrocardiography (ECG) showed ventricular premature contractions and complete right bundle branch block [left ventricular ejection fraction (LVEF) % = 65%].

Eleven months prior, the patient experienced unexplained intermittent palpitations, with dizziness, fatigue, chest tightness, and shortness of breath. He was admitted to a local hospital. Twenty-four hour Holter monitoring in the patient showed frequent ventricular extrasystoles, paroxysmal ventricular tachycardia, and right bundle branch block. Echocardiography revealed LVEF of 60% with no obvious abnormalities in cardiac structure or function. Cardiac magnetic resonance (CMR) imaging revealed abnormal signals in the right ventricular surface of the ventricular septum, and late gadolinium enhancement (LGE) (Figure 1). Based on these findings, the patient was diagnosed with multifocal ventricular tachycardia. Therefore, the patient underwent cardiac catheter ablation and received bisoprolol (5 mg/d), amiodarone (0.2 g/d).

Surgery and medication did not improve the patient's symptoms within the following 7 months. In local hospital repeat CMR imaging showed that LGE was aggravated (Figure 1). Fluorine-18 fluorodeoxyglucose positron emission tomography (FDG-PET) demonstrated intense multifocal cardiac uptake in the interventricular septum and right ventricle without abnormal lesions in other parts of the body (Figure 2). Adenosine technetium-99m (99mTc)-sestamibi myocardial perfusion imaging showed that blood perfusion was decreased in the middle and basal segments of the ventricular septum. The doctor considered that arrhythmia might be caused

TABLE 1 The patient's time line.

| Time line | |
|---|---|
| 2021.7<br>First hospitalization | The patient was admitted due to chest tightness and palpitation, electrocardiogram showed complete right bundle branch block, No obvious abnormalities were found on coronary angiography.<br>CMR imaging revealed abnormal signals in the right ventricular surface of the ventricular septum, and significant LGE.<br>Patient underwent cardiac catheter ablation and drug therapy |
| 2022.4<br>Second hospitalization | Repeat CMR imaging showed LGE were aggravated.<br>FDG-PET showed significant metabolic increase in ventricular septum and right ventricle, and no abnormal metabolic lesions were observed in other organs of the body. |
| 2022.6<br>Third hospitalization | Patient received the last CMR to accurately EMB. It was eventually diagnosed as ICS, received an ICD and drug therapy. |
| 2022.8<br>Follow-up | During 2 months after discharge, the patient had no symptoms of palpitations. FDG-PET showed that the area of increased glucose metabolism in the original lesion was reduced, indicating the effectiveness of immunosuppressive therapy. |

CMR, cardiac magnetic resonance; FDG-PET, Fluorine-18 fluorodeoxyglucose positron emission tomography; EMB, endomyocardial biopsy.

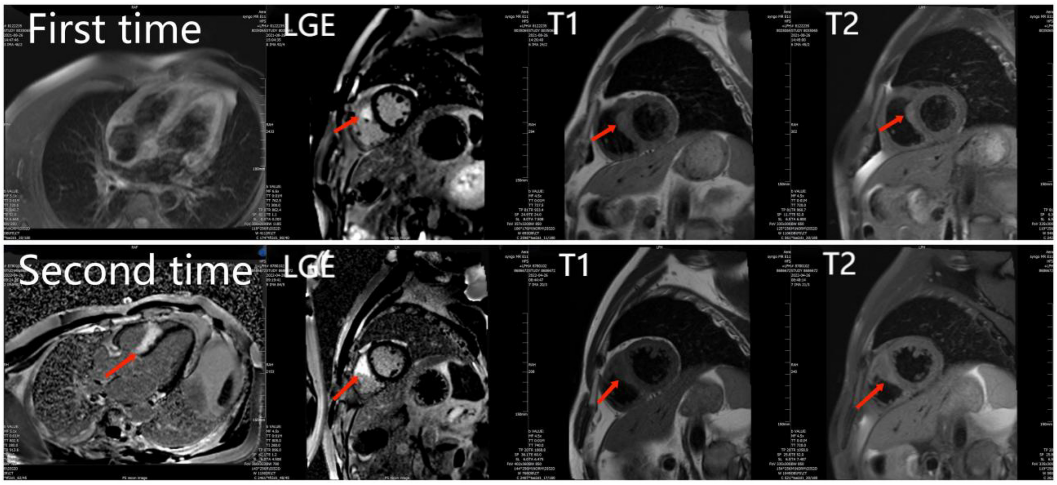


FIGURE 1
The first and second cardiac magnetic resonance show abnormal signals and LGE in the right ventricular surface of the ventricular septum. And the second time LGE was more severe than the first time.

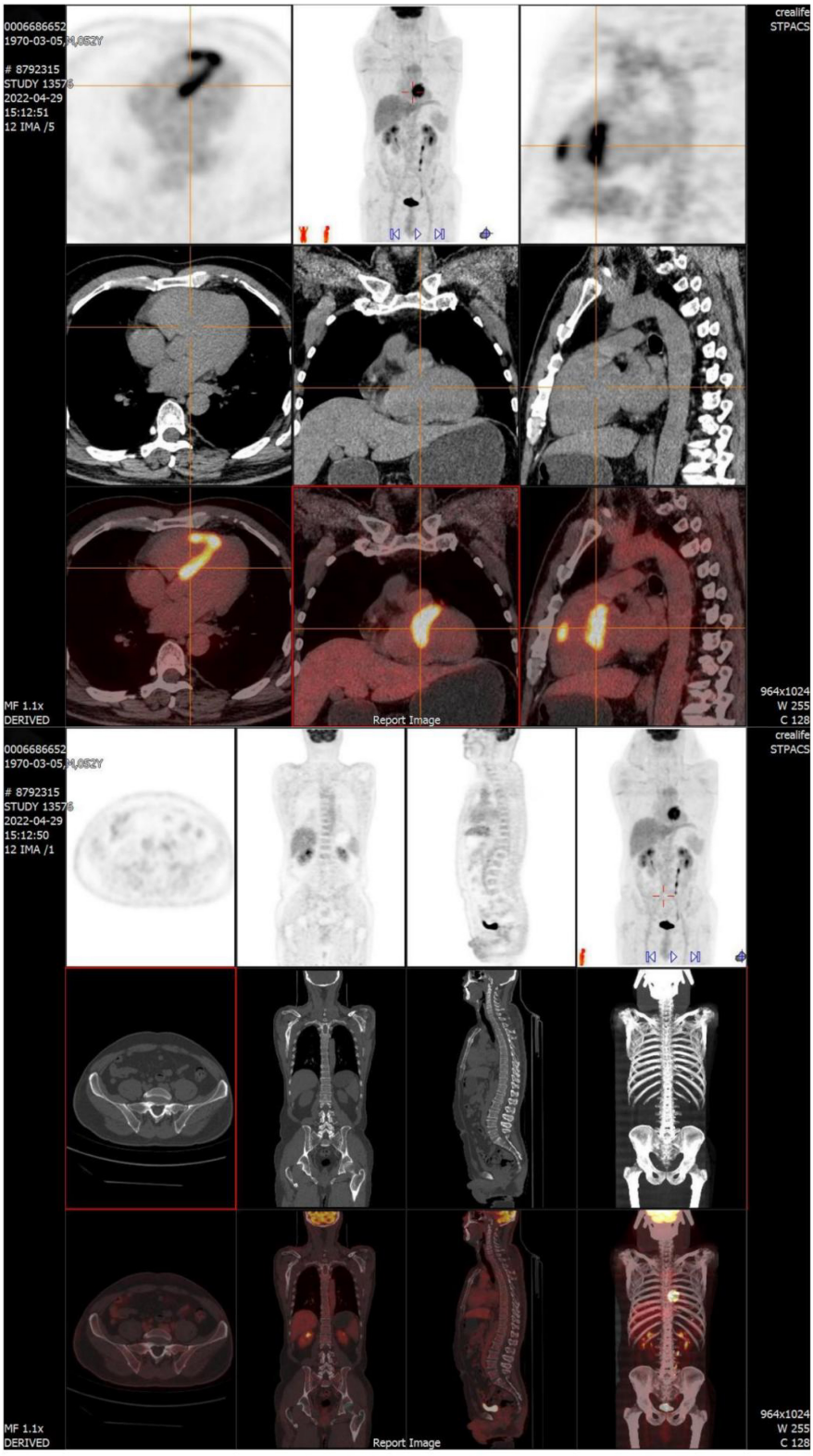


FIGURE 2
FDG-PET reveals intense multifocal cardiac uptake in the interventricular septum and right ventricle, and no abnormal lesions are found in other parts of the body. FDG-PET, Fluorine-18 fluorodeoxyglucose positron emission tomography.

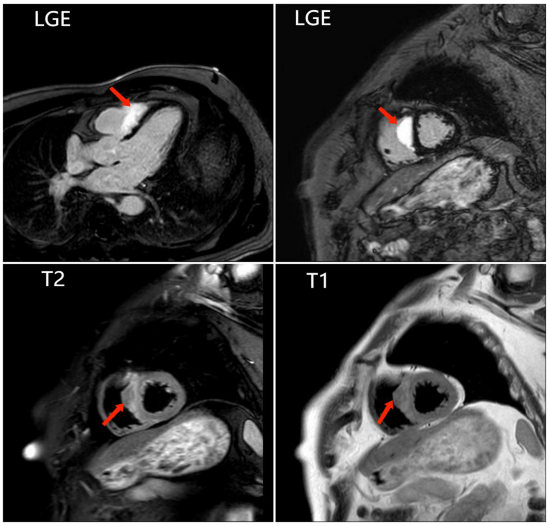


FIGURE 3
The last cardiac magnetic resonance is used for accurately locating the lesion and improving the success rate of the endomyocardial biopsy. Images show abnormal signals in the right ventricular surface of the ventricular septum, and significant LGE.

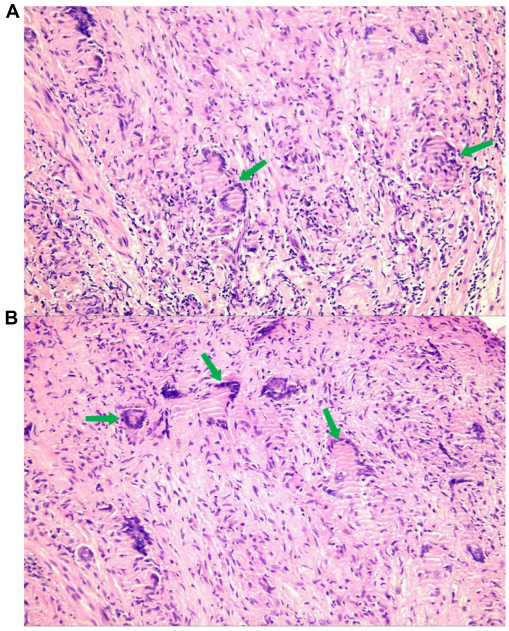


FIGURE 4
A large number of epithelioid nodules composed of epithelioid cells, multinucleated giant cells [**A,B** (green arrow)], and lymphocytes are found in the myocardium and endocardium.

by cardiac tumor, and suggested that the patient should undergo cardiac biopsy in our hospital.

After admission, based on the patient's imaging findings and symptoms, we considered a possible diagnosis of: CS, myocarditis, hypertrophic cardiomyopathy, or myocardial amyloidosis. CS can invade any part of the myocardium. However, transmural involvement of the left and right ventricular walls is the most common. The inflammatory phase of CS is characterized by myocardial granulomatous infiltration, inflammation, and edema. This can lead to local thickening and abnormal movement of the heart muscle. Although both CS and myocarditis manifest cardiac inflammation, myocarditis mostly involves the lateral wall of the heart, whereas CS mostly involves the septum (4). In patients with CS, myocardial granulomatous infiltration can lead to thickening of the myocardial wall, morphologically similar to hypertrophic cardiomyopathy. However, in this case, abnormal FDG-PET uptake foci were observed. Moreover, ECG showed ventricular arrhythmia, and hypertrophic cardiomyopathy was not detected. The most typical imaging features of cardiac amyloidosis are extensive LGE, most prominent in the subendocardial layer. In addition, in CS, subepicardial LGE is observed.

To further clarify the cause of arrhythmia, we performed an EMB. To accurately locate the lesion and improve the success rate of the EMB, the patient underwent the last CMR (**Figure 3**). Using CMR imaging guidance, EMB was taken from interventricular septum tissue of the right ventricle. EMB revealed a large number of epithelioid nodules composed of epithelioid cells, multinucleated giant cells, and lymphocytes in the myocardium and endocardium. However, no necrotic tissue was found on acid-fast staining (–) (**Figure 4**). Based on the clinical manifestations, imaging data, and pathological features, we diagnosed the patient with ICS. Thereafter, the patient received dual-chamber implantable cardioverter defibrillator to prevent sudden death, while prednisone (35 mg/d) was administered to treat sarcoidosis. Additionally, spironolactone (20 mg/d) and daglitazine (10 mg/d) were administered to delay ventricular remodeling.

During 2 months after discharge, the patient had no symptoms of palpitations. The 24-h Holter monitoring showed frequent premature ventricular contractions without further ventricular tachycardia. FDG-PET showed that the area of increased glucose metabolism in the original lesion was reduced, indicating the effectiveness of immunosuppressive therapy (**Figure 5**).

## Discussion

Due to the low incidence and inconsistent diagnostic methods of ICS, it is often missed or misdiagnosed. However, multimodal imaging evaluation is of great significance to guide diagnosis of CS. A Japanese study indicated that approximately 26.8% of patients with CS could be diagnosed with ICS (5). Some studies have shown that patients with ICS might have poor prognosis and are more likely to develop heart failure and other

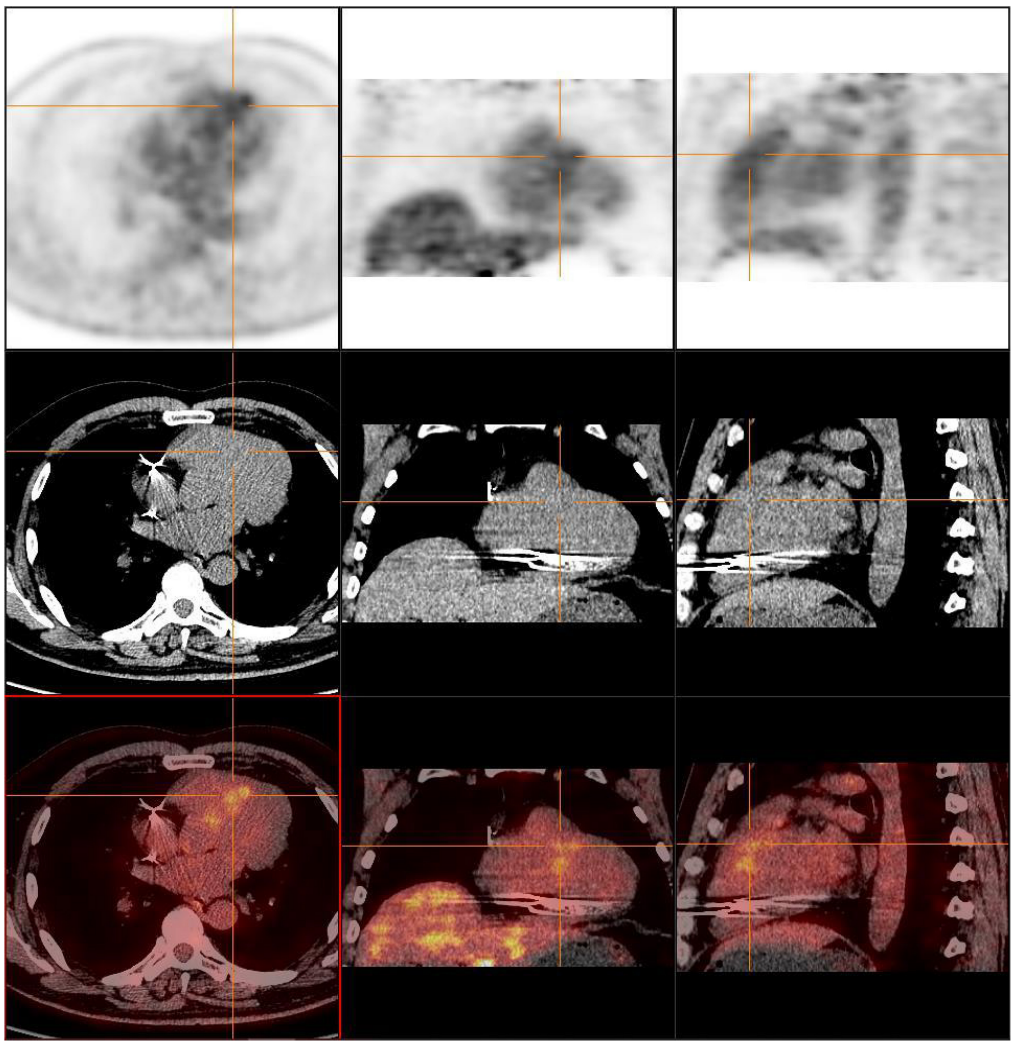

FIGURE 5
FDG-PET showed that the area of increased glucose metabolism in the original lesion was reduced, indicating the effectiveness of immunosuppressive therapy.

adverse cardiac events (6). Therefore, early diagnosis of CS using multimodal imaging is useful for achieving a favorable patient prognosis. Advanced cardiac imaging of CS includes CMR and FDG-PET. A meta-analysis by Zhang et al. showed that CMR imaging had 95% sensitivity and 92% specificity for detection of CS (7). On the one hand, FDG-PET can be used for detecting myocardial inflammation and metabolism of lesions caused by granulomatous infiltration in patients with CS. However, FDG-PET can detect systemic lesions outside the heart and help identify other organs affected by sarcoidosis. CMR focuses on examining deconstruction and perfusion of the heart and can directly reflect exercise ability and degree of fibrosis of the heart. FDG-PET focuses more on the degree of inflammation and metabolism of lesions. The complementary advantages of the two methods can help better diagnose CS, which is the significance of multimodal imaging examinations.

Although some researchers advocate CS diagnosis through clinical manifestations and imaging examination, EMB is the gold standard for CS diagnosis. Owing to the uneven distribution of non-caseous granulomas in the myocardial endocardium, the positive predictive accuracy of EMB is low. In our case, to accurately obtain tissue from the lesion, we used CMR to locate the lesions and thus, obtained positive results. Some studies have reported that the positive predictive value of EMB could reach 89% (8) when the electrolytic voltage profile is consistent with that of the CMR image. Therefore, regarding CS, advanced imaging cannot only screen high-risk patients to assist diagnosis but also guide EMB to improve the detection rate. Based on our experience, advanced imaging examination should be improved in time to prevent missed diagnosis in patients with the following conditions: First, unexplained palpitations, syncope, decreased ejection fraction, or previous heart failure.

Second, unexplained left or right bundle branch block; second or third degree atrioventricular block; atrial arrhythmia; and ventricular arrhythmia occur. Third, unexplained wall thickness and wall motion abnormalities are observed on echocardiography.

Corticosteroid immunosuppressants are currently the first-line treatment of sarcoidosis as they improve cardiac remodeling and effectively relieve symptoms when used as early as possible after CS diagnosis. Of note, CMR and FDG-PET scans can also be used for evaluating the efficacy of immunosuppressive therapy in patients with CS.

Based on the findings of our case, due to lack of specific biomarkers for detecting CS and ICS, diagnosis is still very difficult. Multimodal imaging examination should be used more frequently in patients with suspected CS or having high-risk factors for CS. Timely and accurate diagnosis has important clinical significance for better follow-up, treatment, and prognosis of patients.

## Data availability statement

The original contributions presented in this study are included in the article/supplementary material, further inquiries can be directed to the corresponding author.

## Ethics statement

The studies involving human participants were reviewed and approved by the Clinical Research Ethics Committee, First Hospital of Lanzhou University. The patients/participants provided their written informed consent to participate in this study. Written informed consent was obtained by the patients/participants for the publication of this case study.

## Author contributions

YW and XN contributed to manuscript writing. JX, GJ, SH, and MB contributed to concept design, manuscript editing, and revision. All authors contributed to the article and approved the submitted version.

## Funding

This work was supported by the Special Fund for Civil-Military Integration Development of Gansu Province (grant no. 2060303), the Science and Technology Program of Gansu Province (grant no. 21JR1RA100), the Scientific Research Project of Health Industry of Gansu Province (grant no. GSWSKY2020-64), and the Foundation of the First Hospital of Lanzhou University (grant no. ldyyyn2020-47).

## Conflict of interest

The authors declare that the research was conducted in the absence of any commercial or financial relationships that could be construed as a potential conflict of interest.

## Publisher's note



## References

1. Hutchinson J. Statement on sarcoidosis. Joint statement of the American Thoracic Society (ATS), the European Respiratory Society (ERS) and the World Association of Sarcoidosis and Other Granulomatous Disorders (WASOG) adopted by the ATS Board of Directors and by the ER. *Am J Respir Crit Care Med.* (1999) 160:55. doi: 10.1164/ajrccm.160.2.ats4-99

2. Baughman RP, Lower EE, du Bois RM. Sarcoidosis. *Lancet.* (2003) 361:1111. doi: 10.1016/S0140-6736(03)12888-7

3. Birnie DH, Kandolin R, Nery PB, Kupari M. Cardiac manifestations of sarcoidosis: diagnosis and management. *Eur Heart J.* (2017) 38:2663–70.

4. Jeudy J, Burke AP, White CS, Kramer GB, Frazier AA. Cardiac sarcoidosis: the challenge of radiologic-pathologic correlation—erratum. *Radiographics.* (2015) 35:1316. Erratum for: Radiographics. 2015;35:657–679. doi: 10.1148/rg.2015154010

5. Tezuka D, Terashima M, Kato Y, Toriihara A, Hirasawa K, Sasaoka T, et al. Clinical characteristics of definite or suspected isolated cardiac sarcoidosis: application of cardiac magnetic resonance imaging and 18F-Fluoro-2-deoxyglucose positron-emission tomography/computerized tomography. *J Card Fail.* (2015) 21:313–22. doi: 10.1016/j.cardfail.2014.12.004

6. Yafasova A, Fosbøl EL, Schou M, Gustafsson F, Rossing K, Bundgaard H, et al. Long-term adverse cardiac outcomes in patients with sarcoidosis. *J Am Coll Cardiol.* (2020) 76:767–77. doi: 10.1016/j.jacc.2020.06.038

7. Zhang J, Li Y, Xu Q, Xu B, Wang H. Cardiac magnetic resonance imaging for diagnosis of cardiac sarcoidosis: a meta-analysis. *Can Respir J.* (2018) 2018:7457369. doi: 10.1155/2018/7457369

8. Casella M, Dello Russo A, Bergonti M, Catto V, Conte E, Sommariva E, et al. Diagnostic yield of electroanatomic voltage mapping in guiding endomyocardial biopsies. *Circulation.* (2020) 142:1249–60. doi: 10.1161/CIRCULATIONAHA.120.046900

frontiers | Frontiers in Cardiovascular Medicine

TYPE Case Report
PUBLISHED 18 October 2022
DOI 10.3389/fcvm.2022.1013044



OPEN ACCESS

EDITED BY
Zhongchan Sun,
Guangdong Academy of Medical Sciences, China

REVIEWED BY
Quanmei Ma,
Guangdong Provincial People's Hospital, China
Guang Tong,
Guangdong Provincial People's Hospital, China

*CORRESPONDENCE
Yun Zhang
zhangyun@sdu.edu.cn

SPECIALTY SECTION
This article was submitted to Cardiovascular Imaging, a section of the journal Frontiers in Cardiovascular Medicine

RECEIVED 06 August 2022
ACCEPTED 27 September 2022
PUBLISHED 18 October 2022

CITATION
Ma L, Yang J, Liu Y, Wang F, Liu T, Wang Y, Sun H, Zhang C and Zhang Y (2022) Case report: Acute ST-elevation myocardial infarction and cardiogenic shock caused by a giant right sinus of Valsalva aneurysm and right coronary artery compression.
*Front. Cardiovasc. Med.* 9:1013044.
doi: 10.3389/fcvm.2022.1013044



# Case report: Acute ST-elevation myocardial infarction and cardiogenic shock caused by a giant right sinus of Valsalva aneurysm and right coronary artery compression

Lianyue Ma[1], Jianmin Yang[1], Yan Liu[1], Fang Wang[2], Tongtao Liu[1], Ying Wang[1], Hourong Sun[3], Cheng Zhang[1] and Yun Zhang[1]*

[1]The Key Laboratory of Cardiovascular Remodelling and Function Research, Chinese Ministry of Education, Chinese National Health Commission and Chinese Academy of Medical Sciences, The State and Shandong Province Joint Key Laboratory of Translational Cardiovascular Medicine, Department of Cardiology, Qilu Hospital of Shandong University, Jinan, China, [2]Department of Radiology, Qilu Hospital of Shandong University, Jinan, China, [3]Department of Cardiac Surgery, Qilu Hospital of Shandong University, Jinan, China

A sinus of Valsalva aneurysm (SVA) is a rare aortic disease that may be congenital or acquired. Patients with an intact SVA are usually asymptomatic, whereas a ruptured SVA may cause acute chest pain and dyspnea. We present a rare case of acute ST-elevation myocardial infarction and cardiogenic shock in a 51-year-old man. Emergency coronary angiography revealed a giant aneurysm with an absence of flow in the right coronary artery. Both two-dimensional echocardiography and computed tomography angiography showed a giant right SVA, which ruptured into the pericardial sac and led to extrinsic compression of the right coronary artery. Surgical repair combined with coronary bypass grafting was performed. Unfortunately, the patient died from low cardiac output syndrome and postoperative multiple organ failure. This case highlights that the possibility of SVA rupture should be considered in acute myocardial infarction cases and that echocardiography and coronary computed tomography angiography are important in providing an accurate and rapid SVA diagnosis.

KEYWORDS

**sinus of Valsalva aneurysm, acute myocardial infarction, echocardiography, computed tomography angiography, right coronary artery compression, case report**

## Introduction

A sinus of Valsalva aneurysm (SVA) is a rare cardiac anomaly, with an approximately 0.09% estimated prevalence in the general population (1). Men are two to four times more likely to be affected than women (2, 3). The incidence of ruptured SVA is approximately five times higher in Asians than in Westerners (4). SVAs are most common in the right coronary sinus, followed by the noncoronary and the left coronary sinuses. Although it can be acquired (2, 5, 6) from trauma, infections, and degenerative diseases, it is more frequently congenital. SVA pathology includes the absence of elastic media tissue between the aortic sinus and the hinge line of the aortic annulus, which weakens the aortic wall and results in aneurysmal formation (3). Unruptured SVAs are mostly asymptomatic unless there are complications. In contrast, ruptured SVAs usually cause severe damage and lead to diverse clinical manifestations such as chest pain, dyspnea, tachycardia, or fatigue. Acute myocardial infarction (AMI) may be caused by compression or thrombotic occlusion of the coronary artery (7, 8). An SVA ruptures into the pericardium is fatal owing to pericardial tamponade, with sudden cardiac arrest as the first symptom (9). Herein, we report a giant, ruptured right SVA (RSVA) that extrinsically compressed the right coronary artery (RCA) and presented as acute ST-elevation myocardial infarction and cardiogenic shock.

## Case description

A 51-year-old man who had previously been in good condition with no history of smoking or cardiovascular diseases was admitted to a local hospital after presenting with abrupt chest pain, nausea, and emesis for 2 h. He was hemodynamically unstable (blood pressure, 82/50 mmHg; pulse, 48 beats/min). The 18-lead electrocardiogram revealed sinus bradycardia, second-degree atrioventricular block, and ST-segment elevation in leads II, III, aVF, and V3R-V5R (Figure 1). The myoglobin, creatine kinase-MB, troponin I, and N-terminal pro-brain natriuretic peptide levels were 399.6 ng/ml (reference value, <70.0 ng/ml), 66.12 ng/ml (reference value, <5.0 ng/ml), 2.39 ng/ml (reference value, <0.1 ng/ml), and 6,037.0 pg/ml (reference value, ≤300 pg/ml), respectively. The low-density lipoprotein cholesterol level was 2.16 mmol/L (reference value, 0–3.7 mmol/L). The D-dimer level was 0.55 μg/ml (reference value, <0.5 μg/ml). The blood creatinine was 76 μmol/L (reference value, 44–123 μmol/L), with

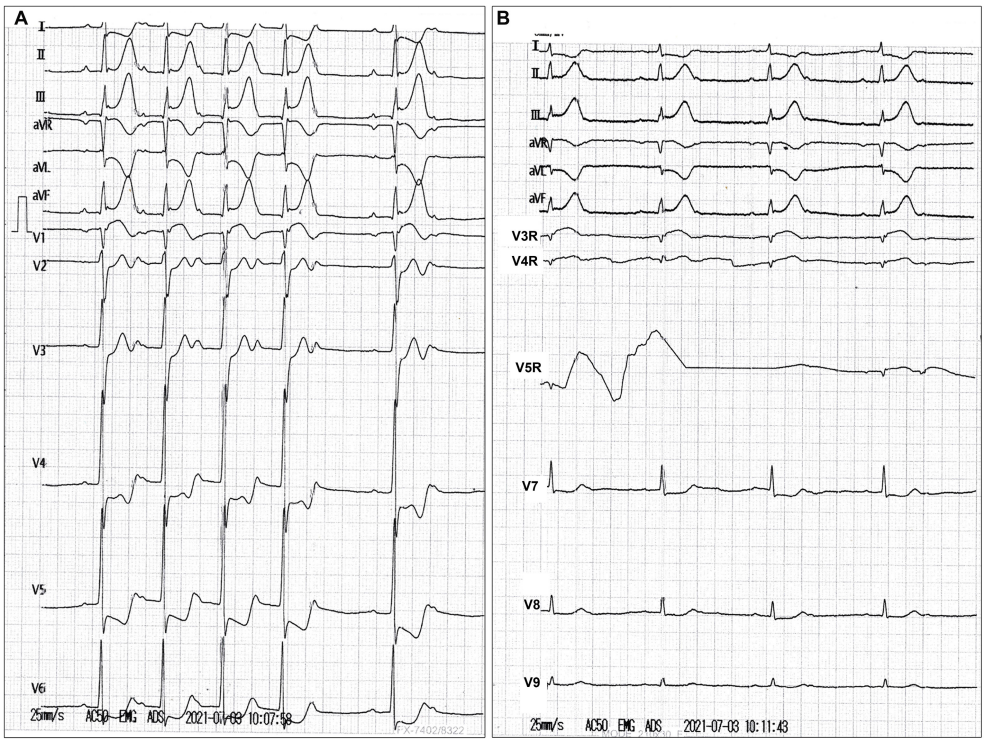


FIGURE 1
**(A,B)** Electrocardiography images.

10.3389/fcvm.2022.1013044

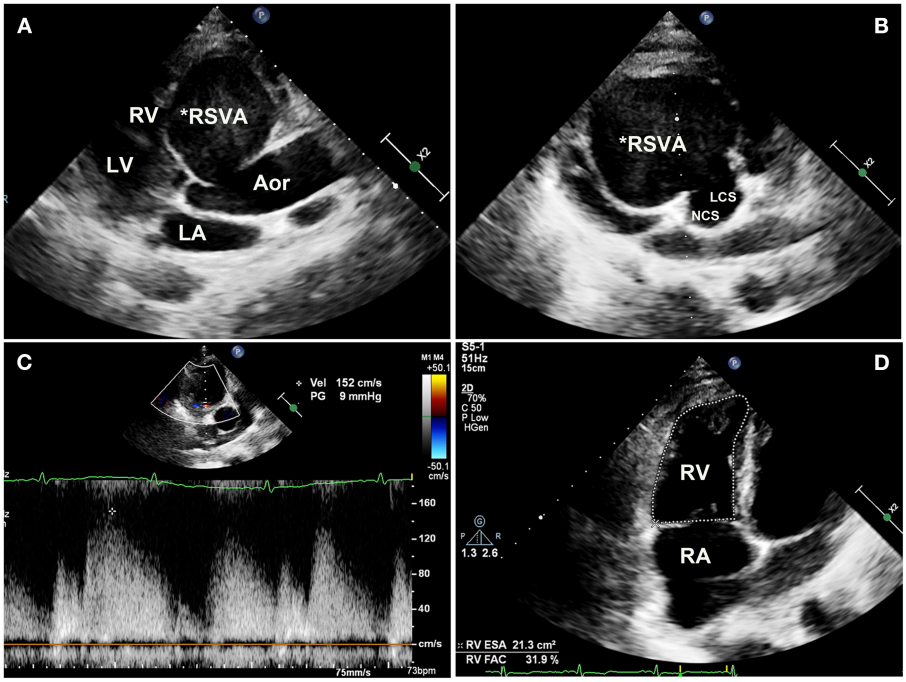


FIGURE 2
Transthoracic echocardiography images. **(A)** Transthoracic echocardiography showing a giant right sinus of Valsalva aneurysm in the long-axis view and **(B)** the aortic root. **(C)** The compressed RCA is displaced with an accelerating velocity of 150 cm/s. **(D)** The right ventricular systolic fraction is reduced (31.9% RVFAC). RSVA, right sinus of Valsalva aneurysm; RV, right ventricle; LV, left ventricle; LA, left atrium; Aor, aorta; NCS, noncoronary sinus; LCS, left coronary sinus; RA, right atrium; RVFAC, right ventricular fractional area change.

a eGFR of 99.69 ml/(min*1.73 $m^2$). The patient's liver function was mildly impaired (Child-Pugh A level, no hepatic encephalopathy and ascites, 19.8 μmol/L of bilirubin, 32.3 g/L of albumin, PT-INR 1.04). Loading doses of aspirin and clopidogrel were administered. Emergency coronary angiography revealed persistent swirling of contrast within a large aneurysmal dilatation with an absence of flow in the RCA (Supplementary Video 1). No significant stenosis of the left coronary artery, but a myocardial bridge of the left anterior descending artery was observed (Supplementary Video 2). Bedside echocardiography showed a huge aneurysm (62 mm × 56 mm) close to the right atrium, an enlarged right heart, and severe tricuspid regurgitation. No pericardial effusion was observed. He was subsequently transferred to our hospital.

On physical examination, his blood pressure was 93/70 mmHg with dopamine infusion, and he had a pulse rate of 128 beats/min. No heart murmurs were auscultated. However, the patient's blood pressure became stable after the dopamine infusion was discontinued. Transthoracic echocardiography (Supplementary Video 3) demonstrated a giant RSVA in a prothrombotic state with a small degree of pericardial effusion (Figures 2A,B). The RCA was displaced and compressed with an accelerating velocity (Figure 2C). The inferoposterior left ventricular and lateral right ventricular wall motions were abnormal. The right heart was enlarged and right ventricular systolic function was reduced (right ventricular fractional area change of 31.9%, tricuspid annular plane systolic excursion of 13 mm, Figure 2D, Supplementary Video 4). The left ventricular ejection fraction was 51%. The inferior vena cava diameter was 25 mm, with <50% inspiratory collapse. Coronary computed tomography angiography (CTA) revealed a huge RSVA (65 mm × 70 mm) with contrast medium leakage into the pericardial sac, revealing a rupture of the RSVA (Figures 3A,B); however, it did not show signs of tamponade. The RCA was severely compressed and stretched by the giant aneurysm (Figure 3C) and its proximal segment was relatively slender (Figure 3D).

Cardiac surgery was performed using standard cardiopulmonary bypass with moderate hypothermia. Pericardial adhesion was extensive, and there was severe blood loss. After opening the pericardial sac, a huge, dull red aneurysm was seen (Supplementary Figure 1A). Aortic incision was performed, and the aneurysm was explored, revealing no thrombus and a size of 60 mm × 50 mm × 40 mm. The RSVA

Abbreviations: SVA, sinus of Valsalva aneurysm; RSVA, right SVA; AMI, acute myocardial infarction; CTA, computed tomography angiography; RCA, right coronary artery; LCOS, low cardiac output syndrome.

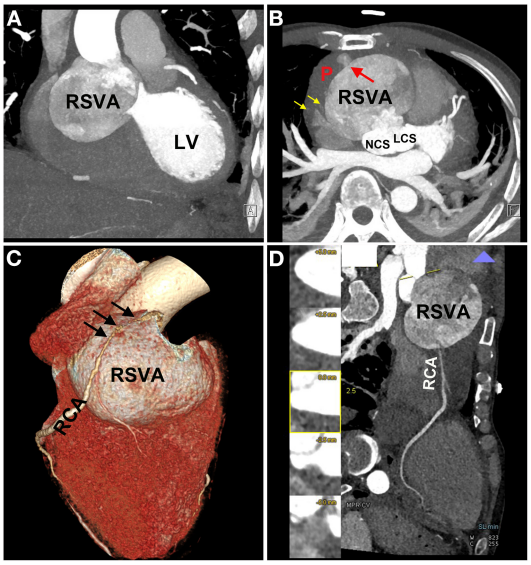


FIGURE 3
Coronary computed tomography angiography (CTA) images. CTA images showing the RSVA **(A)**, which ruptured to the pericardium [red arrow **(B)**], and some contrast medium leakage into the pericardial sac [yellow arrows **(B)**]; the severely compressed RCA is stretched across the aneurysmal surface [black arrows **(C)**]; the proximal segment of RCA was relatively slender **(D)**. RSVA, right sinus of Valsalva aneurysm; LV, left ventricle; NCS, noncoronary sinus; LCS, left coronary sinus; RCA, right coronary artery.

diagnosis was confirmed, and the RSVA wall appeared fragile and bled profusely. Unfortunately, the perforation was too small to be detected. The orifice of the RSVA neck was ~25 mm in diameter and was closed with a continuous suture and a bovine epicardial patch of suitable size (Supplementary Figures 1B,C). The RCA was confirmed to originate from the aneurysm, and its proximal segment was displaced and severely compressed along with the right ventricle. Thereafter, the RCA was bypassed with a saphenous vein graft. The intraoperative blood flow of the vein graft, measured with a flowmeter, was 130 ml/min. Ventricular fibrillation occurred, and sinus rhythm was restored after one electrical defibrillation. Subsequent cardiopulmonary bypass weaning was successful, and the mediastinal pericardial drainage tube was retained. Exactly 10 units of red blood cells, 1,200 ml fresh plasma, 28 units of cryoprecipitate, and one therapeutic dose of platelets were transfused owing to hemorrhage during surgery. Furthermore, prothrombotic agents, including factor VII, human prothrombotic complex, and human fibrinogen, were also used.

The patient was transferred to the cardiac care unit after surgery. The patient showed signs and symptoms indicative of low cardiac output syndrome (LCOS), manifested as hypotension (80–110/40–70 mmHg with dobutamine), tachycardia (101–123 beats/min in sinus rhythm), poor perfusion (week pulses, cold extremities) and oliguria (0.4 ml/kg/h in the case of diuretics). Central venous pressure values ranged from 16 to 22 mmHg. Laboratory examination demonstrated an increase in lactate of >2 mmol/L on two successive blood gases (2.2–5.0 mmol/L). Bedside echocardiography showed an enlarged right ventricle with poor mobility. The increased right ventricular pressure interfered with the left ventricle volume capacity, despite a 50% ejection fraction. The inferior vena cava diameter was 17 mm with <50% collapse. Several interventions were initiated as the diagnosis of LCOS was established, including administering appropriate dosages of analgesia and sedation, continuing mechanical ventilation, maintaining mild hypothermia in the patient, treating tachyarrhythmias promptly, optimizing preload, intra-aortic balloon pump assistance, and pharmacotherapeutic agents enhancing contractility to improve cardiac output. The patient presented disseminated intravascular coagulation, manifesting reduced platelet count ($<100*10^9$/L), prolonged thrombin time (>3 s), and elevated fibrin-related markers (D-dimer >10-fold limit of normal). The patient's liver and renal function were aggravated progressively. On the second day, ventricular tachycardia was reported. The patient died on the third day after surgery.

Timeline is shown in Table 1.

## Discussion

Sinus of Valsalva aneurysms leading to AMI are reportedly associated with direct compression (7) or thrombotic occlusion of the coronary artery (8). In our case, the giant RSVA manifested as an acute ST-elevation myocardial infarction with several probable contributing mechanisms. First, RCA compression by the giant aneurysm resulted in a severe coronary oxygen supply-demand mismatch. Second, RCA displacement and stretching across the aneurysmal surface may have disturbed the coronary blood flow. Finally, the echocardiographic prothrombotic state suggested hypercoagulation, which might have led to a detached thrombus forming in the giant RSVA, traveling into the RCA. Another feature was the RSVA rupture into the pericardium. An SVA rupture into the pericardium is fatal owing to pericardial tamponade (9). Cardiogenic shock could have resulted from the AMI or the pericardial tamponade. In this case, despite preoperative transthoracic echocardiography and coronary CTA demonstrating RSVA rupture into the pericardium, the pericardial effusion was small, and the patient's blood pressure gradually stabilized without vasoactive agents or pericardiocentesis. Thus, the leading causes of the cardiogenic shock may have been AMI and severe right heart failure rather than pericardial tamponade. Extensive pericardial adhesion and a tiny perforation might have caused limited pericardial effusion. These two concurrent features make this case uncommon.

TABLE 1 The patient's admission timeline, diagnosis, and treatment.

| Day | Events |
|---|---|
| 30 h prior | The patient presented with abrupt chest pain, nausea, and emesis for 2 h and was admitted to a local hospital |
| | Physical examination: blood pressure, 82/50 mmHg; pulse, 48 beats/min |
| | Electrocardiogram: sinus bradycardia, second-degree atrioventricular block, and ST-segment elevation in leads II, III, aVF, and V3R-V5R |
| | Laboratory tests: elevated myoglobin, creatine kinase MB, troponin I, and N-terminal pro-brain natriuretic peptide |
| | Emergency coronary angiography: a giant aneurysm with an absence of flow in the RCA |
| | Bedside echocardiography: a huge aneurysm, enlarged right heart, severe tricuspid regurgitation, no pericardial effusion |
| 1 | The patient was admitted into our hospital |
| 3 | 24-h Holter monitor results: sinus rhythm, premature atrial contraction, frequent multifocal premature ventricular contraction, ST-segment, and T-wave changes |
| 8 | Transthoracic echocardiography: a giant RSVA in a prothrombotic state, with a small pericardial effusion. The RCA was displaced and compressed, regional wall movement abnormalities, reduced right ventricular systolic function, and dilated inferior vena cava. Tricuspid regurgitation and pulmonary artery hypertension were reduced than before |
| | Coronary computed tomography: a huge RSVA (65 mm × 70 mm), which ruptured into the pericardial sac. The RCA was severely compressed and stretched by the giant aneurysm |
| 14 | Thoracic computed tomography: bilateral pneumonia, pleural effusion, sachet-like iso-density structure in front of the ascending aorta |
| 18 | Preoperative transthoracic echocardiography: a giant RSVA in a prothrombotic state, reduced inferior vena cava's diameter and tricuspid regurgitation |
| 19 | Cardiac surgery: The diagnosis of RSVA was confirmed. The perforation was too small to be detected. Combined repair of the ruptured RSVA and coronary artery bypass grafting were performed. Ventricular fibrillation occurred once during the surgery |
| 21 | Bedside echocardiography: enlarged right ventricle with poor function. Electrocardiogram: ventricular tachycardia |
| 22 | The patient died owing to LCOS and multiple organ failure |

Echocardiographic findings of a ruptured SVA were first reported in 1974 (10), and the usefulness of two-dimensional and Doppler echocardiography in assessing such aneurysms was well documented thereafter. Transesophageal echocardiography may provide more information about the aneurysm and its rupture. Both electrocardiogram-gated cardiac CTA and cardiac magnetic resonance imaging can provide excellent anatomic depiction, and cardiac magnetic resonance imaging can provide valuable functional information (11). The echocardiographic exam in this report showed an anatomic abnormality. Therefore, it was possible to evaluate the size and location of the aneurysmal sac. However, myocardial viability detected by single photon emission computed tomography, positron emission tomography, or cardiac magnetic resonance imaging was not performed for financial and safety reasons, which is a limitation of the case. Turbulent fluid was detected inside the SVA. However, the SVA perforation was not detected because of its position or small size. Coronary CTA findings were in line with those of the echocardiography, and the aneurysm was observed to originate from the right coronary sinus, while the aneurysm sac was filled with heterogeneously mixed contrast agents because of its large size. The RCA originated from the right anterior upper part of the RSVA. The proximal segment of the RCA was relatively slender owing to the extrinsic compression of the giant aneurysm, and the relevant positional relationship and SVA perforation location were detected.

The mainstay treatment option for SVA is surgical intervention. Early aggressive treatment is recommended for ruptured SVA to prevent endocarditis or lesion enlargement, which leads to worse symptoms necessitating more extensive repair (2). Surgical strategies include aneurysm resection, patch repair, Bentall procedures, aneurysm closure with concomitant aortic valve replacement, and transcatheter closure (2, 12, 13). So the surgery was finally performed because of the RSVA's rupture and prothrombotic state in this patient. However, the RSVA of this patient might have been through chronic rupture and repaired repeatedly; as seen in the surgery, the pericardial adhesion was extensive, and the wall of the RSVA was thickened, fragile, and abundant in blood vessels. The surgeons thought removing the RSVA at that time was difficult; thus, we performed surgical repair instead. However, the RSVA wall was too fragile to bleed profusely. The limitation of our management was that we focused more on managing AMI and the giant RSVA and neglected the effect of tricuspid regurgitation on right heart function. In hindsight, Bentall procedures and tricuspid valvuloplasty might be more suitable for this patient. The lesson learned from this patient was that we should pay more attention to comprehensive and individualized treatments.

## Conclusion

Acute myocardial infarction caused by a ruptured SVA is a rare cardiac condition that often carries a poor prognosis. This case demonstrates that the possibility of an SVA rupture should be considered in AMI cases. Echocardiography

and coronary CTA evaluation are important in providing an accurate and rapid SVA diagnosis. Surgical intervention is still the mainstay and most effective treatment for a ruptured SVA.

## Data availability statement

The original contributions presented in the study are included in the article/Supplementary material, further inquiries can be directed to the corresponding author.

## Ethics statement

The studies involving human participants were reviewed and approved by Ethics Committee of Shandong University Qilu Hospital. The patients/participants provided their written informed consent to participate in this study.

## Author contributions

LM and JY contributed to the manuscript writing. YL and FW contributed to the collection of figures. LM, TL, YW, HS, and CZ contributed to the clinical treatment of this case. YZ contributed to the review of the manuscript. All authors approved the submitted version.

## Funding

This work was supported by a grant from the National Natural Science Foundation of China (81800382), the key Research and Development Plan of Shandong Province (No. 2021SFGC0503).

## Conflict of interest

The authors declare that the research was conducted in the absence of any commercial or financial relationships that could be construed as a potential conflict of interest.

## Publisher's note



## Supplementary material

The Supplementary Material for this article can be found online at: https://www.frontiersin.org/articles/10.3389/fcvm.2022.1013044/full#supplementary-material

## References

1. Smith WA. Aneurysm of the sinus of Valsalva, with report of 2 cases. *JAMA.* (1914) 62:1878–80. doi: 10.1001/jama.1914.02560490024006

2. Takach TJ, Reul GJ, Duncan JM, Cooley DA, Livesay JJ, Ott DA, et al. Sinus of Valsalva aneurysm or fistula: management and outcome. *Ann Thorac Surg.* (1999) 68:1573–77. doi: 10.1016/S0003-4975(99)01045-0

3. Ott DA. Aneurysm of the sinus of Valsalva. *Semin Thorac Cardiovasc Surg Pediatr Card Surg Annu.* (2006) 9:165–76. doi: 10.1053/j.pcsu.2006.02.014

4. Chu SH, Hung CR, How SS, Chang H, Wang SS, Tsai CH, et al. Ruptured aneurysms of the sinus of Valsalva in oriental patients. *J Thorac Cardiovasc Surg.* (1990) 99:288–98. doi: 10.1016/S0022-5223(19)37013-8

5. Abetti A, Gandet T, Amri AAA, Ibrahimi MO, Rouviere P, Meilhac A, et al. Ruptured right Valsalva sinus into the right atrium due to infective endocarditis: a case report. *Pan Afr Med J.* (2020) 37:65. doi: 10.11604/pamj.2020.37.65.21491

6. Li X, Zhong Y, Rao L, Bai W. A dissecting aneurysm of the sinus of Valsalva involving the inter-ventricular septum in a patient with syphilis and a quadricuspid aortic valve. *Echocardiography.* (2021) 38:1061–3. doi: 10.1111/echo.15055

7. Zhuo GY, Zhang PY, Luo L, Tang Q, Xiang T. Ruptured sinus of Valsalva aneurysm presenting as syncope and hypotension: a case report. *BMC Cardiovasc Disord.* (2021) 21:449. doi: 10.1186/s12872-021-02247-4

8. Hattori TI, Yoshida R, Yoshida Y, Akita S, Kato W, Tajima K, et al. A case of acute myocardial infarction caused by a giant thrombus derived from an aneurysm of the sinus of Valsalva and a bioprosthetic aortic valve. *J Echocardiogr.* (2021) 19:181–2. doi: 10.1007/s12574-020-00464-y

9. Zhu BL, Quan L, Ishida K, Taniguchi M, Oritani S, Kamikodai Y, et al. Fatal traumatic rupture of an aortic aneurysm of the sinus of Valsalva: an autopsy case. *Forensic Sci Int.* (2001) 116:77–80. doi: 10.1016/S0379-0738(00)00365-0

10. Rothbaum DA, Dillon JC, Chang S, Feigenbaum H. Echocardiographic manifestation of right sinus of Valsalva aneurysm. *Circulation.* (1974) 49:768–71. doi: 10.1161/01.CIR.49.4.768

11. Bricker AO, Avutu B, Mohammed TL, Williamson EE, Syed IS, Julsrud PR, et al. Valsalva sinus aneurysms: findings at CT and MR imaging. *Radiographics.* (2010) 30:99–110. doi: 10.1148/rg.301095719

12. Wingo M, de Angelis P, Worku BM, Leonard JR, Khan FM, Hameed I, et al. Sinus of Valsalva aneurysm repairs: operative technique and lessons learned. *J Card Surg.* (2019) 34:400–3. doi: 10.1111/jocs.14041

13. Weinreich M, Yu P-J, Trost B. Sinus of Valsalva aneurysms: review of the literature and an update on management. *Clin Cardiol.* (2015) 38:185–9. doi: 10.1002/clc.22359

frontiers | Frontiers in Cardiovascular Medicine

TYPE Case Report
PUBLISHED 26 October 2022
DOI 10.3389/fcvm.2022.986078



OPEN ACCESS

EDITED BY
Riccardo Liga,
Pisana University Hospital, Italy

REVIEWED BY
Jaganmohan Tharakan,
Cardiologist Researcher India, India
Roberto Spina,
Gosford Hospital, Australia

*CORRESPONDENCE
Mohammadbagher Sharifkazemi
dr.sharifkazemi@gmail.com

SPECIALTY SECTION
This article was submitted to Cardiovascular Imaging, a section of the journal Frontiers in Cardiovascular Medicine

RECEIVED 04 July 2022
ACCEPTED 12 October 2022
PUBLISHED 26 October 2022

CITATION
Sharifkazemi M, Mohseni-Badalabadi R, Hosseinsabet A and Hajizeinali A (2022) Case report: Multimodal imaging diagnosis of a giant coronary artery fistula: A report of two cases. *Front. Cardiovasc. Med.* 9:986078. doi: 10.3389/fcvm.2022.986078



# Case report: Multimodal imaging diagnosis of a giant coronary artery fistula: A report of two cases

Mohammadbagher Sharifkazemi[1]*, Reza Mohseni-Badalabadi[2], Ali Hosseinsabet[2] and Alimohammad Hajizeinali[3]

[1]Department of Cardiology, Nemazee Hospital, Shiraz University of Medical Sciences, Shiraz, Iran, [2]Department of Cardiology, Tehran Heart Center, Tehran University of Medical Sciences, Tehran, Iran, [3]Department of Interventional Cardiology, Tehran Heart Center, Tehran University of Medical Sciences, Tehran, Iran

Being a very rare cardiac disease, most cases of coronary artery fistula (CAF) are genetic. Complications such as coronary steal syndrome, myocardial infarction, heart failure, or tamponade can manifest following the abnormal communication that the fistula creates between the coronary arteries and cardiac chambers or major vessels and the subsequent shunt. Most CAFs are small and asymptomatic, making diagnosis difficult. In symptomatic patients, the initial diagnostic workup is generally made with chest radiography and electrocardiography. Other imaging modalities have also been suggested to improve diagnostic accuracy. Cardiac catheterization and coronary angiography are currently the gold standard for diagnosis and planning the intervention, as they can recognize the quantum of the shunt as well as complications of a fistulous track (e.g., aneurysm formation, thrombus, leak, and the number of openings to the receiving chamber/vessel); however, this invasive method may be associated with risk. Herein, we report two patients with giant CAFs, one from the left circumflex artery to the coronary sinus and the other to the superior vena cava. Moreover, we describe how multimodal imaging, including two- and three-dimensional transesophageal echocardiography, coronary cineangiography, coronary computed tomography angiography, and enhanced chest computed tomography, can facilitate diagnosis and estimate the disease course in such patients. We believe that using multimodal imaging cannot only help the initial diagnosis regarding the presence of a CAF and the accurate anatomical site of the fistula in the patient but can also help predict the disease course and choose the most suitable treatment modality. Therefore, we suggest multimodal imaging be done to diagnose patients suspected of CAF. However, invasive cineangiography should be necessarily followed, regardless of whether an intervention is planned or not.

KEYWORDS

**coronary vessels, coronary artery disease, multimodal imaging, fistula, vascular fistula**

## Introduction

Coronary artery fistula (CAF) is among the rare cardiac diseases comprising about 0.002% of the general population and 0.4% of all cardiac malformations (1). It is mainly a congenital heart disease but can also be acquired from trauma, infection, or as a result of an iatrogenic injury such as intracardiac operations, transcutaneous myocardial biopsy, and coronary angioplasty (2).

Coronary artery fistula induces an abnormal communication between the coronary arteries and cardiac chambers or major vessels of systemic or pulmonary circulation without an interposed capillary bed. Consequently, blood is drawn away from the normal cardiac circulation (known as coronary "steal" syndrome), widening pulse pressure (1, 3). About 60% of fistulas arise from the right coronary artery, and 90% drain to the right chamber (4, 5). A large amount of shunt drainage into the venous side of the systemic circulation increases blood volume in the right heart structures and induces pulmonary arterial hypertension (PAH); untreated cases may develop right-sided heart failure or cardiac tamponade as a result of rupture or thrombosis of fistula or arterial aneurysm (1, 3, 4). However, when the fistula drains to the left atrium or left ventricle, the left heart volume is only increased, producing run-off from the aorta, resulting in no shunt (1, 3, 4).

Despite being described nearly two centuries ago in 1841, the real incidence and clinical course of CAF have not been well-defined since more than half of the cases have a small fistula and are accordingly asymptomatic and clinically undetectable. Patients with large CAFs may present with an unexplained systolic-diastolic heart murmur (with a crescendo-decrescendo pattern) or conduction abnormalities, atrial fibrillation, and ventricular tachyarrhythmia on physical examination. CAF-associated complications such as myocardial infarction or chronic myocardial ischemia can be detected on an electrocardiogram (ECG) and by volume overload on a chest radiograph; however, these modalities are insufficient for accurate diagnosis of CAF itself (4). More accurate imaging modalities, such as two- and three-dimensional transthoracic and transesophageal echocardiograms (2D and 3D TTE and TEE), Doppler echocardiography, enhanced chest computed tomography (CT), and coronary computed tomography angiography (CCTA), aid and facilitate diagnosis of the fistula site, origin, and terminus (4). In almost all intervention centers, 2D and 3D TEE and TTE are used in the supplement to cineangiography for verifying the exact anatomy of this anomaly and successful CAF closure (6), which further shows the supplementary role of modern imaging techniques. Herein, we describe and compare the disease course of two patients with CAFs, left circumflex artery (LCx), one to the coronary sinus and the other LCx to superior vena cava, to emphasize the role of multimodal imaging in the diagnosis and prognosis in patients suspected of CAF.

## Case presentation

### Case#1: Giant coronary artery fistula between proximal left circumflex artery and coronary sinus

A 43-years-old woman had a long history of mitral valve (MV) prolapse and tricuspid regurgitation, for which she had undergone MV replacement with a bioprosthetic MV (mosaic #31) plus tricuspid valve repair 12 years ago. Two years after her operation, the results of routine follow-up echocardiography and 2D TEE raised the possibility of a connection between the left circumflex artery and coronary sinus (**Supplementary Figure 1**), confirmed by more investigations such as conventional coronary angiography and CCTA. At that time, the patient refused cardiac surgery and missed her follow-up appointments for a long period.

She was referred to our center by the cardiologist echocardiographer for doing a transesophageal echocardiographic evaluation of valve function to rule out malfunction of the bioprosthetic MV. Her chief complaint was progressive shortness of breath, and 2D TTE examination revealed an excess transmitral gradient (peak gradient of 24 mmHg and mean gradient of 11 mmHg) accompanied by severe PAH (systolic pulmonary artery pressure = 65 mmHg) with an insignificant right to left shunt.

In the recent referral of the patient, 3D TEE was performed, which clearly identified CAF courses and low-velocity flow throughout the whole cardiac cycle, which drained into the coronary sinus (venous system) (**Figure 1**). Moreover, coronary cineangiography (**Figure 2**) and contrast-enhanced CT scan of the chest, as well as CCTA (**Figure 3**), demonstrated the anatomical course of a giant CAF clearly. Therefore, she was referred to an interventionist, but the patient refused further therapeutic intervention once again. As the patient was not evaluated using angiography before surgery, we cannot be sure about the cause, and it might have been iatrogenic.

### Case#2: Giant coronary artery fistula between proximal left circumflex artery and superior vena cava

A 28-year-old man with a history of frequent bouts of paroxysmal atrial fibrillation for several months was scheduled for elective electrical cardioversion and referred to our echocardiography center for TEE on the same day of cardioversion. He had no other remarkable history. TTE

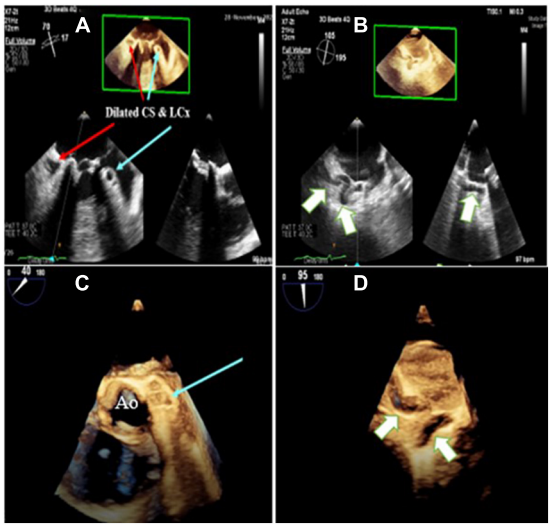


FIGURE 1
Three-dimensional zoom mid esophageal echocardiography **(A)** shows dilated left circumflex artery (LCX; light blue arrow) and coronary sinus (CS), **(B)** tortuous, giant coronary fistula (white arrow), **(C,D)** mid esophageal full volume illustrating the same findings.

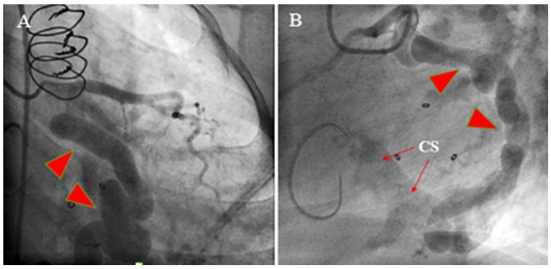


FIGURE 2
Coronary artery cineangiography in 30° RAO (left; **A**) and 60° LAO (right; **B**) projections show a giant coronary artery (red isosceles triangles) starting from the proximal left circumflex artery and terminating in the same artery (narrow arrows).

results showed the top normal size of both atria and left ventricle, normal biventricular systolic function with no PAH or significant left to right shunt (Qp/Qs = 1.2) (**Figure 4**). TEE (2D and 3D) showed CAF courses and low-velocity flow throughout the whole cardiac cycle, which drained into the superior vena cava (**Supplementary Figure 2**). Moreover, coronary cineangiography (**Figure 5**) and enhanced chest CT (**Figure 6**) clearly demonstrated the anatomical course of a giant CAF. He underwent cardioversion, and the rhythm resumed to normal sinus rhythm; however, he preferred to leave the hospital and postpone CAF therapeutic intervention.

Patients gave consent for all steps of the diagnostic procedure and cooperated with the physician. The heart team was open to listening to patients' opinions and reflected them in the medical records, but, both patients decided to postpone the suggested treatments.

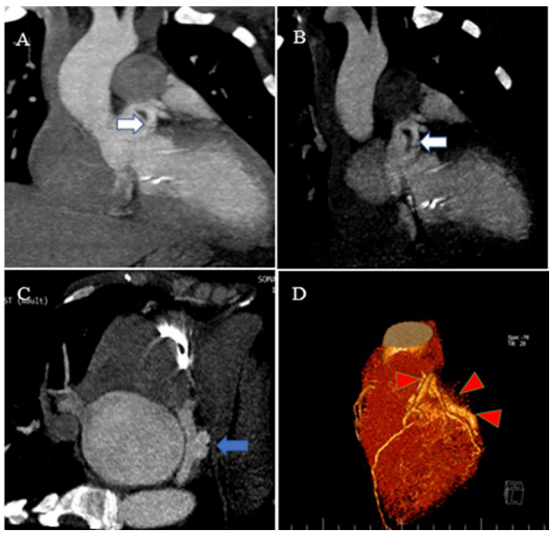


FIGURE 3
Contrast-enhanced CT scan of the chest, as well as CCTA, show the proximal site of a giant fistula originating from the left circumflex artery (white arrow), draining into the coronary sinus and forming a pouch (blue arrow). Reconstruction of coronaries illustrates a giant fistula (red color arrowheads).

## Discussion

In these two case reports, we described how multimodal imaging, including 2D and 3D TEE, coronary cineangiography, and contrast-enhanced CT scan of the chest as well as CCTA, could verify the exact anatomy of CAF, as documented in the provided figures. The first case was suspected of CAF using 2D TEE 10 years ago, 2 years after valvular replacement surgery, but she did not follow her problem until she became symptomatic (progressive shortness of breath). Therefore, her symptoms were suspected to be related to malfunction of the bioprosthetic MV, which was likely to undergo degenerative changes and become stenotic (considering the transmitral gradient of peak 24 and mean 11 at rest with severe PAH); in other words, we assume that CAF had a small or even no role in her symptoms. The second case was scheduled to be managed by electrical cardioversion for his paroxysmal atrial fibrillation, which was found to be related to his CAF using multimodal imaging.

These two patients did not have two of the most common symptoms reported for CAF, namely chest pain and murmur. Also, shortness of breath, the third common symptom, was only observed in one case #1 (7). Furthermore, the types of CAF were not the common ones previously reported, such as coronary to the pulmonary artery or cardiac chamber (8). The clinical course of these two patients depicts the rarity of CAF.

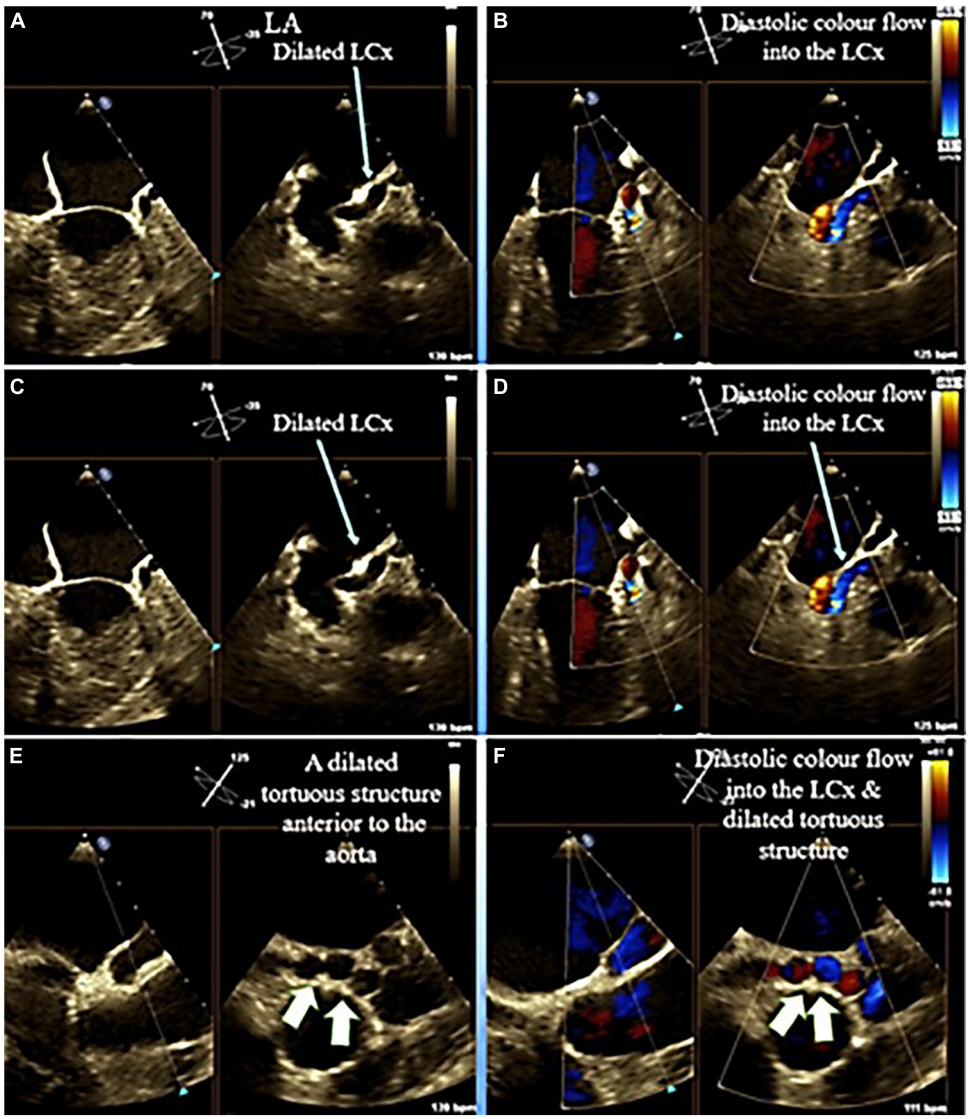


FIGURE 4
Mid esophageal echocardiography in different views illustrates dilated left circumflex (light blue arrow) as well as a giant tortuous structure (fistula) (white arrow) posterior to the aorta.

Physicians and cardiologists may easily miss this significant condition considering the diversity of its clinical symptoms. In our patients, the involved coronary artery and the drainage site of the fistula were as common as those previously reported. Among 56 patients diagnosed with CAF by CCTA, only one had coronary to superior vena cava fistula (8), and among 29 patients with LCX CFA, the site of fistula drainage was coronary sinus in only one patient (9). Another distinctive feature of the two cases presented here was the large size of the CAF, which has rarely been reported previously (10).

The clinical course of these two patients necessitates careful and close examinations using more accurate diagnostic methods alongside routine methods such as ECG and TTE. Here, both cases were diagnosed as CAF only after being examined with TEE. TTE and TEE play a key role in depicting CAF anatomy and hemodynamic changes with the advantage of lacking ionizing radiation or contrast material (4). Some studies have ascertained that CCTA was the modality of choice for CAF diagnosis (11, 12).

For multimodal imaging, we used coronary cineangiography, and contrast-enhanced CT scan of the chest as well as CCTA. Besides being able to diagnose CAF, these images could also verify the size of the fistula and disease course (to the right or left heart and resulting shunt). Performing pre-treatment coronary angiography has also been suggested in such patients since it can determine more

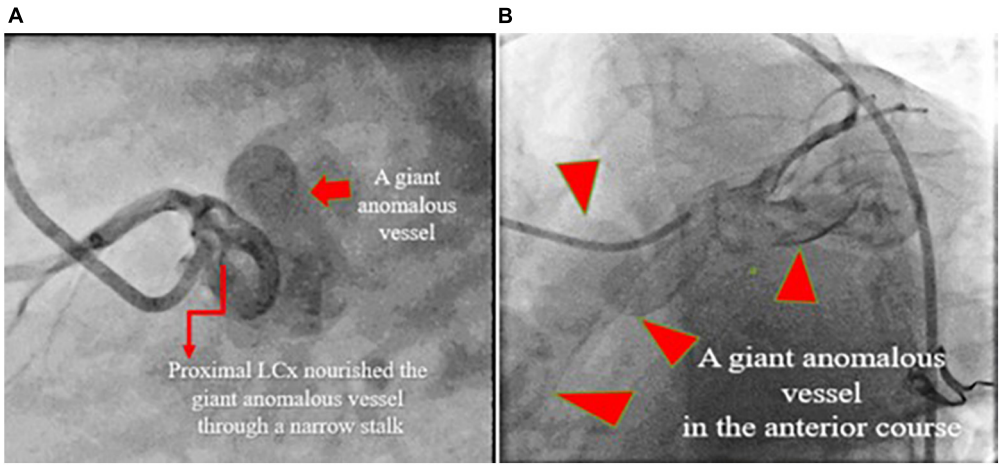


FIGURE 5
Coronary artery cineangiography in 70° LAO (left; **A**) and 30° LAO (right; **B**) projections show a giant coronary fistula (red isosceles triangles) starting from the proximal left circumflex artery.

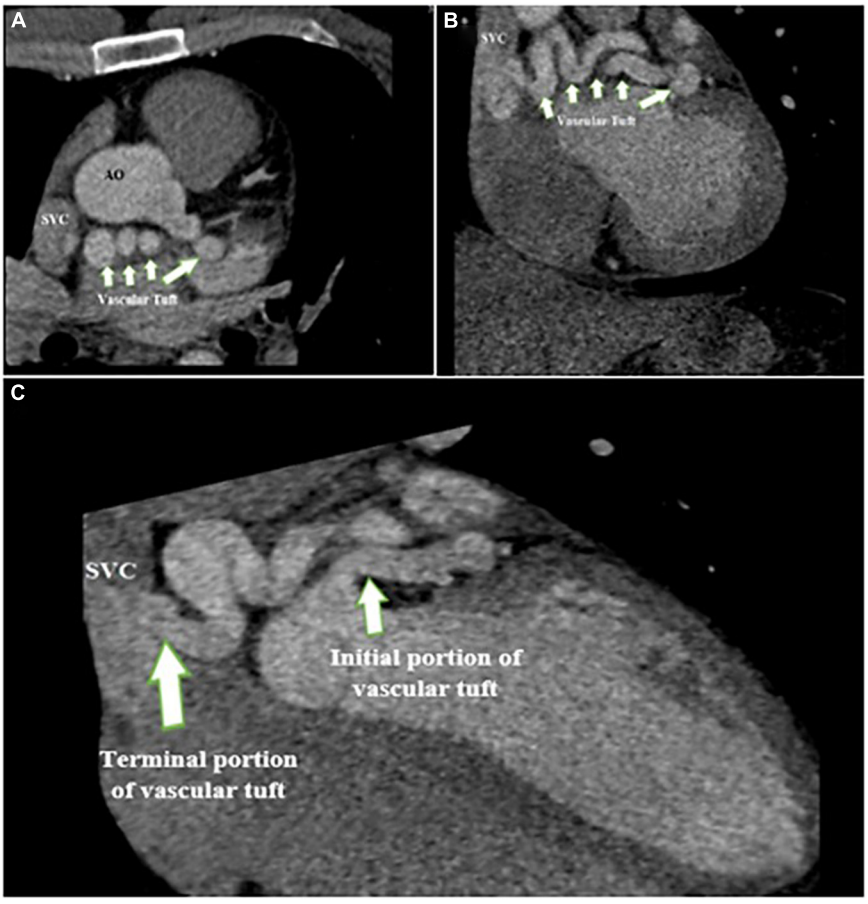


FIGURE 6
Contrast-enhanced CT scan of the chest shows the proximal site of giant fistula (white arrow) originating from the left circumflex artery with drainage into the superior vena cava.

accurate details of the patients' conditions, including blood flow patterns, device landing zones, and surgical ligation sites, which may not be fully evident on CT or magnetic resonance images (13); however, it imposes a greater risk because of its invasiveness, compared with CCTA. In a large-scale study on 12,457 patients undergoing coronary angiography, 112 patients had coronary anomalies, among whom only 10.7% were found to have CAF; therefore, the overall prevalence of CAF was 0.096% (14). Similarly, in another study, CAF was found in 0.08% of 11,350 patients who underwent coronary angiography (15). Improved imaging techniques following the development of modern technology may also have influenced the more accurate frequencies reported. Other imaging methods, such as intravascular ultrasound and optical coherence tomography, have also been suggested for the diagnosis and treatment of plaque vulnerability (16), coronary artery aneurysm (17), and dissection (18); however, the diagnostic accuracy of these imaging methods has not been established in CAF, and more studies are required in this regard.

Incorporating these multimodal imagings when dealing with patients with CAF enables physicians to benefit from the advantages of each, which also facilitates complete planning of the treatment strategy and may also help reduce long-term adverse outcomes (19). However, currently, physicians select an imaging modality compatible with their own clinical experience, as there are no specific guidelines determining the gold standard imaging modality for CAF detection. Further studies are also required to determine the effect of imaging modalities on patients' outcomes.

The mainstay of CAF management includes surgical closure versus percutaneous transcatheter closure (TCC) (20). Since CAFs are rare, and there are few studies on the patients' outcomes and suitability of treatments, it is difficult to determine the most appropriate management. CAF occlusion in 33 patients using TCC (with the placement of coils in 31, detachable balloons in 10, umbrella devices in 2, covered stent in 1, and a combination of detachable balloons and coils in 2) was successful in 83% of the patients and complete closure in 91% at follow-up (21). Although TCC has been suggested since 1982, patients may require re-catheterization or may develop complications, such as transient ischemic changes on ECG and unretrieved device embolization, which may result in death (21). Surgery is mainly used in cases requiring cardiopulmonary bypass for correction of additional cardiac lesions, including patent ductus arteriosus, atrial septal defect, mitral/aortic regurgitation, RCA atresia (i.e., a rare congenital malformation characterized by the absence of right coronary ostium), and coarctation (21). The closure is rigorously suggested in pediatric patients with congenital CAFs, and TCC is suggested as an effective treatment method with fewer complications (19, 22). Studies on the adult population have also reported that TCC was a safe and effective method for the treatment of CAFs (23, 24). In our study, both cases refused the suggested treatment; therefore, we cannot discuss the outcome of treatment in these patients. Further studies are required to determine the long-term outcome of CAF treatment.

## Conclusion

Here, we reported two cases of giant LCX CAF, who were not diagnosed during routine examinations by the cardiologist and were referred for echocardiographic examination with other clinical suspicions. The use of multimodality imaging for these two patients was found as an effective tool for verifying the size of the fistula, the exact anatomic site, source and drainage site, and the resulting shunt. Therefore, we anticipate that using multimodal imaging is beneficial in initial diagnosis, accurate anatomical site of fistula, and prediction of disease course. Therefore, we suggest multimodal imaging be performed in patients suspected of CAF.

## Data availability statement

The raw data supporting the conclusions of this article will be made available by the authors, without undue reservation.

## Ethics statement

Ethical review and approval was not required for the study on human participants in accordance with the local legislation and institutional requirements. The patients/participants provided their written informed consent to participate in this study. Written informed consent was obtained from the individual(s) for the publication of any potentially identifiable images or data included in this article.

## Author contributions

MS and RM-B performed echocardiographies and reviewed coronary angiographies and CCTAs. AHO performed echocardiographies. AHA performed coronary angiographies. MS condensed and collated visualizations for this manuscript. All authors have made substantial contributions to treatment planning, provided the literature review, drafted the manuscript, revised it critically, and gave final approval for publishing.

## Conflict of interest

The authors declare that the research was conducted in the absence of any commercial or financial relationships that could be construed as a potential conflict of interest.

## Publisher's note



## Supplementary material

The Supplementary Material for this article can be found online at: https://www.frontiersin.org/articles/10.3389/fcvm.2022.986078/full#supplementary-material

SUPPLEMENTARY FIGURE 1
The parasternal long-axis view in TTE shows **(A)** dilated coronary sinus (white arrow), **(B)** a well-seated bioprosthetic mitral valve in AC4 view, **(C)** mid esophageal view in two-dimensional transesophageal echocardiography, showing a tortuous, giant vascular tuft; coronary artery fistula (white arrow), and **(D)** blue and red colors in color Doppler study indicates "to and fro" movement of the vascular tuft regarding the probe.

SUPPLEMENTARY FIGURE 2
Mid esophageal full volume illustrating dilated left circumflex (light blue arrow).

## References

1. Mangukia CV. Coronary artery fistula. *Ann Thorac Surg.* (2012) 93:2084–92. doi: 10.1016/j.athoracsur.2012.01.114

2. Huang Y-K, Lei M-H, Lu M-S, Tseng C-N, Chang J-P, Chu J-J. Bilateral coronary-to-pulmonary artery fistulas. *Ann Thorac Surg.* (2006) 82:1886–8. doi: 10.1016/j.athoracsur.2006.02.040

3. Loukas M, Germain AS, Gabriel A, John A, Tubbs RS, Spicer D. Coronary artery fistula: a review. *Cardiovasc Pathol.* (2015) 24:141–8. doi: 10.1016/j.carpath.2014.01.010

4. Yun G, Nam TH, Chun EJ. Coronary artery fistulas: pathophysiology, imaging findings, and management. *Radiographics.* (2018) 38:688–703. doi: 10.1148/rg.2018170158

5. Qureshi SA. Coronary arterial fistulas. *Orphanet J Rare Dis.* (2006) 1:51. doi: 10.1186/1750-1172-1-51

6. Esper SA, Fink R, Rhodes JF, Harrison JK, Mackensen GBA. Coronary artery fistula successfully closed with the precise guidance of three-dimensional echocardiography. *J Cardiothorac Vasc Anesth.* (2014) 28:194–5. doi: 10.1053/j.jvca.2013.11.016

7. Verdini D, Vargas D, Kuo A, Ghoshhajra B, Kim P, Murillo H, et al. Coronary-pulmonary artery fistulas. *J Thorac Imaging.* (2016) 31:380–90. doi: 10.1097/RTI.0000000000000232

8. Lim JJ, Jung JI, Lee BY, Lee HG. Prevalence and types of coronary artery fistulas detected with coronary CT angiography. *AJR Am J Roentgenol.* (2014) 203:W237–43. doi: 10.2214/AJR.13.11613

9. Hou B, Ma W-G, Zhang J, Du M, Sun H-S, Xu J-P, et al. Surgical management of left circumflex coronary artery fistula: a 25-year single-center experience in 29 patients. *Ann Thorac Surg.* (2014) 97:530–6. doi: 10.1016/j.athoracsur.2013.09.015

10. Gupta V, Truong QA, Okada DR, Kiernan TJ, Yan BP, Cubeddu RJ, et al. Giant left circumflex coronary artery aneurysm with arteriovenous fistula to the coronary sinus. *Circulation.* (2008) 118:2304–7. doi: 10.1161/CIRCULATIONAHA.108.781617

11. Saboo SS, Juan Y-H, Khandelwal A, George E, Steigner ML, Landzberg M, et al. MDCT of congenital coronary artery fistulas. *AJR Am J Roentgenol.* (2014) 203:W244–52. doi: 10.2214/AJR.13.12026

12. Early S, Meany T, Fenlon H, Hurley J. Coronary artery fistula; coronary computed topography–the diagnostic modality of choice. *J Cardiothorac Surg.* (2008) 3:41. doi: 10.1186/1749-8090-3-41

13. Reddy G, Davies JE, Holmes DR, Schaff HV, Singh SP, Alli OO. Coronary artery fistulae. *Circ Cardiovasc Interv.* (2015) 8:e003062. doi: 10.1161/CIRCINTERVENTIONS.115.003062

14. Yildiz A, Okcun B, Peker T, Arslan C, Olcay A, Bulent Vatan M. Prevalence of coronary artery anomalies in 12,457 adult patients who underwent coronary angiography. *Clin Cardiol.* (2010) 33:E60–4. doi: 10.1002/clc.20588

15. Sercelik A, Mavi A, Ayalp R, Pestamalci T, Gümüsburun E, Batiraliev T. Congenital coronary artery fistulas in Turkish patients undergoing diagnostic cardiac angiography. *Int J Clin Pract.* (2003) 57:280–3.

16. Hoang V, Grounds J, Pham D, Virani S, Hamzeh I, Qureshi AM, et al. The role of intracoronary plaque imaging with intravascular ultrasound, optical coherence tomography, and near-infrared spectroscopy in patients with coronary artery disease. *Curr Atheroscler Rep.* (2016) 18:57. doi: 10.1007/s11883-016-0607-0

17. Dutary J, Zakhem B, De Lucas CB, Paulo M, Gonzalo N, Alfonso F. Treatment of a giant coronary artery aneurysm: intravascular ultrasound and optical coherence tomography findings. *J Interv Cardiol.* (2012) 25:82–5. doi: 10.1111/j.1540-8183.2011.00659.x

18. Alfonso F, Paulo M, Gonzalo N, Dutary J, Jimenez-Quevedo P, Lennie V, et al. Diagnosis of spontaneous coronary artery dissection by optical coherence tomography. *J Am Coll Cardiol.* (2012) 59:1073–9. doi: 10.1016/j.jacc.2011.08.082

19. Valente AM, Lock JE, Gauvreau K, Rodriguez-Huertas E, Joyce C, Armsby L, et al. Predictors of long-term adverse outcomes in patients with congenital coronary artery fistulae. *Circ Cardiovasc Interv.* (2010) 3:134–9. doi: 10.1161/CIRCINTERVENTIONS.109.883884

20. Cheng TO. Management of coronary artery fistulas: percutaneous transcatheter embolization versus surgical closure. *Catheter Cardiovasc Interv.* (1999) 46:151–2. doi: 10.1002/(SICI)1522-726X(199902)46:2<151::AID-CCD7>3.0.CO;2-G

21. Armsby LR, Keane JF, Sherwood MC, Forbess JM, Perry SB, Lock JE. Management of coronary artery fistulae: patient selection and results of transcatheter closure. *J Am Coll Cardiol.* (2002) 39:1026–32. doi: 10.1016/S0735-1097(02)01742-4

22. Mottin B, Baruteau A, Boudjemline Y, Piéchaud FJ, Godart F, Lusson JR, et al. Transcatheter closure of coronary artery fistulas in infants and children: a french multicenter study. *Catheter Cardiovasc Interv.* (2016) 87:411–8. doi: 10.1002/ccd.26320

23. Ilkay E, Celebi OO, Kacmaz F, Ozeke O. Percutaneous closure of coronary artery fistula: long-term follow-up results. *Postepy Kardiol Interwencyjnej.* (2015) 11:318–22. doi: 10.5114/pwki.2015.55603

24. Gowda ST, Latson LA, Kutty S, Prieto LR. Intermediate to long-term outcome following congenital coronary artery fistulae closure with focus on thrombus formation. *Am J Cardiol.* (2011) 107:302–8. doi: 10.1016/j.amjcard.2010.09.018

frontiers | Frontiers in Cardiovascular Medicine

TYPE Case Report
PUBLISHED 09 November 2022
DOI 10.3389/fcvm.2022.985644



OPEN ACCESS

EDITED BY
Ali Yilmaz,
University Hospital Münster, Germany

REVIEWED BY
Aleksander Dokollari,
Lankenau Medical Center,
United States
Antonio Maria Calafiore,
Department of Cardiovascular
Sciences, Italy

*CORRESPONDENCE
David Chung Wah Siu
cwdsiu@hku.hk
Lixue Yin
yinlixue_cardiac@163.com

SPECIALTY SECTION
This article was submitted to
Cardiovascular Imaging,
a section of the journal
Frontiers in Cardiovascular Medicine

RECEIVED 04 July 2022
ACCEPTED 24 October 2022
PUBLISHED 09 November 2022

CITATION
Zhou M, Un K-c, Wong CK, Wong OY,
Siu DCW, Yin L, Chan DT-l and
Lam SCC (2022) Case report:
Recurrent severe mitral regurgitation
due to ruptured artificial chords after
transapical Neochord mitral valve
repair.
*Front. Cardiovasc. Med.* 9:985644.
doi: 10.3389/fcvm.2022.985644



# Case report: Recurrent severe mitral regurgitation due to ruptured artificial chords after transapical Neochord mitral valve repair

Mi Zhou[1], Ka-chun Un[1], Chun Ka Wong[1], On Yat Wong[2], David Chung Wah Siu[1]*, Lixue Yin[3]*, Daniel Tai-leung Chan[4] and Simon Cheung Chi Lam[1]

[1]Cardiology Division, Department of Medicine, Queen Mary Hospital, The University of Hong Kong, Hong Kong, Hong Kong SAR, China, [2]Department of Anesthesiology, Queen Mary Hospital, The University of Hong Kong, Hong Kong, Hong Kong SAR, China, [3]Cardiovascular Ultrasound and Non-Invasive Cardiology Department, Sichuan Provincial People's Hospital, Chengdu, China, [4]Department of Cardiothoracic Surgery, Queen Mary Hospital, The University of Hong Kong, Hong Kong, Hong Kong SAR, China

Transapical Neochord mitral valve repair has been proven to be a technically safe procedure to correct primary mitral regurgitation (MR). Recurrent MR due to ruptured artificial chords is rare. Here, we present 2 cases of recurrent severe MR due to the detached or partially ruptured artificial chords after the Neochord procedure.

KEYWORDS

**valvular heart disease, mitral regurgitation, mitral valve (MV) repair, cardiac intervention, echocardiography**

## Introduction

The early phase of degenerative mitral regurgitation (MR) is characterized by compensatory adaptions, demonstrated with normal left ventricular ejection fraction (LVEF), dilated left ventricle, or eccentric hypertrophy (1). In this stage, most of the patients are asymptomatic or present with non-specific symptoms related to lung infections (cough, sputum, fever). Gradually, an uncorrected MR would lead to irreversible remodeling of the left ventricle and present with cardiac dysfunction, pulmonary hypertension, and poor outcome (1, 2). To date, the evidence of transapical Neochord (DS1000 System) mitral valve repair in reducing MR in suitable patients with chronic severe primary MR has been well-established (3, 4). Further, several clinical trials have been carried out in European and United States to compare the safety and performance of the NeoChord procedure with conventional open surgical repair (ClinicalTrials.gov NCT01777815, NCT02803957). Here, we report two patients with recurrent severe MR after the Neochord procedure due to the ruptured or loosed artificial chords.

10.3389/fcvm.2022.985644

## Patient 1: Recurrent severe MR due to detached artificial chords

A 71-year-old woman repeatedly presented to the outpatient department for cough, whitish sputum, and progressive shortness of breath (SOB) since 2018. Physical examination indicated that vital signs were stable (BP: 124/71 mmHg, Temperature: 37.0°C, *P*: 70 beats/min, $SPO_2$: 98%), and lower limb edema. ECG: normal. Cardiac enzyme: unremarkable. Chest X-ray: bilateral lower zone haziness, blunted bilateral costophrenic angle. The symptoms were resolved after treatment with augmentin, Lasix, and oxygen treatment (2L/min). Subsequent transthoracic echocardiography (TTE) and transesophageal echocardiography (TEE) showed that normal-sized left ventricle with preserved LVEF (55–60%); severe anterior directed MR due to prolapse P2 and P3 segment. She underwent Neochord repair with 4 artificial chords implanted, residual trivial MR with a mean trans-mitral gradient of 4 mmHg. The patient followed a regular postoperative valvular evaluation by TTE every 6 months after being discharged from the hospital. Twenty-four months after discharge, she was admitted to the cardiac clinic again for a severe SOB and heart failure symptoms (New York heart association functional class 3–4) and decreased exercise tolerance. Conventional and 3-D TTE showed severe anterior directed MR due to the detached artificial chords (Figure 1).

## Patient 2: Recurrent severe MR due to partially ruptured artificial chords

A 58-year-old man was repeatedly referred to the respiratory clinic for cough, sputum, and fever since 2003. He was founded with posterior mitral valve prolapse with mild MR in 2013. He felt palpitation and exertional dyspnea in March 2019. TTE and TEE revealed severe MR due to P1, and P2 leaflet prolapse; borderline LV cavity size with LVEF ~65%. Holter: sinus tachycardia, several episodes of supraventricular contractions, and premature ventricular contractions. On examination, his vital signs were stable (BP: 129/71 mmHg, *p*: 86 beats/min). He underwent Neochord mitral valve repair with 3 artificial chords, with residual trivial MR and a mean trans-mitral gradient of 2–4 mmHg. Thirty months after he was discharged from the hospital, he was admitted to the hospital again for an exertional SOB. TTE indicated severe anterior directed MR due to partially ruptured artificial chords (Figure 2).

# Discussion

Off-pump transapical Neochord mitral valve repair has been proven to be a technically safe and achievable procedure to correct MR from grade 3+/4+ to ≤ 2+ (5). Type A or type B anatomy which featured isolated-/multi-segments prolapse

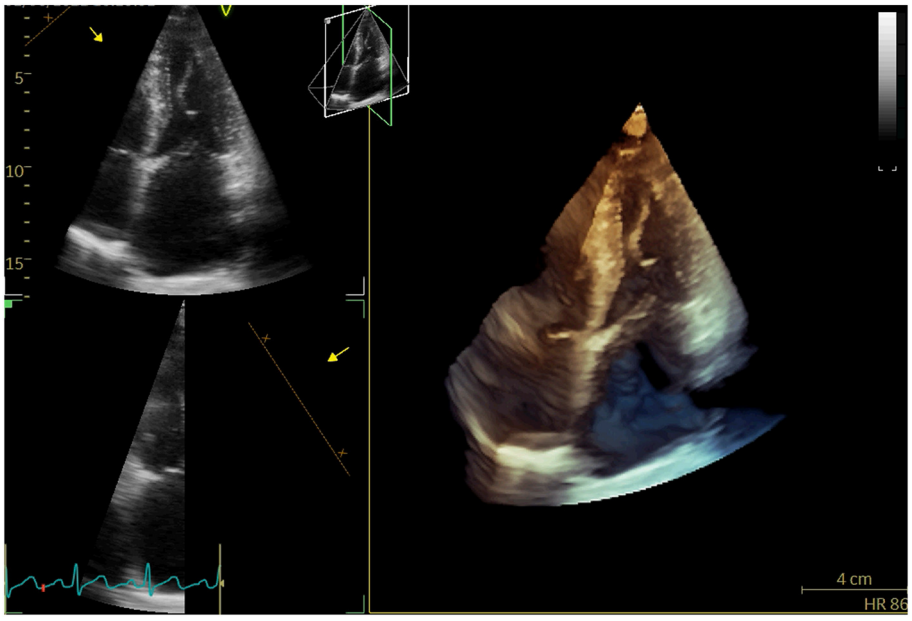


FIGURE 1
3D-TTE revealed detached artificial chords.

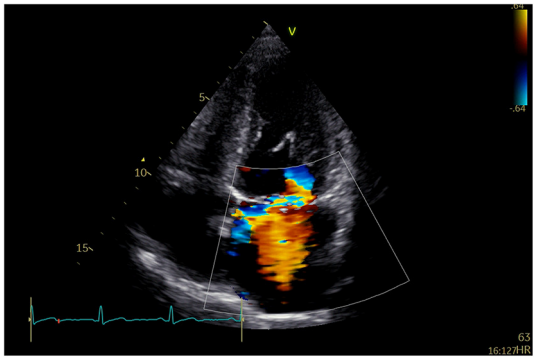

FIGURE 2
TTE revealed recurrent severe MR due to partially ruptured artificial chords.

or flail of the posterior mitral leaflet was considered the optimized selection for Neochord implantation. Type C and type D anatomy was defined as anterior or bileaflet prolapse with or without paracommissural involvement and annular calcifications, which has been reported to meet 80% of the primary endpoint (moderate or less MR without the need for reoperation after Neochord repair at 1 year) compared to the type A (92%) and type B (88%) anatomy (4). In addition, the leaflet-to-annulus index (LAI) >1.25 will be taken into account before the procedure, as it is an essential predictor of a good outcome. Functional MR or MR due to endocarditis and ischemic heart disease should be excluded from Neochord mitral valve repair (3, 6). In our study, these two patients (type B MV anatomy and LAI ≥1.25) are preferred to receive the transapical Neochord repair compared to the conventional open mitral valve surgery because of its mini-invasive and off-pump nature. Procedural success was achieved in those two patients because residual MR evaluated immediately after surgery was trivial.

The incidence of recurrent severe MR after transapical Neochord procedure is 11% in the first year (4). Reasons for recurrent MR with a moderate or above degree are complicated, including inappropriate patient, new prolapse/re-prolapse of leaflet, leaflet tethering caused by LV dysfunction, calcification, untreated/residual leaflet prolapse, leaflet curling, over-tensioning of the treated leaflet, and ventricular dilation (7).

Recurrent MR due to ruptured artificial chords is rare. Early-intermediate rupture is defined as the rupture occurring within 1–3 years after the Neochord procedure. Reasons for early-intermediate rupture are unclear, probably due to the inflammatory response, chords injured intraoperatively, or intracardiac stress (8, 9). Late rupture is defined as rupture occurring 6–14 years postoperatively that may result from artificial chord calcification (10). Our two patients reached the primary outcome at 1 year and severe MR reoccurred at postoperative 24–30 months. Elective reoperation is scheduled for our two patients. In the absence of histopathological analysis of recurrent severe MR, we hypothesized that the early-intermediate failure was likely due to LV reverse remodeling leading to the loose of artificial chords or changes of intracardiac stress exceeding the strength of the artificial chords.

Although the results of transapical Neochord implantation for the correction of mitral regurgitation are very encouraging, more reliable evidence based on a large cohort study is needed to evaluate the short-term and long-term outcomes. In this context, our case series might provide a clue that artificial chords can loosen or partially rupture in the early- intermediate period after mitral valve repair.

## Data availability statement

The original contributions presented in the study are included in the article/supplementary material, further inquiries can be directed to the corresponding authors.

## Author contributions

MZ, DS, and LY contributed to the conception of the manuscript. MZ, CW, K-cU, OW, SL, and DC organized the data collection. MZ wrote the first draft of the manuscript. All authors contributed to manuscript revision, read, and approved the submitted version.

## Conflict of interest

The authors declare that the research was conducted in the absence of any commercial or financial relationships that could be construed as a potential conflict of interest.

## Publisher's note

# References


1. Gaasch WH. Meyer TE. Left ventricular response to mitral regurgitation. *Circulation*. (2008) 118:2298–303. doi: 10.1161/CIRCULATIONAHA.107.755942

2. Patel H, Desai M, Tuzcu EM, Griffin B. Kapadia S. Pulmonary hypertension in mitral regurgitation. *J Am Heart Assoc*. (2014) 3:e000748. doi: 10.1161/JAHA.113.000748

3. Colli A, Adams D, Fiocco A, Pradegan N, Longinotti L, Nadali M, et al. Transapical neochord mitral valve repair. *Ann Cardiothorac Surg*. (2018) 7:812–20. doi: 10.21037/acs.2018.11.04

4. Colli A, Manzan E, Besola L, Bizzotto E, Fiocco A, Zucchetta F, et al. One-year outcomes after transapical echocardiography-guided mitral valve repair. *Circulation*. (2018) 138:843–5. doi: 10.1161/CIRCULATIONAHA.118.033509

5. Ahmed A, Abdel-Aziz TA, AlAsaad MMR, Majthoob M. Transapical off-pump mitral valve repair with NeoChord implantation: a systematic review. *J Card Surg*. (2021) 36:1492–8. doi: 10.1111/jocs.15350

6. Colli A, Manzan E, Rucinskas K, Janusauskas V, Zucchetta F, Zakarkaite D, et al. Acute safety and efficacy of the neochord procedure. *Interact Cardiovasc Thorac Surg*. (2015) 20:575–81. doi: 10.1093/icvts/ivv014

7. Colli A, Besola L, Bizzotto E, Fiocco A, Denas G, Bellu R, et al. Mechanisms of recurrent regurgitation after transapical off-pump mitral valve repair with neochord implantation†. *Eur J Cardio Thoracic Surgery*. (2019) 56:479–87. doi: 10.1093/ejcts/ezz048

8. Kudo M, Ryohei Y, Okamoto K. Recurrent mitral regurgitation due to ruptured ePTFE neochordae after mitral valve repair by the loop technique: a report of case. *Ann Thoracic Cardiovasc Surgery*. (2014) 20(Suppl. 7):746–9. doi: 10.5761/atcs.cr.13-00240

9. Yamashita MH, Skarsgard PL. Intermediate and early rupture of expanded polytetrafluoroethylene neochordae after mitral valve repair. *Ann Thorac Surg*. (2011) 92:341–3. doi: 10.1016/j.athoracsur.2011.01.042

10. Luthra S, Ismail A, Tsang G. Calcific degeneration and late fracture of expanded polytetrafluoroethylene neochords after mitral valve repair. *JTCVS Techniques*. (2020) 1:34–6. doi: 10.1016/j.xjtc.2019.11.012

frontiers | Frontiers in Cardiovascular Medicine

TYPE Case Report
PUBLISHED 17 November 2022
DOI 10.3389/fcvm.2022.1008308



OPEN ACCESS

EDITED BY
Grigorios Korosoglou,
GRN Klinik Weinheim, Germany

REVIEWED BY
Mariya Kronlage,
Heidelberg University Hospital, Germany
Anastasios Psyllas,
MHW Germany, Germany
Georgios A. Pitoulias,
Aristotle University of Thessaloniki, Greece

*CORRESPONDENCE
Jianzhong Xu
jianzhongxv@outlook.com

SPECIALTY SECTION
This article was submitted to Cardiovascular Imaging, a section of the journal Frontiers in Cardiovascular Medicine

RECEIVED 31 July 2022
ACCEPTED 26 October 2022
PUBLISHED 17 November 2022

CITATION
Hong M, Kang Y, Xu J and Wang J (2022) Case report: Recurrence of hypertension after renal artery angioplasty due to the progression of focal renal fibromuscular dysplasia. *Front. Cardiovasc. Med.* 9:1008308. doi: 10.3389/fcvm.2022.1008308



# Case report: Recurrence of hypertension after renal artery angioplasty due to the progression of focal renal fibromuscular dysplasia

Mona Hong, Yuanyuan Kang, Jianzhong Xu* and Jiguang Wang

Department of Hypertension, Ruijin Hospital, Shanghai Institute of Hypertension, Shanghai Jiao Tong University School of Medicine, Shanghai, China

Whether fibromuscular dysplasia (FMD) is a progressive disease, remains unclear. We reported a case of focal renal artery FMD that slowly progressed to a branching artery over a few years after the angioplasty without in-stent restenosis, which reconfirms that focal FMD is progressive and that such progression may be segmental. Stenting may be an option for young, risk factor-free patients with focal FMD.

KEYWORDS

**hypertension, fibromuscular dysplasia (FMD), renal artery, progression, in-stent restenosis**

## Introduction

Fibromuscular dysplasia (FMD) is a non-inflammatory, non-atherosclerotic vascular disease that may involve medium-sized arteries throughout the body and most commonly affects the renal arteries. When the renal artery is involved, the most frequent finding is hypertension (1). In young patients with recent onset of hypertension, percutaneous balloon angioplasty with bailout stenting is recommended as first-line therapy with the goal of curing hypertension (2). While restenosis occurs in more than 25% of patients with FMD within 1 year after balloon angioplasty (3), studies showed that the rate of restenosis after stenting in patients with atherosclerotic renal artery stenosis was about 10% and renal arteries that received balloon angioplasty developed restenosis earlier than arteries that received a stent (4).

Whether FMD is a progressive disease and the factors associated with disease progression remain unclear (5). Although several older studies suggested that FMD in the majority of patients progressed with time (6), the current expert consensus is that multifocal FMD of the carotid arteries is not a progressive disease (3), whereas focal FMD progresses remains unclear.

## Case description

A 31-year-old woman was referred to our hospital due to recurring elevated blood pressure for half a year. The patient first came to our hospital 8 years ago for new-onset hypertension. Investigation of probable secondary hypertension was initiated with renal disease. Renal function was preserved, with no abnormalities, and urea and creatinine levels were also normal. Kidney ultrasound showed asymmetric kidneys (right 93*35 mm, left 116*53 mm) and renal artery computed tomography angiography revealed stenosis in the mid-portion of the right kidney artery. After Takayasu and other arteritis were excluded, renal artery FMD was diagnosed. Subsequently, catheter-based renal angiography confirmed focal stenosis in the mid-portion of the right renal artery (Figure 1A, Supplementary Video 1), and a bare metal stent was implanted because of dissection after balloon dilation (Figure 1B, Supplementary Video 2). The blood pressure returned to normal (120–130/60–70 mm Hg) without any antihypertensive drugs after the procedure. The patient was recommended dual antiplatelet therapy for half a year. During the past 8 years, she monitored her blood pressure regularly, and it remained normal. She noticed 6 months ago that her blood pressure gradually increased, peaking at 180/120 mm Hg. She came to our hospital again. Biochemical tests revealed significantly elevated plasma renin activity (5.9 ng/ml/hour) and aldosterone levels (1,005.35 pg/ml) with hypokalemia (2.7 mmol/L). Then in-stent restenosis was suspected, so she was admitted to the ward for further examination. Renal angiography was performed again. However, no obvious in-stent restenosis was observed, but severe stenosis was found in the right inferior renal branch artery (Figure 1C, Supplementary Video 3), which was totally normal 8 years ago (Figures 1A,B). Intravascular ultrasound (IVUS) images revealed that eccentric intimal thickening caused stenosis of the branch artery (Figure 1E, Supplementary Video 5) and no neointimal hyperplasia in the stent (Figure 1F, Supplementary Video 6). Balloon angioplasty was performed for the branch artery and the lesion vessel was dilated successfully (Figure 1D, Supplementary Video 4). One week after the procedure, the patient was normotensive without any antihypertensives. At 1-year follow-up, the patient's blood pressure remained normal.

## Discussion

We reported a case of focal renal artery FMD that slowly progressed to a branching artery over a few years after the angioplasty without in-stent restenosis, which reconfirmed that focal FMD was progressive and that such progression may be segmental. Stenting may be an option for young, risk factor-free patients with focal FMD.

In the presented case, the renal arterial flow in the right kidney was adequate, only the branch artery blood flow was reduced. The diagnosis of renovascular hypertension was supported by renin angiotensin aldosterone system activation. The plasma renin activity and aldosterone levels were increased with hypokalemia. One similar case has been reported previously (7).

The expert consensuses recommend that balloon angioplasty without stenting is currently the first-line revascularization technique in FMD-related renal artery stenosis (2, 3). While there is no evidence that renal artery balloon angioplasty alone is superior to the stent in patients with FMD. The mechanisms of restenosis in stented lesions differ from those in balloon-dilated lesions. In balloon-dilated lesions, late constriction of the external elastic membrane after angioplasty plays a more significant role in causing restenosis than dose neointimal proliferation which is the main cause of restenosis in the stent. Since most patients with FMD undergo balloon dilation alone, the restenosis rate after stenting is unknown. In our focal FMD case, no significant neointimal hyperplasia occurred after stenting. The possible reasons were that the patient was young, had no smoking history, no diabetes, no dyslipidemia, and blood pressure returned to normal after stenting. The absence of the above risk factors may be the possible reason for the absence of neointimal hyperplasia in the stent.

Whether FMD is a progressive disease and the factors associated with disease progression remain unclear (5). It is the consensus of US experts that progression in multifocal FMD is an uncommon occurrence (3). Whether focal FMD will progress is uncertain, the progress of focal FMD to multifocal FMD has been reported recently (8). The present case is the first to report focal renal artery FMD that slowly progressed to a branching artery over a few years, with no progression at the original lesion. This observation reconfirms that focal FMD is progressive and that such progression may be segmental. In addition, IVUS images, in this case, revealed intimal hyperplasia leading to the progression of the renal branch artery. Takayasu arteritis was further ruled out because Takayasu arteritis was more often characterized by adventitial hyperplasia (9), and Takayasu arteritis was more prone to in-stent restenosis than to progression in other artery segments.

In conclusion, focal FMD is a progressive disease with a segment of progression. Stenting may be an option for young, risk-free patients with focal FMD.

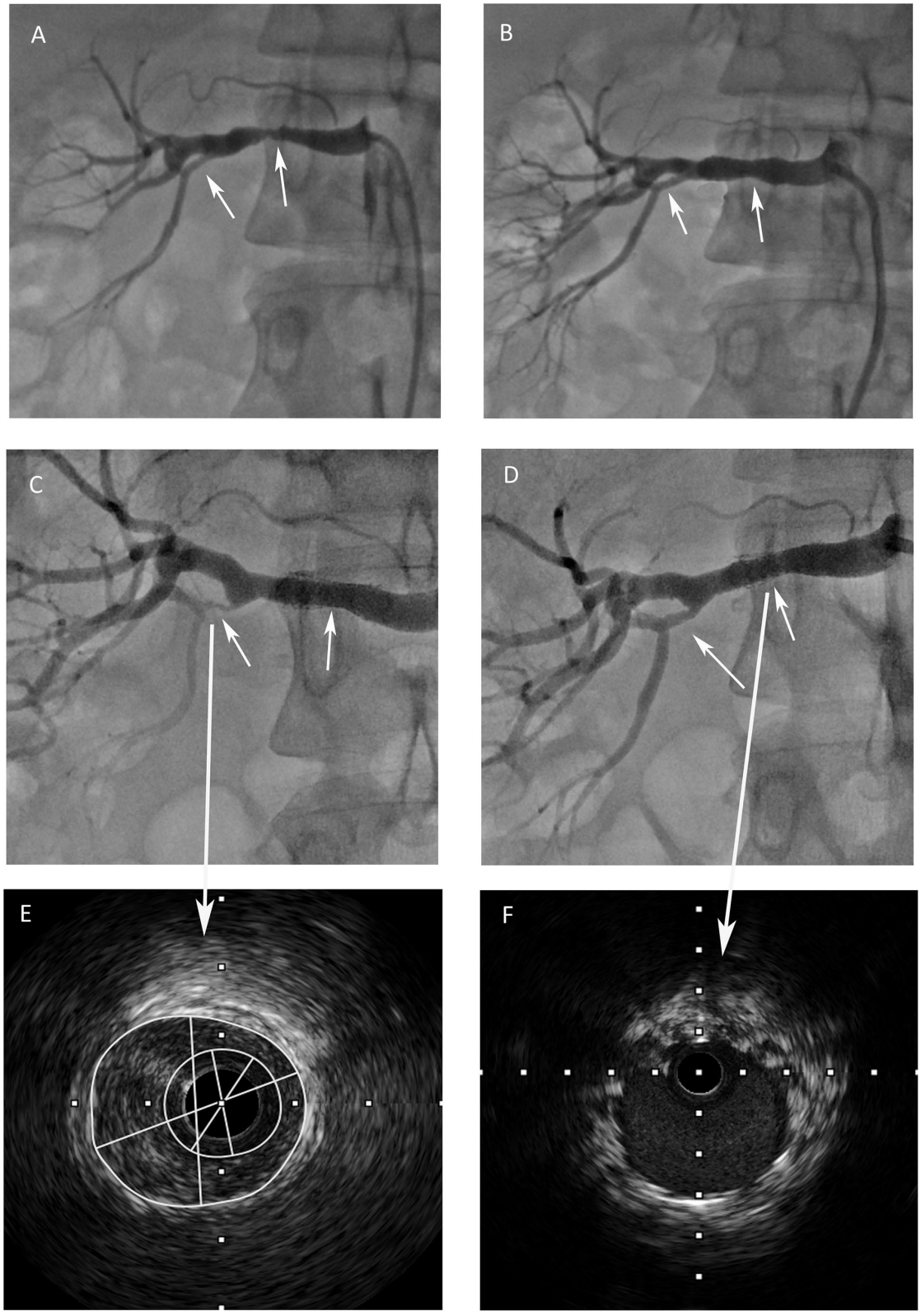


FIGURE 1
**(A)** Renal angiography revealed focal stenosis in the mid-portion of the right renal artery and the right inferior renal branch artery was normal. **(B)** After a stent was implanted into the renal artery, the right inferior renal branch artery was still normal. **(C)** Severe stenosis was found in the right inferior renal branch artery, no obvious in-stent restenosis was observed. **(D)** The lesion vessel was dilated successfully and the renal blood flow was restored after the procedure. **(E)** Intravascular ultrasound image revealed eccentric intimal thickening of the branch artery. **(F)** Intravascular ultrasound image revealed that no obvious neointimal hyperplasia in the stent.

## Data availability statement

The original contributions presented in the study are included in the article/Supplementary material, further inquiries can be directed to the corresponding author.

## Ethics statement

Ethical review or approval was not required for the study on human participants in accordance with the local legislation and institutional requirements. The patient provided their written informed consent to participate in this study. Written informed consent was obtained from the individuals for the publication of any potentially identifiable images or data included in this article.

## Author contributions

JX performed the intervention together with YK. MH drafted the manuscript. JX and JW contributed to manuscript design, drafting, and critical revision. All authors have critically read and reviewed this article, approved the version to be published, and agreed to be accountable for all aspects of the work in ensuring that questions related to the accuracy or integrity of any part of the work are appropriately investigated and resolved.

## Conflict of interest

The authors declare that the research was conducted in the absence of any commercial or financial relationships that could be construed as a potential conflict of interest.

## Publisher's note

All claims expressed in this article are solely those of the authors and do not necessarily represent those of their affiliated organizations, or those of the publisher, the editors and the reviewers. Any product that may be evaluated in this article, or claim that may be made by its manufacturer, is not guaranteed or endorsed by the publisher.

## Supplementary material

The Supplementary Material for this article can be found online at: https://www.frontiersin.org/articles/10.3389/fcvm.2022.1008308/full#supplementary-material

SUPPLEMENTARY VIDEO 1
Renal angiography showed focal stenosis in the mid-portion of the right renal artery.

SUPPLEMENTARY VIDEO 2
A bare metal stent was implanted because of dissection after balloon dilation.

SUPPLEMENTARY VIDEO 3
Severe stenosis was found in the right inferior renal branch artery.

SUPPLEMENTARY VIDEO 4
Balloon angioplasty was performed for the branch artery and the lesion vessel was dilated successfully.

SUPPLEMENTARY VIDEO 5
Intravascular ultrasound revealed that eccentric intimal thickening caused stenosis of the branch artery.

SUPPLEMENTARY VIDEO 6
Intravascular ultrasound revealed no neointimal hyperplasia in the stent.

## References

1. Olin JW, Froehlich J, Gu X, Bacharach JM, Eagle K, Gray BH, et al. The United States Registry for Fibromuscular Dysplasia: results in the first 447 patients. *Circulation.* (2012) 125:3182–90. doi: 10.1161/CIRCULATIONAHA.112.091223

2. Persu A, Giavarini A, Touze E, Januszewicz A, Sapoval M, Azizi M, et al. European consensus on the diagnosis and management of fibromuscular dysplasia. *J Hypertens.* (2014) 32:1367–78. doi: 10.1097/HJH.0000000000000213

3. Olin JW, Gornik HL, Bacharach JM, Biller J, Fine LJ, Gray BH, et al. Fibromuscular dysplasia: state of the science and critical unanswered questions: a scientific statement from the American Heart Association. *Circulation.* (2014) 129:1048–78. doi: 10.1161/01.cir.0000442577.96802.8c

4. Takahashi EA, McKusick MA, Bjarnason H, Piryani A, Harmsen WS, Misra S. Treatment of in-stent restenosis in patients with renal artery stenosis. *J Vasc Interv Radiol.* (2016) 27:1657–62. doi: 10.1016/j.jvir.2016.05.041

5. Gornik HL, Persu A, Adlam D, Aparicio LS, Azizi M, Boulanger M, et al. First international consensus on the diagnosis and management of fibromuscular dysplasia. *J Hypertens.* (2019) 37:229–52. doi: 10.1097/HJH.0000000000002019

6. Goncharenko V, Gerlock AJ Jr, Shaff MI, Hollifield JW. Progression of renal artery fibromuscular dysplasia in 42 patients as seen on angiography. *Radiology.* (1981) 139:45–51. doi: 10.1148/radiology.139.1.7208940

7. Skraeddergaard A, Nyvad J, Christensen KL, Horlyck A, Mafi HM, Reinhard M. Difficulty and importance of diagnosing stenosis of renal branch artery in fibromuscular dysplasia: a case report. *Blood Press.* (2021) 30:416–20. doi: 10.1080/08037051.2021.1993735

8. Chen Y, Dong H, Jiang X, Zou YB. Unifocal progressed to multifocal renal artery fibromuscular dysplasia. *Eur Heart J Case Rep.* (2022) 6:ytab522. doi: 10.1093/ehjcr/ytab522

9. Sharma S, Sharma S, Taneja K, Bahl VK, Rajani M. Morphological mural changes in the aorta in non-specific aortoarteritis (Takayasu's arteritis): assessment by intravascular ultrasound imaging. *Clin Radiol.* (1998) 53:37–43. doi: 10.1016/S0009-9260(98)80032-9

frontiers | Frontiers in Cardiovascular Medicine

TYPE Case Report
PUBLISHED 24 November 2022
DOI 10.3389/fcvm.2022.957779



OPEN ACCESS

EDITED BY
Francesco Bandera,
University of Milan, Italy

REVIEWED BY
Domenico De Santis,
Sapienza University of Rome, Italy
Syed Amir Gilani,
University of Lahore,Pakistan

*CORRESPONDENCE
Jiangquan Liao
liaojiangquan@163.com

†These authors have contributed equally to this work

SPECIALTY SECTION
This article was submitted to Cardiovascular Imaging, a section of the journal Frontiers in Cardiovascular Medicine

RECEIVED 31 May 2022
ACCEPTED 07 November 2022
PUBLISHED 24 November 2022

CITATION
Liao J, Wang Y, Shao M, Wang Y, Du J, Li X, Yang P, Fu D, Dong Z and Liu M (2022) An unusual contrast-induced encephalopathy following percutaneous coronary intervention in patients with cerebrovascular abnormalities: A case report. *Front. Cardiovasc. Med.* 9:957779. doi: 10.3389/fcvm.2022.957779



# An unusual contrast-induced encephalopathy following percutaneous coronary intervention in patients with cerebrovascular abnormalities: A case report

Jiangquan Liao[1*†], Yan Wang[1†], Mingjing Shao[1†], Yanling Wang[2], Jinhang Du[1], Xianlun Li[1], Peng Yang[1], Dongliang Fu[1], Zhe Dong[1] and Mengru Liu[1]

[1]National Integrated Traditional and Western Medicine Center for Cardiovascular Disease, China-Japan Friendship Hospital, Beijing, China, [2]Department of Cardiovascular and Respiratory Medicine, Beijing Nuclear Industry Hospital, Beijing, China

**Introduction:** Contrast-induced encephalopathy (CIE) is a complication associated with the administration of iodinated contrast, which usually happens minutes to hours after contact with contrast, and fully recovers within 72 h. The clinical manifestations of CIE are diverse, and the pathological mechanism is not explicit.

**Methods:** We report the case of a 66-year-old female who suffered from a delayed CIE following the administration of iodinated contrast agent. Symptoms were severe. Imaging examination, biochemical and etiological detection were performed timely. The course of neurological symptoms was atypical. Her complex complications of hypothyroidism and cerebrovascular abnormalities contributed to more challenges, which were also clues to the diagnosis. With prompt and active treatment, the patient recovered fully over 10 days.

**Discussion:** The diagnosis standard of CIE highly depends on the association with the contact of contrast and the exclusion of other nervous system diseases. Complicated clinical circumstances and individual specificity can

lead to different clinical manifestations of CIE, making it even more difficult to diagnose and treat. Prompt and dynamic imaging examination would provide great value in the diagnosis and evaluation of CIE. Timely diagnosis and intervention may be the key to its satisfying prognosis.

KEYWORDS

contrast-induced encephalopathy, percutaneous coronary intervention, blood-brain barrier, hypothyroidism, cerebrovascular abnormalities

## Introduction

Contrast-induced encephalopathy (CIE) is a rare neurological complication associated with the intra-arterial administration of iodinated contrast. The incidence of CIE associated was estimated between 0.05 and 0.11% for diagnostic intravascular coronary angiography (ICA) and between 0.3 and 0.4% for percutaneous coronary intervention (PCI) (1). Its clinical manifestations are diverse, and the diagnosis of CIE is usually exclusionary (2). CIE can lead to various neurological symptoms within minutes to a few hours after the injection of contrast. Most of the symptoms would disappear with the removal of the contrast agent by kidney within 72 h. With prompt and active treatment, sequela usually does not occur. Herein, we present a patient with cerebrovascular abnormalities who suffered from a delayed CIE following PCI and fully recovered over 10 days.

## Case report

A 66-year-old female was hospitalized due to 1 month of chest tightness and unexplained medium pericardial effusion diagnosed 1 week before admission by echocardiogram. The previous history includes kidney trauma and hematuria caused by an impact 3 years ago, with no sequela. The blood test indicated cardiac troponin T (cTnT) 0.117 ng/mL (normal range < 0.014 ng/mL). Electrocardiogram showed T wave inversion in V4-6. ICA was performed through the right radial artery, revealing moderate to severe stenosis in the left anterior descending branch (LAD), and one drug-eluting stent (DES) was implanted according to standard procedure. There is no complication during the PCI procedure. Approximately 100 ml of iopromide (62.34 g iopromide per 100 ml) (Bayer Pharma AG), a non-ionic hypotonic contrast agent, was administered during the procedure. Local anesthetic (1% lidocaine) was administered prior to ICA, and 6,000 iu intra-arterial heparin was administered during PCI.

Blood tests reported later that day showed that the thyroid function was very low, with free thyroxine 4 0.12 ng/dL (normal range 0.93 to 1.7 ng/dL), free thyroxine 3 0.27 pg/mL (normal range 2.0 to 4.4 pg/mL), thyrotropin 63.87 uIU/mL (normal range 0.27 to 4.2 uIU/mL), and thyroid antibody high off the chart. We considered hypothyroidism resulting from Hashimoto's thyroiditis. Other abnormalities in blood tests included serum creatinine 123.5 umol/L (normal range 63.5 to 106 umol/L), Na + 131 mmol/L (normal range 135 to 145 mmol/L), total cholesterol (TC) 7.45 mmol/L (normal range < 1.7 mmol/L), and low-density lipoprotein cholesterol (LDL-C) 4.1 mmol/L (normal range < 3.4 mmol/L). Dual antiplatelet (aspirin 100 mg/d and clopidogrel 75 mg/d), enhanced lipid-lowering (atorvastatin 20 mg/d and ezetimibe 10 mg/d) were administered.

Forty-eight hours after PCI, she began to suffer from severe headaches, speech disorder, trance, uncooperative in physical examination, and slow pupil light reflex. Cranial CT scan was performed immediately and showed no evidence of intracranial hemorrhage but multiple old infarcts, white matter degeneration, and brain atrophy (**Figure 1**). About 62 h after PCI, her temperature began to rise and deteriorated into loss of consciousness, eyes stared to the right, dull pupil light reflex, no response to pain stimulation of limbs, spasticity, and suspicious positive pathological signs of the left lower limb. Urgent brain MRI showed multiple ischemic and infarct foci, right parietal and occipital cortex swelling with abnormal signals, expansion of supratentorial ventricular system, and degeneration of brain white matter (comparison of MRI is shown in **Figure 2**). Blood tests revealed no significant changes. Lumbar puncture and cerebrospinal fluid examination, antinuclear antibody spectrum test, electroencephalogram were conducted, but no results with clear diagnostic significance were found. Cranial MRA showed distal internal carotid artery occlusion, bilateral anterior and middle cerebral arteries occlusion, abundant and disordered collateral circulation at the circle of the basal artery and bilateral basal ganglia, all of which were classified as moyamoya disease (**Figure 3**).

In other hospitals, a family member provided a medical history of an uncertain diagnosis of congenital cerebrovascular dysplasia with an uncertain imaging examination. Multidisciplinary consultation was conducted, and myxedema coma caused by hypothyroidism, brain edema caused by hyponatremia, intracranial infection, brain

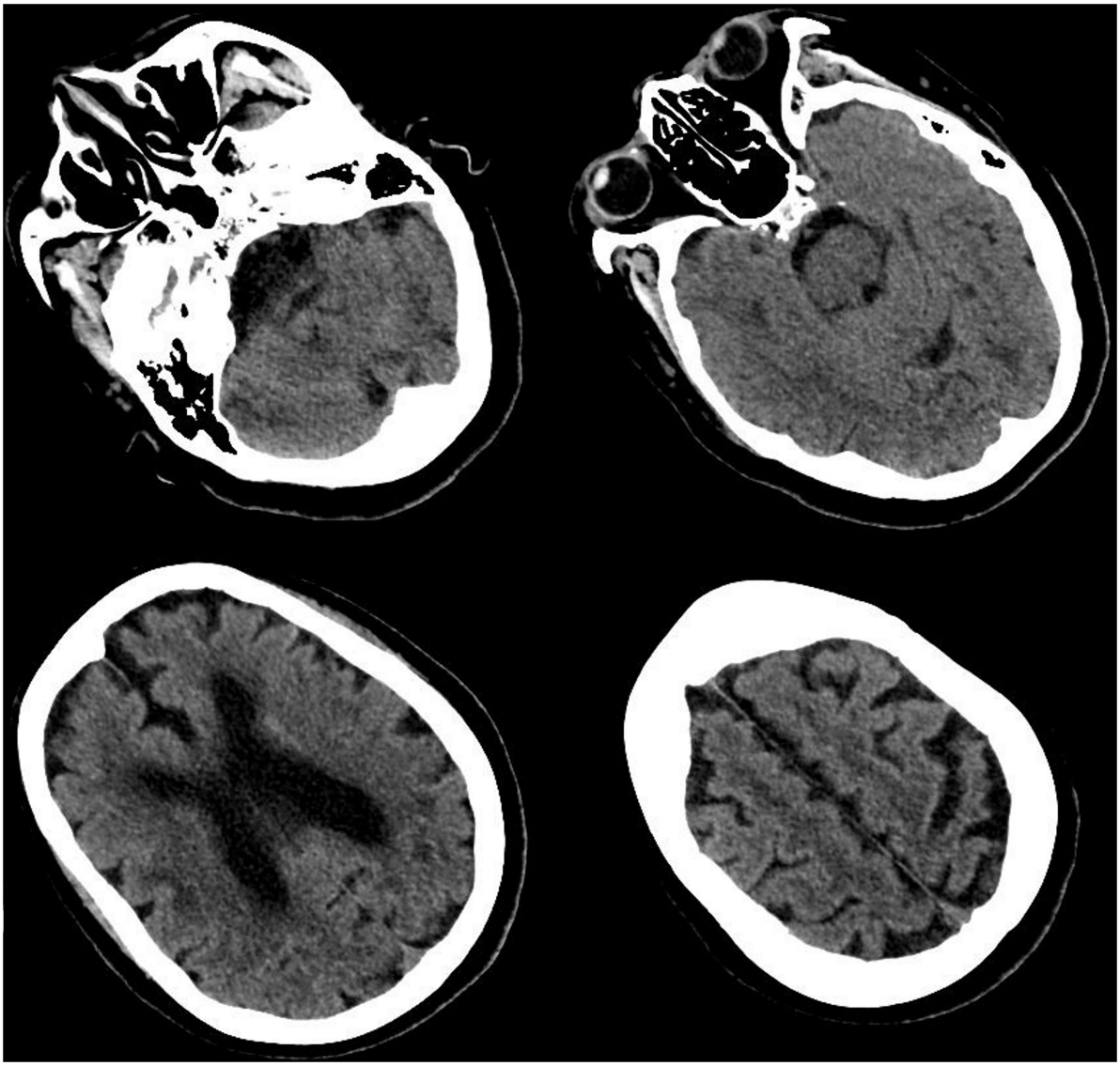

FIGURE 1
Cranial computed tomography (CT) scan. CT scan showed multiple cerebral infarction, white matter degeneration, brain atrophy, with no sign of cerebral hemorrhage or space-occupying lesion.

tumor, and other nervous system diseases were excluded. The diagnosis of CIE was performed. The treatment of CIE was engaged during these examinations. Dexamethasone, mannitol, parenteral nutrition solution, thyroxine, and glucose sodium chloride supplement were performed.

Seventy-five hours after the onset of these symptoms (5 days after PCI), the patient regained consciousness and was capable of simple conversation. Ten days after her consciousness, she had fully recovered and discharged from the hospital. During her last 10 days in the hospital, her physical activity gradually recovered, but she experienced dysphoria and disorientation several times. Two weeks after discharge, she returned to the outpatient clinic with no sign of discomfort. Physical and chemical examinations were within normal range. Echocardiogram showed no sign of pericardial effusion. MRI showed that the right parietal and occipital cortex swelling with abnormal signals disappeared (comparison of MRI is shown in **Figure 2**). Yet she has lost memory from the onset of neurological symptoms to fully recover.

## Discussion

Contrast-induced encephalopathy was first reported in Fischer-Williams et al. (3), which is a rare complication of the administration of contrast agent. The clinical

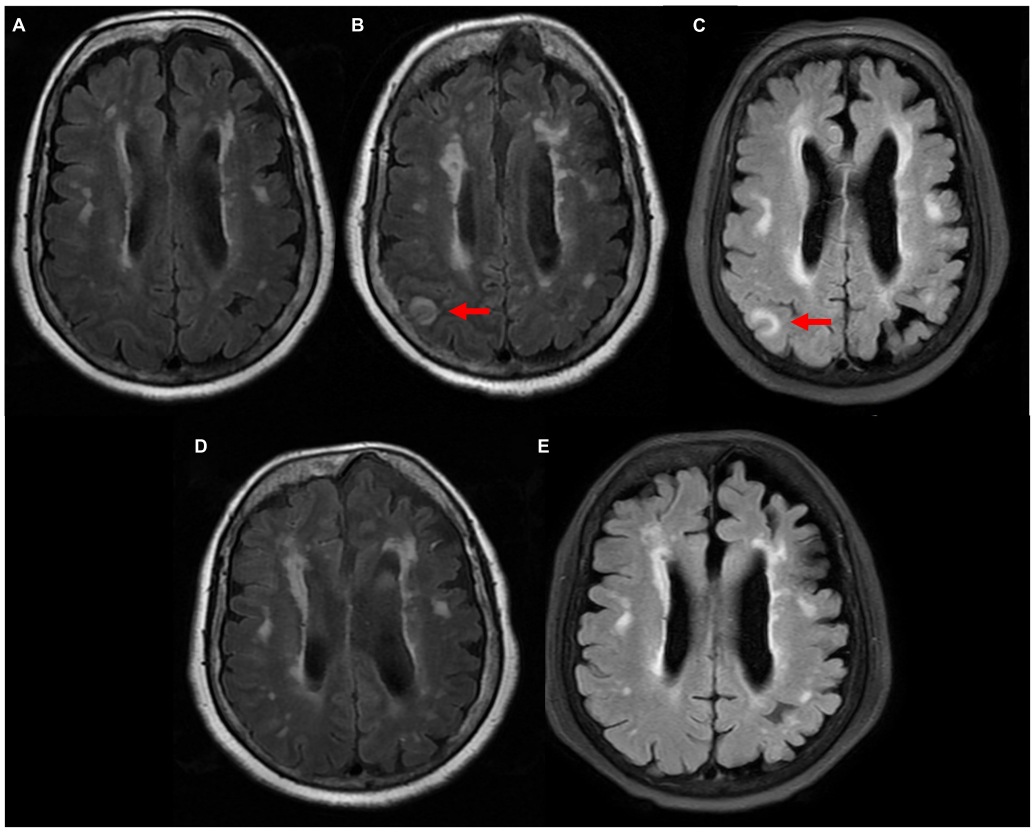


FIGURE 2
Comparison of magnetic resonance imaging (MRI) T2 flair sequence. **(A)** 4 years ago patient suffered from moderate headache and performed MRI scan in our clinic department. It showed multiple ischemic infarcts, white matter degeneration, brain atrophy, with no sign of abnormal signal. **(B)** 24 h after neurological symptoms, right parietal and occipital cortex swelling with abnormal signals was observed. **(C)** 72 h after neurological symptoms, right parietal and occipital cortex swelling with abnormal signals remained. **(D)** 12 days after neurological symptoms, abnormal signals disappeared. **(E)** 50 days after neurological symptoms, no sign of new abnormal signal.

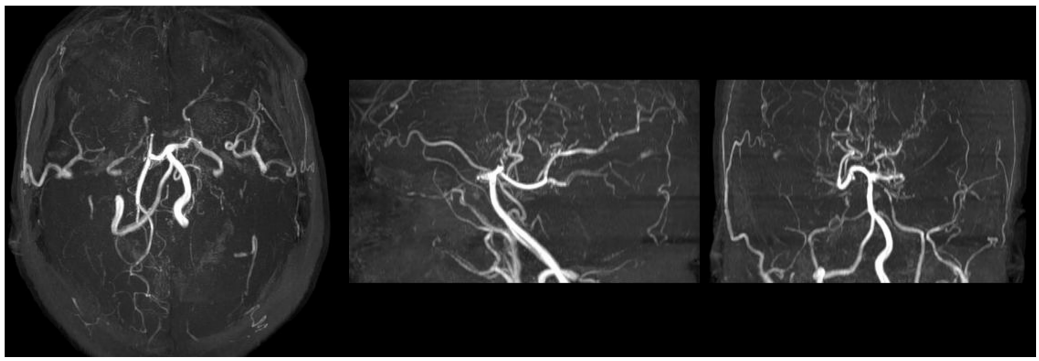

FIGURE 3
Maximum Intensity Projection sequence of MRA scan after neurological symptoms. MRA scan showed distal internal carotid artery occlusion, bilateral anterior and middle cerebral arteries occlusion, abundant and disordered collateral circulation at the circle of basal artery and bilateral basal ganglia, considered moyamoya disease.

manifestations of CIE are different signs of neurological dysfunction which usually are transient. CIE is sometimes indefinitely diagnosed, requires admission of an iodinated contrast agent, a short interval between exposure to contrast and onset of symptoms, full recovery from neurological symptoms within days, and is excluded from other

pathological processes. CIE happens 0.5 to 18 h after the administration of the iodinated contrast agent, according to present reports (4). With or without treatment, symptoms usually resolve spontaneously within 48 to 72 h, as the contrast agent is eliminated by the kidneys (5). Typical radiological findings of CIE include cerebral edema and cortical enhancement.

The pathological mechanism of CIE is not explicit. Current understanding of CIE is the dysfunction of the blood–brain barrier (BBB) and neurotoxicity caused by iodine-based contrast. Under normal conditions, the BBB can block the iodinated compounds out of the nervous system. When the integrity of the BBB is disrupted and the contrast agent permeates the central nervous system, it causes injury through direct neuronal toxicity (1). The high iodine concentration in contrast, increased neuronal excitability due to receptor activation, and lipid solubility of the contrast medium have all contributed to the contrast's neurotoxicity (6–8).

The main risk factors of CIE are not certain due to the lack of the statistic data. Renal dysfunction (decreased glomerular filtration rate) as one of the major risk factors is well-established (9, 10). Other than that, previous stroke and heart failure are major risk factors for CIE (11).

In this case, there were many unusual features we can find during the procedure. First, the neurological symptoms happened 48 h after the administration of the contrast agent, which was longer than ever reported cases of CIE. Second, the neurological symptoms were fully resolved but had lasted for over 10 days. Other than these, she was accompanied by renal dysfunction, hypothyroidism, hyponatremia, pericardial effusion, and moyamoya disease. Among these diseases, moyamoya disease (MMD) is a chronic occlusive cerebrovascular disease characterized by partial progressive stenosis at the end of the internal carotid artery and abnormal vascular network at the bottom of the brain (12). Narducci et al. (13) first demonstrated that the BBB was impaired in patients with MMD with a retrospective study.

With all these leading evidence, we supposed the following pathophysiological process. Following contrast agent administration, the BBB, which had been compromised by MMD, was unable to keep the contrast out of the nervous system. Contact with iodine-based contrast led to neurotoxicity. Hyponatremia, attributed to hypothyroidism, deteriorated the impairment of BBB, and cerebral edema. Low metabolic level and renal dysfunction which are attributed to hypothyroidism had led to a delayed elimination of contrast. These may explain the delayed and prolonged procedure of CIE, and the changes in imaging abnormalities abided by the symptoms. Lateral evidence for the diagnosis of CIE are that we treated her with a standard treatment of CIE, including dexamethasone, mannitol, and nutrition support. Biochemical and etiological detection of cerebrospinal fluid did not return diagnostic results. Brain tumor was also excluded after the re-examination of MRI. Hence we have strong confidence that this is the first reported delayed CIE following PCI in patients with cerebrovascular abnormalities.

In conclusion, CIE is a rare complication of the administration of iodinated contrast agent, with varied clinical manifestations. The diagnosis standard of CIE is not definite, which highly depends on the association with the contact of contrast and the exclusion of other nervous system diseases. Prompt and dynamic imaging examination would provide great value in the diagnosis and evaluation of CIE. The pathological mechanism of CIE is not explicit, which leads to only supportive treatment, not etiological treatment in clinical practice. Complicated clinical circumstances and individual specificity make it even more difficult to handle. Timely diagnosis and intervention may be the key to its satisfying prognosis.

## Data availability statement

The original contributions presented in this study are included in the article/supplementary material, further inquiries can be directed to the corresponding author.

## Ethics statement

Ethical review and approval was not required for the study on human participants in accordance with the local legislation and institutional requirements. The patients/participants provided their written informed consent to participate in this study. Written informed consent was obtained from the individual(s) for the publication of any potentially identifiable images or data included in this article.

## Author contributions

JL, YW, and MS supervised and revised the manuscript. YLW, JD, and XL drafted the manuscript. PY, DF, ZD, and ML processed the clinical information and imaging. All authors contributed to the article and approved the submitted version.

## Funding

This work was supported by the National Natural Science Foundation of China (Nos. 81803923 and 81903988), Young Elite Scientists Sponsorship Program by CAST (2018QNRC2-C10),

and Science Research Fund of China-Japan Friendship Hospital (No. 2017-2-QN-13).

## Conflict of interest

The authors declare that the research was conducted in the absence of any commercial or financial relationships that could be construed as a potential conflict of interest.

## Publisher's note



## References

1. Spina R, Simon N, Markus R, Muller DW, Kathir K. Contrast-induced encephalopathy following cardiac catheterization. *Catheter Cardiovasc Interv.* (2017) 90:257–68. doi: 10.1002/ccd.26871

2. Hamra M, Bakhit Y, Khan M, Moore R. Case report and literature review on contrast-induced encephalopathy. *Future Cardiol.* (2017) 13:331–5. doi: 10.2217/fca-2016-0075

3. Fischer-Williams M, Gottschalk PG, Browell JN. Transient cortical blindness. An unusual complication of coronary angiography. *Neurology.* (1970) 20:353–5. doi: 10.1212/WNL.20.4.353

4. Fernando TG, Nandasiri S, Mendis S, Senanayake S, Gooneratne IK, Navinan R, et al. Contrast-induced encephalopathy: a complication of coronary angiography. *Pract Neurol.* (2020) 20:482–5. doi: 10.1136/practneurol-2020-002524

5. Dattani A, Au L, Tay KH, Davey P. Contrast-induced encephalopathy following coronary angiography with no radiological features: a case report and literature review. *Cardiology.* (2018) 139:197–201. doi: 10.1159/000486636

6. Tuohimaa PT, Melartin E, Dabb R. Neurotoxicity of iothalamates and diatrozoates (2 parts). *Invest Radiol.* (1970) 5:29. doi: 10.1097/00004424-197005010-00003

7. Mennini T, Bernasconi P, Fiori MG. Neurotoxicity of nonionic low-osmolar contrast media. A receptor binding study. *Invest Radiol.* (1993) 28:821–7. doi: 10.1097/00004424-199328090-00012

8. Wible JH Jr., Barco SJ, Scherrer DE, Wojdyla JK, Adams MD. Neurotoxicity of non-ionic X-ray contrast media after intracisternal administration in rats. *Eur J Radiol.* (1995) 19:206–11. doi: 10.1016/0720-048X(94)00599-8

9. Chisci E, Setacci F, de Donato G, Setacci C. A case of contrast-induced encephalopathy using iodixanol. *J Endovasc Ther.* (2011) 18:540–4. doi: 10.1583/11-3476.1

10. Yu J, Dangas G. Commentary: new insights into the risk factors of contrast-induced encephalopathy. *J Endovasc Ther.* (2011) 18:545–6. doi: 10.1583/11-3476C.1

11. Chu YT, Lee KP, Chen CH, Sung PS, Lin YH, Lee CW, et al. Contrast-induced encephalopathy after endovascular thrombectomy for acute ischemic stroke. *Stroke.* (2020) 51:3756–9. doi: 10.1161/STROKEAHA.120.031518

12. Fujimura M, Bang OY, Kim JS. Moyamoya disease. *Front Neurol Neurosci.* (2016) 40:204–20. doi: 10.1159/000448314

13. Narducci A, Yasuyuki K, Onken J, Blecharz K, Vajkoczy P. In vivo demonstration of blood-brain barrier impairment in Moyamoya disease. *Acta Neurochir (Wien).* (2019) 161:371–8. doi: 10.1007/s00701-019-03811-w

frontiers | Frontiers in Cardiovascular Medicine

TYPE Case Report
PUBLISHED 14 December 2022
DOI 10.3389/fcvm.2022.1055000



OPEN ACCESS

EDITED BY
Riccardo Liga,
Pisana University Hospital, Italy

REVIEWED BY
Andreas Giannopoulos,
University Hospital Zürich, Switzerland
Lin Yang,
Affiliated Hospital of North Sichuan Medical College, China

*CORRESPONDENCE
Hoai Thi Thu Nguyen
hoainguyen1973@gmail.com

SPECIALTY SECTION
This article was submitted to Cardiovascular Imaging, a section of the journal Frontiers in Cardiovascular Medicine

RECEIVED 27 September 2022
ACCEPTED 22 November 2022
PUBLISHED 14 December 2022

CITATION
Nguyen HTT, Pham VT, Duong HD, Kirkpatrick JN, Taylor WR and Pham HM (2022) Concomitant intramyocardial and hepatic hydatid cysts diagnosed by multi-modality imaging: A rare case report. *Front. Cardiovasc. Med.* 9:1055000. doi: 10.3389/fcvm.2022.1055000



# Concomitant intramyocardial and hepatic hydatid cysts diagnosed by multi-modality imaging: A rare case report

Hoai Thi Thu Nguyen[1,2*], Viet Tuan Pham[1], Hung Duc Duong[1], James N. Kirkpatrick[3,4], Walter Robert Taylor[5,6] and Hung Manh Pham[1,7]

[1]Vietnam National Heart Institute, Bach Mai Hospital, Hanoi, Vietnam, [2]Department of Internal Medicine, VNU-University of Medicine and Pharmacy, Hanoi, Vietnam, [3]Cardiovascular Division, Department of Medicine, University of Washington Medical Center, Seattle, WA, United States, [4]Department of Bioethics and Humanities, University of Washington Medical Center, Seattle, WA, United States, [5]Mahidol Oxford Tropical Medicine Research Unit, Bangkok, Thailand, [6]Centre for Tropical Medicine and Global Health, University of Oxford, Oxford, United Kingdom, [7]Department of Cardiology, Hanoi Medical University, Hanoi, Vietnam

Cardiac echinococcosis is a potentially fatal form of hydatid disease; yet, its diagnosis and treatment are challenging due to the variability in its clinical manifestations and due to its various unpredictable preoperative complications. Multi-modality imaging is shown to provide important guidance for the treatment and decision-making. We report a rare case of a 50-year-old woman who had concomitant cardiac and hepatic hydatid cysts. She presented with abdominal pain and elevated eosinophilic white blood cells. The initial abdominal ultrasound and computerized tomography revealed a large cyst in the liver. An intramyocardial cyst was detected by two-dimensional echocardiography. Three-dimensional echocardiography increased the confidence level of two-dimensional echocardiography by displaying the three-dimensional volume of the cyst and allowing visualization of its spatial characteristics and the relationships with adjacent cardiac structures, which was subsequently confirmed at surgery. Multi-detector computed tomography and magnetic resonance imaging helped localize and define the typical morphological features of the cyst. Serology and antigen detection were used for diagnosis. This rare case underlines the integration of clinical, multi-modality imaging, and pathological data in the diagnosis of concomitant intramyocardial and hepatic hydatid cysts. Surgical resection of cysts and anthelmintic medication were successful in the management of this patient.

KEYWORDS

**hydatid cyst, cardiac echinococcosis, intramyocardial hydatid cyst, three-dimensional echocardiography, multi-modality imaging**

## Introduction

Echinococcosis in humans occurs as a result of infection by the larval stages of the taeniid cestodes of the genus *Echinococcus*. When present, hydatid involvement often manifests as cystic lesions in many organs (1), which can be symptomatic due to expansion and mass effect or due to rupture that occasionally leads to anaphylaxis and death. Cardiac hydatid cysts are found in fewer than 2% of cases of hydatidosis (2). The diagnosis is challenging because of the long latency between the infection and the manifestation of the disease (3). Decision-making regarding therapy for cardiac hydatid cysts depends on their locations, size, hemodynamic influences, and the risk of rupture. Two-dimensional (2D) and three-dimensional (3D) echocardiography, multi-detector computed tomography (MDCT), and magnetic resonance imaging (MRI) can show the cystic nature of the mass and its relation to the cardiac chambers.

In this article, we report a rare case of a female patient who presented with abdominal pain and elevated eosinophilic white blood cells. Multi-modality imaging showed an unexpected intramyocardial hydatid cyst and a large hepatic cyst with a definitive diagnosis confirmed by pathology of samples that were acquired during surgery.

## Case presentation

A 50-year-old female farmer from a Northern Midland province of Vietnam complained of right upper quadrant and epigastric pain, which was described as a dull ache that had been present for 2 months. In addition, she experienced an intermittent "stinging" sensation in the chest. She was otherwise well and denied weight loss, malaise, fever, rash, and gastrointestinal or respiratory symptoms. Her medical history was normal. She had many dogs as pets in her house. Findings on physical examination were unremarkable. The 12-lead electrocardiogram (ECG) with sinus rhythm at 76 beats per minute and 24-h ambulatory ECG were normal. A chest X-ray examination showed a normal cardiothoracic index and clear lung fields. The patient had eosinophilia (eosinophilic white blood cell 22.1%) in association with a mild increase in plasma liver enzymes (AST:39U/L, ALT: 56U/L) and the erythrocyte sedimentation rate (1h/2h:30/36). Other blood and urine test results were normal.

Abdominal ultrasound demonstrated an echo-lucent lesion measuring 150 × 80 mm in the right lobe of the liver. An abdominal computed tomography scan with contrast was performed to assess the tissue characteristics, size, and evidence of local complications and detect other visceral cysts. The cyst was described as an encapsulated structure measuring 115 × 86 mm, with a thin capsule containing homogeneous liquid. The biliary tract was normal on both abdominal ultrasound and CT scan. Cerebral and pulmonary cysts were ruled out by head and chest CT scans, respectively.

Transthoracic echocardiography (TTE) revealed a drop-like and echo-lucent intramural structure measuring 29 × 21 mm, bulging into the left ventricle from the myocardium of the left ventricular lateral wall and moving synchronously with the cardiac cycle (Figure 1A). On Doppler echocardiography, no color flow was observed within the cystic cavity. Neither the aortic valve nor the mitral valve was influenced by the cyst. The cardiac cyst did not cause intracardiac obstruction. Left ventricular (LV) and right ventricular (RV) dimensions and function and systolic pulmonary artery pressure were normal. These findings were compatible with the patient's clinical functional class (New York Heart Association Classification I).

Three-dimensional transthoracic echocardiography (3D-TTE) was performed to image the cyst in multiple planes. In total three different modalities of 3D echocardiography, including live 3D (narrow-angle), 3D zoom, and full volume (wide angle), were acquired and then cropped to visualize the cyst using "en-face" views. The cyst was round and unilocular, with liquid content and well-defined edges; its wall looked homogeneously smooth and hyper-echogenic when seen from outside and inside (Figures 1B–D and Supplementary Videos 1–3). Cystic sludge was hypo-echogenic. The 3D dataset was used to measure cyst size (28 × 21 × 22 mm), and color Doppler confirmed that it was not vascularized. Enhanced description of the cyst with 3D-TTE helped in the differential diagnosis and aided in the understanding of the surrounding structures. There were no mitral prolapse, no mitral annular dilation, and no mitral regurgitation seen on 3D-TTE.

On cardiac CT images, the lesion looked primarily intracavitary. Contrast-enhanced MDCT of the heart showed an encapsulated, rounded and fluid-attenuated, non-calcified structure along the LV lateral wall measuring 32 mm × 24 mm, its morphologic features looked similar to that of the hepatic cyst which was shown in the Figure 2A. There was no enhancement seen following IV contrast. Coronary MDCT excluded coronary stenosis; coronary aneurysm, which may have mimicked some of the findings on echo; and coronary compression caused by the cyst. In computed tomographic 3D volume-rendered images, the cyst was also clearly seen not in contact with coronary arteries (Figures 2B–E).

Cardiac MRI also demonstrated a single intramuscular cystic mass located at the anterolateral papillary muscle attaching to LV lateral free wall and protruding into the ventricular cavity (Figure 2F and Supplementary Video 4). The cyst was not enhanced by gadolinium and was measured at 24 × 23 × 30 mm. Myocardial perfusion and enhancement were normal. LVEF and cardiac indexes were 77% and 2.8 l/min/m$^2$, respectively. The flow void on CMR confirmed the normal activity of the cardiac valves without intracardiac obstruction.

We performed serological enzyme-linked immunosorbent assay (ELISA) tests for *Entamoeba histolytica*, *Strongyloides*, *Toxocara*, and *Echinococcus* and examined stool for the eggs of

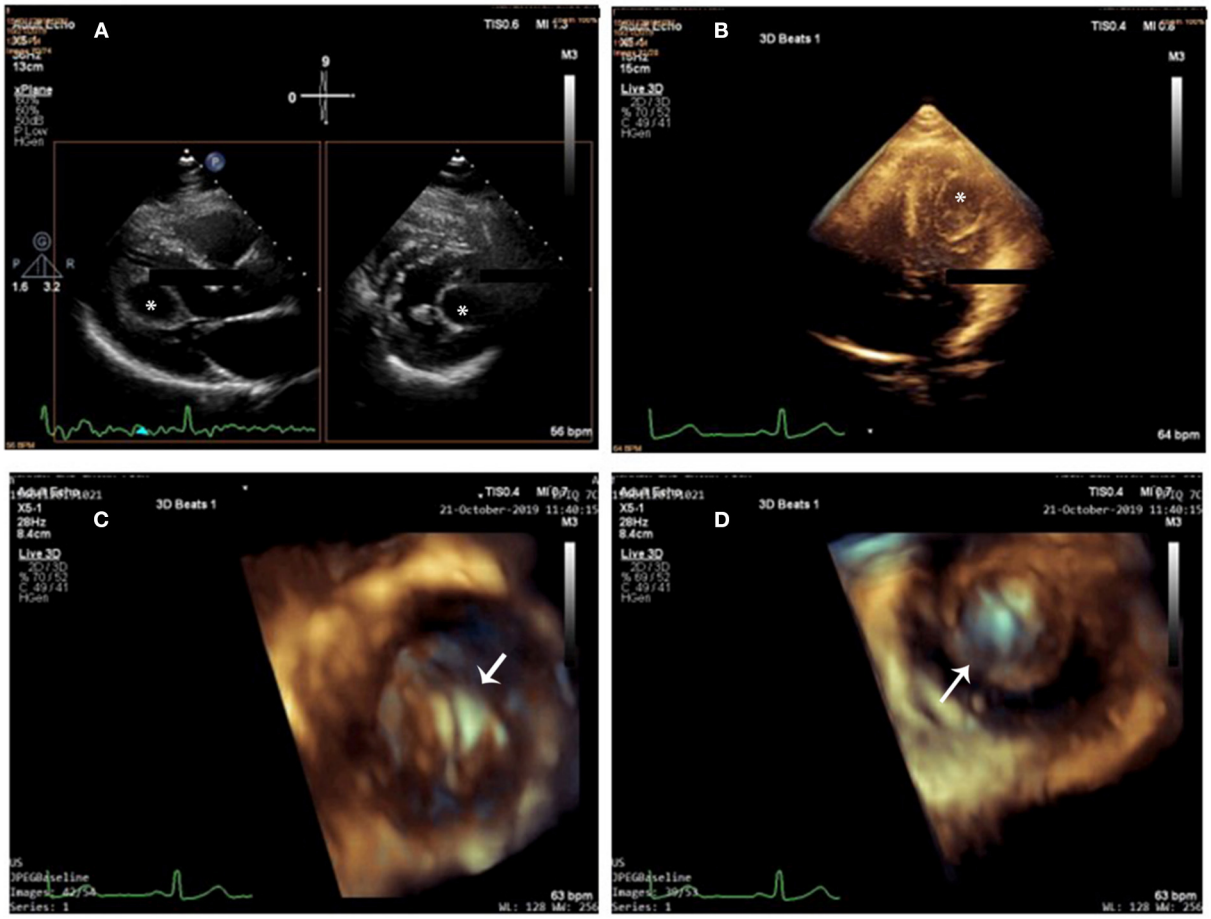


FIGURE 1
Cardiac cyst on 2D-TTE and 3D-TTE. **(A)** 2D X-plane imaging showed a drop-like and echo-lucent intramural structure (star) bulging into the left ventricle from the myocardium of the left ventricular lateral wall. **(B)** 3D full-volume imaging: The cyst was round and unilocular, with liquid content and well-defined edges (star). **(C,D)** 3D zoom imaging (en-face view) from outside **(C)** and from inside **(D)** perspectives (arrow), the cyst wall looked homogeneously smooth and hyper-echogenic. Cystic sludge was hypo-echogenic.

*Fasciola hepatica*. All results were negative. Because the hepatic cyst was very large and appeared to be at risk for rupture, surgical removal was attempted. However, only a partial cystectomy was possible because it was located too deeply in the liver tissue. The experienced surgeons resected the tip of the cyst and drained all the fluid inside. *Echinococcus* larvae were found in the histological specimen of the hepatic cyst wall (Figures 3A,B). She was treated with albendazole 400 mg b.i.d for 8 weeks before the cardiac surgery.

Since there were concerns for cyst rupture because of the mechanical contractility of the left ventricle, cardiac surgery was undertaken by the experienced cardiothoracic surgeons in the cardiovascular operating room to remove the cyst under cardiopulmonary bypass to minimize the risk of cyst leakage. The anterior papillary muscle containing the cyst was pale and swollen, and on exposure, the cyst was an opalescent white and smooth sphere containing clear yellow liquid (Figures 3C–E). The fluid was aspirated completely. Intravenous solumedrol was applied to the cyst to prevent an allergic reaction. The cyst cavity was excised intact, and the affected papillary muscle was reattached. The cystic fluid contained larvae at different stages that had specific morphological characteristics of *Echinococcus granulosus*, according to the designation of the World Health Organization and the World Organization for Animal Health (Figures 3F,G) (4).

After the cardiac cystectomy, the eosinophilic count decreased significantly (13.1% at 4 days post-operation). Post-operative TTE showed an LV cavity devoid of masses, normal LV systolic function, and trivial mitral regurgitation. The patient continued receiving albendazole 200 mg b.i.d for 2 more weeks. Post-operative 12-lead and 24-h ambulatory ECGs were normal. At 1, 6, and 12 months after cardiac surgery, the patient felt well-without symptoms, and her blood tests, abdominal ultrasound, and echocardiographic LV and RV systolic functions were normal. However, the 12-month 2D-TTE revealed mild to moderate mitral regurgitation due to prolapsed A1 and

10.3389/fcvm.2022.1055000

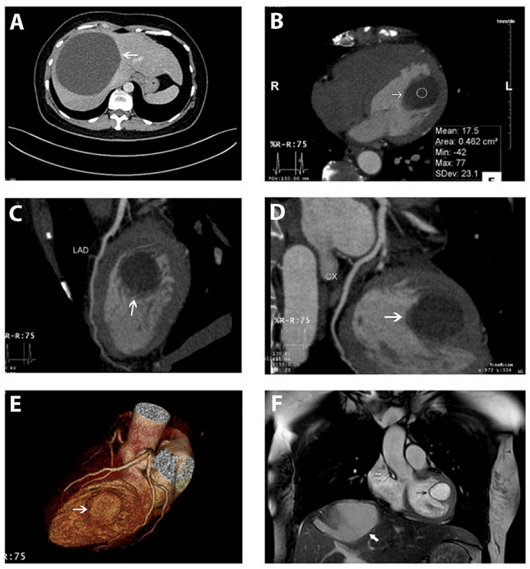


FIGURE 2
Hepatic cyst and the cardiac cyst on CT and on MRI. **(A)** A giant hepatic cyst was seen on the abdominal CT scanner (white arrow). **(B–E)** An encapsulated, rounded, and fluid-attenuated non-calcified structure along the LV lateral wall (white arrow) and its spatial relationship with coronary arteries (left anterior descending, circumflex) on MDCT. **(F)** Cardiac cyst (black arrow) and the hepatic cyst (white arrow) were simultaneously depicted on MRI. The cardiac cyst was a single intramuscular cyst located at the anterolateral papillary muscle attached to the LV lateral free wall, protruding into the LV cavity, not enhanced by the gadolinium. Myocardial perfusion and enhancement were normal.

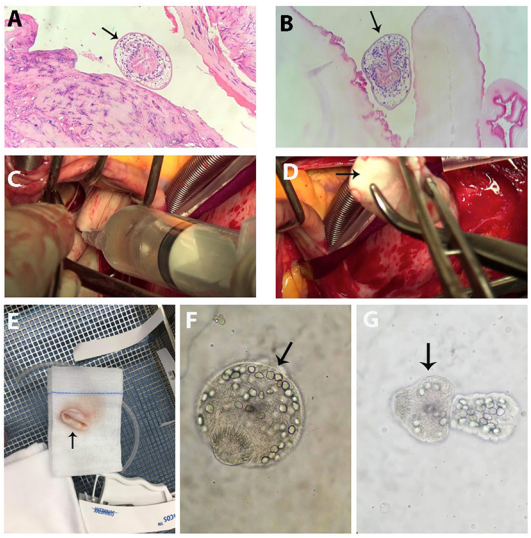


FIGURE 3
Surgical findings and Echinococcus larvae. **(A,B)** Echinococcus larvae (arrow) in the hepatic cyst specimen. **(C)** Cardiac cyst fluid that looked clear yellow was aspirated. **(D)** Opalescent white and smooth sphere cyst (arrow) was totally removed from the heart. **(E)** Cyst specimen (arrow). **(F,G)** Echinococcus larvae at different stages (arrow) in the cardiac cyst fluid.

A2 segments that were confirmed by 3D transesophageal echocardiography (3D-TEE) (Figures 4A–D); the prolapse was probably due to resection of the anterior papillary muscle at the time of cyst removal. The 3D-TTE and 3D-TEE showed no abnormal structures in the LV cavity, and the LV dimensions and ejection fraction were within normal limits and without any significant changes from the previous echo studies.

## Discussion

Cystic echinococcosis, caused by *Echinococcus granulosus*, is common in pastoral areas. In Southeast Asian countries such as Thailand, Vietnam, and Indonesia, *Echinococcus* is very rare (5). In Vietnam, only two cases of cystic lung echinococcosis have been previously reported (6). The liver is the most common site, ~60%, followed by the lungs, ~20%. Hydatid cysts can be found in the pancreas, spleen, pelvis, rectum, kidneys, urinary tract, central nervous system, musculoskeletal system, bone, and skin (7–10). Cardiac hydatid cysts are rare, accounting for fewer than 2% of reported cases; the prevalence of asymptomatic cardiac hydatid cysts is even rarer (2). In Vietnam, our patient was the first cardiac echinococcosis case to be reported.

*Echinococcus granulosus* is a cyclophyllid cestode and is also known as the hydatid worm or dog small tapeworm. The adult worms reside and reproduce in the small intestines of dogs and wild carnivores, defining them as the definitive hosts. Humans and other animals are intermediate hosts (i.e., they harbor the larval stage or asexual forms). They become infected by ingestion of eggs passed in dog feces, and this leads to the development of hydatid cysts. During primary infection, eggs may reach the heart through the lymphatic system or *via* the coronary circulation. Alternatively, cysts in the liver and lungs may rupture and release daughter cysts, larvae, and fragments of the germinal layer, which then settle in the myocardium to produce new cysts. The coronary artery anatomy explains the cardiac distribution of cysts; the most common cardiac location is the left ventricular wall (60%) because the left ventricle receives the largest amount of the coronary blood supply, followed by the right ventricle (10%), interventricular septum (4%), left atrium and left atrial appendage (6%), pulmonary artery (6%), pericardium (7%), and right atrium (3%) (11). Cysts may localize in the ventricular wall, outflow tract, or apex or may spread from the left ventricular wall to the ventricular septum. The pericardium may also be affected, causing acute pericarditis that may lead to constrictive pericarditis over time. By contrast, the endocardium does not react to the presence of hydatid cysts and, therefore, may be more easily invaded by the cyst. Cardiac

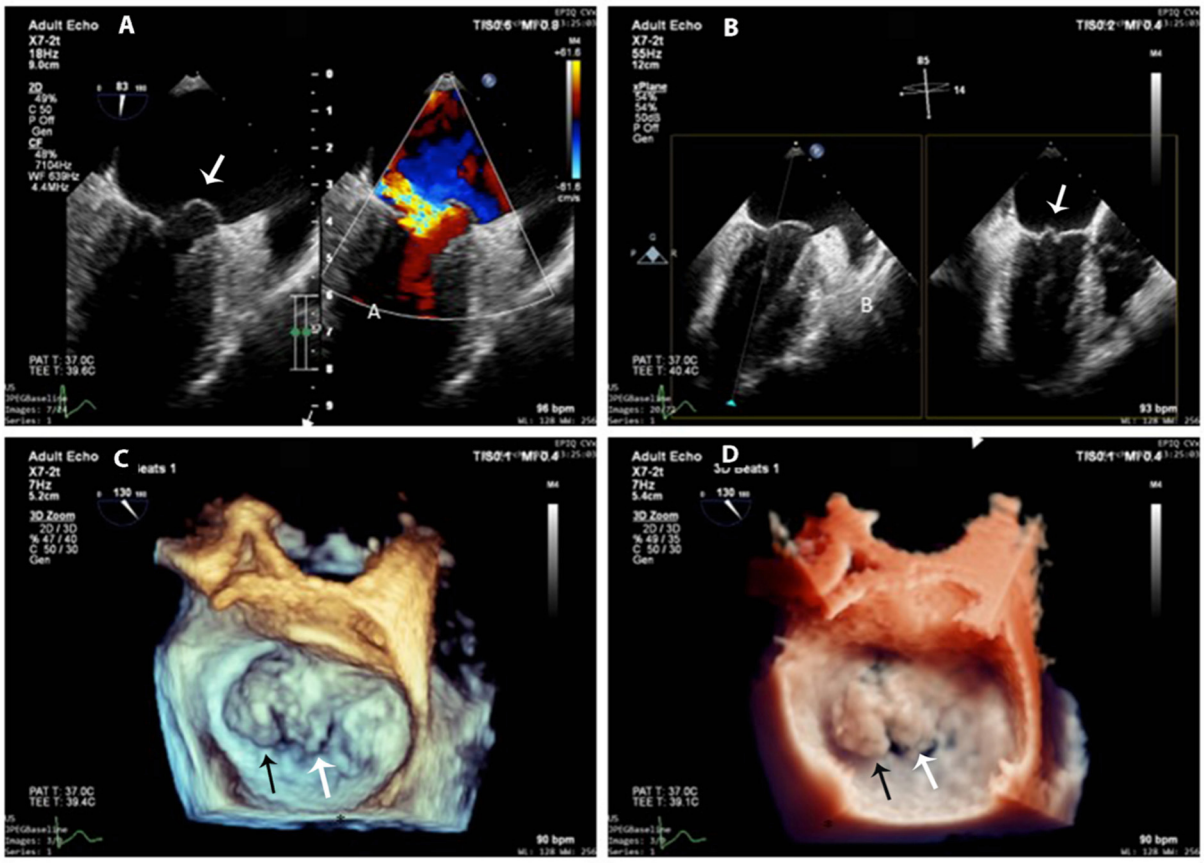


FIGURE 4
3D-TEE at 1-year follow-up. **(A)** Mitral anterior leaflet prolapse (white arrow) on a mid-esophageal two-chamber view (left panel) and the origin of the regurgitation jet with color Doppler (right panel). **(B)** X-plane imaging with two orthogonal views shows exactly the prolapsed scallops (white arrow). **(C,D)** 3D-zoom images of the mitral valve from the left atrial perspective (surgeon's en-face view) show exactly A1 (black arrow) and A2 (white arrow) prolapse **(C)** normal 3D gain vs. **(D)** true view mode.

hydatid cysts are often part of multiple organ involvement (1, 5). Patients may be asymptomatic for many years, while in other patients, symptoms may develop when there is a mechanical obstruction, for example, coronary artery compression, or if the conduction system is compromised by the expanding cyst. Serious complications include cyst rupture leading to acute anaphylactic shock and death, cardiac tamponade also due to a rupture or an expanding cyst, cerebral or peripheral arterial embolism, acute coronary syndrome, arrhythmias, ventricular dysfunction, valvular regurgitation, and sudden unexplained death (12–17).

Electrocardiography may reveal Q-wave or inverted T-wave in leads overlying the affected myocardium or may disclose evidence of conduction abnormalities (12, 13).

2D-TTE is the first-line diagnostic method of choice for cardiac hydatid cysts. It is rapid and portable and can indicate whether the cyst is enclosed or ruptured, whether it communicates with the blood supply within the heart, and whether it is vascularized. Echocardiography can evaluate the cyst mobility, attachment, and hemodynamic consequences and follow the results of treatment. Patients with exposure to or with the presence of echinococcosis in any part of the body should undergo an assessment by echocardiography as part of "staging" this multisystem disease. Our patient had concomitant cardiac and hepatic hydatid cysts but had only abdominal symptoms. She experienced no dyspnea, palpitations, or cough. A lack of cardiovascular signs and symptoms was likely related to the size and the location of the cardiac cyst, making the diagnosis of cardiac hydatid disease difficult. Thus, routine TTE plays an important role in screening for this potentially fatal condition. Mass population screening of cystic *Echinococcus* in endemic areas using portable ultrasound is considered the best method for early diagnosis, especially in asymptomatic cases (9, 10).

The use of live/real-time 3D echocardiography is the newest approach in the assessment of intracardiac cysts, which helps image the cysts in multiple planes from outside and from inside and allows for a volumetric assessment of a cyst over a linear measurement as is obtained with 2D imaging. 3D

echocardiography showed the texture of the cyst and helped confirm the continuity of the cyst to the left ventricular wall by visualization in multiple planes. Full-volume images can be obtained by 3D echocardiography and sectioned in multiple planes to examine and assess intracardiac cysts in terms of their homogeneous or heterogeneous nature, point of attachment, vascularity, and calcifications. The tissue characteristics of the cysts are peculiar to 3D echocardiography, which helps in the determination of their etiology and guides surgical planning. This information is vital, particularly since surgical cyst excision is the treatment of choice for this rare, but life-threatening, disease.

MDCT and MRI provide important details regarding the size, composition, presence of daughter cysts, anatomical location, and extracardiac involvement (9). Contrast-enhanced CT and MRI are helpful for localizing and defining the morphological features of hydatid cysts. MDCT can evaluate the coronary artery system and differentiate cysts from vascular structures. CT is also the best method for detecting cyst wall calcification. MRI is used for detecting tiny cysts, which might be missed when using ultrasound. MRI of a hydatid cyst demonstrates a hypointense lesion on T1-weighted images and a hyperintense lesion on T2-weighted images. The cyst has a defined peripheral wall because of the fibrous content of the pericyst and, therefore, may exhibit mild enhancement on delayed contrast-enhanced CT and MR images, displayed as ring enhancement. Our patient's cyst had no internal enhancement because its contents were avascular. To investigate LV or RV outflow tract obstruction and the status of coronary arteries, cardiac catheterization and angiography may be useful but can cause the rupture of the cyst. Angiography and scintigraphy may be helpful in diagnosing pulmonary hydatid embolism.

For cardiac differential diagnosis, we had to consider myxoma, fibroma, angiosarcoma, lipoma, and teratoma. Myxomas are typically found within the atria, are often pedunculated and attached to the atrial septum, are only rarely found in the left ventricular cavity, and have discrete echo-lucencies representing necrosis/hemorrhage. Fibromas are principally embedded in the myocardium and often manifest in children. Angiosarcomas are highly vascularized and tend to be located in the right atrium. Lipomas can be detected at any age and are seen in the left ventricle, atrial septum, and right atrium; they may also be resident in the subendocardium.

Eosinophilia is presented in <25% of patients with echinococcal cysts due to spontaneous cyst leakage or occult intrabiliary rupture (7). ELISA is the most serological method most commonly used. Sensitivity is high (80–94%) for hepatic hydatid and low for lung hydatid (65%) cysts. Sensitivity is reduced with cysts in certain sites (e.g., brain and eye) and in early and late inactive cysts. Therefore, negative serology does not exclude the diagnosis, as in our patient. Test specificity may be low because of cross-reaction with other parasitic infectious diseases, like filaria, alveolar echinococcosis, cysticercosis, and fascioliasis (1, 7).

Histology is a reliable method to confirm the diagnosis if a suitable sample of hydatid fluid/"sand" can be obtained safely by aspiration. A cyst biopsy may be more hazardous because of a higher risk of leakage, which may lead to seeding or acute anaphylaxis. In our patient, finding larvae in the hepatic cyst established the diagnosis and was important in deciding to perform the cardiac cystectomy. Although asymptomatic and with little apparent effect on cardiac function, the cyst was at high risk of rupture, given its location in the left ventricular wall. Hydatid cysts in the ventricular walls can grow toward either the epicardium or the endocardium. Subepicardial cysts grow more easily toward the pericardial cavity and can have large diameters; subendocardial cysts often have a higher potential for intracavitary growth. Surgical resection should not be delayed since medical therapy does not always result in a cure and may not prevent cyst rupture. Most cysts in the heart are resected under cardiopulmonary bypass, as was performed for our patient, to minimize the intracardiac rupture of the cyst, the hemodynamic deterioration during manipulation, or the accidental tear of the ventricular cavity (1, 7, 18, 19). Unfortunately, our patient developed mild to moderate mitral regurgitation due to prolapsed A1 and A2 segments of the anterior leaflet 12 months after surgery. It was probably related to the reduced function of the anterior papillary muscles of the left ventricle after cyst resection. This underscores the need for follow-up echocardiography to screen for valve dysfunction and residual cysts without exposure to radiation or requirement of iodine or gadolinium contrast agent.

Current guidelines for the management of cystic echinococcosis recommend that surgery be combined with adjunctive medical treatment with albendazole to sterilize the cyst and thus minimize the risk of intraoperative dissemination. Data from previous studies showed that the treatment of hydatid cysts with albendazole lowered the rate of recurrence and reduction of the size and death of the hydatid cysts (2, 20). The dose and duration of albendazole therapy vary in different reports; we treated our patient for 8 weeks with albendazole after her partial hepatic cystectomy and before her cardiac cystectomy; albendazole was continued for 2 weeks post-cardiac surgery. After 1 year, there was no evidence of relapsed hydatid disease on echocardiography and abdominal ultrasound, and the patient completely recovered.

## Conclusion

We present a rare case of *Echinococcus granulosus* from Vietnam, a very low-endemic country for hydatid disease, that involved the left ventricle and the liver. Our patient highlights the need to search for hydatid cysts outside of the liver. It also stresses the importance of 2D echocardiography and the incremental value of live/real-time 3D echocardiography over 2D imaging for the diagnosis of cardiac echinococcosis. It also confirms the roles of cardiac imaging modalities such as

MDCT and MRI. Surgical excision, with adjunctive albendazole, is the best treatment for cardiac cysts to prevent catastrophic complications caused by cystic rupture, regardless of cyst dimensions. The management of hydatid disease should be based on a multidisciplinary approach involving collaboration among cardiologists, radiologists, surgeons, and infectious disease specialists.

## Data availability statement

The original contributions presented in the study are included in the article/Supplementary material, further inquiries can be directed to the corresponding author.

## Ethics statement

The studies involving human participants were reviewed and approved by Bach Mai Hospital. The patients/participants provided their written informed consent to participate in this study. Written informed consent was obtained from the individual(s) for the publication of any potentially identifiable images or data included in this article.

## Author contributions

HN, VP, and JK devised the manuscript concept. HN, VP, HP, WT, and HD belonged to the patient's management team. HN and VP performed two-dimensional/three-dimensional echocardiography. HD was the main surgeon. VP contributed to clinical, imaging, and pathological data collection. HN and VP wrote the manuscript in collaboration with JK, WT, HP, and HD. JK and WT reviewed and edited the manuscript. HN took care of revising and submitting the manuscript. All authors read and approved the final version of the manuscript.

## Acknowledgments

We wish to acknowledge the Vietnam National Heart Institute, Bach Mai Hospital, for providing us with the opportunity to conduct this case report.

## Conflict of interest

The authors declare that the research was conducted in the absence of any commercial or financial relationships that could be construed as a potential conflict of interest.

## Publisher's note

All claims expressed in this article are solely those of the authors and do not necessarily represent those of their affiliated organizations, or those of the publisher, the editors and the reviewers. Any product that may be evaluated in this article, or claim that may be made by its manufacturer, is not guaranteed or endorsed by the publisher.

## Supplementary material

The Supplementary Material for this article can be found online at: https://www.frontiersin.org/articles/10.3389/fcvm.2022.1055000/full#supplementary-material

SUPPLEMENTARY VIDEO 1
3D-full volume imaging: the cyst was bulging into the left ventricle from the myocardium of the left ventricular lateral wall, moving synchronously with the cardiac cycle.

SUPPLEMENTARY VIDEO 2
3D zoom imaging of the cyst from outside perspective.

SUPPLEMENTARY VIDEO 3
3D zoom imaging of the cyst from inside perspective.

SUPPLEMENTARY VIDEO 4
The cardiac cyst and the hepatic cyst were simultaneously depicted on MRI.

## References

1. Higuita NIA, Brunetti E, McCloskey C. Kraft CS. *Cystic Echino.* (2016) 54:518–23. doi: 10.1128/JCM.02420-15

2. Brunetti E, Kern P, Vuitton DA. Expert consensus for the diagnosis and treatment of cystic and alveolar echinococcosis in humans. *Acta Trop.* (2010) 114:1–16. doi: 10.1016/j.actatropica.2009.11.001

3. Botezatu C, Mastalier B, Patrascu T. Hepatic hydatid cyst - diagnose and treatment algorithm. *J Med Life.* (2018) 11:203–9. doi: 10.25122/jml-2018-0045

4. Eckert J, Gemmell MA, Meslin Fo-X, Pawlowski ZS, World Health O. *WHO/OIE Manual on Echinococcosis in Humans and Animals: A Public Health Problem of Global Concern*. edited by Eckert J. Paris: World Organization for Animal Health (2001).

5. Wen H, Vuitton L, Tuxun T, Li J, Vuitton DA, Zhang W, et al. Echinococcosis: advances in the 21st century. *Clin Microbiol Rev.* (2019) 32:. doi: 10.1128/CMR.00075-18

6. Van De N, Le Van D. The first report of two cases of cystic echinococcosis in the lung by Echinococcus ortleppi infection, in Vietnam. *Res Rep Trop Med.* (2017) 8:45–51. doi: 10.2147/RRTM.S122014

7. Moro P, Schantz PM. Echinococcosis: a review. *Int J Infect Dis.* (2009) 13:125–33. doi: 10.1016/j.ijid.2008.03.037

8. Butt A, Khan JA. Cystic echinococcosis: a 10-year experience from a middle-income country. *Trop Doct.* (2020) 50:117–21. doi: 10.1177/00494755198 91338

9. Dietrich CF, Douira-Khomsi W, Gharbi H, Sharma M, Cui XW, Sparchez Z, et al. Cystic echinococcosis, review and illustration of non-hepatic manifestations. *Med Ultrason.* (2020) 22:319–24. doi: 10.11152/mu-2537

10. Kankilic N, Aydin MS, Günendi T, Göz M. Unusual hydatid cysts: cardiac and pelvic-ilio femoral hydatid cyst case reports and literature review. *Braz J Cardiovasc Surg.* (2020) 35:565–72. doi: 10.21470/1678-9741-2019-0153

11. Dursun M, Terzibasioglu E, Yilmaz R, Cekrezi B, Olgar S, Nisli K, et al. Cardiac hydatid disease: CT and MRI findings. *AJR American journal of roentgenology.* (2008) 190:226–32. doi: 10.2214/AJR.07.2035

12. Fennira S, Kamoun S, Besbes B, Ben Mrad I, Zairi I, Ben Moussa F, et al. Cardiac hydatid cyst in the interventricular septum: a literature review. *Int J Infect Dis.* (2019) 88:120–6. doi: 10.1016/j.ijid.2019.09.004

13. Firouzi A, Neshati Pir Borj M, Alizadeh Ghavidel A. Cardiac hydatid cyst: A rare presentation of echinococcal infection. *J Cardiovasc Thorac Res.* (2019) 11:75–7. doi: 10.15171/jcvtr.2019.13

14. Su L, Yu J, Dai C, Liu Y, Peng L. Echinococcosis in left ventricle: a case report. *Medicine).* (2019) 98:e15267. doi: 10.1097/MD.0000000000015267

15. Kulaybi S, Alamri N, Abdalkareem M. Case report: cardiac hydatid cyst. *J Cardiovasc Dis Diagnos.* (2017) 05:297. doi: 10.4172/2329-9517.1000297

16. El Boussaadani B, Regragui H, Bouhdadi H, Wazaren H, Ajhoun I, Laaroussi M, et al. Primary cardiac hydatid cyst presenting with massive pericardial effusion: a case report. *Egypt Heart J.* (2020) 72:51. doi: 10.1186/s43044-020-00085-x

17. Mesrati M, Mahjoub Y, Ben Abdejlil N, Boussaid M, Belhaj M, Limem H, et al. Case Report: Sudden death related to unrecognized cardiac hydatid cyst. *F1000Research*. (2020) 9:23277. doi: 10.12688/f1000research.23277.1

18. O'Connell EM, Nutman TB. Eosinophilia in Infectious Diseases. *Immunol Allergy Clin North Am.* (2015) 35:493–522. doi: 10.1016/j.iac.2015.05.003

19. Baruah N, Saikia PP, Nath M. Off-pump excision of ventricular myocardial hydatid cyst: a case report and review of literature. *Ind J Thora Cardiovasc Surg.* (2021) 37:427–30. doi: 10.1007/s12055-020-01113-w

20. Dehkordi AB, Sanei B, Yousefi M, Sharafi SM, Safarnezhad F, Jafari R, et al. Albendazole and treatment of hydatid cyst: review of the literature. *Infect Disord Drug Targets.* (2019) 19:101–4. doi: 10.2174/1871526518666180629134511

frontiers | Frontiers in Cardiovascular Medicine

TYPE Case Report
PUBLISHED 09 January 2023
DOI 10.3389/fcvm.2022.1020186



OPEN ACCESS

EDITED BY
Sebastian Kelle,
Deutsches Herzzentrum Berlin,
Germany

REVIEWED BY
Nikhil Agrawal,
University of Texas Health Science Center at Houston, United States
Carlos Jerjes-Sanchez,
Escuela de Medicina y Ciencias de la Salud Tec Salud, Tecnológico de Monterrey, Mexico

*CORRESPONDENCE
Xiaona Yu
1440114556@qq.com

†These authors share first authorship

SPECIALTY SECTION
This article was submitted to Cardiovascular Imaging, a section of the journal Frontiers in Cardiovascular Medicine

RECEIVED 15 August 2022
ACCEPTED 16 December 2022
PUBLISHED 09 January 2023

CITATION
Wu S, Wang X, Ren W, Song G, Hou Y, Hu H and Yu X (2023) Case report: Fatal systemic embolism caused by early prosthetic valve endocarditis after Bentall surgery.
*Front. Cardiovasc. Med.* 9:1020186.
doi: 10.3389/fcvm.2022.1020186



# Case report: Fatal systemic embolism caused by early prosthetic valve endocarditis after Bentall surgery

Shaofeng Wu[1†], Xin Wang[1†], Weidong Ren[1], Guang Song[1], Yang Hou[2], Haidi Hu[3] and Xiaona Yu[1*]

[1]Department of Ultrasound, Shengjing Hospital of China Medical University, Shenyang, China, [2]Department of Radiation, Shengjing Hospital of China Medical University, Shenyang, China, [3]Department of Vascular Surgery, Shengjing Hospital of China Medical University, Shenyang, China

Prosthetic valve endocarditis (PVE) is a rare but dangerous complication of Bentall surgery and *Staphylococcus epidermidis* PVE involving multiple valves simultaneously during the early postoperative period has not been reported. A 42 year old patient admitted to intensive care unit with fever 1 month after aortic valve replacement (Bentall procedure). Echocardiography was of great diagnosis value and suggested large, mobile vegetations on both the prosthetic aortic valve and native tricuspid valve. The presence of *Staphylococcus epidermidis* was revealed by multiple blood cultures. Surgery was not performed because of the history of aortic valve replacement 1 month ago. He developed acute right femoral artery thromboembolism, multiple cerebral infarction and splenic infarction during hospitalization and died of cerebral infarction after being discharged. This case underlines that patients with early PVE may have poor prognosis and fatal systemic embolism should be aware of in PVE patients with large vegetations present with dyskinesia, abdominal pain, and limb numbness. The timely echocardiography and vascular ultrasound are primary and reliable diagnostic methods in this scenario.

KEYWORDS

**Bentall surgery, prosthetic valve endocarditis, systemic embolism, staphylococcus endocarditis, echocardiography**

## Highlights

- Early PVE is a rare but dangerous complication of aortic valve replacement.
- Soft tissue infection during the early postoperative period of Bentall surgery may lead to PVE, which can cause a poor prognosis.
- Echocardiography and vascular ultrasound are of great importance and value in the diagnosis of PVE.
- It is necessary to prevent postoperative infection because early PVE cannot be resolved by reoperation.

10.3389/fcvm.2022.1020186

## Introduction

Bentall procedure is the gold standard treatment for patients with ascending aortic aneurysm and aortic valve stenosis or regurgitation (1). PVE is a rare but dangerous consequence after prosthetic valve implantation with an incidence of 0.3–1.2% per patient-year, and the risk for PVE is 1.7% within the first year after operation (2). *Staphylococcus epidermidis* infective endocarditis (IE) is rare within 1 year after valve replacement (3). We herein reported a sporadic case of Staphylococcus IE involving multiple valves and systemic embolisms 1 month after Bentall surgery in a 42-year-old man with Marfan's syndrome.

## Case presentation

A 42-year-old man was admitted to the hospital due to unexplained chest pain and dyspnea. Echocardiography suggested Marfan's syndrome, showing aortic root dilated up to 70 mm and moderate aortic regurgitation. Finally, the patient received aortic root replacement (Bentall surgery) to alleviate clinical symptoms. He has history of hypertension for 1 year. The patient recovered well from the surgery. However, he developed a perianal abscess in the following weeks.

He presented to the emergency department with persistent fever (38°C) and fatigue 1 month after surgery. The blood pressure was 109/71 mmHg, breathing rate was 16 breaths/min, pulse was 88 beats/min, and temperature was 36.5°C. Laboratory results showed white blood cell 19.6 × $10^9$/L, hemoglobin 95 g/L, platelet count 106 × $10^9$/L, C-reactive protein 195 mg/L, B-type natriuretic peptide 761.8 pg/ml, hypersensitivity troponin T 0.174 ng/ml. Electrocardiographic analysis revealed a first-degree atrioventricular block. A heart examination showed a murmur at the aortic area. Transthoracic echocardiogram (TTE) revealed a large (25 mm × 22 mm), iso-echogenic, irregular vegetation on the ventricular side of the prosthetic aortic valve (**Figure 1A**) winging back and forth during the cardiac cycle. In addition, a large (16 mm × 9 mm) tricuspid valve vegetation with obvious mobility was also presented (**Figure 1B**). IE was suspected according to the modified Duke criterion (4). Therefore, vancomycin (1,000 mg, every 12 h) and gentamicin (240 mg, every 8 h) were given for infection control. Rifampin was orally taken (0.3 g, every 8 h). In addition, enoxaparin sodium injection (0.8 ml, every 12 h) and warfarin (5 mg a day) were administered to prevent further vegetation generation. The diagnosis of *Staphylococcus epidermidis* endocarditis was confirmed by blood culture on day 4 after admission. Differential diagnoses included intracardiac thrombus, cardiac myxoma, non-bacterial thrombotic endocarditis and valve calcification.

The recommendation for surgery was considered inappropriate as the patient was still in the convalescent phase of Bentall surgery. Antibiotic treatment was continued.

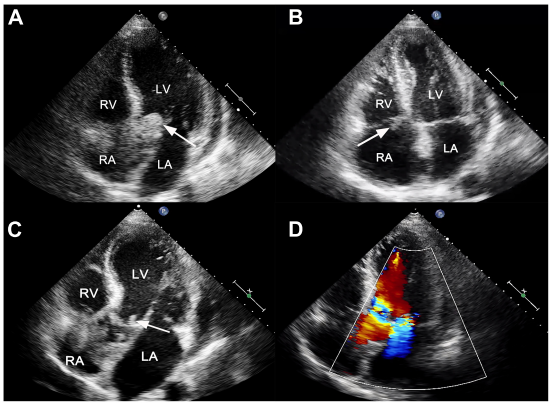


FIGURE 1
**(A)** Transthoracic echocardiogram showed a large, mobile vegetation on the ventricular side of the prosthetic valve (white arrow). **(B)** A vegetation was also visible on the tricuspid valve (white arrow). **(C)** Transthoracic echocardiogram reexamination showed residual vegetations on prosthetic aortic valves with reduced size (white arrow). **(D)** The new mitral valve moderate regurgitation. LA, left atrium; LV, left ventricle; RA, right atrium; RV, right ventricle.

On day 21, he suffered from right lower extremity numbness without an apparent cause. The vascular ultrasound showed hypoechoic mass at the distal end of the right common femoral artery with a size of 38 mm × 11 mm without significant activity (**Figure 2A**), strongly suggesting right common femoral artery embolism, one of the complications of PVE. Color Doppler showed scattered color blood flow signal (**Figure 2B**) and delayed upstroke waveforms (**Figure 2C**). The embolism in the right femoral artery was also confirmed by enhanced CT reconstruction (**Figure 2D**). Our patient immediately underwent arteriotomy to remove the embolism. Macroscopic inspection revealed thrombotic substance and vegetations (**Figure 3A**). Fiber-like material and red blood cell aggregation were shown under the microscope (**Figure 3B**). Pathological examination confirmed the right lower extremity artery embolism.

On day 28, the patient presented with sudden convulsion. Enhanced CT scanning revealed left occipital cerebral embolism (**Figure 2E**). Deproteinized calf serum injection (0.8 g once a day) was given to improve brain blood circulation. He underwent a TTE reexamination on day 31, showing that aortic valve and tricuspid valve vegetations were still present while the aortic valve vegetation was smaller compared with the last time (**Figure 1C**). However, a new mitral valve regurgitation has emerged (**Figure 1D**). Unfortunately, he presented with decreased muscle tone in the right limb on day 35, and the subsequent CT scan showed another new spot of cerebral embolism.

Furthermore, the patient developed abdominal pain, and the CT scan revealed splenic infarction (**Figure 2F**) on day 40. After

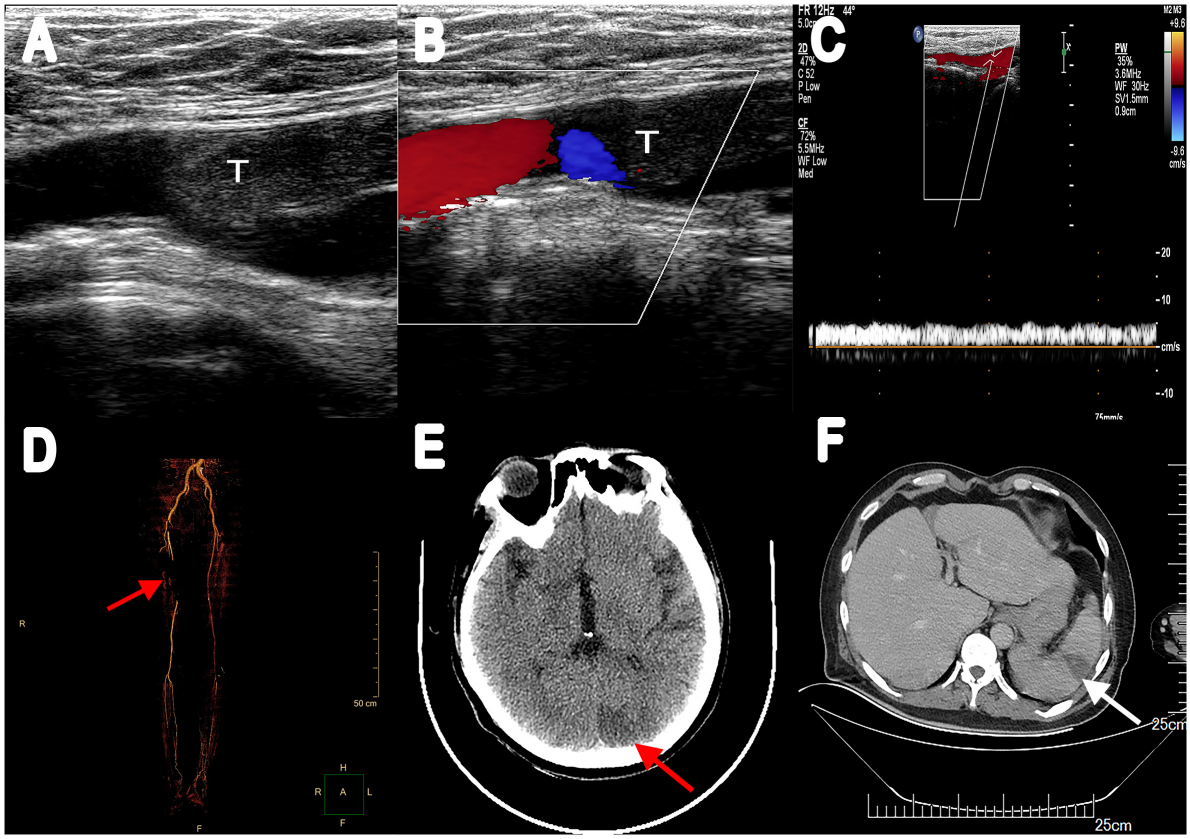


FIGURE 2
**(A)** Vascular ultrasonography showed hypoechoic filling echo was seen at the distal end of the right common femoral artery. **(B)** Color Doppler image displayed there was little color blood flow signal. **(C)** Abnormal spectrum morphology of posterior tibial artery with the significantly reduced blood flow velocity. **(D)** Multiple filling defects of the right femoral artery were observed in three-dimensional reconstruction (red arrow). **(E)** Enhanced CT scanning revealed a low-density lesion in the left occipital lobe (red arrow). **(F)** Abdominal enhancement CT showed wedge-shaped hypodense lesions under the capsule with no enhancement (white arrow). T, thrombus.

7 weeks of antibiotic and anticoagulant therapy, The patient's clinical symptom improved and body temperature was normal (36.5°C). Blood culture was negative. He was discharged after completing 45 days of hospitalization therapy and a follow-up 2 weeks later was advised. Oral warfarin (5 mg/d) was given once daily after discharge to maintain the international normalized ratio between 2 and 3 without significant bleeding tendency. Unfortunately, he died of cerebral infarction on day 55.

## Discussion

PVE is a rare but dangerous complication in patients after aortic valve replacement, with a high mortality rate of 20–40%. Moreover, 80% of death cases are associated with embolic events (1). There are few case reports on PVE complications after Bentall surgery. To our knowledge, this is the first report of the *Staphylococcus epidermidis* PVE complicated with multiple systemic embolisms early after a Bentall procedure.

Patients with cardiac structural abnormalities are vulnerable to IE, including congenital heart disease, prosthetic valve replacement, valvular stenosis, and regurgitation, leading to local hemodynamic abnormalities, where the endocardium is damaged under the constant shock of blood flow. In this scenario, the occurrence of bacteremia, caused by infected focus in other parts of the body, will promote IE. The most common organisms known to cause PVE are Staphylococcus (5). However, early infections (<1 year) caused by low pathogenic pathogens, such as *Staphylococcus epidermidis*, were rare. *Staphylococcus epidermidis* is an opportunistic pathogen mainly distributed in the intestine and has the possibility of invading the human body through soft tissue infection (3).

The most frequent symptom in patients with PVE is fever, arterial embolism, and heart failure. Systemic embolism is a serious complication of PVE, accounting for approximately 21.1% of patients with left-sided IE (6). Vegetation larger than 1 cm in diameter increases the incidence of embolization and mortality. Left-sided IE is always accompanied by splenic infarction and stroke (7, 8). However, concurrent embolization

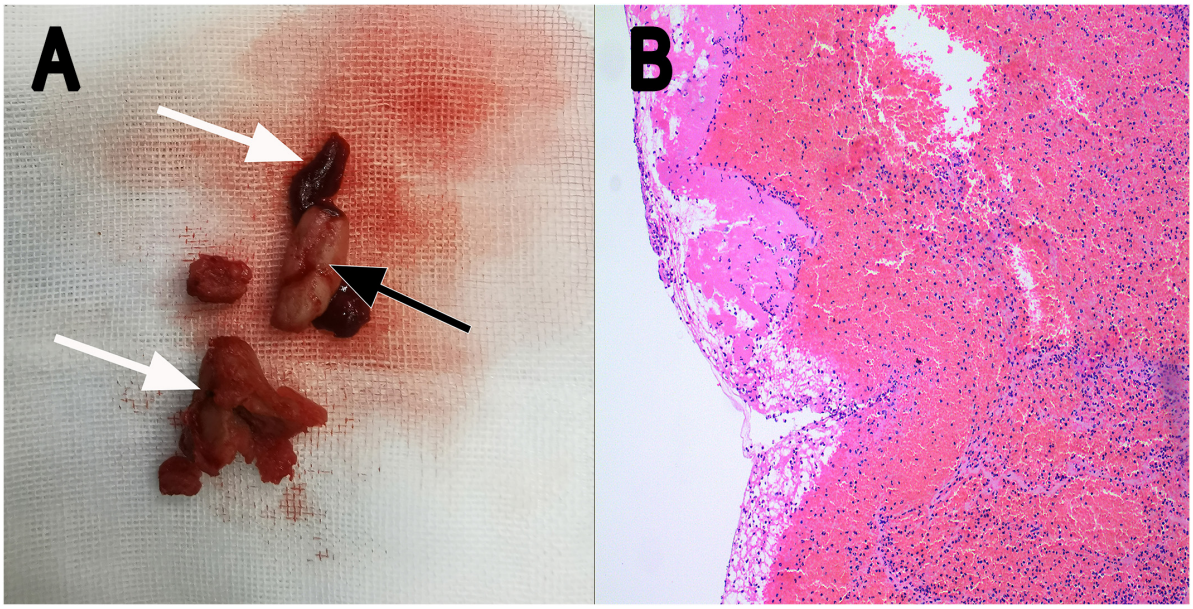


FIGURE 3
**(A)** Thrombotic substance and vegetations removed by surgery in gross appearance (white arrow: thrombotic substance; black arrow: vegetation). **(B)** Fiber-like substance and many red blood cells were seen under the microscope (H&E staining; magnification, ×10). H&E, hematoxylin and eosin.

in the brain and spleen is rare (9). In our case, cerebral and splenic infarctions occurred successively within nine days, caused by the multiple shedding of the large vegetation.

Echocardiography is the preferred technique for the diagnosis of endocarditis. The most common echocardiographic finding is the presence of vegetation and/or abscess on prosthetic valves. New-onset valve regurgitation also indicates higher likelihood of endocarditis. Echocardiography is simple and easy to perform and enables the accurate assessment of the size, location, and morphology of vegetations. Echocardiography must be performed immediately as long as IE is suspected (10). In this case, the echocardiographic findings and blood culture results were quite unequivocal. Large, mobile vegetations are the prerequisite of arterial embolism in PVE.

The fibrinolysis and anticoagulation therapy for IE patients with vegetation remains controversial. The American College of Cardiology/American Heart Association guidelines recommend surgery or the use of slow-infusion, low-dose (25 mg of tissue-type plasminogen activator over 6–24 h without bolus) fibrinolysis protocol as initial treatment (11). It is worth noting that the risk of complications of fibrinolysis therapy is related to thrombosis area and previous stroke history. A thrombus area $\geq$1.6 $cm^2$ has a complication rate of 47% (12). On the other hand, the European Society of Cardiology guidelines are more inclined to surgery (13). Our patient was not received thrombolysis due to the high risk of complications of thrombolytic therapy in this patient with large vegetation on his mechanical aortic valve (25 mm × 22 mm). In addition, some researchers suggest continuing anticoagulant therapy for patients with mechanical valve IE. However, the general recommendation is to discontinue all forms of anticoagulation for at least 2 weeks in patients with mechanical valve IE who have experienced a central nervous system embolic event. This time allows for thrombus organization and prevent the acute hemorrhagic transformation of embolic lesions. Special care should be taken when reintroducing anticoagulants. Intravenous unfractionated heparin is first applied until the activated partial thromboplastin time range from 50 to 70 s and then adjusted dose warfarin is used carefully (14). In our case, huge vegetation on the mechanical aortic valve and continued anticoagulant therapy after cerebral infarction together contribute to the risk of shedding of unstable vegetation, which is considered as the cause of failure of anticoagulation and subsequent recurrent embolism.

The PVE has attracted much more attention due to its high mortality rate. The earlier the diagnosis, the better the prognosis. A multidisciplinary team including cardiology, internal medicine, and infectious diseases should be jointly organized to manage patients with PVE. The absolute indication for early PVE surgery is *Staphylococcus aureus* infection to prevent brain embolization. Serving as the preferred treatment for PVE patients, surgery is also recommended for patients with hemodynamic instability, recurrent infection, or emboli. On the contrary, conservative treatment with antibiotics alone is often associated with adverse outcomes (15). Therefore,

the prevention of PVE should be focused on the antibiotic prophylaxis before and after invasive procedures. Reducing perioperative invasive procedures (such as central venous access and catheterization) is another effective way to reduce bacteremia and subsequent valves contamination. Additionally, more frequent follow-up and monitoring are also necessary for the first year after replacement. Health education is equally important. Our patient was not a candidate for reoperation because of persistent fever and a history of surgery a month ago. Hence, he only received symptomatic treatment, which means the subsequent high risk of development of multi-organ embolisms or even death.

## Conclusion

We report a sporadic case of *Staphylococcus epidermidis* IE involving multiple valves and systemic embolism early after Bentall operation in a patient with Marfan's syndrome. Continuous anticoagulation therapy after cerebral infarction may be the cause of deterioration. This case emphasizes that patients with early PVE may have poor prognosis and systemic embolization should be highly vigilant when PVE patients with large vegetations start to develop dyskinesia, abdominal pain, and limb numbness. Vascular ultrasound and echocardiography serve as the primary and reliable diagnostic methods in this situation.

## Data availability statement

The original contributions presented in this study are included in the article/supplementary material, further inquiries can be directed to the corresponding author.

## Ethics statement

This study was approved by the Ethical Committee of Shengjing Hospital of China Medical University. Written informed consent was obtained from patient's next of kin.

## Author contributions

SW and XW drafted the manuscript and participated in cardiac ultrasonography. XY interpreted and revised the manuscript and conducted the vascular and cardiac ultrasound. WR and GS were involved in echocardiographic diagnosis. YH provided radiology images. HH was the surgeon in the case. All authors contributed to the study conception and design and approved the final manuscript.

## Conflict of interest

The authors declare that the research was conducted in the absence of any commercial or financial relationships that could be construed as a potential conflict of interest.

## Publisher's note

All claims expressed in this article are solely those of the authors and do not necessarily represent those of their affiliated organizations, or those of the publisher, the editors and the reviewers. Any product that may be evaluated in this article, or claim that may be made by its manufacturer, is not guaranteed or endorsed by the publisher.

## References

1. Mangner N, Woitek F, Haussig S, Schlotter F, Stachel G, Höllriegel R, et al. Incidence, predictors, and outcome of patients developing infective endocarditis following transfemoral transcatheter aortic valve replacement. *J Am Coll Cardiol.* (2016) 67:2907–8. doi: 10.1016/j.jacc.2016.03.588

2. Kolte D, Goldsweig A, Kennedy K, Abbott J, Gordon P, Sellke F, et al. Comparison of incidence, predictors, and outcomes of early infective endocarditis after transcatheter aortic valve implantation versus surgical aortic valve replacement in the United States. *Am J Cardiol.* (2018) 122:2112–9. doi: 10.1016/j.amjcard.2018.08.054

3. Bjursten H, Rasmussen M, Nozohoor S, Götberg M, Olaison L, Rück A, et al. Infective endocarditis after transcatheter aortic valve implantation: a nationwide study. *Eur Heart J.* (2019) 40:3263–9. doi: 10.1093/eurheartj/ehz588

4. Li J, Sexton D, Mick N, Nettles R, Fowler V Jr, Ryan T, et al. Proposed modifications to the Duke criteria for the diagnosis of infective endocarditis. *Clin Infect Dis.* (2000) 30:633–8. doi: 10.1086/313753

5. Heuzé C, Lepage L, Loubet P, Duval X, Cimadevilla C, Verdonk C, et al. Infective endocarditis after bentall surgery: usefulness of new imaging modalities and outcomes. *JACC Cardiovasc Imaging.* (2018) 11:1535–7. doi: 10.1016/j.jcmg.2017.12.007

6. Fabri J Jr, Issa V, Pomerantzeff P, Grinberg M, Barretto A, Mansur A. Time-related distribution, risk factors and prognostic influence of embolism in patients with left-sided infective endocarditis. *Int J Cardiol.* (2006) 110:334–9. doi: 10.1016/j.ijcard.2005.07.016

7. Pericas J, Llopis J, Cervera C, Sacanella E, Falces C, Andrea R, et al. Infective endocarditis in patients with an implanted transcatheter aortic valve: clinical characteristics and outcome of a new entity. *J Infect.* (2015) 70:565–76. doi: 10.1016/j.jinf.2014.12.013

8. Mohananey D, Mohadjer A, Pettersson G, Navia J, Gordon S, Shrestha N, et al. Association of vegetation size with embolic risk in patients with infective endocarditis: a systematic review and meta-analysis. *JAMA Intern Med.* (2018) 178:502–10. doi: 10.1001/jamainternmed.2017.8653

9. Chrissoheris M, Ferti A, Spargias K. Early prosthetic valve endocarditis complicating repeated attempts at CoreValve implantation. *J Invasive Cardiol.* (2011) 23:E291–2.

10. Habib G, Lancellotti P, Antunes M, Bongiorni M, Casalta J, Del Zotti F, et al. 2015 ESC guidelines for the management of infective endocarditis: the task force for the management of infective endocarditis of the European society of cardiology (ESC). endorsed by: European association for cardio-thoracic surgery (EACTS), the European association of nuclear medicine (EANM). *Eur Heart J.* (2015) 36:3075–128. doi: 10.1093/eurheartj/ehv319

11. Nishimura R, Otto C, Bonow R, Carabello B, Erwin J III, Fleisher L, et al. 2017 AHA/ACC focused update of the 2014 AHA/ACC Guideline for the management of patients with valvular heart disease: a report of the American college of cardiology/American heart association task force on clinical practice guidelines. *J Am Coll Cardiol.* (2012) 70:252–89. doi: 10.1016/j.jacc.2017.03.011

12. Tong A, Roudaut R, Ozkan M, Sagie A, Shahid M, Pontes Júnior S. Transesophageal echocardiography improves risk assessment of thrombolysis of prosthetic valve thrombosis: results of the international PRO-TEE registry. *J Am Coll Cardiol.* (2004) 43:77–84. doi: 10.1016/j.jacc.2003.08.028

13. Baumgartner H, Falk V, Bax J, De Bonis M, Hamm C, Holm P. 2017 ESC/EACTS guidelines for the management of valvular heart disease. *Rev Esp Cardiol.* (2018) 71:110. doi: 10.1016/j.rec.2017.12.013

14. Baddour L, Wilson W, Bayer A, Fowler V Jr, Tleyjeh I, Rybak M. Infective endocarditis in adults: diagnosis, antimicrobial therapy, and management of complications: a scientific statement for healthcare professionals from the American heart association. *Circulation.* (2015) 132:1435–86.

15. Attaran S, Chukwuemeka A, Punjabi P, Anderson J. Do all patients with prosthetic valve endocarditis need surgery? *Interact Cardiovasc Thorac Surg.* (2012) 15:1057–61. doi: 10.1093/icvts/ivs372

frontiers | Frontiers in Cardiovascular Medicine

TYPE Case Report
PUBLISHED 11 January 2023
DOI 10.3389/fcvm.2022.1091201



OPEN ACCESS

EDITED BY
Sanjeev Bhattacharyya,
Barts Heart Centre, United Kingdom

REVIEWED BY
Apostolos Vrettos,
Barts Health NHS Trust,
United Kingdom
Aliki Tsagkridi,
Barts Heart Centre, United Kingdom

*CORRESPONDENCE
Jianghua Li
✉ 75090935@qq.com

SPECIALTY SECTION
This article was submitted to Cardiovascular Imaging, a section of the journal Frontiers in Cardiovascular Medicine

RECEIVED 06 November 2022
ACCEPTED 21 December 2022
PUBLISHED 11 January 2023

CITATION
Deng Z, Wang X, Liu Q, Li J and Liu H (2023) Case report: Echocardiographic diagnosis of double orifice mitral valve in an asymptomatic woman. *Front. Cardiovasc. Med.* 9:1091201. doi: 10.3389/fcvm.2022.1091201



# Case report: Echocardiographic diagnosis of double orifice mitral valve in an asymptomatic woman

Zixian Deng[1,2], Xiaoyu Wang[1,2], Qiyun Liu[1,2], Jianghua Li[1,2]* and Huadong Liu[1,2]

[1]Department of Cardiology, Shenzhen People's Hospital, Second Clinical Medical College of Jinan University, First Affiliated Hospital of Southern University of Science and Technology, Shenzhen, Guangdong, China, [2]Department of Cardiology, Shenzhen Cardiovascular Minimally Invasive Medical Engineering Technology Research and Development Center, Shenzhen People's Hospital, The Second Clinical Medical College, The First Affiliated Hospital, Southern University of Science and Technology, Jinan University, Shenzhen, China

Double orifice mitral valve (DOMV) is a rare congenital anomaly that is often associated with cardiac malformation. Valve dysfunction usually presents in childhood; therefore, most cases are diagnosed with DOMV in childhood. Its prevalence and prognostic relevance in adulthood are unknown. Here, we report a case of a 38-year-old woman who presented to the outpatient clinic with an abnormal electrocardiogram and was found to have an isolated double orifice mitral valve malformation on transthoracic echocardiography. Echocardiography is the diagnostic tool of choice for patients with double orifice mitral valves. We should familiarize ourselves with the echocardiographic features of DOMV in order to improve the detection.

KEYWORDS

**congenital heart disease, case report, double orifice mitral valve, diagnosis, echocardiography**

## Introduction

Double orifice mitral valve (DOMV) is an extremely rare congenital anomaly that may be due to inadequate fusion of the endocardial cushions during embryonic life, resulting in two separate orifices of the mitral valve into the left ventricle, and can be classified into 3 types: complete bridging, incomplete bridging, and hole type (1). Other structural cardiac abnormalities are usually associated with them and isolated DOMV is rarely present (2). Here, we report an incomplete bridging type of DOMV in an asymptomatic woman.

## Case presentation

A 38-year-old asymptomatic woman with a previous history of subclinical hypothyroidism and long-term use of sodium thyroxine presented to the outpatient clinic with "abnormal ECG for 1 year." No heart murmur was detected. The short

axis view showed two oval-shaped orifices, one large and one small, aligned left and right, with the small hole tendon not visible (Figure 1A). Color Doppler examination showed two bundles of blood flow across the orifice. There was no mitral stenosis (MS) and trivial mitral regurgitation (MR) (peak mitral E wave velocity = 97.2 cm/s, peak gradient = 4 mm Hg, peak mitral A wave velocity = 47.4 cm/s, peak gradient = 1 mm Hg). The remaining valvular structures were not significantly abnormal, and the tricuspid valve had mild regurgitation. The left ventricular ejection fraction and diastolic function were normal. In addition, no other cardiac structural abnormalities were detected. The transesophageal echocardiogram (Figures 1B, C) was consistent with the transthoracic echocardiogram, and the diagnosis of congenital heart disease was confirmed as DOMV. Additional movies are available in the Supplementary material.

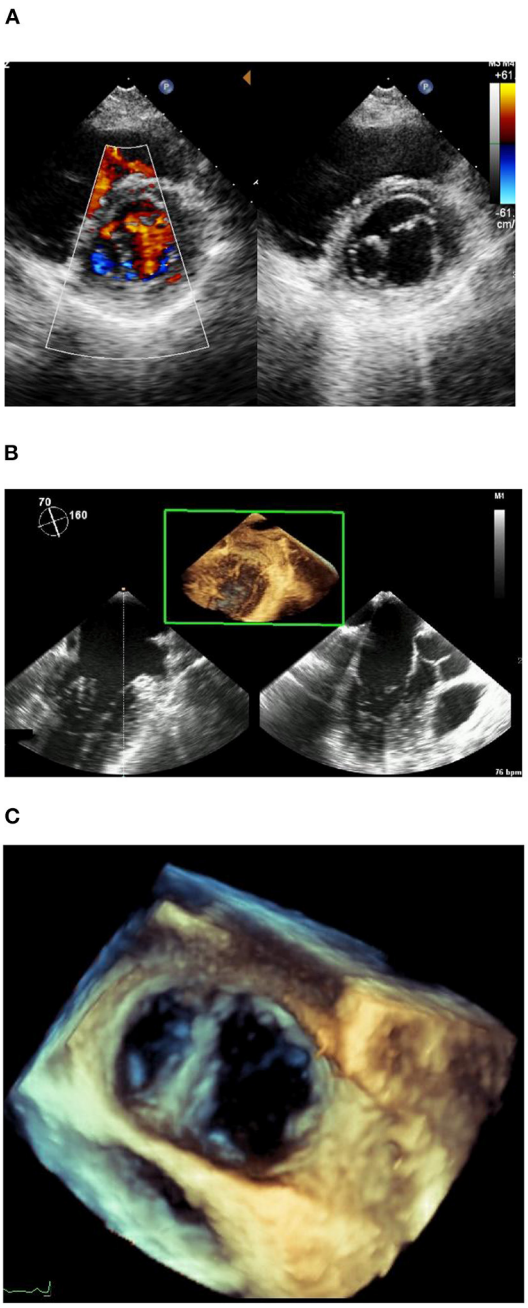


FIGURE 1
**(A)** Short axis of echocardiogram image. **(B)** Transesophageal echocardiogram. **(C)** Transesophageal echocardiogram.

## Discussion

Double orifice mitral valve is an extremely rare congenital anomaly, first reported by Greenfield (3). The etiology of this disease remains unclear. Some scholars believe that DOMV may result from the inadequate fusion of the endocardial cushions during embryonic development (4). Others suggest that it may be related to interstitial abnormalities and atrioventricular sulcus folding abnormalities during endocardial cushion formation in valve tissue or abnormal development of the ventricular myocardium (5). But a small portion is acquired, and when mitral annular calcifications affect the second scallop of the anterior and the posterior leaflet, the mitral valve orifice may split into two, leading to DOMV (6). In addition, iatrogenic interventions are also potential causes of DOMV. As described by Alfieri, DOMV can occur after "edge-to-edge" mitral valve repair, a technique that specifically refers to the suturing together with the middle scallops of the mitral leaflets, which then form a double-barrel opening (7, 8). Due to its rarity, epidemiological data are lacking. Previous retrospective studies and autopsy reports have found the prevalence of DOMV to be between 0.01 and 0.1% (1, 9, 10).

The anatomic feature of DOMV is an accessory bridge of fibrous tissues extending from the center of the posterior mitral valve to the anterior valve dividing the mitral valve into two orifices. DOMV is classified into three types: complete bridge, incomplete bridge, and hole types, with complete bridges accounting for 15% of DOMV and the remaining two accounting for 85% (10, 11). This case was diagnosed as an incomplete bridge type. Moreover, DOMV rarely occurs as an isolated anomaly but is commonly combined with other malformations including atrioventricular septal defect, aortic stenosis, patent arterial duct, and tetralogy of Fallot (12, 13). Therefore, DOMV is usually detected in early childhood. Nevertheless, its prevalence and prognostic relevance in adulthood are unknown. Approximately half of DOMV patients are functionally normal and usually have no obvious signs and symptoms, thus predisposing them to underdiagnosis. In this study, DOMV was also found incidentally.

The ultrasound presentation of DOMV in adults is characteristic. Specifically, two left-right aligned orifices are visible at the level of the short axis of the parasternal mitral valve, showing the typical "spectacle sign." In the left apical two-chamber view, two orifices exist in the mitral valve,

exhibiting the typical "seagull sign" (14). Doppler examination reveals that each valve orifice obtains a corresponding diastolic flow. The present case demonstrates the superiority and importance of echocardiography for the accurate diagnosis of DOMV. In addition, echocardiography can also detect other combined malformations or secondary changes, which can provide a basis for clinical decision-making.

Treatment and prognosis of DOMV depend on the type and severity of mitral valve insufficiency. When it is an isolated DOMV, no management is required with a favorable prognosis (15). Surgical valve repair or replacement (16) should be performed when significant stenosis or insufficiency is present, according to the cause of the lesion and intraoperative exploration findings (17). If associated with other intracardiac or extracardiac malformations, the corresponding lesion should be treated and the DOMV should be managed appropriately. In our case, no significant changes in the structure and function of the heart were observed during the 2-year follow-up, making it unnecessary for this patient to receive treatment. Additionally, we do not intend to take a longer follow-up.

## Conclusions

Double orifice mitral valve does not necessarily have clinical symptoms and signs to draw clinical attention. Therefore, this case report aims to raise awareness of this rare entity and provide all patients with the opportunity for correct and timely diagnosis and appropriate management.

## Data availability statement

The original contributions presented in the study are included in the article/Supplementary material, further inquiries can be directed to the corresponding author.

## Ethics statement

Written informed consent was obtained from the patient for publication of this case report and any accompanying images.

## Author contributions

ZD and XW collected all the clinical data. QL and JL independently reviewed the data. ZD prepared the manuscript. JL and HL proposed the idea for this work. All authors contributed to the article and approved the submitted version.

## Funding

This study was supported by the Medical Scientific Research Foundation of Guangdong Province of China (no. A2018530), the Shenzhen People's Hospital Research Cultivation Project (nos. SYJCYJ202014 and SYLCYJ202119), the Sanming Project of Medicine in Shenzhen (no. SZSM201412012), the Shenzhen Key Medical Discipline Construction Fund (no. szxk003), and the Science and Technology Planning Project of Shenzhen Municipality (no. JCYJ20190806153207263).

## Conflict of interest

The authors declare that the research was conducted in the absence of any commercial or financial relationships that could be construed as a potential conflict of interest.

## Publisher's note

All claims expressed in this article are solely those of the authors and do not necessarily represent those of their affiliated organizations, or those of the publisher, the editors and the reviewers. Any product that may be evaluated in this article, or claim that may be made by its manufacturer, is not guaranteed or endorsed by the publisher.

## Supplementary material

The Supplementary Material for this article can be found online at: https://www.frontiersin.org/articles/10.3389/fcvm.2022.1091201/full#supplementary-material

## References

1. Baño-Rodrigo A, Van Praagh S, Trowitzsch E, Van Praagh R. Double-orifice mitral valve: a study of 27 postmortem cases with developmental, diagnostic and surgical considerations. *Am J Cardiol.* (1988) 61:152–60. doi: 10.1016/0002-9149(88)91322-7

2. Graham FJ, Jenkins SMM. Isolated double-orifice mitral valve in octogenarian. *Eur Heart J Cardiovasc Imaging.* (2018) 19:957. doi: 10.1093/ehjci/jey066

3. Trowitzsch E, Bano-Rodrigo A, Burger BM, Colan SD, Sanders SP. Two-dimensional echocardiographic findings in double orifice mitral valve. *J Am Coll Cardiol.* (1985) 6:383–7. doi: 10.1016/S0735-1097(85)80176-5

4. Krisai P, Wein B, Kaufmann BA. Isolated double-orifice mitral valve: a case report. *BMC Cardiovasc Disord.* (2015) 15:172. doi: 10.1186/s12872-015-0168-0

5. Liu S, Ren W, Ma C, Yang J. Congenital double-orifice mitral valve in asymptomatic patients. *Int Heart J.* (2018) 59:213–5. doi: 10.1536/ihj.17-033

6. Lange M, Bültel H, Wichter T. Calcified mitral stenosis imitates a MitraClip(®) and forms a double orifice. *Eur Heart J.* (2018) 2:yty084. doi: 10.1093/ehjcr/yty084

7. Bhamra-Ariza P, Muller DW. The MitraClip experience and future percutaneous mitral valve therapies. *Heart Lung Circ.* (2014) 23:1009–19. doi: 10.1016/j.hlc.2014.05.021

8. Feldman T, Kar S, Rinaldi M, Fail P, Hermiller J, Smalling R, et al. Percutaneous mitral repair with the MitraClip system: safety and midterm durability in the initial EVEREST (Endovascular Valve Edge-to-Edge REpair Study) cohort. *J Am Coll Cardiol.* (2009) 54:686–94. doi: 10.1016/j.jacc.2009.03.077

9. Romano MMD, Menardi AC, Almeida-Filho OC, Vicente WVA, Evora PRB. Double-orifice mitral valve: an educational presentation. *Braz J Cardiovasc Surg.* (2019) 34:377–9. doi: 10.21470/1678-9741-2018-0615

10. Wójcik A, Klisiewicz A, Szymański P, Rózański J, Hoffman P. Double-orifice mitral valve—echocardiographic findings. *Kardiol Pol.* (2011) 69:139–43.

11. Pillai VV, Karunakaran J. Repair of double orifice left AV valve (DOLAVV) with endocardial cushion defect in adult. *Braz J Cardiovasc Surg.* (2017) 32:338–40. doi: 10.21470/1678-9741-2016-0034

12. Kowalik E, Klisiewicz A, Skrzypczyńska-Banasik U, Hoffman P. Always look at both sides of the heart: a double-orifice mitral valve discovered in a young adult with repaired tetralogy of Fallot. *Cardiol J.* (2019) 26:204–5. doi: 10.5603/CJ.2019.0045

13. Mouine N, Amri R, Cherti M. Unusual findings in secondary hypertension: double orifice mitral associated to aortic coarctation, bicuspid aortic valve, and ventricular septal defect. *Int Arch Med.* (2014) 7:14. doi: 10.1186/1755-7682-7-14

14. Ciampani N, Vecchiola D, Silenzi C, Costantini C, Mazzanti M, Iacobone G, et al. The tensor apparatus in double-orifice mitral valve: interpretation of echocardiographic findings. *J Am Soc Echocardiogr.* (1997) 10:869–73. doi: 10.1016/S0894-7317(97)70048-8

15. Zalzstein E, Hamilton R, Zucker N, Levitas A, Gross GJ. Presentation, natural history, and outcome in children and adolescents with double orifice mitral valve. *Am J Cardiol.* (2004) 93:1067–9. doi: 10.1016/j.amjcard.2004.01.015

16. Zhu D, Chen A, Zhao Q. Surgical repair for isolated congenital double-orifice mitral valve. *Eur J Cardiothorac Surg.* (2011) 39:268–70. doi: 10.1016/j.ejcts.2010.05.030

17. Tani T, Kim K, Fujii Y, Komori S, Okada Y, Kita T, et al. Mitral valve repair for double-orifice mitral valve with flail leaflet: the usefulness of real-time three-dimensional transesophageal echocardiography. *Ann Thorac Surg.* (2012) 93:e97–8. doi: 10.1016/j.athoracsur.2011.11.047

frontiers | Frontiers in Cardiovascular Medicine

TYPE Case Report
PUBLISHED 03 March 2023
DOI 10.3389/fcvm.2023.1036476



OPEN ACCESS

EDITED BY
Grigorios Korosoglou,
GRN Klinik Weinheim, Germany

REVIEWED BY
Saket Singh,
Yale Medicine, United States
Yi Chang,
Chinese Academy of Medical Sciences and Peking Union Medical College, China

*CORRESPONDENCE
Hongmei Xia
✉ xiahm985206@126.com
Zheng Liu
✉ liuzheng@tmmu.edu.cn

†These authors share first authorship

SPECIALTY SECTION
This article was submitted to Cardiovascular Imaging, a section of the journal Frontiers in Cardiovascular Medicine

RECEIVED 04 September 2022
ACCEPTED 06 February 2023
PUBLISHED 03 March 2023

CITATION
Yang G, Lai X, Liang C, Fan W, Fu W, Liu Z and Xia H (2023) Infective endocarditis with anomalous origin of coronary arteries and an abnormal aortic root bulge: A case report. *Front. Cardiovasc. Med.* 10:1036476. doi: 10.3389/fcvm.2023.1036476



# Infective endocarditis with anomalous origin of coronary arteries and an abnormal aortic root bulge: A case report

Guoliang Yang[1†], Xiaoyue Lai[1†], Chunshui Liang[2], Weijie Fan[3], Wanlei Fu[4], Zheng Liu[1*] and Hongmei Xia[1*]

[1]Department of Ultrasound, Xinqiao Hospital, Army Medical University, Chongqing, China, [2]Department of Cardiac Surgery, Xinqiao Hospital, Army Medical University, Chongqing, China, [3]Department of Radiology, Xinqiao Hospital, Army Medical University, Chongqing, China, [4]Department of Pathology, Xinqiao Hospital, Army Medical University, Chongqing, China

**Background:** The aortic bulge sign possibly indicates an arterial aneurysm, pseudoaneurysm, aortic dissection, or aortic diverticulum. The aortic diverticulum is a congenital abnormality of the aorta, mainly known as an aneurysmal remnant of the dorsal fourth aortic arch or ductus arteriosus. However, the diverticulum of another part of the aorta has rarely been reported.

**Case summary:** We report a case of a 24-year-old male with a history of oral ulcer presented with recurrent hyperpyrexia and chest pain. Echocardiography and computed tomography showed the anomalous origin of the coronary arteries, aortic valve vegetations, and a bulge at the aortic root. The patient then received a Bentall procedure. The aorta and aortic valves were replaced by a valved conduit. The bulge with a normal arterial wall at the aortic root was considered to be a diverticulum. The infective endocarditis was verified as a secondary oral-derived streptococcal infection. The patient was discharged 15 days after surgery. Post-operative echocardiography had no positive findings.

**Conclusion:** Our case report highlights the role of multimodal cardiovascular imaging for the diagnostic workup of rare disorders, such as the presence of a diverticulum in the aortic root in a patient with endocarditis and anomalous origin of the right coronary artery.

KEYWORDS

**aortic diverticulum, infective endocarditis, echocardiography, computed tomography, anomalous origin of the coronary artery**

## 1. Introduction

The aortic bulge sign found on imaging possibly indicates an arterial aneurysm, pseudoaneurysm, aortic dissection, or aortic diverticulum. The aortic diverticulum is a congenital abnormality of the aorta, mainly known as an aneurysmal remnant of the dorsal fourth aortic arch or ductus arteriosus (1, 2). However, diverticulum found in other parts of the aorta has rarely been reported except for abnormal vascular pathologies in Marfan's syndrome (3). Here we present an unusual aortic root bulge with infective endocarditis of the native aortic valve associated with concomitant anomalous origin of the coronary artery.

## 2. Case presentation

A 24-year-old male patient with recurrent fever (up to 40°C), palpitation, shortness of breath, and precordial pain after activity over the past 3 weeks was admitted to our hospital. The patient had a history of working in high-altitude areas and recurrent oral ulcers before the onset. The vital signs on admission were as follows: a body temperature of 36.4°C, heart rate of 110 beats per minute, and regular, blood pressure of 118/68 mmHg. Electrocardiogram presented sinus rhythm. Auscultation was notable for a diastolic murmur on the 3rd intercostal area of the left sternal border, and a pistol shot sound in the groin. The patient had no perineal ulcer. The acupuncture test was negative.

Echocardiography showed: left ventricle enlargement; a sonolucent area ~11.5 × 25 mm was located next to the right coronary sinus, which communicated with the dilated aortic root; a flail-like moving flocculent vegetation ~17 mm long was located in the junction area of the right and left aortic valve on the aortic side; the right and left aortic valve leaflets were both impaired, resulting in severe aortic regurgitation (Figures 1A, B); and the right coronary artery showed intramural course and was compressed by the surrounding abscess. It also showed an abnormal opening at the junction of the left and right aortic valves, with only a 2.7 mm wide ostium compared to a 4.3 mm one in the left coronary artery (Figure 1C); the ejection fraction was 69%; mild pulmonary hypertension was presented; and no obvious abnormality was observed in the aortic arch and its branches.

Computed tomographic angiography showed that the right coronary sinus was of an irregular shape, and was pushed to the left by a 2.2 × 1.4 × 2.1 cm cystic structure in the anterior part of the aortic root. Enhancement was observed in the cystic structure, which communicated with the aorta (Figure 2A); the left coronary artery arose from above the left coronary sinus; the right coronary artery arose from above the junction of the left and right coronary sinus, and the proximal segment was surrounded by the abscess (5.1 × 2.0 cm), resulting in mild-to-moderate stenosis (Figures 2B, C). Coronary angiography was not performed. Cranial MRI indicated no intracranial infection.

Initial laboratory results were notable for leukocyte of 14.91 × $10^9$/L, albumin 28.4 g/L, procalcitonin 0.38 ng/ml, and C-reactive protein was 110.2 mg/L. Hemoglobin was 105 g/L. Cardiac troponin I (cTnI) was 0.23 pg/ml. N-terminal pro-b-type natriuretic peptide (BNP) was 609.51 pg/ml. The pre-operative blood culture result was negative. The clinical evidence suggested infective endocarditis, aortic insufficiency, aortic root abscess, and coronary heart disease.

The patient then received a Bentall procedure to replace the damaged aorta and valves with a 23# valved conduit. The intraoperative findings were listed as follows: the left atrium was enlarged; there was abundant vegetation in the damaged aortic valves; and a bulge was found next to the right coronary sinus, with a complete three-layer structure (intima, media, and adventitia). The bulge communicated with the aortic root and was also full of vegetation, which compressed the right coronary sinus and blocked the right coronary ostia (Figure 3A). The left and right coronary arteries both started at the left coronary sinus and were ~4 mm apart. The right coronary artery showed ~3 mm intramural course, surrounded by purulent exudate and tissue edema. Surgical debridement was performed to clear all vegetation and remove the damaged aortic valve leaflets and part of the valvular annulus (Figure 3B). The portion of the aortic valve annulus under the right coronary sinus was reconstructed with a bovine pericardial patch. The bulge was preserved outside the conduit to have better support for the unstable annulus. A 23#SJM valved conduit was inserted, with perforation in the corresponding position of the ostia of the coronary arteries. Stenosis in the right coronary disappeared soon after the compression was removed. The coronary arteries were then anastomosed to the conduit at the assumed positions with buttons. After the surgery, the patient was sent to the intensive care unit with tracheal intubation and received intravenous ceftriaxone 2 g/day for at least 4 weeks as an anti-infective therapy.

The intraoperative and post-operative blood cultures were both negative. Therefore, we performed a post-operative high-throughput sequencing examination, which showed oral streptococcal infection. The patient then received cardiotonic therapy, anti-inflammatory treatment, and other necessary symptomatic support. Post-operative echocardiography showed that the artificial aortic conduit and valves were in normal position and functioned well (Figure 4A). The closure of the bulge was successful, with no blood flow signal inside (Figure 4B). No stenosis or obstruction was observed in the opening of the coronary arteries. Post-operative blood routine examination showed that the leukocyte returned to normal at 9.21 × $10^9$/L. The patient described that the chest pain disappeared and was discharged 15 days after the surgery. Four weeks after surgery, the follow-up echocardiography showed no positive finding.

## 3. Discussion

This is a case of an abnormal aortic root bulge, with infective endocarditis, anomalous origin of coronary arteries, and surrounding abscess. The patient was initially characterized by a recurrent oral ulcer, which was confirmed to be an oral streptococcal infection by high-throughput sequencing results. The coronary arteries originated from above the coronary sinus, together with the significantly-sized bulge compressing the right coronary sinus, leading to the local hemodynamic change. This change facilitated streptococcal colonization and vegetation and finally resulted in the formation of an aortic root abscess. The patient showed manifestations of myocardial ischemia, including chest pain, enlarged left ventricle, and abnormal BNP level. We assumed the cause was stenosis of the right coronary artery, which was the dominant coronary artery of this patient. Stenosis in the right coronary artery may result from multiple reasons: (1) anomalous origin, (2) blocked ostium under vegetations, (3) intramural course, and (4) proximal compression by the peripheral abscess.

The possible diagnosis of an aneurysm, pseudoaneurysm, and Valsalva sinus aneurysm were all considered pre-operatively, based on the morphology and location of the aneurysm-like bulge. Surgical exploration revealed its communication with the aortic root, but the bulge was a different structure from the coronary sinuses. More intriguingly, the surgical findings showed complete

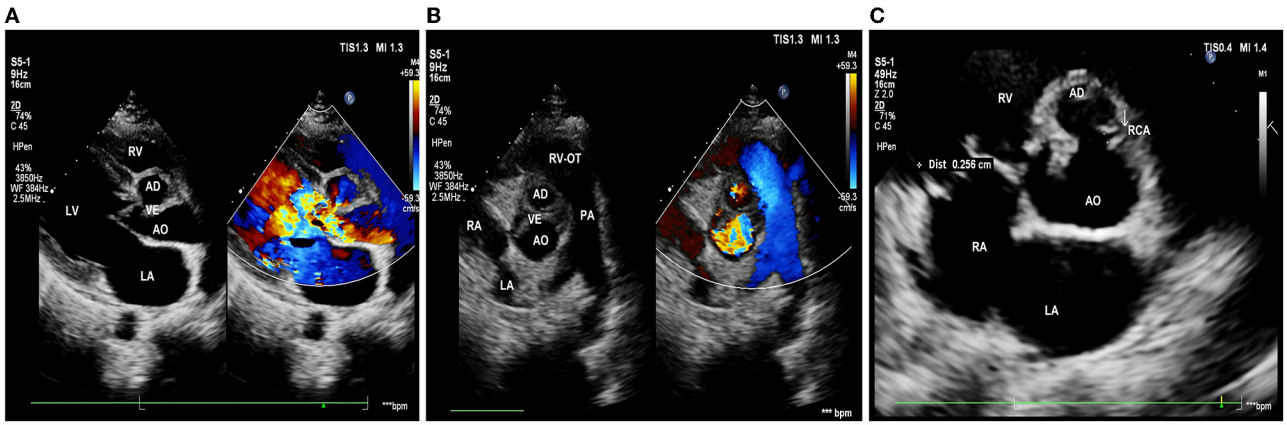


FIGURE 1
Pre-operative echocardiography. **(A)** Long-axis view of the left ventricle shows aortic valves thickening and flail motion, and color Doppler shows massive aortic regurgitation. **(B)** Short-axis view of the great arteries shows that the bulge in the aortic root communicates with the aorta, with vegetations in the aortic valve. **(C)** The right coronary artery (white arrow) is restrictive; LA, left atrium; LV, left ventricle; RV, right ventricle; AO, aorta; RVOT, right ventricular outflow tract; PA, pulmonary artery; RCA, right coronary artery; AD, aortic disease; and VE, valvular excrescence.

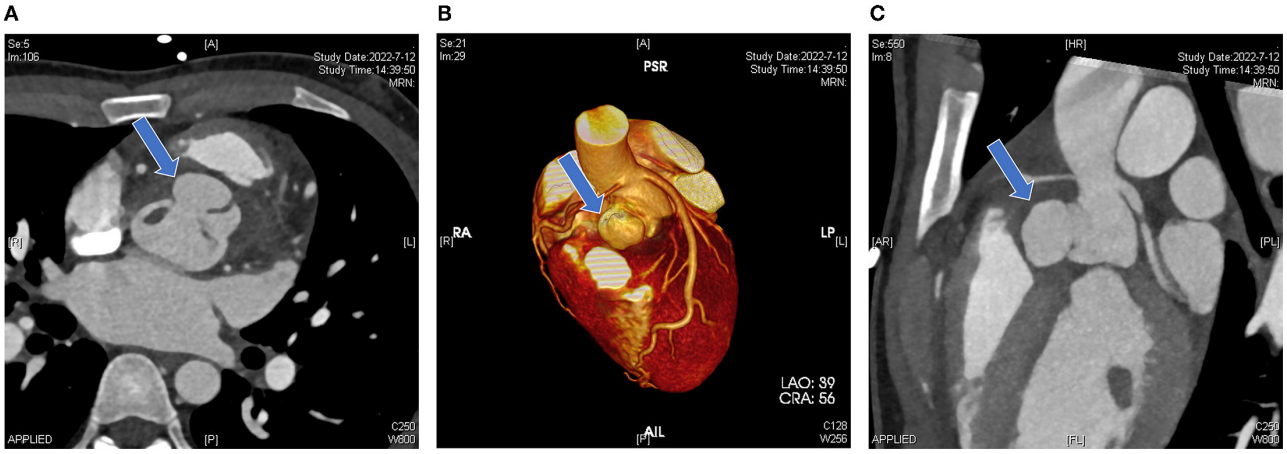


FIGURE 2
Pre-operative computed tomography. **(A)** Irregular morphology of the coronary sinuses with local anterior protrusion (blue arrow). **(B)** A three-dimensional reconstruction image shows that the left coronary artery arises from above the left coronary sinus and the right coronary artery arises from above the junction of the left and right coronary sinuses. The aortic root bulge is shown in the blue arrow. **(C)** Sagittal view showing the vertical position of the bulge (blue arrow).

intima, media, and adventitia layers. Therefore, we considered the bulge to be most likely a diverticulum with the available evidence, mainly the intraoperative findings about a complete, smooth, thick, and elastic arterial wall of this structure. However, it was unfortunate in this case that we failed to perform a pathological examination because the bulge had to be preserved for safety reasons. On the one hand, the structure was necessary to support the unstable aortic annulus. On the other hand, the bulge was so big that it fell under the level of the aortic annulus, so removing the bulge might have hurt the sinoatrial node nearby.

Another possible diagnosis, of Behcet's disease in the aorta, was also considered due to the initial presentations and a history of recurrent oral ulcers. The clinical characteristics of Behcet's disease include recurrent mucosae ulcers and skin lesions. The diagnosis was rejected based on the negative result of the skin acupuncture test, which would be positive if the acupunctured skin area showed continuously expanding lesions.

The enlightenment of this interesting case is to provide a possible and necessary diagnosis consideration of diverticulum, other than pseudoaneurysm or Valsalva sinus aneurysm when an aneurysm-like structure is found at the aortic root by radiography or echocardiography. The key point of differentiating a diverticulum from a pseudoaneurysm or a Valsalva sinus aneurysm is that a diverticulum has complete intima, media, and adventitia layers structures. While the wall of a pseudoaneurysm, usually presented as a continuous interruption of the artery wall, is mainly composed of fibrous tissue, and the wall of a Valsalva sinus aneurysm is weak and thin and associated with characterized coronary sinus dilation (4, 5). The ultrasonic features of a diverticulum are very similar to normal aortic walls, while the

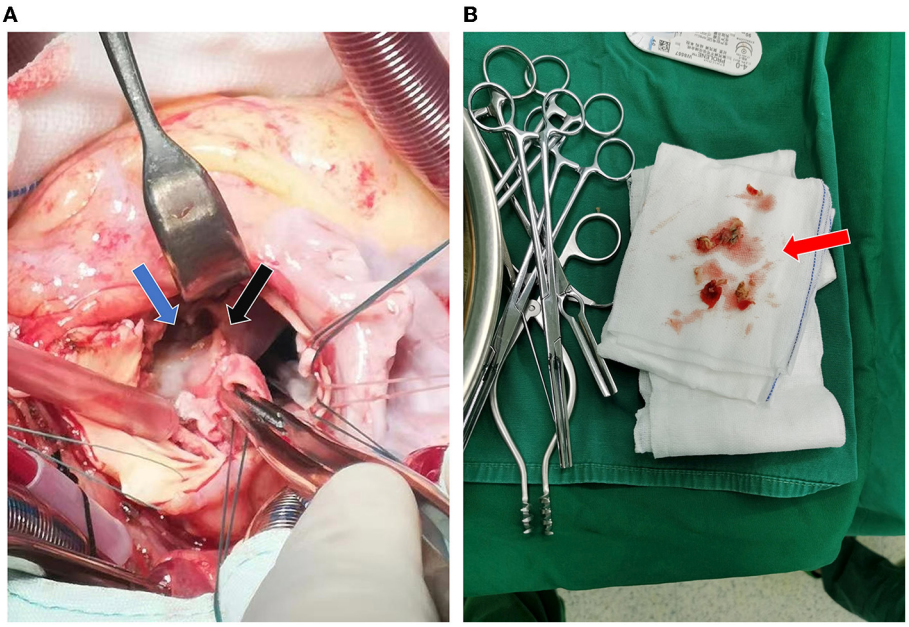


FIGURE 3
Intraoperative findings. **(A)** The aortic root bulge (blue arrow) filled with vegetation and damaged at the right coronary annulus (black arrow). **(B)** Intraoperative removal of the damaged aortic valve and part of the annulus (red arrow).

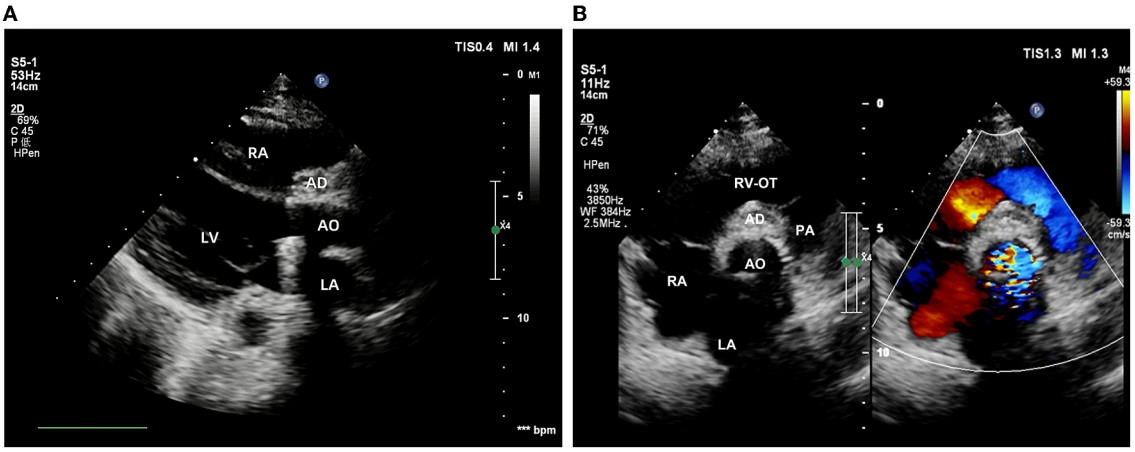


FIGURE 4
Post-operative echocardiography. **(A)** The position and function of the artificial valved conduit are normal. **(B)** The aortic root bulge is successfully closed without an internal blood flow signal.

other two diseases are different (4, 6). Therefore, distinguishing the ultrasonic features of the wall of a newfound aneurysm-like structure on echocardiography can be very important pre-operatively. However, post-operative histopathological examination is still the gold standard to confirm the diagnosis of an aortic bulge.

## 4. Conclusion

We report a case of infective endocarditis with an aortic root abscess, which was verified as a secondary oral-derived streptococcal infection in an abnormal aortic root bulge, and associated with anomalous origin of the coronary arteries and right coronary artery stenosis. The onset of the disease is rapid and life-threatening. Timely correct diagnosis and treatment are particularly important in similar cases. Due to its extremely abnormal appearance, it can be easily ignored or misdiagnosed on the first clinic visit. The enlightenment of this case is that when an aneurysm-like structure is found at the aortic root by radiography or echocardiography, the possibility of an aortic diverticulum should be considered.

## Data availability statement

The original contributions presented in the study are included in the article/Supplementary material, further inquiries can be directed to the corresponding authors.

## Ethics statement

The studies involving human participants were reviewed and approved by Xinqiao Hospital Ethics Committee. The patients/participants provided their written informed consent to participate in this study. Written informed consent was obtained for the publication of this case report.

## Author contributions

GY, CL, and HX were the main participants in the process of the case study. GY, CL, and WFu organized the data. XL and GY contributed to the manuscript. HX revised and approved the manuscript. ZL provided guidance and administrative and technical support. All authors read and approved the submitted version of the manuscript for publication.

## Conflict of interest

The authors declare that the research was conducted in the absence of any commercial or financial relationships that could be construed as a potential conflict of interest.

## Publisher's note



## Supplementary material

The Supplementary Material for this article can be found online at: https://www.frontiersin.org/articles/10.3389/fcvm.2023.1036476/full#supplementary-material

## References

1. Kommerell B. Verlagerung des osophagus durch eine abnorm verlaufende arteria subclavia dextra (arteria lusoria). *Fortschr Geb Rontgenstr*. (1936) 54:590–5.

2. Backer CL, Bharadwaj SN, Eltayeb OM, Forbess JM, Ropescu AR, Mongé MC. Double aortic arch with kommerell diverticulum. *Ann Thorac Surg*. (2019) 108:161–6. doi: 10.1016/j.athoracsur.2019.01.062

3. Thomas GP, Purkayastha S, Athanasiou T, Darzi A. General surgical manifestations of Marfan's syndrome. *Br J Hosp Med*. (2008) 69:270–4. doi: 10.12968/hmed.2008.69.5.29359

4. Restrepo CS, Lane MJ, Murillo H. Cardiac aneurysms, pseudoaneurysms, and diverticula. *Semin Roentgenol*. (2012) 47:262–76. doi: 10.1053/j.ro.2011.11.011

5. Cao S, Zhou Q, Hu B, Guo RQ. A bulging left ventricular wall in three-vessel coronary artery disease: true aneurysm, pseudoaneurysm, or diverticulum? *Coronary Artery Disease*. (2015) 26:184–5. doi: 10.1097/MCA.0000000000000183

6. Nakano H, Shimakura T, Katsumata T, Shimamura Y, Yabuki A, Matsuda N. A case report–successful surgical treatment of prosthetic aortic valve detachment with enlargement of sinuses of Valsalva caused by the recurrence of aortitis. *Nihon Kyobu Geka Gakkai Zasshi*. (1993) 41:523–7.

frontiers | Frontiers in Cardiovascular Medicine

TYPE Case Report
PUBLISHED 16 March 2023
DOI 10.3389/fcvm.2023.1138390



OPEN ACCESS

EDITED BY
Masaki Izumo,
St. Marianna University School of Medicine, Japan

REVIEWED BY
Yukio Sato,
St. Marianna University School of Medicine, Japan
Takeji Saitoh,
Hamamatsu University School of Medicine, Japan

*CORRESPONDENCE
Wei Feng
✉ wfeng@cmu.edu.cn

SPECIALTY SECTION
This article was submitted to Cardiovascular Imaging, a section of the journal Frontiers in Cardiovascular Medicine

RECEIVED 05 January 2023
ACCEPTED 22 February 2023
PUBLISHED 16 March 2023

CITATION
Miao Y, Zhang Y, Yue L, Guan S and Feng W (2023) Case report: Novel three-dimensional echocardiographic methods mapping aortic root pseudoaneurysm secondary to blood culture-negative endocarditis with bicuspid aortic valve involvement.
Front. Cardiovasc. Med. 10:1138390.
doi: 10.3389/fcvm.2023.1138390



# Case report: Novel three-dimensional echocardiographic methods mapping aortic root pseudoaneurysm secondary to blood culture-negative endocarditis with bicuspid aortic valve involvement

Yue Miao, Yanchao Zhang, Ling Yue, Shuang Guan and Wei Feng*

Department of Ultrasound, The Fourth Hospital of China Medical University, Shenyang, China

**Background:** Infective endocarditis (IE), though uncommon, is a potentially lethal disease. Blood culture-negative endocarditis (BCNIE) accounts for 2.5%–31% of all cases of IE and can lead to life-threatening complications, including aortic root pseudoaneurysm. It is associated with considerable diagnostic and therapeutic dilemmas. TrueVue and TrueVue Glass include the latest two technologies applied in advanced three-dimensional echocardiography, which allow for novel photorealistic images of cardiac structures, and provide abundant previously unavailable diagnostic information. Herein, based on a series of novel three-dimensional echocardiographic methods, we report a case of BCNIE with aortic valve involvement, leading to aortic valve perforation and prolapse, and developing into a giant aortic root pseudoaneurysm.

**Case summary:** In this study, we presented a case of a 64-year-old man exhibiting symptoms of intermittent fever, asthenia, and dyspnea following light exertion. Physical examination, laboratory tests, and electrocardiograms were suspected of IE, though the results of blood cultures were exactly negative. Three-dimensional transthoracic echocardiography, as well as a series of novel advanced techniques, was adopted to clearly visualize the lesions of the aortic valve and aortic root. However, despite active medical treatment modalities, the patient eventually suffered from a sudden, unexpected death 5 days later.

**Conclusion:** BCNIE with aortic valve involvement and development into a giant aortic root pseudoaneurysm is a rare and serious clinical event. In addition, TrueVue and TrueVue Glass offer unprecedented photographic stereoscopic images, enhancing the diagnostic performance of such structural heart diseases.

KEYWORDS

infective endocarditis, blood culture-negative endocarditis, pseudoaneurysm, three-dimensional echocardiography, TrueVue, TrueVue Glass

## Introduction

Infective endocarditis (IE), though uncommon, is a substantial cause of morbidity with an annual incidence of 3–10/100,000 cases, leading to a huge burden on society worldwide (1). Blood culture-negative endocarditis (BCNIE) accounts for 2.5%–31% of all cases of endocarditis, which is often accompanied by considerable diagnostic and therapeutic

dilemmas (2). Additionally, peri-annular spread of endocarditis contributes to tissue necrosis and peri-annular abscess, and in rare cases, precipitates pseudoaneurysm, which is a life-threatening complication (3). Currently, there is a lack of reports concerning patients with BCNIE with aortic valve involvement and development of a giant aortic root pseudoaneurysm; its early identification and accurate diagnosis remain formidable clinical challenges.

Advances in echocardiography techniques over the past few years have played an integral and vital role in the diagnosis of IE. Recent enhancements in three-dimensional echocardiography (3DE) have been further improved as a result of novel transducers, software, and trans-illumination techniques, which provide plentiful and previously unavailable diagnostic information. Meanwhile, the TrueVue technique allows for novel photorealistic images of cardiac structures with a freely movable virtual light source integrated into the data set, effectively enhancing the depth perception and augmenting the visualization of anatomical structures (4). In addition, the TrueVue technology can be modified into a transparent mode, named TrueVue Glass, focusing on the blood pool–tissue interface; however, the tissue itself remains transparent, which leads to highlighted borders of the chambers, valves, and vessels within the heart (5).

Herein, in the current study, we present a case suspected of BCNIE with aortic valve involvement, causing aortic valve perforation, and prolapse, and development into a giant aortic root pseudoaneurysm with novel 3DE imaging technologies.

## Case description

The included case concerned a 64-year-old man who presented with a medical history of diarrhea and intermittent low-grade fever for 2 months. The patient received repeated, inadequate antibiotic treatments at other medical institutions prior to admittance to our Department of Cardiovascular Disease. The patient arrived at our Department of Cardiovascular Disease for further diagnostics because of the worsened symptoms, including dyspnea following light exertion, asthenia, and more frequent bouts of fever in the last few days.

During physical examination, the patient was conscious and responded well, in addition to having an anemic appearance and a fever of 37.5°C. A Levine's grading scale II/VI systolic blowing murmur was auscultated in the apex area. Additionally, a diastolic murmur could be heard in the second auscultation area of aortic valve. Breath sounds in both lungs were rough. In addition, the patient's heart rate was 80 beats/min, blood pressure was 120/60 mmHg, and respiratory rate was 18 breaths/min. Laboratory tests illustrated an increase in the white blood cell count ($12.90 \times 10^3$/μL), B-type natriuretic peptide (1,367.38 pg/mL), C reactive protein (99 mg/L), and procalcitonin (0.155 mg/dL). The patient was mildly anemic with a hemoglobin level of 90 g/L. Moreover, the levels of antistreptolysin O and rheumatoid factors were both normal. Biochemical tests for antinuclear antibodies and functional tests for the thyroid were negative. Interestingly, three consecutive sets of blood cultures were all found to be negative. The thoraco-abdominal computed tomography (CT) revealed the presence of bilateral pleural effusion, bilateral pulmonary inflammation, cardiac enlargement, and splenic infarction. Furthermore, the electrocardiogram revealed the presence of sinus rhythm and non-specific T-wave changes.

As the diagnosis of IE was suspected, the patient was followed-up with an ultrasonic examination. Two-dimensional transthoracic echocardiography (2D-TTE) was then performed on an EPIQ CVx cardiac ultrasound system (Epiq CVX, Philips Medical Systems, Andover, MA, United States) with a S9-2 (2–9 MHz) probe. The results illustrated a large aneurysm with the sac-like structure in the left frontal aortic root and communicated with it (**Figure 1A**). However, the number of aortic cusps could not be confirmed in the short-axis view, as it was highly calcified and scattered with vegetations, leading to mild stenosis (peak systolic velocity: 2.9 m/s) (**Figure 1B**). In addition, we identified a local prolapse and perforation of the aortic valve with a moderate regurgitation by multibeam (**Figures 1C–F**). Meanwhile, there was little pericardial effusion. In addition, left ventricular end-diastolic diameter (64 mm) and left ventricular end-systolic diameter (41 mm) revealed dilatation of the left ventricle. The left ventricular ejection fraction was calculated to be 48%. Moreover, tricuspid regurgitation was mild with a pressure gradient of 43 mmHg across the tricuspid valve. There were no other valvular pathologies or other anomalies.

The three-dimensional transthoracic echocardiography (3D-TTE) was performed using an X5-1 (1–5 MHz) probe because the 2D-TTE cannot provide sufficient information. Based on the traditional 3DE imaging technology (**Figure 2A**), we launched the new TrueVue imaging mode. The virtual light source was introduced and placed inside the aneurysm, which transmitted light from the inside out, improving the border definition (**Figure 2B**). Next, we initiated the Glass mode to obtain a transparent rendering effect for further evaluation (**Figures 2C–F**). In this mode, we can obtain a 360° display of aneurysmal morphology and deformation in the cardiac cycle with a click, as well as its neck. In addition, we can also cut off the aneurysm to observe its contour. As a whole, the dimensions of the aneurysm and neck were measured to be 3.62 cm × 2.37 cm × 2.60 cm and 0.22 $cm^2$ in size, respectively, without obvious deformation or evidence of rupture. In addition, when the light source was strategically placed behind the aortic valve, the TrueVue imaging mode vividly revealed a bicuspid aortic valve with two leaflets in the left anterior and the right posterior directions, and a straight-line aortic valve closure shape (**Figure 3A**). The left anterior leaflet prolapsed with a perforation of 0.24 $cm^2$ (**Figures 3B,C**).

In summary, the diagnosis of aortic valve endocarditis was suspected on the basis of characteristic echocardiographic evidence and overall clinical presentation, leading to aortic valve perforation, and prolapse, and aortic root pseudoaneurysm. Antibiotic therapy was initiated immediately with the combined use of vancomycin and gentamycin. Unfortunately, the patient's family refused to provide consent documentation for additional surgery. Despite the active medical treatment modalities, the patient eventually suffered from a sudden, unexpected death

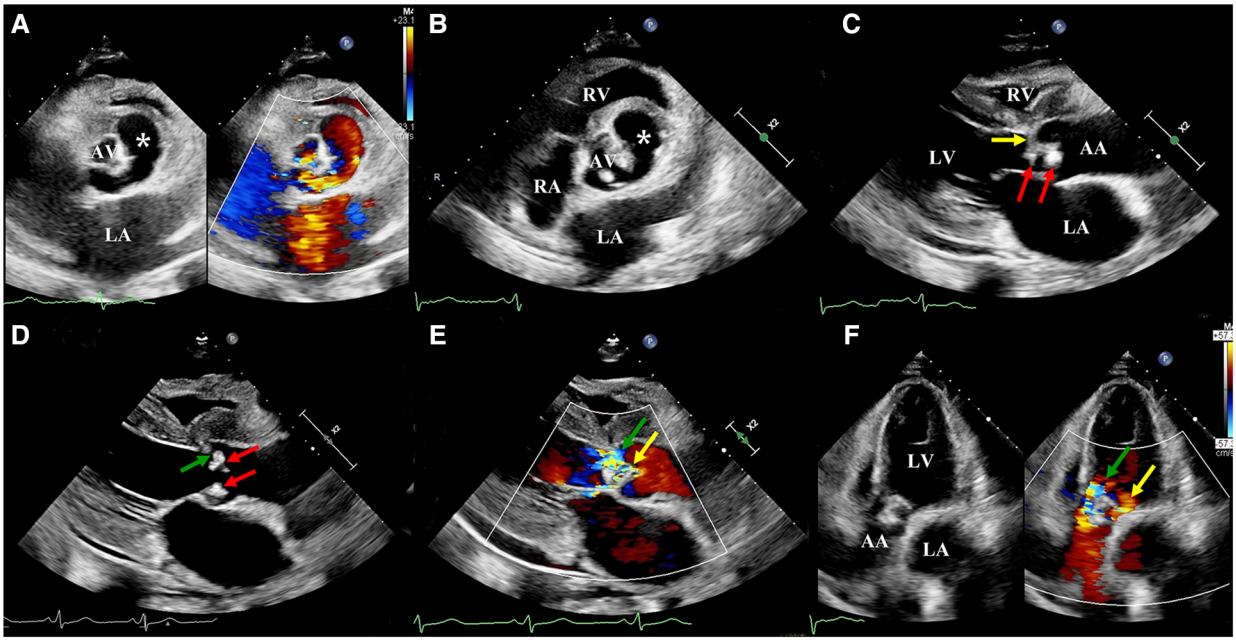


FIGURE 1
Two-dimensional transthoracic echocardiography: (**A**) A large sac-like aneurysm (white asterisk) located on the left front of the aortic root and communicating with it. (**B**) The number of aortic cusps could not be confirmed, as they were highly calcified and scattered with vegetation. (**C**) Aortic valve scattered with vegetations (red arrow) and local leaflets prolapsed (yellow arrow). (**D**) Aortic valve scattered with vegetation (red arrow) and local leaflet perforated (green arrow). (**E**) Parasternal long-axis view, color Doppler revealed two main aortic regurgitant jets, indicative of perforation (green arrow) and prolapsus (yellow arrow). (**F**) Apical five-chamber view, color Doppler revealed two main aortic regurgitant jets, indicative of perforation (green arrow) and prolapsus (yellow arrow). LA, left atrium; LV, left ventricle; RV, right ventricle; AA ascending aorta.

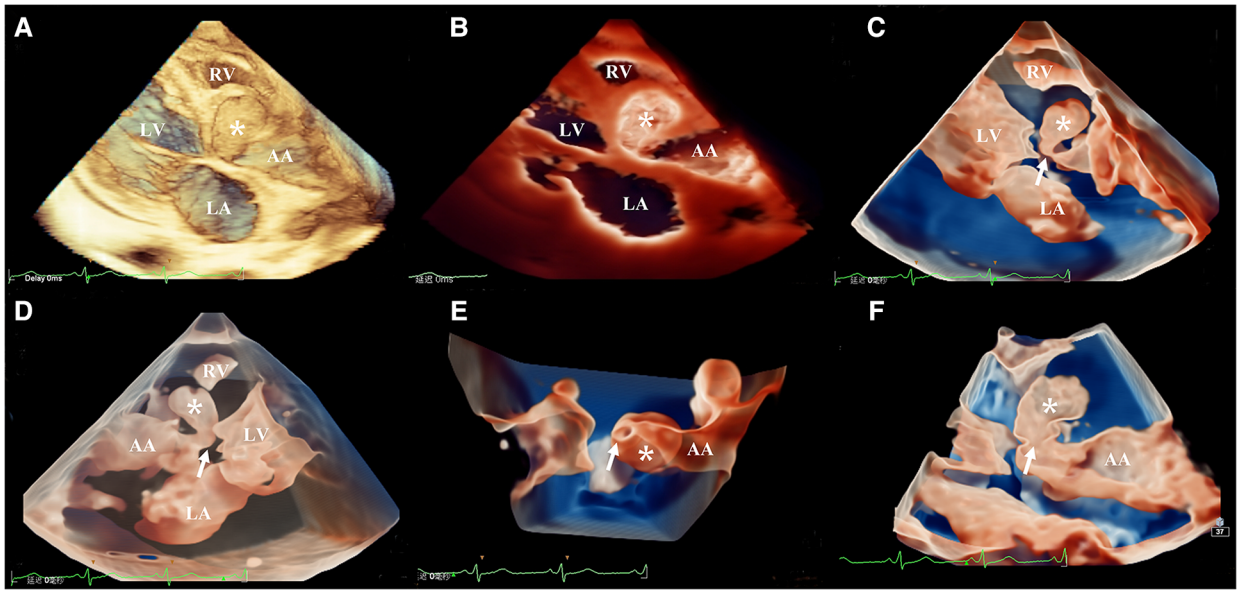


FIGURE 2
Head-to-head comparisons among traditional three-dimensional transthoracic echocardiography (**A**), TrueVue (**B**), and TrueVue Glass (**C–F**) in the evaluation of the aortic root pseudoaneurysm (white asterisk, its neck: white arrow). Different views of pseudoaneurysm in the TrueVue Glass mode: en face (**C**), dorsal (**D**), bottom (**E**), and internal (**F**) perspective. TrueVue Glass increased the degree of tissue transparency, providing a translucent view, and allowing one to visualize the full view of pseudoaneurysm, as well as its neck. LA, left atrium; LV, left ventricle; RV, right ventricle; AA ascending aorta.

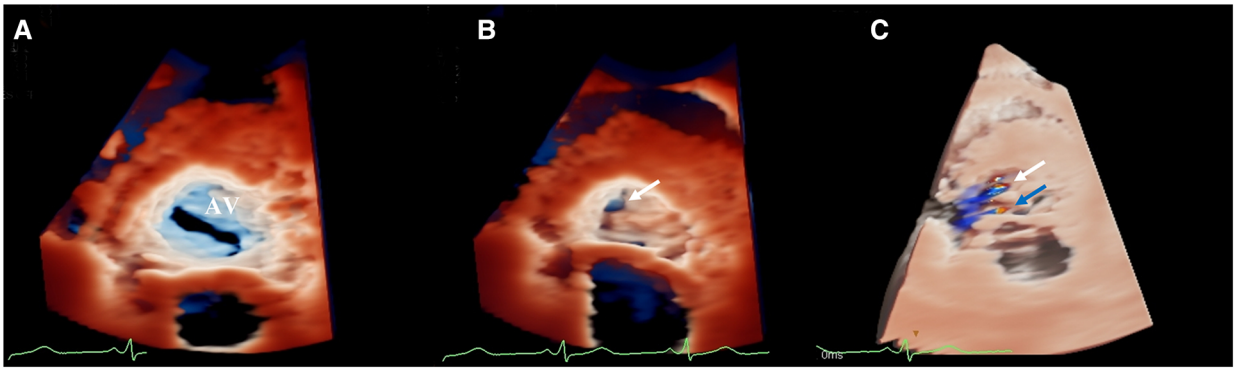


FIGURE 3
(A) TrueVue vividly revealed a bicuspid aortic valve. (B) TrueVue clearly showed an echolucent area at the ten o'clock position of the left anterior leaflet, suggesting an area of perforation of 0.24 $cm^2$ (white arrow). (C) TrueVue merged with three-dimensional color Doppler clearly demonstrated the origin of two different aortic regurgitant jets. One originated from the perforation (white arrow), and the other originated from the prolapsus (blue arrow). AV, aortic valve.

5 days later. Given the lack of family consent, we did not perform an autopsy.

## Discussion

In accordance with the modified Duke criteria, the case reported in the current study fulfilled one major criterion (echocardiography findings) and two minor criterions (fever >38°C and splenic infarction) for inclusion in the study. The diagnosis would at best be classified as "possible" IE (6). The Duke criteria are known for its emphasis on the positive blood cultures, along with echocardiography findings. However, the sensitivity of the criteria for the diagnosis of BCNIE is ambiguous (7). BCNIE refers to IE in which no causative microorganism can be grown employing routine blood culture methods (8). Accordingly, a complete clinical examination is warranted for detection of any accessible infectious focus, which can lead to an early diagnosis in patients with suspected endocarditis, and sometimes can be more effective than blood cultures. Similarly, in our case, the diagnosis of IE benefited from a series of novel three-dimensional echocardiographic methods. Usually, BCNIE, a consequence of previous antibacterial treatment, is commonly precipitated by gram-positive cocci, such as Staphylococci, Streptococci, and Enterococci (9). Other causes include endocarditis related to fastidious, also referred to as the "HACEK" group and the intracellular bacteria that cannot be routinely cultured in blood using the currently available techniques (10). The patient in our study received repeated, inadequate antibiotic treatments at other medical institutions prior to admittance to our Department of Cardiovascular Disease, which may constitute the primary reason for the negative blood culture.

A study revealed that patients with BCNIE present with a higher rate of complications, such as valve rupture and perforation, requiring immediate surgical intervention, compared with those with blood culture-positive endocarditis (BCPIE) (11). Pseudoaneurysm is a rare complication of IE yet possesses a high risk of mortality with inadvertent rupture; accordingly, it requires prompt identification and correct diagnosis (12). Given the typical echocardiographic findings, the patient was indicated for surgery. However, the patient's family was hesitant to proceed with the operation and did not provide additional consent documentation for surgery. Unfortunately, this patient suffered from a sudden unexpected death on the 5th day after the echocardiographic diagnosis. In addition, a previous study conducted by EURO-ENDO registry has indicated an increase of the short-term and long-term mortality in patients with BCNIE relative to those with BCPIE, whereas reduced mortality can be achieved through surgery. This eventually emphasizes that additional efforts are warranted both to improve the etiological diagnosis of IE and to identify BCNIE cases in a timely manner before progressive disease potentially contraindicates surgery (13).

It is well-established that echocardiography plays a crucial role in the diagnosis of IE. Although two-dimensional echocardiography (2DE) and traditional 3DE can provide some diagnostic information, their disadvantages are obvious. The 2DE cannot tell the spatial structure characteristics directly and needed multiple ultrasound sections to clarify the anatomical definition, which was time-consuming, and the diagnosis depended more on the experience of imaging readers, which was not conducive to the care of emergent patients. The image derived from traditional 3DE is usually not clear enough and does not consistently provide adequate detail information or depth perception. Taking the aneurysmal neck as an example, there were certain difficulties for traditional 3DE to display it plainly, due to its smaller and thinner structure. In comparation, the photo-realistic techniques with a higher resolution allows for more realistic images of cardiac structures, by superimposing a virtual light source, which can be moved around and through the aneurysm, making realistic light and shadow effects to highlight the target structures, augmenting our understanding of the anatomical morphology. Studies have shown that novel 3DE rendering techniques can better delineate borders, orifices,

cavities, and other structural abnormalities compared with 2DE and traditional 3DE, increasing the diagnostic confidence of readers and improving communication between the surgeon and the imaging specialist (4, 14, 15). To the best of our knowledge, this is the first case diagnosed with BCNIE with aortic valve involvement, leading to aortic valve perforation, and prolapse and development into a giant aortic root pseudoaneurysm using a series of novel three-dimensional echocardiographic methods. In the past, the description of pseudoaneurysms was primarily dependent on the CT. Relative to CT, novel 3D rendering techniques are more convenient and faster, especially the TrueVue Glass mode, which allows for an all-around display of an aortic root pseudoaneurysm with a click. In addition, the region of interest of images can be directly zoomed and rotated with two fingers on the touch screen. More importantly, given the fact that some structures are very mobile, real-time imaging with the help of 3DE can often visualize these structures better than cardiac CT or magnetic resonance imaging. Therefore, with the rapid development of novel 3D rendering techniques, the diagnosis of structural heart diseases will become much more efficacious in the coming years, continuously improving the prognosis and management of such patients.

## Conclusion

BCNIE with aortic valve involvement and development into a giant aortic root pseudoaneurysm is a rare but serious cardiac disease. The case included in the current study endorsed 3D transillumination rendering techniques for the detection of such structural heart disease.

## Data availability statement

The original contributions presented in the study are included in the article/**Supplementary Material**, further inquiries can be directed to the corresponding author.

## Ethics statement

The studies involving human participants were reviewed and approved by the ethics committee of The Fourth Affiliated Hospital of China Medical University. The patients/participants provided their written informed consent to participate in this study.

## Author contributions

YM drafted the main manuscript. YZ contributed to acquire ultrasound images. LY and SG collected data about patient clinical information. WF reviewed and revised the manuscript. All authors contributed to the article and approved the submitted version.

## Conflict of interest

The authors declare that the research was conducted in the absence of any commercial or financial relationships that could be construed as a potential conflict of interest.

## Publisher's note

All claims expressed in this article are solely those of the authors and do not necessarily represent those of their affiliated organizations, or those of the publisher, the editors and the reviewers. Any product that may be evaluated in this article, or claim that may be made by its manufacturer, is not guaranteed or endorsed by the publisher.

## Supplementary material

The Supplementary Material for this article can be found online at: https://www.frontiersin.org/articles/10.3389/fcvm.2023.1138390/full#supplementary-material.

## References

1. De Stasio V, Delahaye F, Moreau-Triby C, Pozzi M, Si-Mohamed S, Douek P, et al. Integrated imaging evaluation in infective endocarditis: a pictorial essay on clinical cases of extracardiac complications. *Int J Infect Dis.* (2021) 105:62–7. doi: 10.1016/j.ijid.2021.02.013

2. El-Gaaly M, Tomlinson JS, Ezzo T. Small vessel vasculitis associated with culture-negative infective endocarditis related to a cardiac device: a case report. *Eur Heart J Case Rep.* (2022) 6(8):ytac294. doi: 10.1093/ehjcr/ytac294

3. Chiocchi M, D'Errico F, De Stasio V, Di Tosto F, Pugliese L, Di Donna C, et al. Pseudoaneurysm of the aortic root following aortic valve endocarditis—a case with 2 rare life—threatening complications. *Radiol Case Rep.* (2021) 16(12):3703–7. doi: 10.1016/j.radcr.2021.08.066

4. Tamborini G, Mantegazza V, Garlasche A, Muratori M, Fusini L, Ali SG, et al. Head to head comparison between different 3-dimensional echocardiographic rendering tools in the imaging of percutaneous edge-to-edge mitral valve repair. *J Cardiovasc Dev Dis.* (2021) 8(7):73. doi: 10.3390/jcdd8070073

5. Sun F, Tan X, Sun A, Zhang X, Liang Y, Ren W. Rare double orifice mitral valve malformation associated with bicuspid aortic valve in turner syndrome: diagnosed by a series of novel three-dimensional echocardiography and literature review. *BMC Cardiovasc Disord.* (2021) 21(1):377. doi: 10.1186/s12872-021-02184-2

6. Li JS, Sexton DJ, Mick N, Nettles R, Fowler VG, Ryan T, et al. Proposed modifications to the duke criteria for the diagnosis of infective endocarditis. *Clin Infect Dis.* (2000) 30(4):633–8. doi: 10.1086/313753

7. Lamas CC, Eykyn SJ. Blood culture negative endocarditis: analysis of 63 cases presenting over 25 years. *Heart.* (2003) 89(3):258–62. doi: 10.1136/heart.89.3.258

8. Habib G, Lancellotti P, Antunes MJ, Bongiorni MG, Casalta J-P, Del Zotti F, et al. 2015 ESC guidelines for the management of infective endocarditis. *Eur Heart J.* (2015) 36(44):3075–123. doi: 10.1093/eurheartj/ehv319

9. Yang Y-F, Si F-F, Chen T-T, Fan L-X, Lu Y-H, Jin M. Early surgical intervention in culture-negative endocarditis of the aortic valve complicated by abscess in an infant:

a case report. *World J Clin Cases*. (2021) 9(35):11016–23. doi: 10.12998/wjcc.v9.i35.11016

10. Tattevin P, Watt G, Revest M, Arvieux C, Fournier PE. Update on blood culture-negative endocarditis. *Med Mal Infect*. (2015) 45(1–2):1–8. doi: 10.1016/j.medmal.2014.11.003

11. Zamorano J, Sanz J, Moreno R, Almeria C, Rodrigo JL, Samedi M, et al. Comparison of outcome in patients with culture-negative versus culture-positive active infective endocarditis. *Am J Cardiol*. (2001) 87(12):1423–5. doi: 10.1016/s0002-9149(01)01570-3

12. Afonso L, Kottam A, Reddy V, Penumetcha A. Echocardiography in infective endocarditis: state of the art. *Curr Cardiol Rep*. (2017) 19(12):127. doi: 10.1007/s11886-017-0928-9

13. Kong WKF, Salsano A, Giacobbe DR, Popescu BA, Laroche C, Duval X, et al. Outcomes of culture-negative vs. culture-positive infective endocarditis: the ESC-EORP EURO-ENDO registry. *Eur Heart J*. (2022) 43(29):2770–80. doi: 10.1093/eurheartj/ehac307

14. Karagodin I, Addetia K, Singh A, Dow A, Rivera L, DeCara JM, et al. Improved delineation of cardiac pathology using a novel three-dimensional echocardiographic tissue transparency tool. *J Am Soc Echocardiogr*. (2020) 33(11):1316–23. doi: 10.1016/j.echo.2020.08.005

15. Genovese D, Addetia K, Kebed K, Kruse E, Yamat M, Narang A, et al. First clinical experience with 3-dimensional echocardiographic transillumination rendering. *JACC Cardiovasc Imaging*. (2019) 12(9):1868–71. doi: 10.1016/j.jcmg.2018.12.012

frontiers | Frontiers in Cardiovascular Medicine

TYPE Case Report
PUBLISHED 22 March 2023
DOI 10.3389/fcvm.2023.1098154



OPEN ACCESS

EDITED BY
Antonios Karanasos,
Hippokration General Hospital, Greece

REVIEWED BY
Chiara Lestuzzi,
Santa Maria degli Angeli Hospital Pordenone, Italy
Goverdhan Puri,
Post Graduate Institute of Medical Education and Research (PGIMER), India

*CORRESPONDENCE
Hoai Thi Thu Nguyen
hoainguyen1973@gmail.com

SPECIALTY SECTION
This article was submitted to Cardiovascular Imaging, a section of the journal Frontiers in Cardiovascular Medicine

RECEIVED 14 November 2022
ACCEPTED 06 March 2023
PUBLISHED 22 March 2023

CITATION
Le AN, Nguyen AV, Nguyen TN, Kirkpatrick JN, Nguyen HT and Nguyen HTT (2023) Cardiac metastasis mimicking STEMI—impact of point-of-care ultrasound on clinical decision-making: A case report.
Front. Cardiovasc. Med. 10:1098154.
doi: 10.3389/fcvm.2023.1098154



# Cardiac metastasis mimicking STEMI—impact of point-of-care ultrasound on clinical decision-making: A case report

Anh Ngoc Le[1], Anh Van Nguyen[1,2], Trang Ngoc Nguyen[3], James N. Kirkpatrick[4,5], Huyen Thi Nguyen[3] and Hoai Thi Thu Nguyen[1,6]*

[1]Vietnam National Heart Institute, Bach Mai Hospital, Hanoi, Vietnam, [2]Department of Cardiology, Hanoi Medical University, Hanoi, Vietnam, [3]Radiology Center, Bach Mai Hospital, Hanoi, Vietnam, [4]Cardiovascular Division, Department of Medicine, University of Washington Medical Center, Seattle, WA, United States, [5]Department of Bioethics and Humanities, University of Washington Medical Center, Seattle, WA, United States, [6]Department of Internal Medicine, VNU – University of Medicine and Pharmacy, Hanoi, Vietnam

**Introduction:** The manifestations of cardiac metastases are extremely variable depending on their location and extension.
**Case presentation:** A 62-year-old man was admitted to the cardiac emergency department presenting with chest pain, worsening shortness of breath and palpitations. He had a history of esophageal squamous cell carcinoma treated with chemoradiotherapy, and he was not diagnosed with cardiovascular disease before. The electrocardiogram showed significant ST-segment elevations in leads II, III, and aVF. Initially, the patient was diagnosed with ST-segment elevation myocardial infarction. A cardiac point-of-care ultrasound was performed immediately revealing two large heterogeneous masses in the left ventricular wall and the apex, which changed the diagnosis and the management strategy. There was no significant change in serial cardiac biomarkers in the setting of persistent STE. Thoracic computed tomography and cardiac magnetic resonance confirmed that the patient was suffering from cardiac and lung metastases.
**Conclusion:** ECG findings of localized and prolonged STE without Q waves or changes in biomarkers may suggest myocardial tumor invasion, especially in the cancer setting. Cardiac point-of-care ultrasound is an effective, convenient, noninvasive imaging modality to guide real-time clinical decision-making.

KEYWORDS
cardiac metastasis, ST-segmental elevation, point-of-care ultrasound, myocardial infarction, case report

## Introduction

Cardiac metastases account for 95% to 99% of cardiac tumors (1, 2). The exact incidence of cardiac metastatic disease is unknown. A study of post-mortem examinations showed that the proportion of in-hospital deceased patients who had cardiac metastases was 9.1% which was highly variable depending on the types of primary tumors, from 1.0% in prostate carcinoma to 48.4% in mesothelioma (2). Clinical silence is prevalent in most cases (3). The manifestations of cardiac metastases are extremely variable depending on their location and extension (4, 5). We report a case of myocardial metastatic with ST-segment elevation (STE) on electrocardiogram (ECG) and intramyocardial masses noted on cardiac point-of-care ultrasound (POCUS).

## Case presentation

A 62-year-old man without cardiac history was admitted to the cardiac emergency department complaining of chest pain, worsening shortness of breath, and palpitations for 5–6 weeks. His medical history included esophageal squamous cell carcinoma (ESCC) which was treated with chemoradiotherapy for 1.5 years. The treatment strategy was completed 6 months ago.

On admission, the physical examination revealed extreme frailty with a BMI of 16.2 kg/m$^2$, heart failure signs including elevated jugular venous pressure, rales in the lungs, peripheral edema, hepatomegaly, and low blood pressure of 75/40 mmHg. Oxygen saturation was 89% while breathing ambient air. A 12-lead ECG showed rapid atrial fibrillation, and significant convex STE in leads II, III, and aVF with the presence of reciprocal ST depression in the precordial leads (Figure 1A). No prior ECG was available for comparison. Initially, the patient was diagnosed with ST-segment elevation myocardial infarction (STEMI). However, because he had hemodynamic instability and had a history of ESCC, we decided to perform a cardiac POCUS immediately for a more comprehensive assessment before transferring the patient to the catheterization laboratory for urgent percutaneous coronary intervention (PCI). The echocardiogram showed two large masses in the left ventricular wall and the apex. The left ventricular systolic function was low. Because of these echo findings, the PCI was deferred. Treatment was initiated with oxygen, dobutamine, furosemide, digitalis, and enoxaparin.

Serial hs-cTnT measurements and ECGs were obtained. A comprehensive transthoracic echocardiogram (TTE) was performed on the following day. On serial ECGs, STE persisted

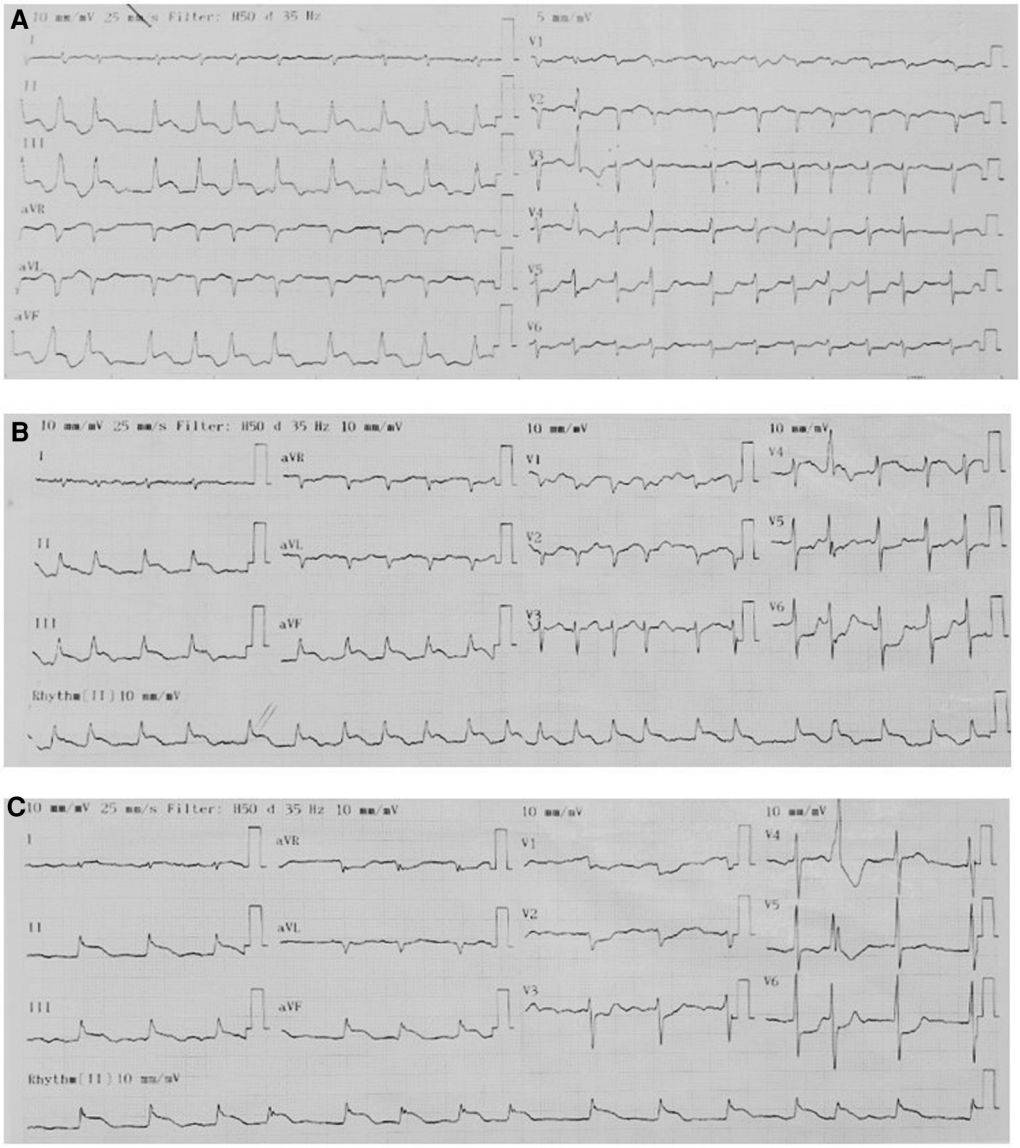


FIGURE 1
Serial ECGs. The pattern of ECGs was persistent, including atrial fibrillation, right axis deviation, poor R-wave progression, profound STE in leads II, III, and aVF with the presence of reciprocal ST depression in the precordial leads. (A) On admission. (B) 1 h later. (C) Before discharge.

and there was no development of pathological Q waves (**Figures 1B, C**). Laboratory studies showed that hs-cTnT stabilized at a high level: on admission 0 h 173.1 ng/L, 1 h 167.3 ng/L, 3 h 159 ng/L, on discharge 180 ng/L (<14 ng/L); elevated N-terminal pro-B-type brain natriuretic peptide (NT-pro-BNP) was 1391 pmol/L < 14.47 pmol/L). TTE unveiled two large heterogeneous masses, which were characterized by ill-defined borders: one involved the lateral, inferior and posterior portion of the left ventricular wall, and another involved the apex and ventricular septum portion (**Figure 2**). The involved ventricular walls were significantly thickened and akinetic, which did not correspond to coronary perfusion territories. Left ventricular systolic dysfunction (biplane left ventricular ejection fraction of 35%), and right ventricular systolic dysfunction (tricuspid annular plane systolic excursion of 15 mm and fractional area change of 30%) were detected.

This patient was referred for a thoracic multidetector computed tomography (MDCT) scan and cardiac magnetic resonance imaging (CMR) for further evaluation of imaging characteristics of the cardiac masses, and other lesions.

On thoracic MDCT, the mediastinal window showed infiltrative lesions causing abnormal wall thickening of the interventricular septum toward the apex, as well as of the inferior, posterior, and lateral walls of the left ventricle corresponding to the lesions observed on TTE. These lesions extended beyond the myocardium to the pericardial fat. The left anterior descending (LAD) artery and the left circumflex (LCx) artery were encased completely and compressed mildly. The adjacent pericardium was irregularly thickened (**Figure 3F**). These lesions were new in comparison with the pre-treatment film (**Figure 4C**). The ESCC was significantly diminished, and there was no longer abnormal esophageal wall thickening (**Figures 4A, B**; **Figure 3E**). On lung window, two new

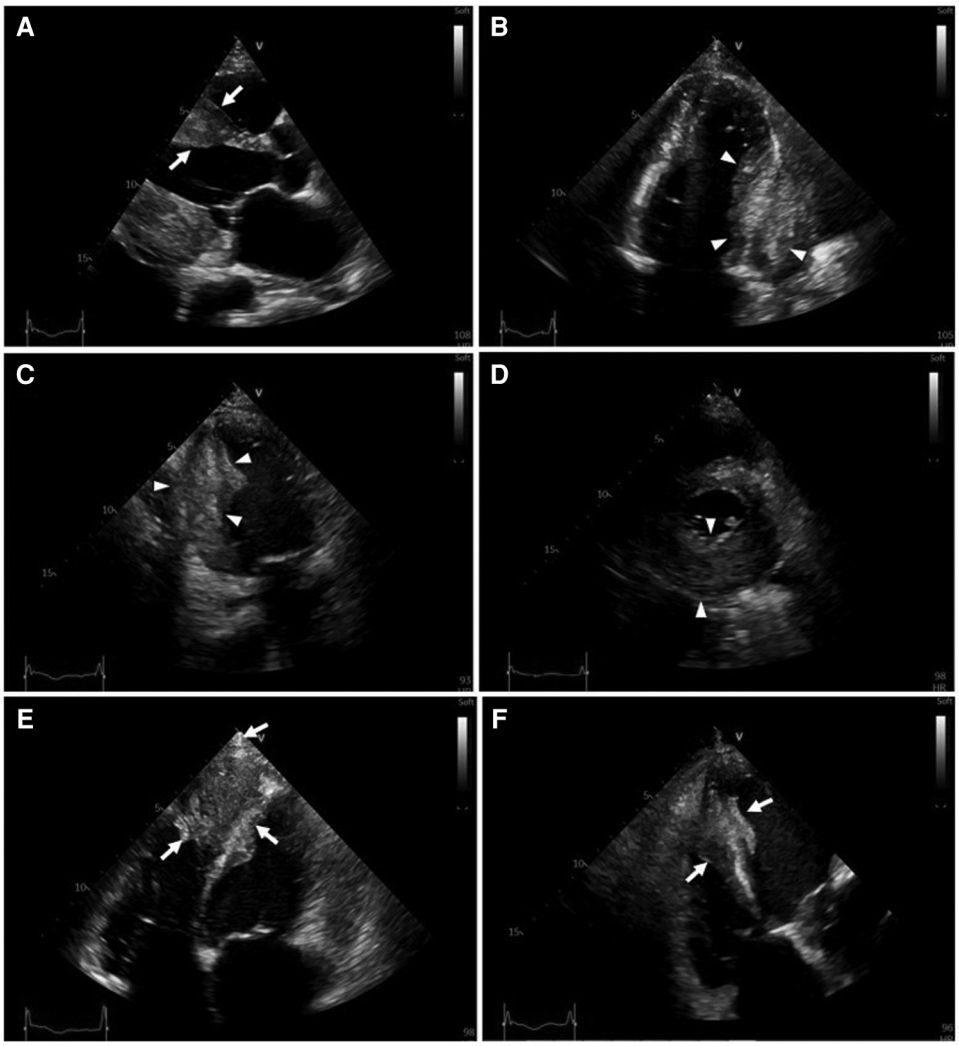


FIGURE 2
Transthoracic two-dimensional echocardiography (2D-TTE). 2D-TTE reveals two large heterogeneous masses characterized by ill-defined borders: one involving the lateral, inferior and posterior portions of the left ventricular wall *(white arrowheads)*, and another involving the apex and ventricular septum *(white arrows)*. (**A**) Parasternal long-axis view. (**B**) Four-chamber view. (**C**) Two-chamber view. (**D**) Parasternal short-axis view at the papillary muscle level. (**E**) Modified four-chamber view. (**F**) RV-focused apical four-chamber view.

10.3389/fcvm.2023.1098154

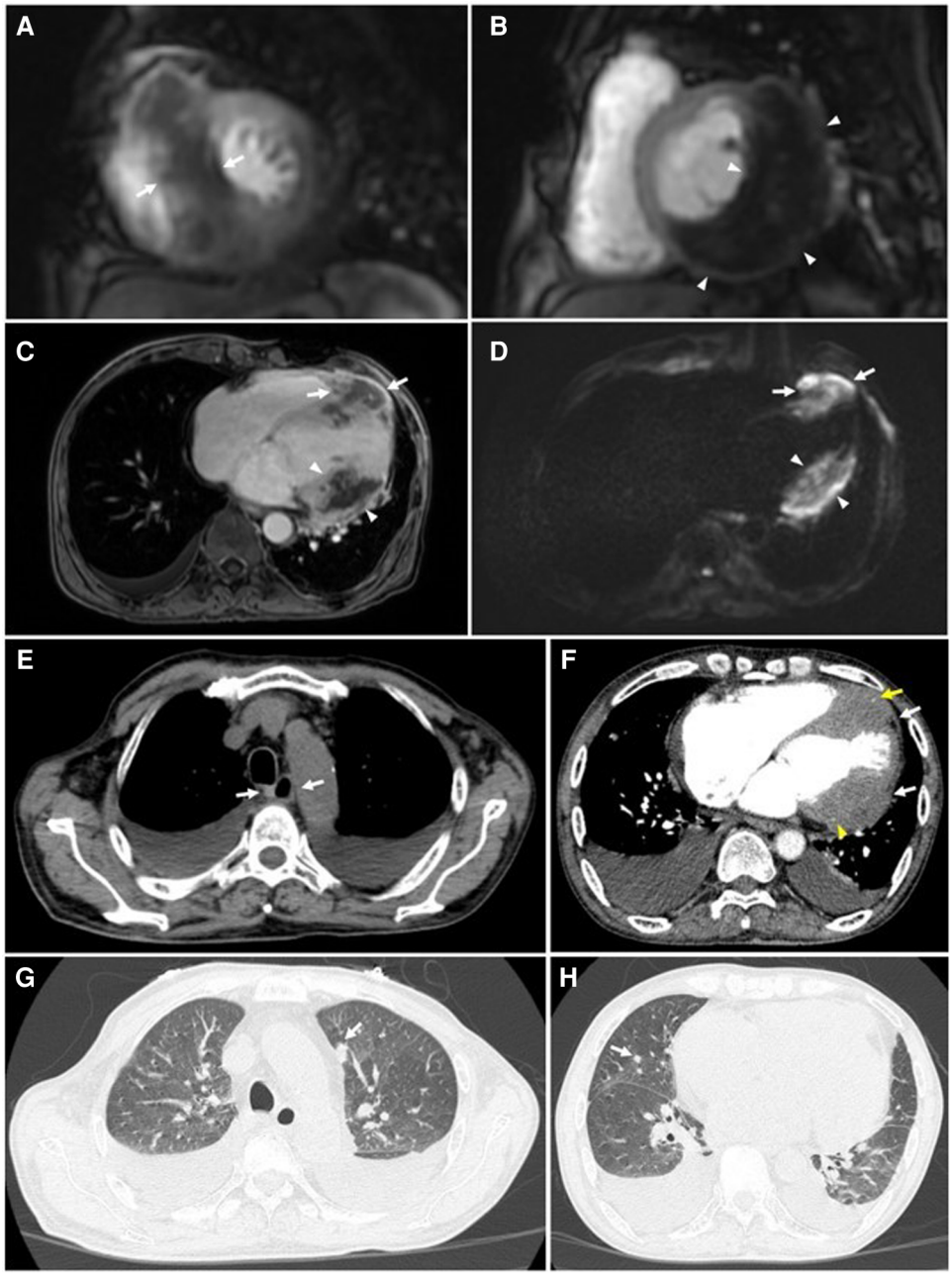


FIGURE 3
Cardiac magnetic resonance and thoracic computed tomography were obtained 6 months after completion of chemoradiotherapy. CMR: (**A to D**) Tumors of the interventricular septum *(white arrows)* and inferior-lateral left ventricular wall *(white arrowheads)* do not demonstrate enhancement on short-axis first-pass perfusion images (**A & B**) and axial post-contrast T1-weighted images (**C**) suggestive of necrosis. These lesions demonstrate restricted diffusion on the axial diffusion-weighted images (DWI) (**D**). (**E**) No abnormal thickening of the esophageal wall is seen on the mediastinal window *(white arrows)*. (**F**) Tumors of the interventricular septum and inferior-lateral left ventricular wall invade the left anterior descending (LAD) artery *(yellow arrows)* and left circumflex (LCx) artery *(yellow arrowheads)*, respectively. These lesions also extend to the pericardium *(white arrows)*. (**G & H**) Metastatic nodules in the upper lobe of the left lung and the middle lobe of the right lung are seen on the lung window *(white arrows)*.

well-defined solid nodules in the left upper lobe and the right middle lobe were detected (**Figures 3G, H**) compared to before treatment (**Figure 4D**). On CMR, two tumors enhanced mildly on first pass perfusion images but had peripheral heterogeneous enhancement in post-contrast T1-weighted images with central necrosis. In addition, the tumors appeared to have restricted diffusion on the diffusion-weighted imaging (DWI) (**Figure 3** A to D).

Although the patient declined invasive coronary angiography and coronary computed tomography angiography, the unremarkable change in serial cardiac biomarkers in the setting of persistent STE strongly argued against STEMI. It was concluded that the patient suffered from cardiac and lung metastases from ESCC. The changes in ECGs were attributed to the patient's cardiac metastases. Given his disease progression

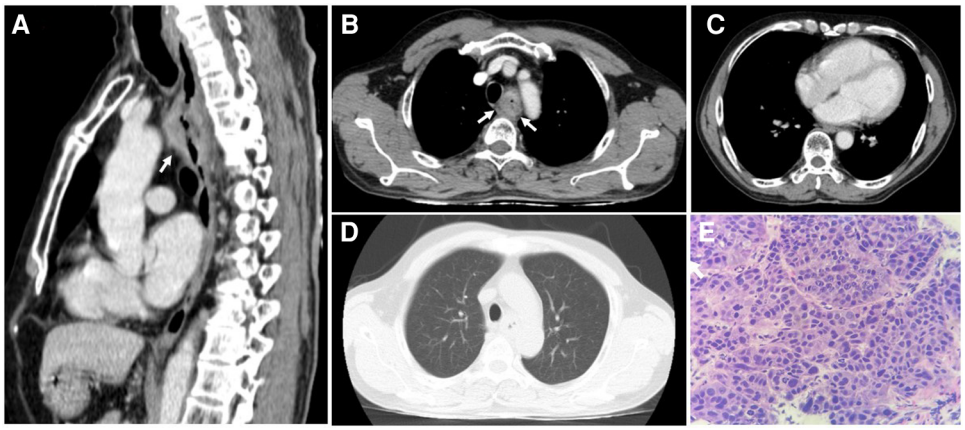


FIGURE 4
The thoracic computed tomography and histopathology before treatment strategy for esophageal squamous cell carcinoma. (**A & B**) The sagittal and axial planes demonstrate that the upper esophageal tumor does not invade the surrounding structures *(white arrows)*. (**C**) The mediastinal window demonstrates normal thickness and density of ventricular and atrial walls. (**D**) No parenchymal lesions are seen on the lung window. (**E**) Hematoxylin and eosin-stained esophageal tissue at 400 × magnification showed tumor cells that possess enlarged, hyperchromasia, coarse nucleus; visible nucleoli and large cytoplasm. The tumor cells demonstrate disarray and loss of polarity in the desmoplastic stroma.

and poor prognosis, the patient refused further diagnosis methods during this admission and wished to pursue palliative treatment. The patient was referred to the local hospital for palliative care. He passed away from multiple organ failure one month later.

## Discussion

Cardiac metastases are usually diagnosed on imaging or autopsy incidentally (1, 2). Primary tumor can metastasize to the heart through four pathways, including hematogeneous, lymphatic, or transvenous spread, or direct invasion. Each metastatic pathway has a different target tissues (6). Pericardial involvement is the most common (69.4%), which may result in pericardial effusion and tamponade, followed by epicardial or myocardial metastases, at 34.2% and 31.8%, respectively (4). A mere 5% of cardiac metastasis involves the endocardium (4). The clinical manifestations of myocardial metastasis depend not only on the degree of metastatic infiltration but also on the location (4). Life-threatening complications include arrhythmias (complete atrioventricular block due to disruption of the cardiac conduction system by cardiac metastases, atrial fibrillation, and ventricular fibrillation, among others), and congestive heart failure (4, 5, 7). Rarely, myocardial metastases may result in cardiac rupture, cardiac tamponade, and sudden death (5). Endocardial and intracavitary lesions may occasionally lead to inflow and outflow obstruction of the heart chambers (4, 5). The coronary arteries may be injured by neoplasm-induced coronary embolism, perivascular compression of the coronary arteries, or invasion of the coronary arteries (4, 5).

Regarding ECG changes in cardiac metastasis, the most common abnormalities are ST-T changes (nonspecific ST-T changes, T wave inversion, ST-segment depression, STE) (8). Myocardial metastasis can result in conduction disturbances, atrial arrhythmias, ventricular arrhythmias, which may be hard to control by antiarrhythmic medications (7–10). Low-voltage and electric alternans may indicate a pericardial effusion and tamponade (8).

STEMI is the most common cause of STE. However, STE can be found in a wide range of conditions, including normal variants, left bundle-branch block, acute pericarditis and myocarditis, electrolytes disturbances, the Brugada syndrome,arrhythmogenic right ventricular cardiomyopathy, early repolarization, transient STE after transthoracic cardioversion, and Prinzmetal's angina (11, 12). STE in the setting of cancer can be seen in many situations, for example, myocardial metastasis, tumor emboli within a coronary artery (13), coronary artery invasion or compression by surrounding metastatic lesions (14) or cancer therapy-related cardiovascular toxicity (coronary vasospasm, accelerated atherosclerosis and plaque rupture, and coronary thrombosis and embolism (15–17).

Our patient presented with localized, persistent STE without development of pathological Q waves. Comprehensive assessment of coronary artery injuries in our patient was not possible because he refused to undergo either coronary computed tomography angiography or coronary angiography. Nevertheless, the stable hs-cTnT and ECG pattern strongly suggested the absence of STEMI.

Although STE related to myocardial metastasis is rare, it has been published in several case reports recently (18–23) and in a large series by Lestuzzi (24). Of note, evolutionary changes occurring in STEMI are not seen in patients with cardiac metastases mimicking STEMI (18, 19, 21–23). These ECGs features seem to be a sign of myocardial metastases. In patients with intracardiac, pericardial, or paracardiac neoplastic masses, 86% of patients with STE suffered from myocardial infiltration detected by two-dimensional echocardiography (24). In addition,

the localization of STE reflects the location of the cardiac infiltration (18–24).

The mechanism of this phenomenon is the same as that of STE in STEMI. Malignant cardiac infiltration results in a change in the electrical properties of the myocardium, leading to the differences in the action potential between the involved and the normal myocardium. An injury current results, which manifests on the ECG as STE (21, 25).

Withholding reperfusion therapy in a patient suffering from STEMI for time consuming diagnostic testing is inadvisable as it results in a delay in therapy. Routine echocardiography before primary PCI is therefore not recommended. Emergency echocardiography is indicated in patients with cardiac arrest, cardiogenic shock, hemodynamic instability or suspected mechanical complications, and in cases in which the diagnosis of STEMI is uncertain (26). Clinical use of POCUS has been extensively described in medical literature since the early 2000s (27). One study found that POCUS confirmed a suspected clinical diagnosis in 50% of cases and changed the diagnosis in 23%, with a change in treatment plan in 53% (28). With the evolution of handheld ultrasound systems and the increasing evidence supporting in clinical practice, POCUS is considered as an effective and emerging tool for the frontline clinician. Recently, the use of cardiac POCUS has increased significantly and become standard in many emergency departments and critical care settings (29). The advantages of POCUS including low cost, time efficiency, ease of use, and accuracy are the backbone of its wide implementation in making diagnoses, clinical monitoring, and guiding procedures (30). In the literature, the number of cardiac POCUS publication has increased yearly. The proportion of emergency medicine and cardiology authors were 38.5% and 20.8%, respectively, decreased over the last decade, while those of anesthesiology and critical care have increased (31). In our patient cardiac POCUS changed the diagnosis and the management strategy. This case reinforces the importance of POCUS in real-time clinical decisions, especially in patients with complicated presentation.

## Conclusion

Metastases to the myocardium and pericardium may mimic acute STEMI which requires timely diagnosis and emergent coronary revascularization. Investigating STEMI-mimicker in the right clinical setting can be important before committing patients to reperfusion strategies. ECG findings of localized and prolonged STE may suggest myocardial tumor invasion, especially in the cancer setting. Cardiac POCUS is a convenient, noninvasive imaging modality to guide real-time clinical decision-making.

## Data availability statement

The raw data supporting the conclusions of this article will be made available by the authors, without undue reservation.

## Ethics statement

The studies involving human participants were reviewed and approved by Bach Mai Hospital. The patients/participants provided their written informed consent to participate in this study. Written informed consent was obtained from the individual(s) for the publication of any potentially identifiable images or data included in this article.

## Author contributions

HTTN, ANL, JNK devised the manuscript concept. AVN, ALN, HTTN belonged to patient's management team. HTTN, ANL performed cardiac point-of-care ultrasound and two-dimensional echocardiography. ANL contributed to clinical, imaging and pathological data collection. TNN, HTN interpreted the MDCT and CMR data. ANL wrote the manuscript in collaboration with HTTN, TNN, HTN. HTTN and JNK revised the manuscript. HTTN submitted the manuscript. All authors contributed to the article and approved the submitted version.

## Acknowledgments

We wish to thank the Vietnam National Heart Institute, Bach Mai hospital for providing us with the opportunity to conduct this case report.

## Conflict of interest

The authors declare that the research was conducted in the absence of any commercial or financial relationships that could be construed as a potential conflict of interest.

## Publisher's note



## Supplementary material

The Supplementary Material for this article can be found online at: https://www.frontiersin.org/articles/10.3389/fcvm.2023.1098154/full#supplementary-material.

# References


1. Lam KY, Dickens P, Chan AC. Tumors of the heart. A 20-year experience with a review of 12,485 consecutive autopsies. *Arch Pathol Lab Med.* (1993) 117(10):1027–31. PMID: 8215825

2. Butany J, Leong SW, Carmichael K, Komeda M. A 30-year analysis of cardiac neoplasms at autopsy. *Can J Cardiol.* (2005) 21(8):675–80. PMID: 16003450

3. Klatt EC, Heitz DR. Cardiac metastases. *Cancer.* (1990) 65(6):1456–9. doi: 10.1002/1097-0142(19900315)65:6<1456::AID-CNCR2820650634>3.0.CO;2-5

4. Bussani R, De-Giorgio F, Abbate A, Silvestri F. Cardiac metastases. *J Clin Pathol.* (2007) 60(1):27–34. doi: 10.1136/jcp.2005.035105

5. Reynen K, Köckeritz U, Strasser RH. Metastases to the heart. *Ann Oncol.* (2004) 15(3):375–81. doi: 10.1093/annonc/mdh086

6. Goldberg AD, Blankstein R, Padera RF. Tumors metastatic to the heart. *Circulation.* (2013) 128(16):1790–4. doi: 10.1161/CIRCULATIONAHA.112.000790

7. Casella M, Carbucicchio C, Dello Russo A, Tundo F, Bartoletti S, Monti L, et al. Radiofrequency catheter ablation of life-threatening ventricular arrhythmias caused by left ventricular metastatic infiltration. *Circ Arrhythm Electrophysiol.* (2011) 4(2):e7–10. doi: 10.1161/CIRCEP.110.961193

8. Cates CU, Virmani R, Vaughn WK, Robertson RM. Electrocardiographic markers of cardiac metastasis. *Am Heart J.* (1986) 112(6):1297–303. doi: 10.1016/0002-8703(86)90363-7

9. Juan Ó, Esteban E, Sotillo J, Alberola V. Atrial flutter and myocardial infarction-like ECG changes as manifestations of left ventricle involvement from lung carcinoma. *Clin Transl Oncol.* (2008) 10(2):125–7. doi: 10.1007/s12094-008-0166-0

10. Lestuzzi C, Miolo G, Tartuferi L, Pecoraro R, De Paoli A, Dametto E, et al. Ventricular arrhythmias due to glomangiosarcoma cardiac metastases. *JACC CardioOncology.* (2021) 3(1):150–3. doi: 10.1016/j.jaccao.2020.11.015

11. Wang K, Asinger RW, Marriott HJL. ST-Segment Elevation in conditions other than acute myocardial infarction. *N Engl J Med.* (2003) 349(22):2128–35. doi: 10.1056/NEJMra022580

12. Merlo AC, Pescetelli F, Ameri P, Porto I. Not every ST-segment elevation is a STEMI. *JACC Case Rep.* (2021) 3(2):283–5. doi: 10.1016/j.jaccas.2020.11.019

13. Aragon J. A rare noncardiac cause for acute myocardial infarction in a 13-year-old patient. *Cardiol Rev.* (2004) 12(1):31–6. doi: 10.1097/01.crd.0000090895.81497.16

14. Cook MA, Sanchez EJ, Lopez JJ, Bloomfield DA. Acute myocardial infarction: a rare presentation of pancreatic carcinoma. *J Clin Gastroenterol.* (1999) 28(3):271–2. doi: 10.1097/00004836-199904000-00022

15. Lyon AR, López-Fernández T, Couch LS, Asteggiano R, Aznar MC, Bergler-Klein J, et al. 2022 ESC guidelines on cardio-oncology developed in collaboration with the European hematology association (EHA), the European society for therapeutic radiology and oncology (ESTRO) and the international cardio-oncology society (IC-OS). *Eur Heart J.* (2022) 43(41):4229–361. doi: 10.1093/eurheartj/ehac244

16. Medepalli LC, Mahmood TS, Liberman H, Medepalli AM, Bagwell TW. Diagnosis and management of a patient with 5-fluorouracil-induced ST elevation and nonsustained ventricular tachycardia as a late presentation of cardiotoxicity and successful 5-fluorouracil rechallenge. *Cureus.* (2022) 14(10):e30489. doi: 10.7759/cureus.30489

17. Vošmik M, Hodek M, Buka D, Sýkorová P, Grepl J, Paluska P, et al. Cardiotoxicity of radiation therapy in esophageal cancer. *Rep Pract Oncol Radiother.* (2020) 25(3):318–22. doi: 10.1016/j.rpor.2020.02.005

18. Chen T. Persistent ST-segment elevation due to cardiac metastasis. *BMJ Case Rep.* (2017):bcr-2017-220621. doi: 10.1136/bcr-2017-220621

19. Hartman RB, Clark PI, Schulman P. Pronounced and prolonged ST segment elevation: a pathognomonic sign of tumor invasion of the heart. *Arch Intern Med.* (1982) 142(10):1917–9. doi: 10.1001/archinte.1982.00340230165026

20. Gard JJ, Bader W, Enriquez-Sarano M, Frye RL, Michelena HI. Uncommon cause of ST elevation. *Circulation.* (2011) 123(9):e259–61. doi: 10.1161/CIRCULATIONAHA.110.002477

21. Xu J, Cui F, Wang D, Liu J, Zhou R. Profound anterior ST-segment elevation in a patient with lung cancer and echocardiographic evidence of right ventricle metastasis. *CASE.* (2022) 6(2):59–62. doi: 10.1016/j.case.2021.11.001

22. Pan KL, Wu LS, Chung CM, Chang ST, Lin PC, Hsu JT. Misdiagnosis: cardiac metastasis presented as a pseudo-infarction on electrocardiography. *Int Heart J.* (2007) 48(3):399–405. doi: 10.1536/ihj.48.399

23. Viscuse PV, Foley TA, Michelena HI. Persistent ST-segment elevation: a Pandora's Box. *Circulation.* (2018) 138(11):1166–8. doi: 10.1161/CIRCULATIONAHA.118.036584

24. Lestuzzi C, Nicolosi GL, Biasi S, Piotti P, Zanuttini D. Sensitivity and specificity of electrocardiographic ST-T changes as markers of neoplastic myocardial infiltration. *Chest.* (1989) 95(5):980–5. doi: 10.1378/chest.95.5.980

25. Harris TR, Copeland GD, Brody DA. Progressive injury current with metastatic tumor of the heart. *Am Heart J.* (1965) 69(3):392–400. doi: 10.1016/0002-8703(65)90277-2

26. Ibanez B, James S, Agewall S, Antunes MJ, Bucciarelli-Ducci C, Bueno H, et al. 2017 ESC guidelines for the management of acute myocardial infarction in patients presenting with ST-segment elevation. *Eur Heart J.* (2018) 39(2):119–77. doi: 10.1093/eurheartj/ehx393

27. Lee L, DeCara JM. Point-of-Care ultrasound. *Curr Cardiol Rep.* (2020) 22(11):149. doi: 10.1007/s11886-020-01394-y

28. Baker DE, Nolting L, Brown HA. Impact of point-of-care ultrasound on the diagnosis and treatment of patients in rural Uganda. *Trop Doct.* (2021) 51(3):291–6. doi: 10.1177/0049475520986425

29. Kirkpatrick JN, Grimm R, Johri AM, Kimura BJ, Kort S, Labovitz AJ, et al. Recommendations for echocardiography laboratories participating in cardiac point of care cardiac ultrasound (POCUS) and critical care echocardiography training: report from the American society of echocardiography. *J Am Soc Echocardiogr.* (2020) 33(4):409–422.e4. doi: 10.1016/j.echo.2020.01.008

30. Díaz-Gómez JL, Mayo PH, Koenig SJ. Point-of-Care ultrasonography. Ingelfinger JR, editor. *N Engl J Med.* (2021) 385(17):1593–602. doi: 10.1056/NEJMra1916062

31. Pattock AM, Kim MM, Kersey CB, Liu L, Kirkpatrick JN, Adedipe A, et al. Cardiac point-of-care ultrasound publication trends. *Echocardiography.* (2022) 39(2):240–7. doi: 10.1111/echo.15297

frontiers | Frontiers in Cardiovascular Medicine

TYPE Case Report
PUBLISHED 24 March 2023
DOI 10.3389/fcvm.2023.1123789



OPEN ACCESS

EDITED BY
Grigorios Korosoglou,
GRN Klinik Weinheim, Germany

REVIEWED BY
Alexandros Kallifatidis,
St.Luke's Hospital, Greece
Moritz Montenbruck,
Katholisches Marienkrankenhaus GmbH,
Germany

*CORRESPONDENCE
Bruna Punzo
✉ bruna.punzo@synlab.it

†These authors have contributed equally to this work

SPECIALTY SECTION
This article was submitted to Cardiovascular Imaging, a section of the journal Frontiers in Cardiovascular Medicine

RECEIVED 14 December 2022
ACCEPTED 27 February 2023
PUBLISHED 24 March 2023

CITATION
Punzo B, Baldi D, Ranieri B, Cavaliere C and Cademartiri F (2023) Multimodality imaging of a cardiac paraganglioma: A case report. Front. Cardiovasc. Med. 10:1123789. doi: 10.3389/fcvm.2023.1123789



# Multimodality imaging of a cardiac paraganglioma: A case report

Bruna Punzo[1]*, Dario Baldi[1], Brigida Ranieri[1], Carlo Cavaliere[1†] and Filippo Cademartiri[2†]

[1]IRCCS SYNLAB SDN, Naples, Italy, [2]Department of Radiology, Fondazione Toscana Gabriele Monasterio/CNR, Pisa, Italy

Cardiac paragangliomas (PGLs) are rare extra-adrenal tumors that arise from chromaffin cells of the sympathetic ganglia. PGLs are often diagnosed incidentally, in the absence of symptoms, or with symptoms related to cardiovascular dysfunction. Cardiac computed tomography (CCT) and cardiac magnetic resonance (CMR) can be used to accurately determine the lesion morphology and position as well as providing detailed tissue characterization. A multimodal imaging approach, not yet standardized, could be useful either in diagnosis and monitoring or in treatment planning. In the case reported here, CCT and CMR were performed to define lesion anatomy, and a reconstruction was generated using cinematic rendering (CR) to characterize the PGL angioarchitecture.

KEYWORDS

case report, cardiac paraganglioma, neuroendocrine tumor, CCT, CMR

## Introduction

According to the World Health Organization's tumor classification scheme, paragangliomas (PGLs) are rare neuroendocrine tumors arising from extra-adrenal parasympathetic or sympathetic ganglia neural crest cells (1).

Cardiac PGLs are extremely rare tumors (<1% of all primary cardiac tumors) originating from visceral paraganglial cells of the left atrium or the aorta. Cardiac PGLs are most commonly observed in the left atrium and they are functional in 35%–50% of patients with symptoms related to catecholamine excess (2, 3). Clinically, these patients may present without symptoms or with generalized disorders such as hypertension, dyspnea, or cardiovascular risk factors.

These lesions can be evolutive, leading to serious complications such as bleeding and cardiac failure. Radiologic findings acquired by computed tomography (CT) and magnetic resonance (MR) play an essential role in cardiac PGL management and can provide further anatomic and tissue characterization.

Currently, the most commonly used tool to provide 3D images from CT data is volume rendering (VR). The cinematic rendering (CR) algorithm has recently been introduced; this supports interpretation for diagnosis of various cardiac pathologies and treatment planning by creating complex lighting effects such as refraction, providing high levels of detail in terms of shadowing and depth, and visualizing high-density and high-contrast structures (4).

In this study, we report the case of a patient with severe rest dyspnea, on whom cardiac computed tomography (CCT) and cardiac magnetic resonance (CMR) imaging were

Abbreviations
CCT, cardiac computed tomography; CMR, cardiac magnetic resonance; CR, cinematic rendering; CT, computed tomography; ICA, invasive coronary angiography; MR, magnetic resonance; PGL, paraganglioma; VR, volume rendering.

performed to characterize a vascularized paracardiac mass suggested by a previous invasive coronary angiography (ICA) addressing a possible angioma.

CR reconstruction using the CCT dataset was employed to better evaluate the anatomical details, including course and tortuosity of the vessels (e.g., coronaries, cardiac veins, and large vessels) involved in the mass vascular supply.

## Case description

A 46-year-old man, a candidate for aortic valve replacement, was referred to us after an invasive coronary angiogram (ICA; **Figure 1**; **Supplementary Movie 1**) showed a large cardiac mass encasing the left coronary artery; there was no coronary artery stenosis. The patient presented with a family history of atherosclerotic coronary artery disease, hypertension treated with lecardipine and lobizide, type 2 insulin-dependent diabetes mellitus, and obesity (BSA = 2.10 $m^2$). The patient provided written informed consent for this study.

CCT was performed (**Figures 2F–J**; **Supplementary Movies 2 and 3**) using a third-generation dual source CT scanner (DSCT; Somatom Force, Siemens Healthineers, Erlangen, Germany). Initially, a non-contrast CT prospectively ECG-triggered high-pitch spiral acquisition was performed for calcium score evaluation. Subsequently, an angiographic CT scan with retrospective ECG gating and automated attenuation-based anatomical tube current modulation (CARE Dose 4D, Siemens) was acquired. Tube voltage was adjusted by using the automated attenuation-based tube voltage selection functionality (CAREkV, Siemens). For the angiographic scan, 70 mL of iodinated contrast agent (Iomeprol 400 mgI/mL, Iomeron 400, Bracco, Italy) was injected at 5.5 mL/s, followed by 50 mL of saline at the same flow rate. Data were reconstructed using a dedicated third-generation Advanced Modeled Iterative Reconstruction device (ADMIRE, Siemens Healthineers, Erlangen, Germany) using medium-sharp convolution kernels (Bv36 and Bv40), a strength level of 3, and a section thickness of 0.75 mm with an increment of 0.4 mm and a pixel matrix of 512 × 512. Postprocessing was performed using a dedicated workstation (Syngo.Via VB10B, Siemens Healthineers, Erlangen, Germany), and MIP, c-MPR, 3D volume rendering, and cinematic rendering images were generated.

CCT showed a solid mass above the basal anterior wall of the left ventricle, characterized by intense, progressive, and inhomogeneous contrast enhancement, and a capsule; the core of the lesion was hypovascular/necrotic; in addition, the lesion showed complete encasing of the left main coronary artery, the proximal-middle segment of the left anterior descending (LAD) coronary artery, and the proximal segment of the left circumflex coronary artery. CR reconstruction of the CCT dataset was employed to better evaluate the anatomical details involved in the mass vascular supply.

The patient also underwent CMR imaging (**Figures 2A–E**) on a 1.5 T scanner (Achieva dStream 1.5 T, Philips) with a 32-channel body coil. The CMR protocol consisted of cine sequences sBTFE in three cardiac planes (two and four chambers and short axis);

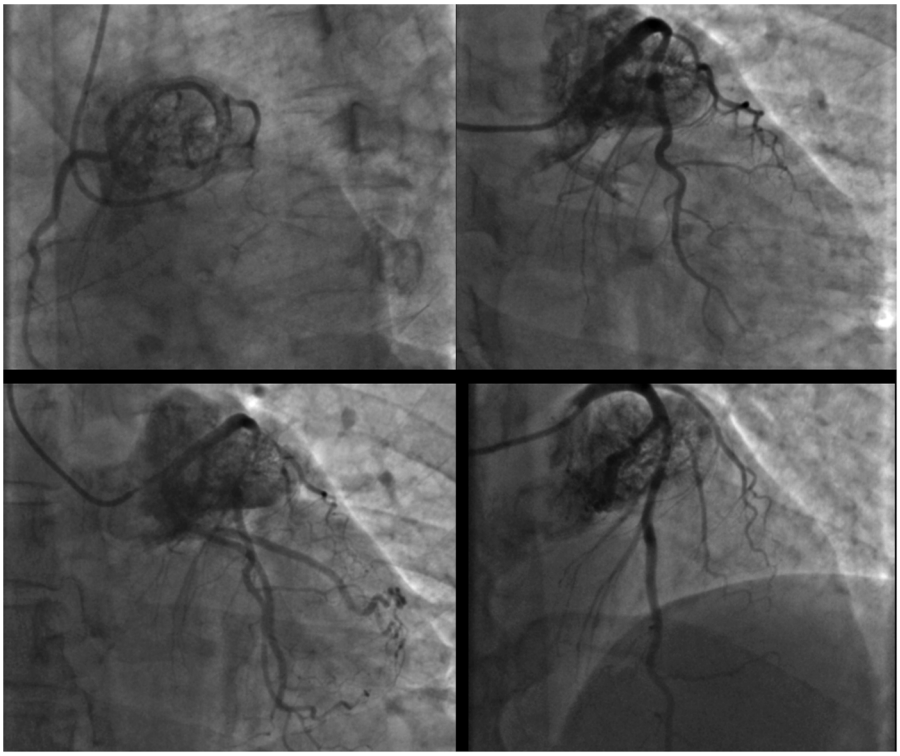

FIGURE 1
Coronary angiogram in different oblique projections showing a large cardiac mass encasing the left coronary artery.

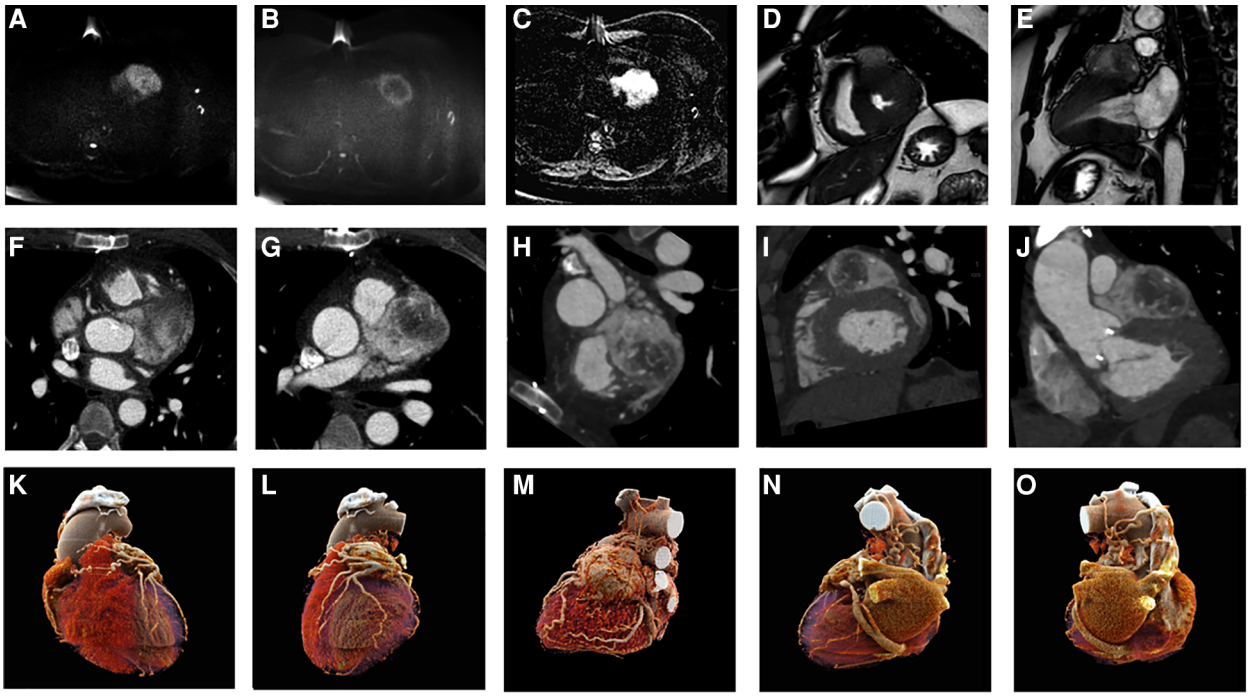


FIGURE 2
CMR acquisition (**A–E**): DWI b 0 and b 1,000 (**A,B**) and ADC map (**C**) showing high cellularity of the lesion; balanced gradient echo sequence in short axis and two chambers (**D,E**), showing morphology and extension of a PGL. CCT acquisition (**F–J**): axial (**F,G**) and oblique planes highlighting the morphology, position, and contrast of the PGL. CR reconstructions in different planes (**K–O**).

T2 STIR and DWI of the entire left ventricle in the short-axis plane; tissue characterization sequences (T1 native MOLLI and T2* mapping); delayed enhancement PSIR-TFE for the evaluation of early or late gadolinium enhancement.

CMR findings were as follows: well-circumscribed ovoid/spherical lesions and typical hyperintensity on T2 imaging sequences, with the other features similar to CCT.

The location and evidence on the morphological, functional, and metabolic features of the mass all pointed to a solid, hypervascular, capsulated, non-infiltrative, neuro-endocrine type of tumor; even though serum catecholamines were within normal ranges, the diagnosis was non-excreting cardiac PGL.

The patient is now in follow-up, mainly with CMR for 2.5 years, and the morphological features of the mass are stable. Multimodality imaging of atypical cardiac masses is warranted for proper diagnosis and follow-up.

## Discussion

Extra-adrenal PGLs are solid hypervascularized tumors originating from the chromaffin cells of the sympathetic ganglia. PGLs are exceptionally rare (<1% of all cardiac primary tumors), and their diagnosis and treatment usually follow very different paths and approaches.

In our case, the mass is attached to the left upper anterolateral portion of the heart and incorporates an important tract of the left coronary artery as well as having contiguity relationships with the majority of adjacent structures.

These aspects, as also reported in the literature, make any surgical removal procedure extremely complex and risky, although the possibility of cardiovascular morbidity and mortality without treatment remains high, given the possible compression/invasion of neighboring structures.

Prognostic factors are represented by tumor attenuation, contrast enhancement, detailed understanding of the feeding vessel, and close proximity to surrounding blood vessels and vital structures (5, 6).

CCT and CMR, thanks to multiple 2D postprocessing techniques, are available to facilitate evaluation of the anatomy, which is often complex and challenging in patients with cardiac PGL.

CCT, thanks to its high spatial resolution and contrast, was able to evaluate the entire solid nodular mass at the base of the LV and its relationship with the surrounding arterial and venous vessels. The lesion was found to have stretched and shifted both the anterior descending coronary artery and the left circumflex artery, which, however, was not providing vascular supply.

In this context, to develop a clear understanding of the PGL angioarchitecture, CR reconstructions were generated.

Briefly, under this approach, 2D reconstructed slices composed of isotropic voxels from standard clinical CT acquisitions are stacked to create a volume, and light is passed through the volume to create a 3D visualization. However, compared to VR, CR makes use of a more sophisticated lighting model that creates photorealistic images with improved detail and produces

shadowing effects that allow for robust visualization of the relative positions of structures.

3D visualizations of CT data can be invaluable in the investigation of complex anatomy and pathology, and pathological findings concerning neighboring structures can be identified and visualized (7).

3D CR is helpful for surgeons because it provides information on spatial relationships and a subjective perspective on the relevant organ (8).

Similar to VR, CR provides the best visualizations of high-density and high-contrast structures such as contrast-enhanced small vessels, but at the same time, it provides more natural and photorealistic illumination of the rendered data (9), highlighting relevant information in anatomically complex regions, as in congenital cardiopathies (10).

The applications of CR are numerous and varied, including medical education, easy disease detection, and improved description and classification of lesions. Recently, examples of the advantages of CR in the context of cardiovascular pathologies have been presented and this method has been qualitatively compared with other 3D postprocessing methods (11, 12). Moreover, realistic shadowing effects and different windowing options are likely to meet with more approval in imaging providing surgical and procedural guidance (13).

In our case, multiplanar reconstruction images still represented the gold standard in classification and preoperative treatment planning; however, the 3D volume rendering and cinematic rendering images provided a more exhaustive global overview of the vascular complexity of the lesion.

For morphological evaluation and tissue characterization, acquisition of a CMR scan is useful in the differential diagnosis and monitoring of cardiac masses. Through this investigation, the study of the cardiac planes enables localization of the lesion and determination of its relationship with the surrounding structures. The morphological characteristics of hyper/hypointensity are suitable to discriminate the lesion, and its relationships with other structures are much better highlighted.

In this case, the lesion showed obvious signal restriction in DWI sequence, and furthermore, the use of gadolinium (LGE) highlighted capsular hyperenhancement of the mass in post-contrast PSIR-TFE sequences, emphasizing its high vascularity.

CMR is now in routine use, but the examination process is lengthy, and it may not be available at every facility.

Both CCT and CMR are useful for further evaluation of these masses. Attenuation on CCT, tissue characterization on CMR, pattern and degree of contrast enhancement, and presence or absence of blood flow on cine CMR images can help differentiate among pericardial masses.

CMR provides incremental prognostic value over clinical factors such as left ventricular ejection fraction and coronary artery disease. In (14), CMR had high diagnostic accuracy in a patient with suspected cardiac tumors.

In our case, CMR contributed useful information, such as the morphological characteristics of hyper/hypointensity, signal restriction in DWI, and enhancement postgadolinium injection.

This case study shows the ability of a multimodal morphological imaging approach, using images obtained with CCT and CMR, to correctly identify, locate, and characterize cardiac PGLs and monitor non-operable lesions over time.

In challenging circumstances, extra-adrenal PGL and metastases can be localized using nuclear medicine methods such as SPECT and MIBG with neurotransmitter analogs, and metabolic radiotracers represent the final step for accurate functional characterization of a PGL and exclusion of a malignant component.

For this type of lesion with complex morphology, not only do additional visualization techniques such as CR provide descriptions and detailed representations of the lesion, its anatomy, and its relationship to the surrounding structures, but they also act as support for both diagnosis and management of complex cardiovascular lesions. In vitro analyses should be performed to characterize the functional status of PGLs, a feature that, combined with the vascular relationships of the lesion, deeply influences the management of these patients.

In conclusion, no standalone scans allow for comprehensive diagnosis of PGLs, although PET/MR technology and, more recently, radiomics techniques can attempt to solve issues related to morpho-functional assessment and benign/malign differentiation. In order to accomplish the aim of establishing the optimal ways to make use of these techniques, more studies with larger samples are needed.

## Data availability statement

The datasets presented in this study can be found in online repositories. The names of the repository/repositories and accession number(s) can be found in the article/**Supplementary Material**.

## Ethics statement

The studies involving human participants were reviewed and approved by IRCCS Fondazione Pascale. The patients/participants provided their written informed consent to participate in this study. Written informed consent was obtained from the participant/patient(s) for the publication of this case report.

## Author contributions

CC and FC contributed equally to the case study. All authors contributed to the article and approved the submitted version.

## Funding

This work was partially funded by the Italian Ministry of Health: projects “ricerca corrente” and “RCR-2019-23669118_005 CARDIO—Carditox-CT study.”

## Conflict of interest

The authors declare that the research was conducted in the absence of any commercial or financial relationships that could be construed as a potential conflict of interest.

## Publisher's note

All claims expressed in this article are solely those of the authors and do not necessarily represent those of their affiliated organizations, or those of the publisher, the editors and the reviewers. Any product that may be evaluated in this article, or claim that may be made by its manufacturer, is not guaranteed or endorsed by the publisher.

## Supplementary material

The Supplementary Material for this article can be found online at: https://www.frontiersin.org/articles/10.3389/fcvm.2023.1123789/full#supplementary-material.

## References

1. Nemeth A, Schlensak C, Popov A. Extended resection of a cardiac paraganglioma – a rare neuroendocrine manifestation of the heart. *J Card Surg*. (2020) 35(3):700–2. doi: 10.1111/jocs.14440

2. Yadav PK, Baquero GA, Malysz J, Kelleman J, Gilchrist IC. Cardiac paraganglioma. *Circ Cardiovasc Interv*. (2014) 7(6):851–6. doi: 10.1161/CIRCINTERVENTIONS.114.001856

3. Bhojwani N, Huang J, Garg V, Yang M, Oliveira GH, Rajiah P. Utility of $^{18}$F-fluorodeoxyglucose positron emission tomography/magnetic resonance imaging in the diagnosis of cardiac paraganglioma. *Indian J Nucl Med*. (2017) 32(4):380–2. doi: 10.4103/ijnm.IJNM_93_17

4. Eid M, De Cecco CN, Nance JW, Caruso D, Albrecht MH, Spandorfer AJ, et al. Cinematic rendering in CT: a novel, lifelike 3D visualization technique. *Am J Roentgenol*. (2017) 209(2):370–9. doi: 10.2214/AJR.17.17850

5. Saththasivam P, Herrera E, Jabbari OA, Reardon M, Sheinbaum R. Cardiac paraganglioma resection with ensuing left main coronary artery compromise. *J Cardiothorac Vasc Anesth*. (2017) 31(1):236–9. doi: 10.1053/j.jvca.2016.05.048

6. Tella SH, Jha A, Taïeb D, Horvath KA, Pacak K. Comprehensive review of evaluation and management of cardiac paragangliomas. *Heart*. (2020) 106(16):1202–10. doi: 10.1136/heartjnl-2020-316540

7. Glöckler M, Halbfaß J, Koch A, Achenbach S, Dittrich S. Multimodality 3D-roadmap for cardiovascular interventions in congenital heart disease – a single-center, retrospective analysis of 78 cases. *Catheter Cardiovasc Interv*. (2013) 82(3):436–42. doi: 10.1002/ccd.24646

8. Lawler LP, Corl FM, Fishman EK. Multi-detector row and volume-rendered CT of the normal and accessory flow pathways of the thoracic systemic and pulmonary veins. *Radiographics*. (2002) 22(Suppl 1):S45–60.

9. Baldi D, Tramontano L, Punzo B, Orsini M, Cavaliere C. CT cinematic rendering for glomus jugulare tumor with intracranial extension. *Quant Imaging Med Surg*. (2020) 10(2):522. doi: 10.21037/qims.2019.12.13

10. Frangi AF, Neiessen WJ, Viergever MA. Three-dimensional modeling for functional analysis of cardiac images – a review. *IEEE Trans Med Imaging*. (2001) 20(1):2–5. doi: 10.1109/42.906421

11. Rowe SP, Fritz J, Fishman EK. CT evaluation of musculoskeletal trauma: initial experience with cinematic rendering. *Emerg Radiol*. (2018) 25:93–101. doi: 10.1007/s10140-017-1553-z

12. Rowe SP, Johnson PT, Fishman EK. Initial experience with cinematic rendering for chest cardiovascular imaging. *Br J Radiol*. (2018) 91:20170558.

13. Vannier MW, Marsh JL, Warren JO. Three dimensional CT reconstruction images for craniofacial surgical planning and evaluation. *Radiology*. (1984) 150:179–84. doi: 10.1148/radiology.150.1.6689758

14. Shenoy C, Grizzard JD, Shah DJ, Kassi M, Reardon MJ, Zagurovskaya M, et al. Cardiovascular magnetic resonance imaging in suspected cardiac tumour: a multicentre outcomes study. *Eur Heart J*. (2021) 43(1):71–80. doi: 10.1093/eurheartj/ehab635

frontiers | Frontiers in Cardiovascular Medicine

TYPE Case Report
PUBLISHED 30 March 2023
DOI 10.3389/fcvm.2023.1117711



OPEN ACCESS

EDITED BY
Riccardo Liga,
Pisana University Hospital, Italy

REVIEWED BY
Francesca Mantovani,
Azienda USL-IRCCS di Reggio Emilia, Italy
Maria D'Armiento,
University of Naples Federico II, Italy

*CORRESPONDENCE
Hoai Thi Thu Nguyen
✉ hoainguyen1973@gmail.com

SPECIALTY SECTION
This article was submitted to Cardiovascular Imaging, a section of the journal Frontiers in Cardiovascular Medicine

RECEIVED 06 December 2022
ACCEPTED 13 March 2023
PUBLISHED 30 March 2023

CITATION
Bui STT, Nguyen PH, Nguyen TN, Kirkpatrick JN, Nguyen VK and Nguyen HTT (2023) Multivalvular involvement associated with Libman-Sacks endocarditis detected by multimodality imaging: A case report. Front. Cardiovasc. Med. 10:1117711. doi: 10.3389/fcvm.2023.1117711



# Multivalvular involvement associated with Libman-Sacks endocarditis detected by multimodality imaging: A case report

Son Tran Thanh Bui[1], Phuong Hoang Nguyen[2], Trang Ngoc Nguyen[3], James N. Kirkpatrick[4], Viet Khoi Nguyen[3] and Hoai Thi Thu Nguyen[1,5]*

[1]Vietnam National Heart Institute, Bach Mai Hospital, Hanoi, Vietnam, [2]Allergy and Clinical Immunology Center, Bach Mai Hospital, Hanoi, Vietnam, [3]Radiology Center, Bach Mai Hospital, Hanoi, Vietnam, [4]Cardiovascular Division, Department of Medicine, University of Washington Medical Center, Seattle, United States, [5]Department of Internal Medicine, VNU—University of Medicine and Pharmacy, Hanoi, Vietnam

Libman-Sacks endocarditis accounts for 6–11 percent of systemic lupus erythematosus patients and is associated with varying degrees of valvular dysfunction, increased risk for stroke and transient ischemic attacks, and increased mortality. In previous studies, left-sided valvular Libman-Sacks vegetations were more frequently detected than right sided vegetations; reported cases of bilateral involvement is very rare. A comprehensive clinical assessment and the multimodality imaging is of utmost importance in the management of systemic lupus erythematosus. In this case report, we describe a 31-year-old female patient with uncontrolled systemic lupus erythematosus initially presented with gastrointestinal symptoms but eventually had a vegetation-like structure on the posterior leaflet of the mitral valve which was revealed during routine echocardiography. Two-dimensional/three-dimensional transthoracic and transesophageal echocardiography, cardiac magnetic resonance, and cardiac computed tomography further characterized the mitral valve vegetation and revealed an additional vegetation of the pulmonary valve. Echocardiography remains the cornerstone for the detection of Libman-Sacks vegetations. Cardiac MRI and cardiac CT are useful in characterizing lesion size and effects and may prove particularly helpful in the assessment of right-sided or multivalvular endocarditis. The presence of focal brain lesions on brain MRI prompted antithrombotic therapy.

KEYWORDS

Libman-Sacks endocarditis, three-dimensional echocardiography, cardiac magnetic resonance, cardiac computed tomography, multimodality imaging, nonbacterial thrombotic endocarditis, white matter hyperintensity

## Introduction

Libman-Sacks endocarditis (LSE) is a form of nonbacterial thrombotic endocarditis (NBTE) and is found in 6%–11% of patients with systemic lupus erythematosus (SLE) (1). Most LSE cases are clinically silent. However, the presence of Libman-Sacks vegetations is associated with varying degrees of valvular dysfunction, increased risk for stroke and transient ischemic attacks, and increased mortality (1, 2). Early detection and initiation of medical therapy may resolve LSE and prevent valvular deterioration (3). In

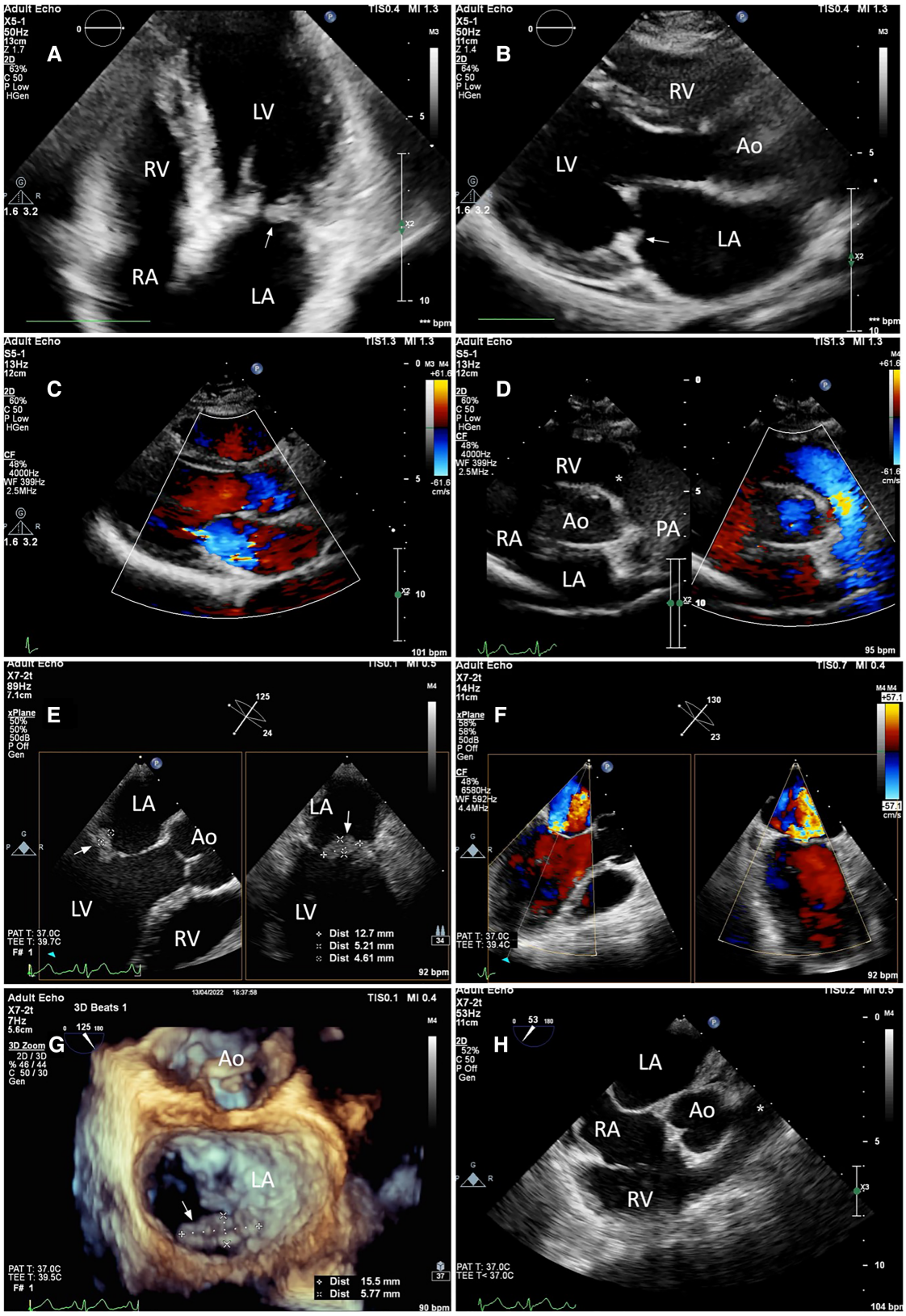


FIGURE 1
Still-frame images of the mitral and pulmonary valves on TTE (A–D) and TEE (E–H). (A,B) TTE apical four-chamber and parasternal long axis views revealed a well-circumscribed, sessile mass with heterogeneous echotexture which was firmly attached to the atrial side of the posterior leaflet of the mitral valve (white arrow). The mitral valve leaflets were thickened. (E) The maximum diameter of the mass was measured using 2D Xplane imaging at the mid-esophageal level. (G) From the left atrial perspective (en-face view), the vegetation was seen attached to the atrial side of the P2 and P3 portions of the posterior leaflet (white arrow) with 3-dimensional zoom-mode. (C,F) mild-to-moderate central mitral regurgitation was seen on both TTE and TEE with color Doppler. (D,H) The pulmonary valve as visualized on the parasternal short-axis and mid-esophageal right ventricle inflow-outflow view was unremarkable (asterisk). Annotations: LA, left atrium; LV, left ventricle; RA, right atrium; RV, right ventricle; Ao, Aorta; PA, pulmonary artery.

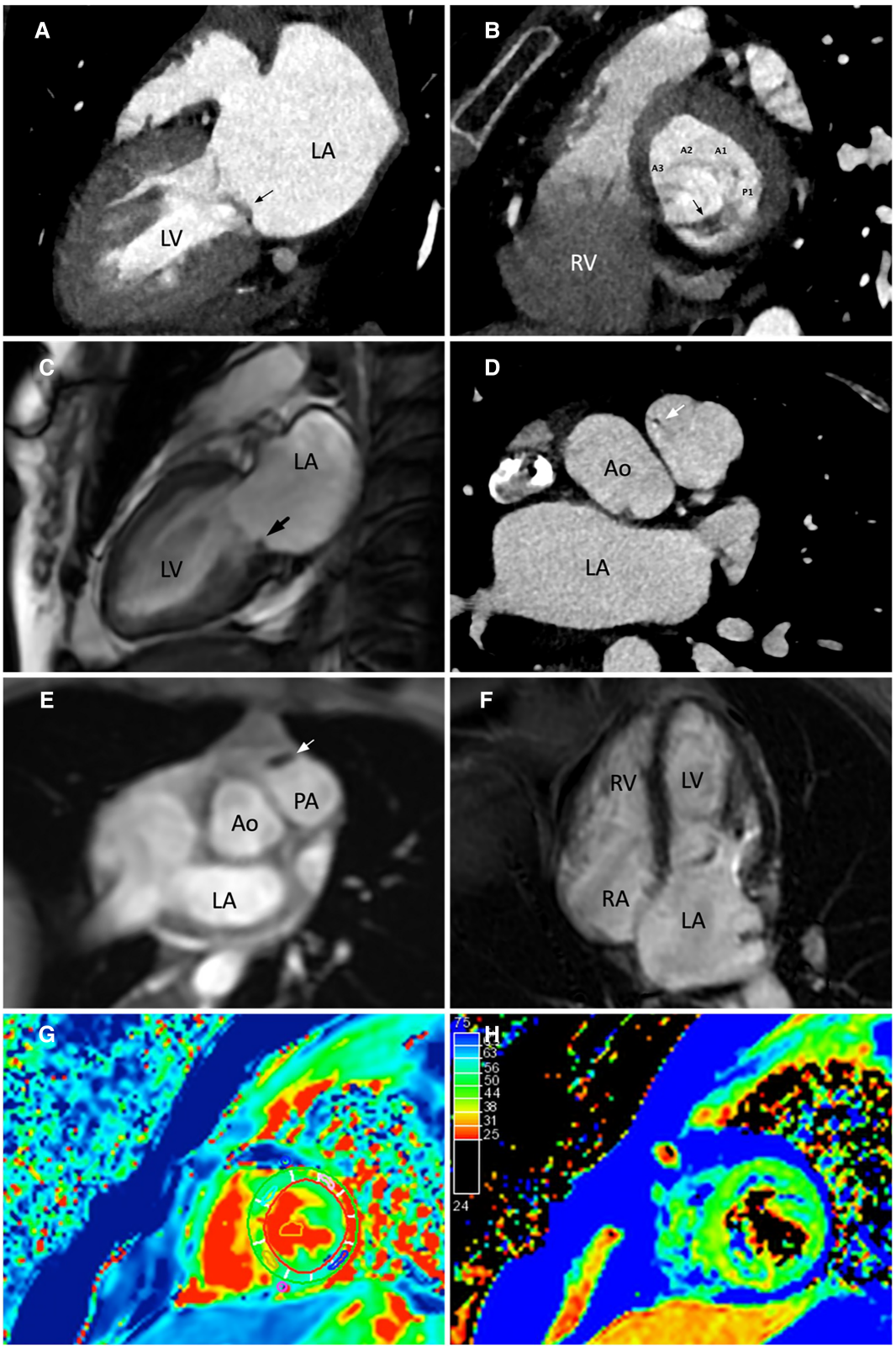


FIGURE 2
Evaluation of the mitral and pulmonary valve vegetations using cardiac computed tomography (CT) and cardiac magnetic resonance (CMR). (**A**,**C**) CT 2-chamber view and cine-CMR still image in end-systole showing a non-homogeneous, isodense mass involving the posterior leaflet of the mitral valve. (**B**) CT short axis view of the mitral valve from a basal short axis slice demonstrated the attachment of the vegetation to the P2 and P3 portions of the posterior mitral leaflet. The mitral valve was seen from a left ventricular perspective. (**D**,**E**) Transverse CT and CMR images through the right ventricular outflow tract showed a small oscillating mass on the anterior cusp of the pulmonary valve. (**F**) The myocardium showed no late gadolinium enhancement. (**G**,**H**) Normal findings on native-T1 and T2-weighted mapping images. Annotations: LA, left atrium; LV, left ventricle; RA, right atrium; RV, right ventricle; Ao, Aorta.

previous studies, left-sided valvular Libman-Sacks vegetations were more frequently detected than right sided vegetations; reported cases of bilateral involvement is very rare (1). In this case report, we highlight the importance of multimodality imaging in the diagnosis of multivalvular involvement in LSE. Our case report was presented in line with the CARE criteria (4).

## Case presentation

A 31-year-old woman diagnosed with SLE 12 years prior presented to our immunology clinic. She complained of a one-month history of general swelling of the whole body and diarrhea. Her SLE was not well-controlled and was predominantly hematological during her previous flares. She had a prior history of intolerance to hydroxychloroquine and was taking methylprednisolone and mycophenolate mofetil at the time of admission. She was positive for SARS-CoV-2 one month prior to admission without any symptom. Her review of systems was negative for underlying valvular disease, previous episodes of rheumatic fever, antiphospholipid syndrome (APS), and intravenous drug abuse.

On examination, the patient had normal vitals, was afebrile, and had generalized edema. A thorough cardiovascular evaluation was unremarkable with no cardiac murmurs and

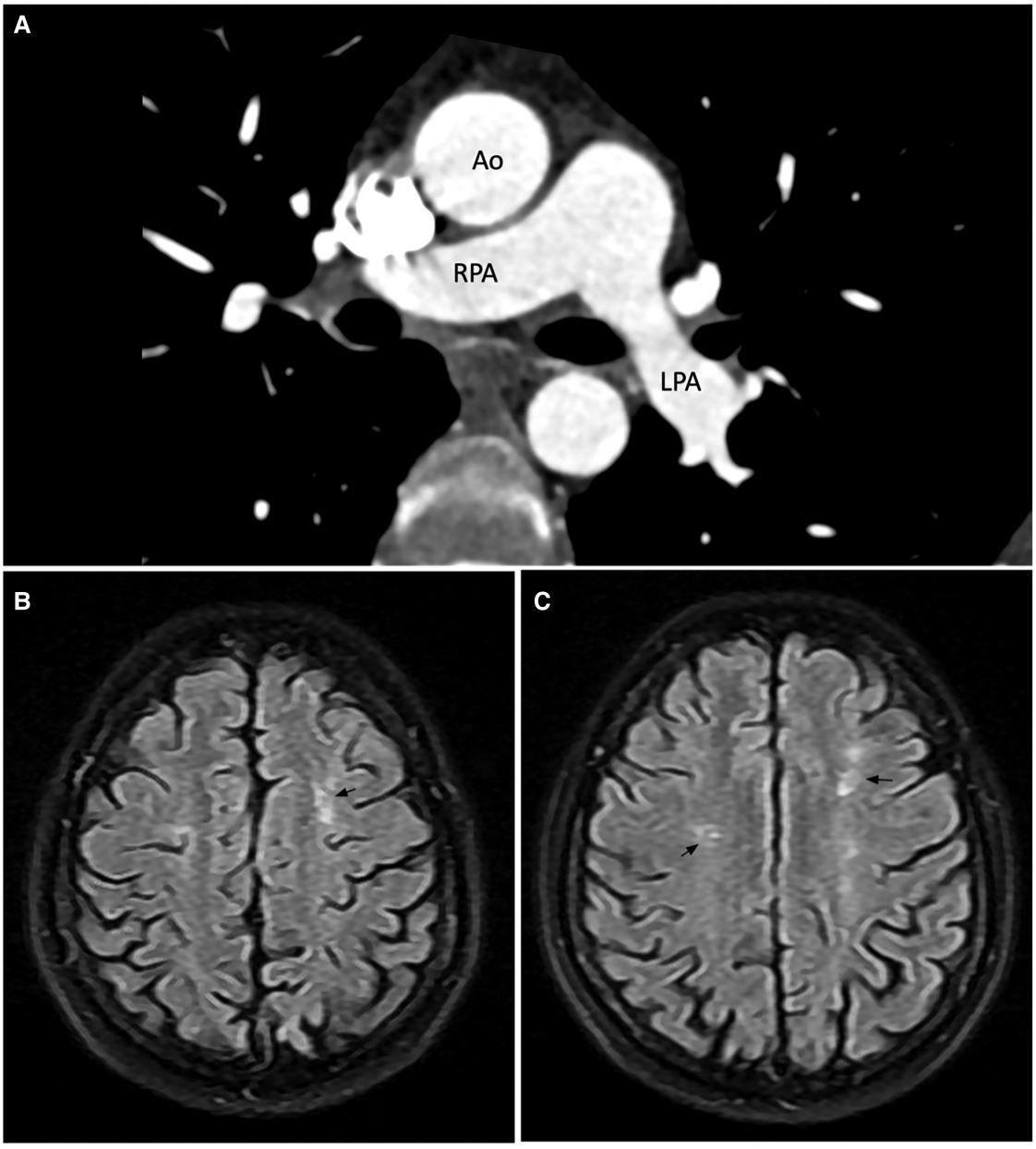


FIGURE 3
Computed tomography pulmonary angiogram (**A**) and brain magnetic resonance imaging scan (**B,C**). (**A**) No large pulmonary emboli on CTPA. (**B,C**) Axial FLAIR image showed bilateral hyperintense white matter lesions in the frontal lobes. The number of lesions is more than expected for the patient's age. Annotations: Ao, aorta; RPA, right pulmonary artery; LPA, left pulmonary artery.

normal jugular venous pressure. Examination of the integumentary system did not show any purpura, splinter hemorrhage, oral ulcers, or alopecia. Notable initial laboratory findings were as follows: mild normocytic anemia with negative Coombs tests, thrombocytopenia ($45 \times 10^9$ per liter), leukocytosis ($17.12 \times 10^9$ per liter), decreased C3 levels (0.45 g/L), severe hypoalbuminemia (8.6 mg/L) without evidence of proteinuria or hematuria, within-normal range liver and renal function tests. Her procalcitonin level was mildly elevated (0.166 ng/ml). The C-reactive protein, interleukin-6, high-sensitivity cardiac troponin and N-type brain natriuretic peptide were in normal ranges. Her coagulation studies showed a prothrombin time and fibrinogen level within normal limits but mildly elevated D-dimer level (0.95 mg/L). The immunologic study was positive for antinuclear antibodies and anti-double-stranded DNA. Screening for antiphospholipid (aPL) antibodies was negative. Endoscopic evaluation of the upper and lower gastrointestinal tract with biopsies only revealed lymphoplasmacytic infiltrates without any evidence of celiac disease. Her SLEDAI-2K score was 5.

A transthoracic echocardiogram (TTE) revealed a 6-by-13-millimeter mass of heterogeneous echocardiographic texture which was well-circumscribed, oval-shaped, protruding, sessile, and firmly attached to the atrial side of the P2 and P3 portions of the posterior mitral leaflet. The posterior mitral leaflet was diffusely thickened, predominantly at the tip and mid portions. There was no commissural fusion, calcification of the leaflets, or involvement of the subvalvular apparatus. Mild-to-moderate central mitral regurgitation and trivial pericardial effusion were present. To further elucidate the nature of the mass and rule out possible thrombi, 2-dimensional and 3-dimensional transesophageal echocardiography (TEE) was subsequently performed (**Figures 1E–H**). The other valves were morphologically normal. Left ventricular systolic function was preserved with a left ventricular ejection fraction (LVEF) of 74 percent. Two-dimensional left ventricular and right ventricular global longitudinal strain values were normal.

A cardiac magnetic resonance (CMR) demonstrated a preserved LVEF (60.5%) and no regional wall motion abnormalities. Late gadolinium enhancement (LGE) images, native-T1 map, T2 map, and extracellular volume (ECV) map were normal (**Figures 2C–H**). Hence, lupus-induced myocarditis was excluded. The mitral valve vegetation appeared as a non-homogeneous, isodense mass involving the posterior leaflet. Transverse cine images through the right ventricular outflow tract revealed a 1.4-by-2.5-millimeter oscillating mass on the anterior cusp of the pulmonary valve which was not seen on echocardiography. Electrocardiogram-gated cardiac computed tomography (CT) with multiplanar reconstruction was subsequently performed to better delineate the exact dimensions of the vegetations (**Figures 2A,B**). Obstructive lesions were not found on her coronary CT angiography. CT of the abdomen and the pulmonary vasculature was negative for emboli (**Figure 3A**) and possible neoplasms. Deep bilateral white matter hyperintensities (WMH), which were more extensive than expected for the patient's age, were found on her brain magnetic resonance imaging (MRI) scan (**Figures 3B,C**).

A comprehensive investigation for possible infective endocarditis (IE) including three sets of blood cultures, serologic

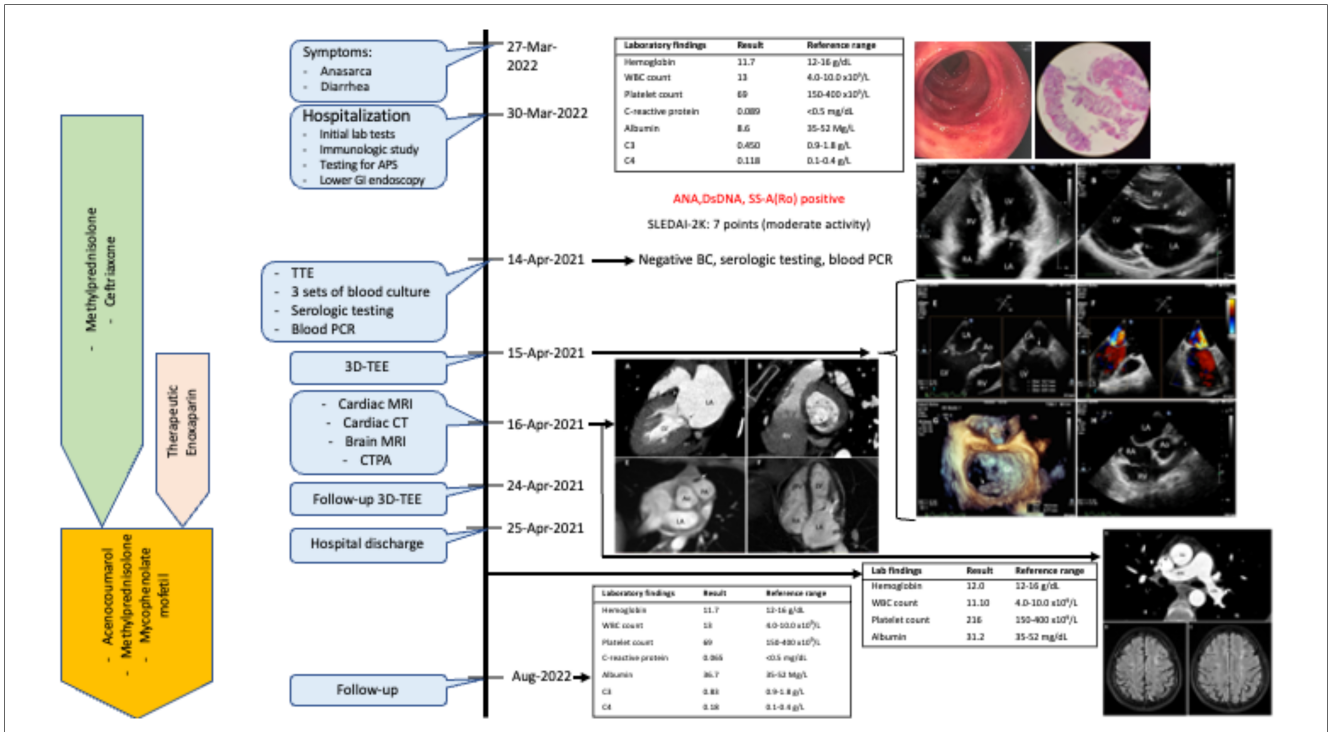


FIGURE 4
Timeline of patient clinical course.

testing for fastidious organisms, and stool sample culture did not reveal any pathogens. The final diagnosis was concomitant mitral and pulmonary valve LSE in a patient with lupus flare and protein-losing enteropathy. The patient was treated with methylprednisolone, systemic anticoagulation with subcutaneous enoxaparin, and intravenous ceftriaxone. After one month of medical therapy, the clinical and laboratory profile improved with a SLEDAI-2K score of 2. A follow-up pre-discharge 3D-TEE showed an unchanged size of the vegetation and severity of mitral regurgitation as compared to earlier echocardiographic studies.

After discharge, the patient maintained long-term therapeutic anticoagulation with acenocoumarol in addition to tapered-dose oral methylprednisolone and mycophenolate mofetil. At 3-month follow-up, she reported total remission of symptoms, and her laboratory tests demonstrated well-controlled SLE. Nonetheless, the Libman-Sacks vegetations and moderate mitral regurgitation persisted on subsequent TTEs. If our patient remains asymptomatic, repeated subsequent TTEs are planned every 1–2 years. The timeline of the patient clinical course is shown in **Figure 4**.

## Discussion

The true prevalence of LSE can reach 50% in autopsy studies (1). LSE is associated with patients having longer lupus duration, higher disease activity, anticardiolipin antibodies, and antiphospholipid syndrome (1). Hence, these populations may warrant screening for LSE, even if asymptomatic.

Despite its clinical significance, LSE is often overlooked during routine echocardiography. The sensitivity of TTE in the detection of LSE is only 11% (1). Most LSE cases are asymptomatic, and a prior SLE diagnosis can also bias echocardiogram interpretations (5). Aside from being more sensitive and specific (6), TEE allows a better understanding of the mechanism of valvular diseases and rules out cardiac thrombi. 3D-TEE has incremental value over 2D-TEE for the detection and characterization of vegetations.

Echocardiography remains the cornerstone for the assessment of cardiac vegetations because it has unrivaled temporal resolution and repeatability. However, it is operator-dependent and is sometimes hindered by body morphology and artifacts from surrounding tissues. Furthermore, due to the complex anatomy and anterior position of the right heart, visualization of the right-sided valves by conventional 2D-TTE and TEE is not optimal, which may explain left-sided predominance of LSE in previous reports. The advent of novel cardiac imaging modalities addresses these difficulties.

CMR is effective in the diagnosis of LSE through direct visualization of vegetations on cine-CMR (steady-state free precession). CMR phase contrast imaging is an appealing new method to quantify regurgitation severity because of its ability to directly measure the flow across a valve. Myocardial tissue characterization using LGE analysis, T1, T2, ECV mapping, and perfusion imaging can identify patients with silent lupus-induced myocardial and pericardial disease (7). Because SLE affects any parts of the heart, CMR is the preferred imaging modality in asymptomatic or oligosymptomatic cases especially when echocardiographic features are abnormal (7). However, vegetations smaller than 3 millimeters are difficult to visualize on CMR due to inferior spatial resolution and partial volume artifact (8).

In comparison with CMR, ECG-gated CCT has a spatial resolution of 0.5–1 millimeters which is excellent at evaluating small structures (9). Nevertheless, it has a lower temporal resolution and requires exposure to radiation and nephrotoxic contrast agents. In our case, the improved spatial resolution allowed better localization and sizing of the pulmonary vegetation previously seen on cine-CMR.

Several conditions to be considered in the differential diagnosis include IE, papillary fibroelastoma, Lambl's excrescences, and cancer-related NBTE. Infective vegetations are often independently highly mobile, elongated, have narrow attachment to its base, and may accompany valve perforation (10). Fibroelastoma rarely causes valvular dysfunction and tends to localize away from the leaflets' free edge (8). Lambls's excrescences appear on echocardiography as undulating hypermobile, strand-like echodensities at the leaflets' coaptation (2). A primary neoplasm was not evident on CT and MRI scans of the thorax, abdomen, and brain. The absence of all forementioned features was ascertained using multimodality imaging.

Treatment mainly involves immunosuppressive therapy for underlying lupus and systemic anticoagulation (11). Surgery in LSE is associated with high mortality and should be reserved only for patients having severe valvular dysfunction, very large vegetations (greater than 2 centimeters), or recurrent thromboembolism despite therapeutic anticoagulation, after weighing the benefits and risks of surgery (3, 11). LSE is associated with cerebrovascular embolism, focal brain lesions, and neuropsychiatric involvement (1, 2). Conversely, patients who exhibit deep WMH on brain MRI scans have increased risk for ischemic stroke (12). Early anti-inflammatory and anti-thrombotic therapy might resolve vegetations-induced valvular dysfunction, improve cerebral perfusion, and avoid the need for surgery (3).

As LSE is highly prevalent among SLE patients with aPL antibodies, most data guiding the choice of antithrombotic agents in LSE was derived from the experience in managing thromboembolic APS. Therapeutic anticoagulation with rivaroxaban in high-risk APS patients (i.e., having triple positive aPL) showed increased risk of recurrent thromboembolic events as compared to conventional vitamin K agonists (VKAs) (13). The 2019 European Society of Cardiology guidelines recommend against the use of DOACs in all APS patients (14). The 2020 International Society on Thrombosis and Haemostasis guidance provided more detailed indications stating that warfarin should be the first-choice treatment in APS with arterial thromboembolic events, triple positivity, small vessel thrombosis, or valvular disease (including LSE), and that DOACs should only be considered in venous APS with single or double positivity or patients who cannot tolerate or have contraindications to

warfarin (15). Mantovani et al. reported the recurrence of thromboembolic events in cancer-related NBTE patients while under therapeutic DOAC (16). Because both cancer-related and auto-immune mediated NBTE share the same spectrum of histopathologic lesions and are associated with hypercoagulable states (17), the use of DOACs in LSE should be cautioned. Although more high-quality trials are needed, available data and guidelines support the use of VKAs in aPL-negative LSE (like our patient). Patients having recurrent thromboembolic events while on oral anticoagulants should be switched to heparin.

## Conclusion

LSE can involve multiple heart valves. Echocardiography remains the cornerstone for its detection, but cardiac MRI and cardiac CT can be useful in characterizing lesion size and effects and may prove particularly helpful in the assessment of right-sided or multivalvular Libman-Sacks endocarditis. The presence of focal brain lesions can guide antithrombotic therapy in asymptomatic, uncomplicated LSE.

## Data availability statement

The original contributions presented in the study are included in the article/Supplementary Materials, further inquiries can be directed to the corresponding author.

## Ethics statement

The studies involving human participants were reviewed and approved by Bach Mai Hospital. The patients/participants provided their written informed consent to participate in this study. Written informed consent was obtained from the individual(s) for the publication of any potentially identifiable images or data included in this article.

## Author contributions

HN, SB, JK devised the manuscript concept. SB, HN, PN belonged to patient's management team. HN, SB performed two-dimensional/three-dimensional echocardiography. TN and VN interpreted the CMR and cardiac CT images. SB wrote the manuscript in collaboration with HN, JK, PN, TN. HN took care of revising and submitting the manuscript. All authors contributed to the article and approved the submitted version.

## Acknowledgments

We wish to thank the Vietnam National Heart Institute, Bach Mai hospital for providing us with the opportunity to conduct this case report.

## Conflict of interest

The authors declare that the research was conducted in the absence of any commercial or financial relationships that could be construed as a potential conflict of interest.

## Publisher's note



## References

1. Moyssakis I, Tektonidou MG, Vasilliou VA, Samarkos M, Votteas V, Moutsopoulos HM. Libman-Sacks endocarditis in systemic lupus erythematosus: prevalence, associations, and evolution. *Am J Med.* (2007) 120:636–42. doi: 10.1016/j.amjmed.2007.01.024

2. Roldan CA, Sibbitt WL, Qualls CR, Jung RE, Greene ER, Gasparovic CM, et al. Libman-Sacks endocarditis and embolic cerebrovascular disease. *JACC Cardiovasc Imaging.* (2013) 6:973–83. doi: 10.1016/j.jcmg.2013.04.012

3. Roldan CA, Sibbitt WL, Greene ER, Qualls CR, Jung RE. Libman-Sacks endocarditis and associated cerebrovascular disease: the role of medical therapy. *PLoS One.* (2021) 16:e0247052. doi: 10.1371/journal.pone.0247052

4. CARE Checklist. *CARE Case Report Guidelines.* Available at: https://www.care-statement.org/checklist (Accessed December 6, 2022).

5. Tape TG, Panzer RJ. Echocardiography, endocarditis, and clinical information bias. *J Gen Intern Med.* (1986) 1:300–4. doi: 10.1007/BF02596207

6. Roldan CA, Qualls CR, Sopko KS, Sibbitt WL. Transthoracic versus transesophageal echocardiography for detection of Libman-Sacks endocarditis: a randomized controlled study. *J Rheumatol.* (2008) 35:224–9. PMID: 18085739.

7. Burkard T, Trendelenburg M, Daikeler T, Hess C, Bremerich J, Haaf P, et al. The heart in systemic lupus erythematosus—a comprehensive approach by cardiovascular magnetic resonance tomography. *PLoS One.* (2018) 13:e0202105. doi: 10.1371/journal.pone.0202105

8. Hoey ETD, Gulati GS, Ganeshan A, Watkin RW, Simpson H, Sharma S. Cardiovascular MRI for assessment of infectious and inflammatory conditions of the heart. *Am J Roentgenol.* (2011) 197:103–12. doi: 10.2214/AJR.10.5666

9. Kuchynka P, Podzimkova J, Masek M, Lambert L, Cerny V, Danek B, et al. The role of magnetic resonance imaging and cardiac computed tomography in the assessment of left atrial anatomy, size, and function. *Biomed Res Int.* (2015) 2015:247865. doi: 10.1155/2015/247865

10. Roldan CA, Tolstrup K, Macias L, Qualls CR, Maynard D, Charlton G, et al. Libman-Sacks endocarditis: detection, characterization, and clinical correlates by three-dimensional transesophageal echocardiography. *J Am Soc Echocardiogr.* (2015) 28:770–9. doi: 10.1016/j.echo.2015.02.011

11. Asopa S, Patel A, Khan OA, Sharma R, Ohri SK. Non-bacterial thrombotic endocarditis. *Eur J Cardiothorac Surg.* (2007) 32:696–701. doi: 10.1016/j.ejcts.2007.07.029

12. Sano E, Arawaka S. White matter hyperintensities as a risk factor for ischemic stroke in patients with systemic lupus erythematosus. *Front Neurol.* (2021) 12:1–6. doi: 10.3389/fneur.2021.738173

13. Pengo V, Denas G, Zoppellaro G, Jose SP, Hoxha A, Ruffatti A, et al. Rivaroxaban vs warfarin in high-risk patients with antiphospholipid syndrome. *Blood*. (2018) 132:1365–71. doi: 10.1182/blood-2018-04-848333

14. Konstantinides SV, Meyer G, Becattini C, Bueno H, Geersing G-J, Harjola V-P, et al. 2019 ESC guidelines for the diagnosis and management of acute pulmonary embolism developed in collaboration with the European respiratory society (ERS). *Eur Heart J*. (2020) 41:543–603. doi: 10.1093/eurheartj/ehz405

15. Zuily S, Cohen H, Isenberg D, Woller SC, Crowther M, Dufrost V, et al. Use of direct oral anticoagulants in patients with thrombotic antiphospholipid syndrome: guidance from the scientific and standardization committee of the international society on thrombosis and haemostasis. *J Thromb Haemost*. (2020) 18:2126–37. doi: 10.1111/jth.14935

16. Mantovani F, Navazio A, Barbieri A, Boriani G. A first described case of cancer-associated non-bacterial thrombotic endocarditis in the era of direct oral anticoagulants. *Thromb Res*. (2017) 149:45–7. doi: 10.1016/j.thromres.2016.11.016

17. Mazokopakis EE, Syros PK, Starakis IK. Nonbacterial thrombotic endocarditis (marantic endocarditis) in cancer patients. *Cardiovasc Hematol Disord Drug Targets*. (2010) 10:84–6. doi: 10.2174/187152910791292484

# Frontiers in
# Cardiovascular Medicine

**Innovations and improvements in cardiovascular treatment and practice**

Focuses on research that challenges the status quo of cardiovascular care, or facilitates the translation of advances into new therapies and diagnostic tools.

---

## Discover the latest Research Topics

See more →

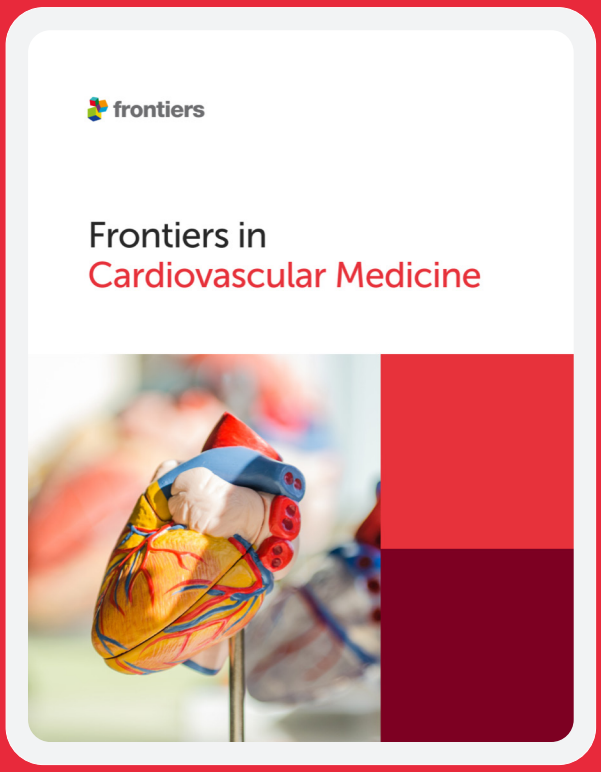


**Frontiers**

Avenue du Tribunal-Fédéral 34
1005 Lausanne, Switzerland
frontiersin.org

**Contact us**

+41 (0)21 510 17 00
frontiersin.org/about/contact